RADC-TR-84-8
Final Technical Report
February 1984

ADAPTIVE TECHNIQUES FOR TROPOSCATTER

Signatron, Inc.

Dr. Mark S. Wallace
Dr. Steen A. Parl
Dr. Alfonso Malaga
Mr. John N. Pierce

APPROVED FOR PUBLIC RELEASE; DISTRIBUTION UNLIMITED

DTIC

JUN 20 84

AD-A142 226

DTIC FILE COPY

ROME AIR DEVELOPMENT CENTER
Air Force Systems Command
Griffiss Air Force Base, NY 13441

84 06 19 016

This report has been reviewed by the RADC Public Affairs Office (PA) and
is releasable to the National Technical Information Service (NTIS). At NTIS
it will be releasable to the general public, including foreign nations.

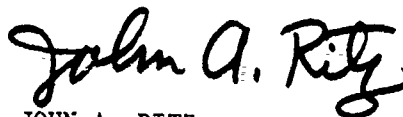RADC-TR-84-8 has been reviewed and is approved for publication.

APPROVED: *[signature]*

        EDWARD E. ALTSHULER
        Project Engineer

APPROVED: *[signature]*

        ALLAN C. SCHELL, Chief
        Electromagnetic Sciences Division

FOR THE COMMANDER: *[signature]*

        JOHN A. RITZ
        Acting Chief, Plans Office

If your address has changed or if you wish to be removed from the RADC
mailing list, or if the addressee is no longer employed by your organization,
please notify RADC (EEPS) Hanscom AFB MA 01731. This will assist us in
maintaining a current mailing list.

Do not return copies of this report unless contractual obligations or notices
on a specific document requires that it be returned.

REPORT DOCUMENTATION PAGE		READ INSTRUCTIONS BEFORE COMPLETING FORM
1. REPORT NUMBER RADC-TR-84-8	2. GOVT ACCESSION NO. AD-A142 226	3. RECIPIENT'S CATALOG NUMBER
4. TITLE (and Subtitle) ADAPTIVE TECHNIQUES FOR TROPOSCATTER		5. TYPE OF REPORT & PERIOD COVERED Final Technical Report Nov 82 – Sep 83
		6. PERFORMING ORG. REPORT NUMBER N/A
7. AUTHOR(s) Dr. Mark S. Wallace Dr. Alfonso Malaga Dr. Steen A. Parl Mr. John N. Pierce		8. CONTRACT OR GRANT NUMBER(s) F19628-82-C-0017
9. PERFORMING ORGANIZATION NAME AND ADDRESS Signatron, Inc. 12 Hartwell Avenue Lexington MA 02173		10. PROGRAM ELEMENT, PROJECT, TASK AREA & WORK UNIT NUMBERS 62702F 46001662
11. CONTROLLING OFFICE NAME AND ADDRESS Rome Air Development Center (EEPS) Hanscom AFB MA 01731		12. REPORT DATE February 1984
		13. NUMBER OF PAGES 292
14. MONITORING AGENCY NAME & ADDRESS(if different from Controlling Office) Same		15. SECURITY CLASS. (of this report) UNCLASSIFIED
		15a. DECLASSIFICATION/DOWNGRADING SCHEDULE N/A

16. DISTRIBUTION STATEMENT (of this Report)

Approved for public release; distribution unlimited.

17. DISTRIBUTION STATEMENT (of the abstract entered in Block 20, if different from Report)

Same

18. SUPPLEMENTARY NOTES

RADC Project Engineer: Edward E. Altshuler (EEPS)

19. KEY WORDS (Continue on reverse side if necessary and identify by block number)

Troposcatter Communications   Implicit Diversity
Phased Array Antennas   Sub-optimal Combiners
Maximal-Ratio Combining
Angle Diversity

20. ABSTRACT (Continue on reverse side if necessary and identify by block number)

This report examines the performance of phased array antennas with
adaptive combining for troposcatter communications. Diversity is commonly
employed to combat fading on troposcatter links. Diversity may be derived
from a phased array by adaptive combining of the element outputs (space
diversity) or equivalently by forming a set of beams via a Butler matrix
transformation (angle diversity).

DD FORM 1473 1 JAN 73   EDITION OF 1 NOV 65 IS OBSOLETE

A number of new results describing the performance of both azimuth and elevation angle diversity systems using phased arrays are derived and performance bounds for both azimuth and elevation diversity are found. A new class of sub-optimal combiners is examined. The effect of implicit diversity on wideband systems is considered. The degradation due to channel measurement errors is also determined. A measurement program is proposed to verify the results. The computer program which performs the common volume integration is described.

Accession For

NTIS GRA&I

DT'C T??

Unannounced

Justification

Distribution/

Availability Codes

Avail and/or

Dist | Special

A|

TABLE OF CONTENTS

TABLE OF CONTENTS (Continued)

TABLE OF CONTENTS (Continued)

TABLE OF CONTENTS (Continued)

TABLE OF CONTENTS (Concluded)

LIST OF FIGURES

LIST OF FIGURES (Continued)

LIST OF FIGURES (Concluded)

LIST OF TABLES

SECTION 1
INTRODUCTION AND SUMMARY

Phased arrays are attractive for troposcatter applications because of their ECCM potential. In a non-hostile environment these capabilities may be used to improve the system performance (i.e., decrease the bit-error-rate or transmitter power) through adaptive combining of the array element outputs. This report examines the potential diversity gains which may be derived from phased array antennas through adaptive combining. The performance of phased arrays is compared with traditional diversity types, such as space, frequency and polarization diversity.

Section 1 contains a summary of the key new results obtained in this study. More details and additional results are contained in the individual subsections. Section 2 describes the basic propagation model used to determine the diversity performance. Different diversity systems are discussed in Section 3, where the equivalence between space and angle diversity is established and a suitable measure of performance selected. Section 4 compares different orders of elevation and azimuth diversity. Section 5 derives the performance of some suboptimum combiners, including a new technique where only the K strongest diversity ports are combined. Section 6 describes the effect of fading, namely that only a finite time is available to measure the channel for optimal combining. Section 7 briefly treats the wideband case where additional diversity is derived from the frequency selective fading of the channel. In Section 8 an experiment is proposed to verify the results. The experiment is configured so that it could be used as a transportable remote sensing tool to get details about the atmospheric reflection and scattering structure. Section 9 describes the computer program used to obtain the troposcatter diversity results presented in this report.

1.1   TROPOSCATTER MODEL

Transhorizon propagation of microwave signals results from turbulent scatter in the troposphere. In our analysis we assume that turbulent scatter is the only mechanism present. The received signals are assumed to be free of diffraction or partial layer reflection components. The scattering is assumed isotropic, so the strength of the scatter in a given direction depends only on the scattering angle. The region of scatterers which are illuminated by the receive and transmit antennas is called the <u>common volume.</u> The signals scattered from various sections of the common volume are assumed independent. The received signal is the sum of a large number of scattered signals which have different amplitudes, phases, and relative delays. For a narrowband system the relative delays of the signals have no effect and the signal experiences Rayleigh fading. To combat this fading diversity is generally employed. In this case a number of signals are present at the receiver. These signals are correlated in general and the system performance depends on the correlations as well as the powers of the various signals.

1.2   COMPUTATION OF TROPOSCATTER SYSTEM PERFORMANCE

The theoretical results we present were generated by a computer program which performs a three-dimensional integration over the common volume. The program determines the power received at various relative delays and the correlation between diversity ports. It includes the effect of the transmit and receive antenna patterns, scatter angle and link geometry. The correlations between diversity ports include the effect of antenna spacing and beam patterns.

1-2

1.3 PERFORMANCE MEASURE

If the transmitted signal is narrowband then the received signal on each diversity port is Rayleigh distributed. The signals on various ports are correlated in general. The short-term statistics of the N-diversity ports are determined by the covariance matrix of the signal levels. Further, the system performance under any performance measure is entirely determined by the eigenvalues of the covariance matrix. The eigenvalues correspond to independent fading components of the channel.

The performance measure we use is the Chernoff bound on the average bit-error-rate (BER) of a digital communications system. If $\{\lambda_i, i = 1, \ldots, n\}$ are the eigenvalues then the Chernoff bound is

$$\phi_0 = \prod_{i=1}^{N} \left(\frac{1}{1 + \lambda_i}\right) .$$

The exact average BER for DPSK modulation is $\phi_0/2$. Although we use this performance measure throughout, the conclusions drawn depend on the eigenvalues and so would remain valid for other performance measures.

Systems are generally specified with a desired average BER. To compare different systems we compare the required SNR (i.e., transmit power required) for a given average error rate.

1.4 DIVERSITY PERFORMANCE BOUND

The best possible diversity system has equal-power independent signals on its diversity ports. The Chernoff bound on the BER for such a system is

$$\phi_0 = \left(\frac{1}{1 + \lambda}\right)^N$$

where λ is the power on one port of the system. A graph of the required SNR (i.e., λ required) to set $\phi_0 = 10^{-4}$, 10^{-6} and 10^{-8} is given in Figure 1-1 for various orders of diversity. Note that the initial SNR gains are large but that diminishing returns are seen with higher order diversity. The magnitude of the gains increases as the SNR gains from the diversity increase. For $\phi_0 = 10^{-8}$ the SNR gains are roughly doubled.

This bound may be achieved by adding receive apertures of the same size which are spaced far enough apart.

1.5 DIVERSITY FROM ARRAY ANTENNAS

Diversity may be derived from phased arrays by dividing the array into subapertures. The element outputs in each subaperture are simply added together, and the subarray outputs may be combined adaptively. We assume throughout that the receive and transmit apertures are the same size. If the receive aperture is subdivided, then the beamwidth of each subaperture is greater than the entire array beamwidth, and the boresight gain of the subapertures is less. The larger beamwidth decreases the aperture-to-medium coupling loss, but the boresight gain also decreases. In addition the subaperture signals are correlated. These effects may be examined in terms of the correlation distance of the received signal.

The signals incident on different parts of the receive aperture are correlated. For a given transmitter beamwidth, we may define correlation lengths in the horizontal and vertical directions, L_h and L_v. The correlation length is roughly the distance by which points must be separated to be uncorrelated. (L_h and L_v are given by the integral of the respective correlation functions divided by their maximum values.) If the array dimensions are a_h by a_v then the antenna gain is nominally

$$G = \frac{4\pi a_h a_v}{\lambda^2} .$$
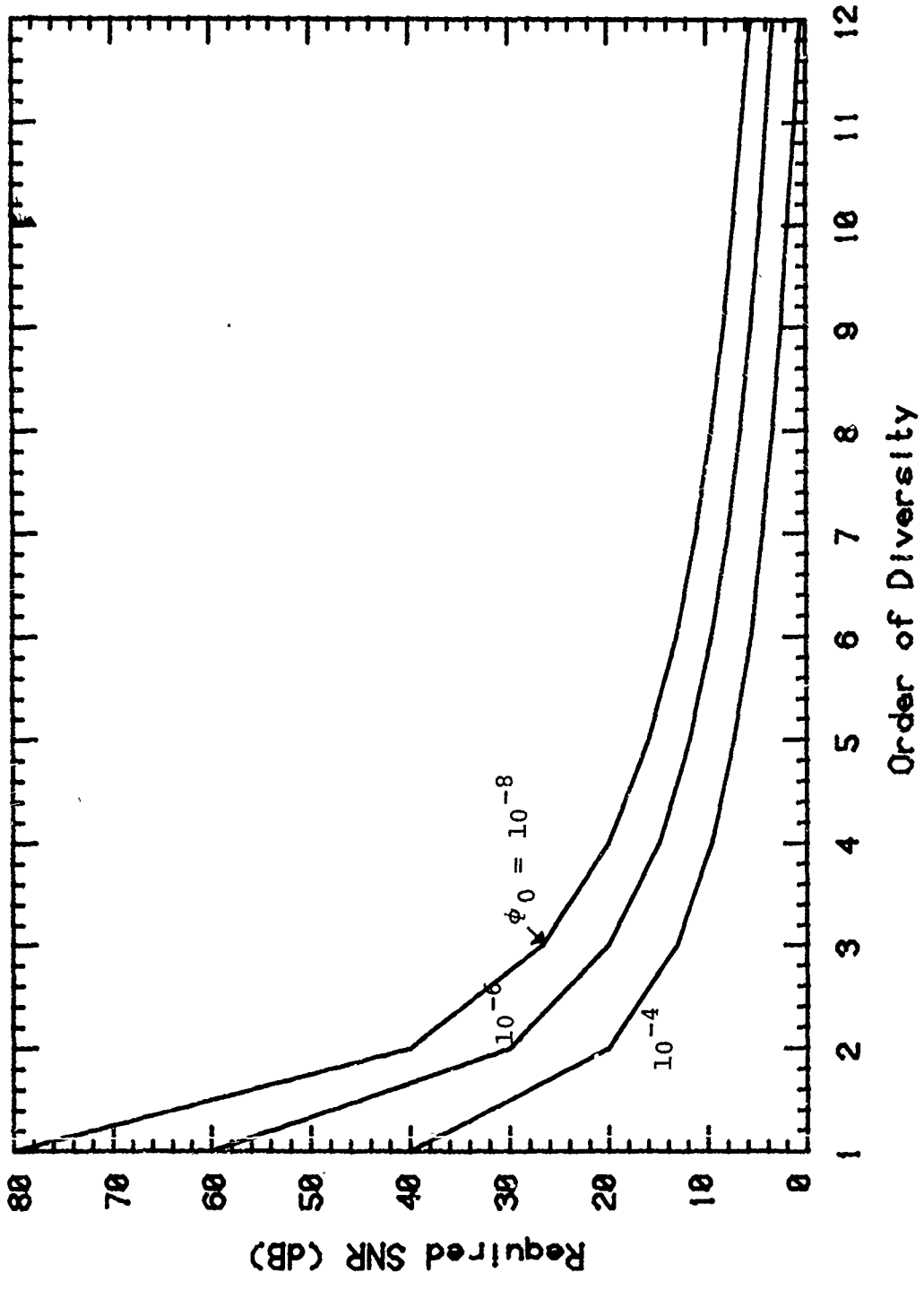
Figure 1-1 Required SNR to Make the Chernoff Bound on BER Equal to 10^{-4}, 10^{-6}, or 10^{-8}.

However the receive coupling loss is roughly

$$L_c = \frac{a_h}{L_h} \cdot \frac{a_v}{L_v} \, ,$$

so the effective gain is

$$\frac{G}{L_c} = \frac{4 \pi L_h L_v}{\lambda^2} \, .$$

Hence subapertures of a large array may have the same effective gain as the entire array. In addition the maximum order of diversity achievable with a given size array is the number of subarrays of dimension $L_v \times L_h$.

It is helpful to examine these effects in terms of different beams formed from the subarrays via a Butler matrix transformation.

1.5.1 Beam Transformation

A Butler matrix transformation of the subarray output yields a set of beams. Each beam has the same beamwidth as the entire array. The direction of boresight gain is different for each beam, so the common volume of each beam is different. The boresight of adjacent beams differ by one half the null beamwidth. Because the beams are orthogonal the signals on each beam are effectively uncorrelated, and the power on each beam gives one eigenvalue of the system.

When subdivision of the array is examined in terms of correlation distance, the maximum order of diversity is known approximately. However, it is difficult to see the benefit of

additional subdivisions near this maximum order. Under a beam transformation additional beams receive less power because they have larger scatter angles or do not intersect the transmit antenna beam. So it is relatively easy to estimate the power which would be received on additional beams.

1.6   ELEVATION ANGLE DIVERSITY

If a square array is subdivided into subsections which are long in the horizontal dimension and short in the vertical direction, the vertical beamwidth of each subarray is greater than its horizontal beamwidth. A beam transformation of these subarray outputs yields a set of beams with different elevation angles. As previously mentioned the beams are orthogonal and the boresight of each beam falls at a null of all other beams.

The array is oriented such that the boresight of the lowest beam is above the horizon. This beam has the lowest scatter angle and so receives the most power. Higher elevation beams receive progressively less power since the scattering angle increases. So the additional eigenvalues from the upper beams are less than the first eigenvalue and the diversity bound may not in general be achieved. However, if the minimum scatter angle is large relative to the beamwidth then the higher beams receive almost the same power as the lowest beam and the bound may be approached.

Calculations of the required SNR to achieve $\phi_0 = 10^{-4}$ for elevation diversity systems of orders 1 to 5 appear in Figure 1-2. The diversity bound is included for comparison. The minimum scatter angle is 1.2° and the beamwidth of the array is 1° (3m x 3m at 5 GHz). The upper elevation beams receive little power so little benefit is derived from them.
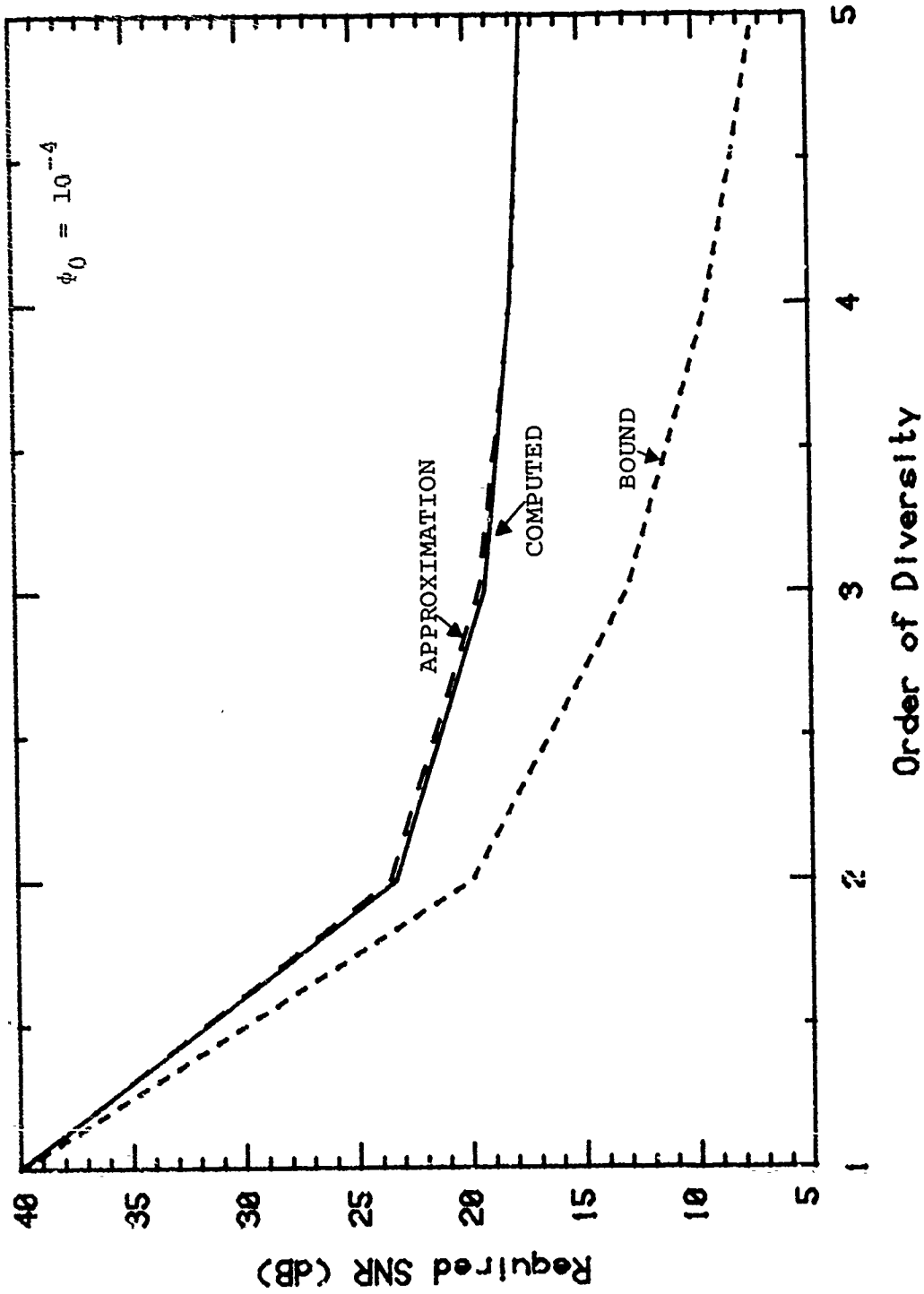
Figure 1-2 Elevation Diversity Performance Computed via 3 Common Volume
Integration for 1.2o Scatter Angle and 1o Beamwidth. Lower
Bound on Performance for Equal Power, Independent Ports.
Approximation Derives Eigenvalues from the Scatter at Bore-
sight for Each Port.

1.6.1 Elevation Diversity Approximation

If the beams are narrow relative to the scatter angle then a simple approximation may be derived. This approximation leads to new general expressions for elevation diversity performance.

For narrow beams the power on each beam depends on the scatter angle at boresight. If β is the beamwidth and Θ_{min} is the minimum scatter angle then the i-th beam boresight is

$$\Theta_i = \Theta_{min} + \frac{1}{2}\beta + (i-1)\beta .$$

The received power goes as $\Theta^{-11/3}$ so

$$\frac{\lambda_i}{\lambda_1} = \left[1 + (i-1)\frac{\beta}{\Theta_1}\right]^{-11/3}$$

where λ_i is the power on the i-th beam. The resulting performance from these eigenvalues is compared with those values generated by the numerical common volume integration in Figure 1-2. The approximation agrees closely.

To continue the comparison Figure 1-3 contains curves of diversity performance vs γ where

$$\gamma = \frac{\beta}{\Theta_1}$$

is the ratio of the beamwidth to the boresight scatter angle of the lowest beam. The curves were computed with various minimum scatter angles and beamwidths. The approximation leads to the following simple expression for Θ_0,

1-9
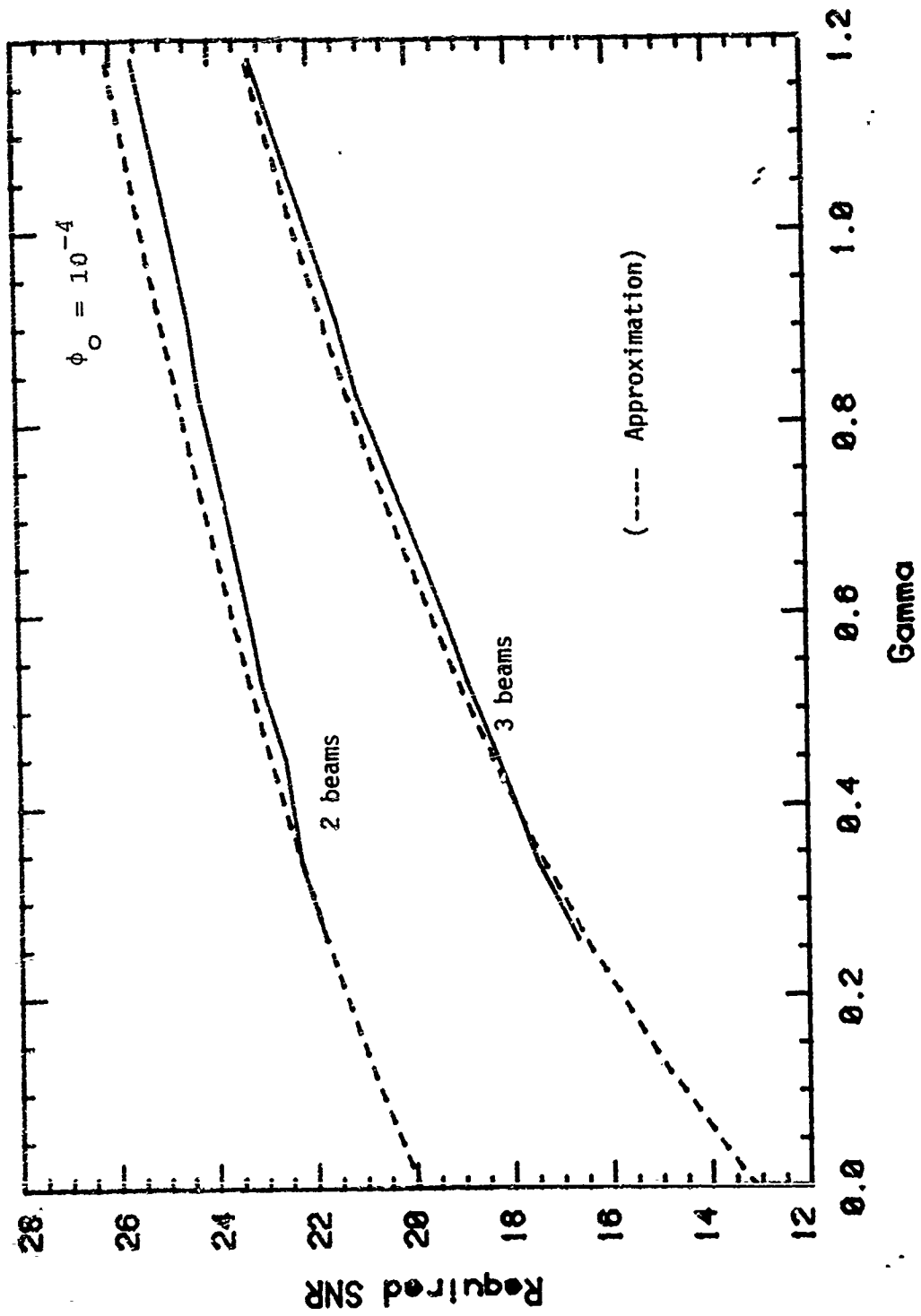
Figure 1-3 Comparison of elevation diversity performance with approximation.

$$\phi_0 = \prod_{i=1}^{n} \frac{1}{1+\sigma[1+(i-1)\gamma]^{-11/3}} \quad .$$

Note that the average BER for DPSK is $\phi_0/2$.

The results agree very closely for small γ, which is to be expected since the beams were assumed narrow. If the receiver and transmitter beamwidths are not narrow, then the -11/3 exponent tends toward -5/3. Similar expressions can be derived in this case but will not be considered here. Thus, the power decreases less rapidly than the approximation would predict and the actual performance is somewhat better (lower required SNR) than the approximation. This is in fact the behavior observed in Figure 1-3. The limiting performance with $\gamma=0$ achieves the diversity bound. Section 4.1 contains the details of the elevation diversity results. Table 4-3 shows how good the simple approximation can be.

1.7 AZIMUTH ANGLE DIVERSITY

If the array is divided into long vertical strips, then the subarray beam patterns are broad in azimuth and narrow in elevation. The beams which result from a beam transformation thus have different boresight <u>azimuth</u> angles. This interpretation makes one key difference betwen azimuth and elevation diversity very clear. Since the transmit and receive arrays have the same beamwidths then some of the azimuth diversity beams do not intersect the transmit antenna beam. In contrast higher elevation angle beams always intersect the transmit beam. Any beams not intersecting the transmit antenna beam receive very little power and so are of little benefit.

1.7.1 Azimuth Diversity Performance Bound

One possible method to improve azimuth diversity performance is to broaden the transmit beam in azimuth. This may be accomplished by transmitting with a subsection of the array. The boresight gain of the transmitter decreases, but the receive beams are illuminated more evenly. Because the boresight gain must decrease in order to illuminate more receive beams, the diversity bound of Section 1.4 cannot, in general, be achieved with fixed size transmit and receive apertures. (An azimuth space diversity system may achieve the bound, but only by using additional apertures.)

Another bound may be derived as follows. If we assume that the scatter angle is large, so that additional azimuth beams have the same scatter angle, then the common volume integration reduces to a one-dimensional integration of the transmit and receive antenna patterns. integration in elevation is required. The same effect is seen at all elevation angles since the scatter angle is assumed large.) Thus, for a given set of receive beams, the optimum transmit beamwidth may be determined.

Table 1-1 gives the average SNR required for $\phi_0 = 10^{-4}$ when the optimum transmit antenna beamwidth ($\propto 1/\alpha$) is used. The loss when the transmit antenna beamwidth is not optimized ($\alpha=1$) is also given for comparison purposes. Beam broadening can improve azimuth diversity performance somewhat, but even with the optimum transmitter beamwidth the azimuth diversity bound is far from the elevation diversity bound.

1.7.2 Computed Azimuth Diversity Performance

Figure 1-4 compares elevation and azimuth diversity performance with their respective bounds. The minimum scatter angle is 1.2° and the beamwidths are 1° (except that the transmit beam is broadened optimally in azimuth for each order of diversity).

Table 1-1

Bound on Azimuth Diversity Gains

(α is the ratio of receiver beamwidth to transmitter beamwidth)

Order of Diversity	Azimuth Diversity Required SNR Bound* (dB)	Optimum α	Loss at α = 1 (dB) (Full Illumination)	Elevation Diversity SNR Bound* (dB)
1	40.0	1	0	40.0
2	22.5	.73	.2	20.0
3	17.4	.45	1.5	13.1
4	15.0	.34	2.3	9.5
5	13.7	.26	3.0	7.3
6	12.8	.22	3.2	5.6
7	12.1	.20	3.7	4.4
8	11.7	.16	3.8	3.4
9	11.3	.16	4.1	2.5
10	11.0	.14	4.2	1.8

* To Achieve $\phi_0 = 10^{-4}$
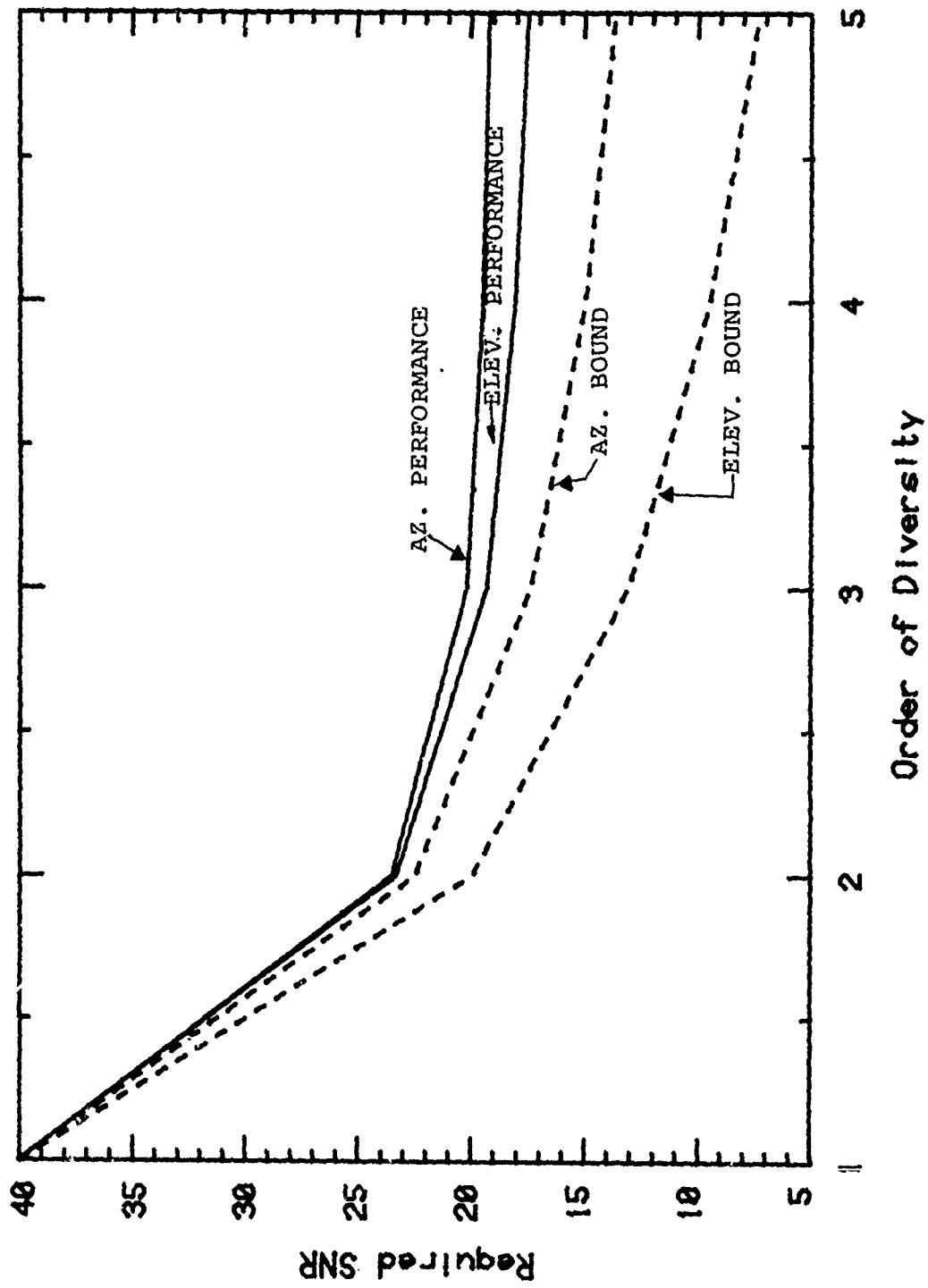
Figure 1-4 Comparison of Azimuth and Elevation Diversity System Performance with their Respective Bounds. Performance Calculated for 1.2° Scatter Angle and 1° Beamwidth.

The conclusion is that in general elevation diversity is more effective than azimuth diversity. In some cases, however, dual azimuth diversity may perform slightly better than dual elevation diversity. For instance, if the minimum scatter angle is 0.7° and the beamwidth is 2°, then a dual azimuth diversity system requires 24.3 dB whereas the elevation system requires 24.5. Because dual azimuth diversity performs reasonably close to dual elevation diversity, a combination of the two is generally the best for high order diversity.

1.8   COMBINED ELEVATION AND AZIMUTH DIVERSITY

If an array is subdivided both vertically and horizontally, a beam transformation yields a rectangular set of beams in elevation and azimuth. That is, the total number of beams is the product of the number in elevation and the number in azimuth.

A number of different orders of diversity are compared in Table 1-2. Different beam selections which result in the same order of diversity are compared. For high order diversity, systems with two azimuth beams and a number of elevation beams perform best. With fourth order diversity, this is especially evident as a 2x2 set of beams is 2.7 dB better than a 4x1 elevation diversity system and 5dB better than a 1x4 azimuth diversity system.

Figure 1-5 presents results for different scatter angles and beamwidths. The 4, 6, and 8 beam systems are formed with 2 azimuth beams and 2, 3, and 4 elevation beams respectively.

The performance of combined elevation and azimuth diversity systems is significantly better than either type alone. So for any angle diversity system of order 4 or higher, a combined azimuth elevation system should be employed.

Table 1-2

Diversity performance by subdividing a given square aperture
(Minimum Scattering Angle 1.2°, Antennas 3m by 3m.
Beamwidth 1°, Square Aperture)

Order of Diversity	No. of Beams in Elevation	No. of Beams in Azimuth	Required SNR	Lower Bound on Required SNR (cf. Table 2-1)
1*	1	1	40.0	40.0
2*	2	1	23.3	20.0
2	1	2	23.5	20.0
3*	3	1	19.3	13.1
3	1	3	20.4	13.1
4	4	1	18.1	9.5
4*	2	2	15.4	9.5
4	1	4	20.0	9.5
6*	3	2	13.6	5.6
6	2	3	14.3	5.6
8*	4	2	13.0	3.4
9*	3	3	12.5	2.5
12*	4	3	12.0	.6

* Optimum Diversity Configuration

Figure 1-5   Required SNR for various orders of diversity achieved by
subdividing optimally a square array. Three cases considered:
1.5m x 1.5m antennas with 0.7° minimum scattering.

1.9 SPACE-ANGLE DIVERSITY EQUIVALENCE

The spaced antennas of a conventional space diversity system may also be considered an array. A beam transformation of the output of two widely separated antennas yields two orthogonal gain patterns with a large number of grating lobes inside the envelope determined by the beamwidth of each antenna. The two voltage patterns vary roughly as sin x and cos x near boresight. If the antennas are brought closer together, then the width of the grating lobes increases. If the antennas have no space between them, then only one grating lobe of each pattern occurs within the main lobe of the individual antenna patterns. This last situation results in beam patterns which are the same as those from a rectangular array divided into square subsections.

Similarly if more antennas are placed between the two space diversity antennas, then the width of the grating lobes stays the same but the number of them decreases. If a continuous linear array is formed, then each gain pattern (in a beam transformation) has a single lobe within the envelope defined by the individual antenna patterns.

1.10 APERTURE SHAPE

Thus far, we have considered subdivision of square antenna arrays only. We now consider rectangular arrays with different vertical and horizontal dimensions. Each antenna is defined by an asymmetry parameter

$$\zeta = \log \frac{a_v}{a_h}$$

where a_v is the vertical dimension and a_h the horizontal. The results are given in Figure 1-6 for fixed area apertures. The
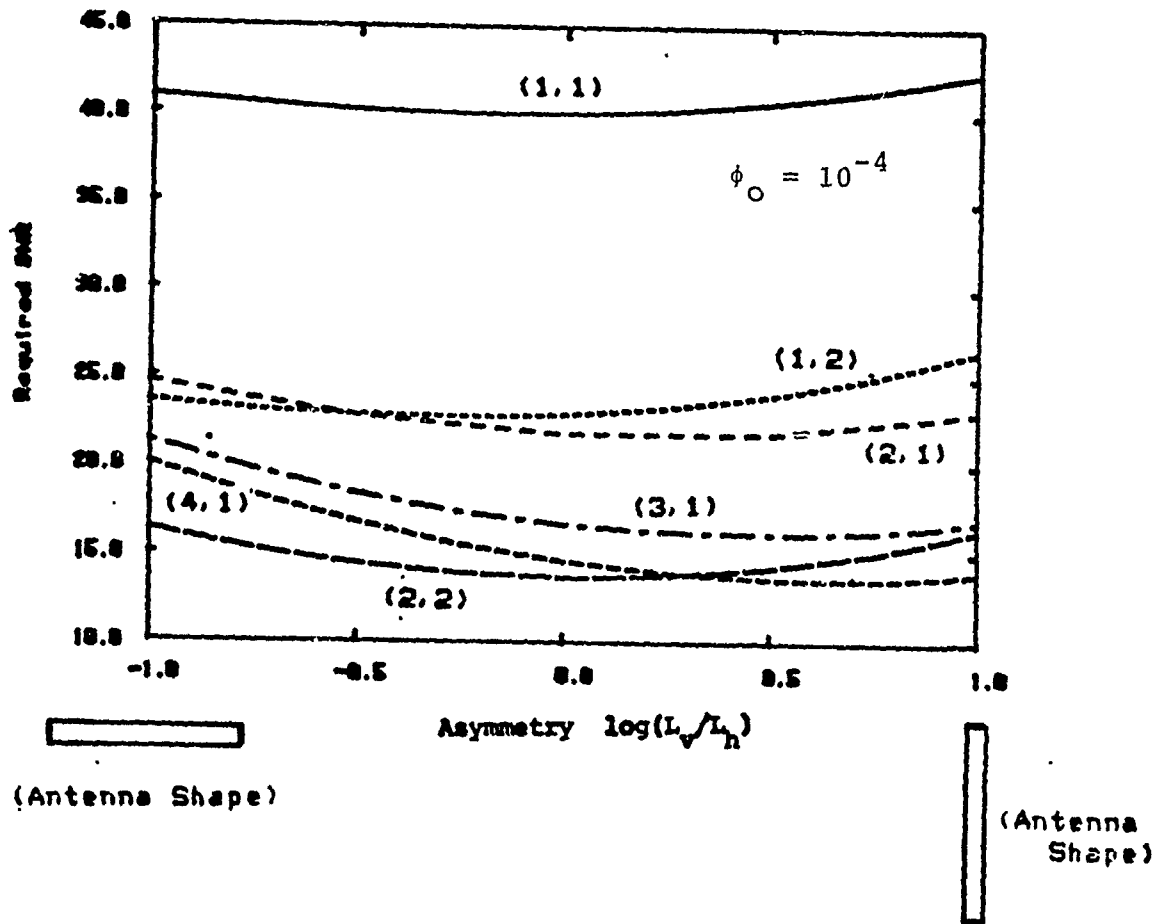
Figure 1-6 Effect of Asymmetry on Various Diversity Systems
with Fixed Area Rectangular Apertures. Diversity
Specified by (# of Elevation Beams, # of Azimuth
Beams).

1-19

diversity systems are specified in terms of two integers (n_e, n_a) corresponding to the number of elevation and azimuth diversity beams, or equivalently, the number of horizontal and vertical divisions of the array. Since practical links are duplex, the transmit and receive apertures are assumed to have the same shape.

For systems with many elevation beams, tall antennas are better, and for azimuth beams wide arrays are better. The basic conclusion is that the subarrays are approximately square. The aperture shape for a given order diversity system should be formed by arranging a number of square subapertures.

1.11 IMPLICIT DIVERSITY FOR WIDEBAND SYSTEMS

The systems considered thus far have been narrow band systems; that is, systems whose signaling interval is long compared to the channel delay spread. For such systems, the troposcatter channel gives Rayleigh fading statistics. For wideband systems, the channel delay spread distorts the transmitted waveform, and equalization may be required. This delay spread may also be used advantageously, since the signals which arrive at different delays fade independently. If it is possible to add these delayed signals coherently, then improved performance is possible. This is called _implicit_ frequency diversity because different frequency components of the transmitted signal fade independently.

The number of independent delayed versions of the signal which are weighted and summed is the order of the implicit diversity system. One implementation of implicit diversity is a tapped-delay line equalizer. The signal is passed through a delay-line and is tapped off at various points to be summed.

The signaling interval and channel delay spread play roughly the same role in implicit diversity as beamwidth and

scatter angle play in angle diversity. If the signaling interval is short compared to the channel delay spread, then large diversity gains are possible.

One major difference between implicit and angle diversity is that if the channel delay spread is long relative to the signaling interval then adjacent symbols are smeared into each other. This is known as intersymbol interference or ISI. Theoretically the effects of ISI may be removed by maximum likelihood decoding, but this process becomes impractical as the delay spread increases.

Despite this consideration, the initial gains from implicit diversity are significant. They taper off more rapidly than the gains from angle diversity, but for most wideband systems 2 or 3 tap equalization (i.e., 2nd or 3rd order diversity) has an important effect.

Figure 1-7 summarizes the major results on implicit diversity. It plots the improvement in SNR (i.e., reduction in required SNR) vs. σ/T, the ratio of channel delay spread to the signaling interval, for various numbers of taps. Note that as σ/T increases, the SNR gains increase initially but then fall or level out. The reason for this behavior is that as the channel delay spread increases the energy in the transmitted pulse is spread out further, and more taps are required to collect this energy. For a fixed number of taps, the delayed signals become less correlated as σ increases (for fixed T), but beyond some level the power on each tap decreases. This contrasts with angle diversity gains, where increasing the scatter-angle-to-beamwidth ratio improves diversity gains for any order of diversity.
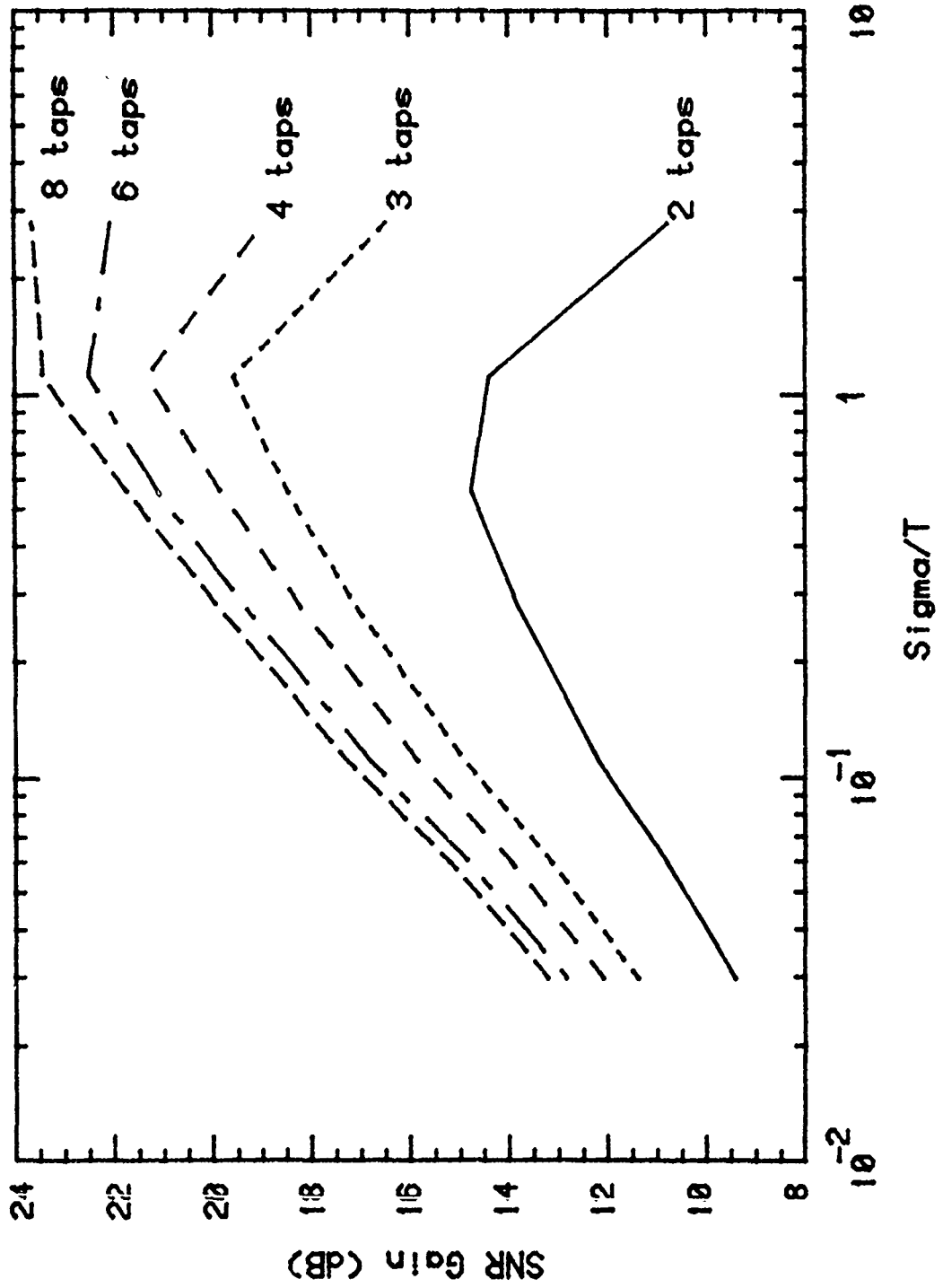
Figure 1-7. Implicit Diversity Gain vs. Channel Delay Spread To Pulse Duration Ratio

1.12 SUB-OPTIMAL COMBINING

The optimal combiner of the signals from N diversity ports is a maximal-ratio combiner which scales each signal by a complex constant and sums them. Maximal-ratio combining may be expensive so sub-optimal techniques are of interest. One possible method is phase-only combining, where the signals are multiplied by a complex constant with magnitude 1. Another possible method is to choose a subset of K of the N signals and combine these optimally. (This subset of K changes as the signals fade.) If the subset consists of a single signal (K=1) then the system is selection diversity, and K=N corresponds to maximal-ratio combining.

For DPSK we have derived a new expression for the average BER of an optimal K of N combiner:

$$BER = \frac{1}{2} \left[1+\rho\right]^{-K} \left(1+\frac{\rho K}{1+K}\right)^{-1} \left(1+\frac{\rho K}{2+K}\right)^{-1} \ldots \left(1+\frac{\rho K}{N}\right)^{-1}, \text{ where}$$

ρ = SNR per diversity branch

Analysis of these methods is done in Section 6. The major results are summarized in Table 1-3. Phase-only combining is at most 1.2 dB worse than maximal ratio combining. In contrast, selection diversity is significantly worse than the optimum method, e.g., it is 3.4 dB worse than the optimum for fourth order diversity (at BER=10^{-4}). Intermediate values of K yield fairly good performance. For instance, if the best 4 of 8 signals are combined then the performance is only 1dB from optimum.

Table 1-3

Comparison of Required SNR for BER = .0001
(DPSK Modulation) for Various Combining Techniques

Order of Diversity (N)	Required SNR for Maximal-Ratio Combiner (dB)	Loss Relative to Maximal-Ratio Combiner (dB)			
		Switch Diversity	Best 2 Of N	Best 4 Of N	Equal Gain Combiner (Approximate)
1	37.0	0	--	--	0
2	18.4	1.5	0	--	0.6
3	12.1	2.5	0.6	--	0.9
4	8.7	3.4	1.0	0	1.0
5	6.5	4.1	1.7	0.2	1.0
6	5.0	4.5	2.1	0.4	1.1
8	2.8	5.4	2.9	1.0	1.2
10	1.3	6.1	3.5	1.4	1.2
12	0.1	6.7	4.1	1.9	1.2

Thus, if a cost is associated with N, the number of ports, and a comparable cost for K, the number of signals combined, then K should be greater than one but less than N. If the cost of downconversion and combining signals is small relative to the cost of ports then maximal-ratio combining should be used. Conversely, if the cost of additional ports is small, then selection diversity is optimum.

1.13 MEASUREMENT INACCURACIES

The channel is assumed frozen, i.e., we assume that the channel may be measured exactly and thus use the optimum combiner weights. However, the addition of measurement errors result in only very slight changes in required SNR for the order diversity systems considered here. For instance, measurement errors for a 6th order system under fairly pessimistic assumptions (one measurement receiver, rapid fading) costs only .5 dB. These effects are discussed in more detail in Section 5.

1.14 PROPOSED MEASUREMENT

Section 8 describes a measurement system which could not only verify the analytical results in this report but also be used to measure the atmospheric structure. It would measure layer reflection at X-band, including height and reflection coefficient of the layer, and turbulent scattering as a function of height. In fact, all parameters necessary to evaluate troposcatter performance with diversity, wideband equalization and advanced modem designs would be determined. The measurement system would be transportable so that geographical and seasonal variations could be measured.

SECTION 2
TROPOSCATTER MODEL

2.1 TROPOSCATTER SIGNAL CHARACTERISTICS

The troposcatter medium may be thought of as consisting of a large number of randomly distributed 'scatterers'. Physically the 'scatterers' are random spatial and temporal fluctuations in the refractive index, or equivalently, the temperature, humidity, and pressure of the atmosphere. Energy incident on a region of the atmosphere containing a number of these scatterers or 'blobs' will be scattered in all directions. In particular if the transmitted signal from a point on the surface of the earth is purely sinusoidal, i.e., a single tone $\exp(j2\pi ft)$, then the scattered signal received at some other location on the surface of the earth consists of the sum of the energy scattered by each blob in the scattering volume. Mathematically it can be expressed as

$$ r = \sum_i A_i e^{j\phi_i} e^{j2\pi ft} $$

where the A_i and ϕ_i are the amplitudes and relative phases of the signals scattered by each blob.

Since the location and 'size' of the blobs varies randomly with time, the amplitudes and phases also vary randomly so that the signal received by a single antenna port can be expressed as

$$ r(t) = A(t)e^{j[2\pi ft + \phi(t)]} $$

where

$$A(t)e^{j\phi(t)} = \sum_i A_i e^{j\phi_i}$$

is the time varying modulation imposed by the scattering medium. The received signal $r(t)$ is a fading signal.

If the scattered signal is received by more than one antenna then the received waveforms $[r_n(t) , n = 1, 2, ..., N]$ are all of the above form,

$$r_n(t) = A_n(t)e^{j\phi_n(t)} .$$

It is convenient to express all of the received waveforms in vector form, i.e.,

$$\underline{r}(t) = \begin{bmatrix} r_1(t) \\ \vdots \\ r_N(t) \end{bmatrix}$$

Each of the components of this vector represents a fading signal. All of the signals have similar statistics, and since they all are a result of scattering from the same medium they will be correlated in general. In adaptive troposcatter several received waveforms are combined adaptively to improve performance.

2.1.1 Fading Statistics

If the scattering volume containing the blobs is large in relation to the wavelength, $\lambda = c/f$ where c is the speed of light and f is the frequency of the incident signal, then the Central Limit Theorem can be applied to characterize the statis-

tics of the received signal. In this case it is simple to show [1] that the amplitude of the received signal A(t) is Rayleigh distributed and its relative phase $\phi(t)$ is uniformly distributed, i.e.,

$$p(A) = \frac{2A}{P_r} e^{-A^2/P_r} \quad , \quad A > 0$$

$$p(\phi) = \frac{1}{2\pi} \quad , \quad 0 < \phi < 2\pi$$

where $P_r = E(A^2)$ is the average received power. In practice the average received power exhibits long term (seasonal) variations which can also be described statistically.

An equivalent statistical description is that the received signal r(t) has a complex Gaussian distribution with zero mean and variance P ,

$$E|r(t)|^2 = P \quad .$$

This is easily generalized to the case of multiple received waveforms represented by a vector $\underline{r}(t)$, where $\underline{r}$ is a complex Gaussian vector with zero mean and covariance matrix $\underline{P}$:

$$E\{\underline{r}\ \underline{r}'\} = \underline{P} \quad .$$

The prime denotes the complex conjugate transposed vector. The covariance matrix $\underline{P}$ is Hermitian. The eigenvalues of this matrix play an important role in the performance evaluation of adaptive troposcatter techniques.

2.1.2 Frequency Selective Fading

The description of the received signal given above applies as long as the transmitted signal is a pure tone, $\exp(j2\pi ft)$, or a narrowband signal, i.e., a signal whose frequency spectrum contains a narrow band of frequencies centered around the frequency f.

When we turn to questions concerning the transmission of wideband signals, however, the mathematical description of the received troposcatter signal must explicitly take into account the fact that differences in path lengths of the signals scattered from different blobs give rise to different propagation time delays, causing a spread in the time of arrival of the received energy. This can be done by expressing the transmitted and received signals, $s(t)$ and $r(t)$, in terms of their frequency spectra, $S(f)$ and $R(f)$, as

$$s(t) = \int_{-\infty}^{\infty} S(f) e^{j2\pi ft} df$$

$$r(t) = \int_{-\infty}^{\infty} R(f) e^{j2\pi ft} df \ .$$

The received signal at each frequency component of $r(t)$ can be written as

$$R(f) = S(f) \sum_{m=1}^{M} \sum_{n=1}^{N_m} A_{mn} e^{j(\phi_n - 2\pi f \tau_m)}$$

where N_m is the number of scattered signals arriving in the time interval $(\tau_m, \tau_m + \delta\tau)$ and ϕ_n is the relative phase of each of these signals. The random amplitude coefficients A_{mn}

represent the power associated with each individual scattered signal arriving at different delays and at different angles. They are usually assumed to be independent (uncorrelated scatter) and thus satisfy:

$$E\left(A_{mn}A_{pq}\right) = \delta_{mp}\delta_{nq} E\left(A_{mn}^2\right) \; .$$

If the total average received power is P_r , then

$$P_r = E \int_{-\infty}^{\infty} \left|R(f)\right|^2 df = \sum_{m=1}^{M} Q_m \int_{-\infty}^{\infty} \left|S(f)\right|^2 df$$

where

$$Q_m = \sum_{n=1}^{N_m} E\left(A_{nm}^2\right) \; .$$

Thus Q_m represents the total relative average power arriving in the delay interval $(\tau_m, \tau_m+\delta\tau)$ where $\delta\tau = \tau_{m+1} - \tau_m = \tau_m - \tau_{m-1}$ and thus is referred to as the delay power impulse response in the limit as $\delta\tau \rightarrow 0$.

The fact that most of the total received signal power arrives over a finite delay interval $0 < \tau < \tau_M$ causes the statistical properties of two frequency components of the received signal to be independent if the frequency separation is large enough. The maximum frequency separation for which the two frequencies are strongly correlated is called the coherence bandwidth. If the bandwidth of the transmitted signal is greater than the coherence bandwidth then the fading is said to be frequency selective. On the other hand if the transmitted bandwidth

2-5

is smaller than the coherence bandwidth, the fading is said to be flat, i.e., frequency independent, and we can ignore delay spread effects. In order to understand this last point it is necessary to establish the relationship between coherence bandwidth and delay spread.

The coherence bandwidth can be determined from the correlation properties of the received signal at two frequencies f_1 and f_2, i.e.,

$$E\{R(f_1)R^*(f_2)\} = S(f_1) S^*(f_2) B(f_1-f_2)$$

where

$$B(f_1-f_2) = \sum_{m=1}^{M} \sum_{n=1}^{N_m} E(A_{mn}^2)e^{-j2\pi(f_1-f_2)\tau_m}$$

$$= \sum_{m=1}^{M} Q_m e^{-j2\pi(f_1-f_2)\tau_m} \quad .$$

The function $B(\Omega)$ is called the two-frequency correlation of the channel and its 'width' is the coherence bandwidth B_C. The product $S(f_1) S^*(f_2)$ can be assumed to be unity when the difference f_1-f_2 is smaller than the bandwidth W of the transmitted signal. Thus if the width of $B(\Omega)$ is greater than the bandwidth, then $E\{R(f_1) R^*(f_2)\}$ is really equal to unity for all $f_1-f_2 \leqslant W$ and the fading at the two frequencies is highly correlated (flat fading). On the other hand, if the width B_C of $B(\Omega)$ is smaller than the bandwidth, W, then frequency components such that $B_C < f_1-f_2 < W$ will fade independently since $E\{R(f_1) R^*(f_2)\} \approx 0$.

From the definition of $B(\Omega)$ it can be seen that in the limit as we let the delay interval $\delta\tau \to 0$, that

$$B(\Omega) = \int_{0}^{\infty} Q(\tau)e^{-j2\pi\Omega\tau}d\tau$$

where $\Omega = f_1 - f_2$, and $Q(\tau)d\tau = Q_m$ is the delay power impulse response. Thus $B(\Omega)$ and $Q(\tau)$ are related by a Fourier transformation. Hence the width of $B(\Omega)$ is approximately equal to the inverse of the width of $Q(\tau)$, i.e., the delay spread.

The simplest definition of the width of $Q(\tau)$ is

$$\delta_Q = \int Q(\tau)d\tau / \max_{\tau} Q(\tau)$$

$$= \max_{\Omega} B(\Omega) / \max_{\tau} Q(\tau)$$

Similarly, the width of $B(\Omega)$ may be defined by

$$\delta_B = \max_{\tau} Q(\tau) / \max_{\Omega} B(\Omega) .$$

Clearly, we then have exactly

$$\delta_Q = 1/\delta_B.$$

Let us call δ_Q the rectangle width of $Q(\tau)$. Other commonly used definitions are

1. 2σ delay spread: $\int \tau^2 Q(\tau)d\tau / \int Q(\tau)d\tau - \left[\int \tau Q(\tau)d\tau / \int Q(\tau)d\tau\right]^2$

2.   99% delay spread: $\tau_2 - \tau_1$, where $\int_{\tau_1}^{\tau_2} Q(\tau)d\tau = 0.99 \int_0^\infty Q(\tau)d\tau$.

Table 2-1 compares the definitions for several analytical shapes of $Q(\tau)$.

The multipath effects generalize to the case of multiple antenna ports.   If we assume a single transmitted waveform $s(t)$ we have

$$\underline{r}(t) \;=\; \int_0^\infty \underline{h}(\tau,t)\, s(t-\tau)d\tau \;\; .$$

where $h_k(\tau,t) = \sum_n A_{kn} e^{i\phi_n} \delta(t-\tau)$ is the impulse response for the channel between the transmitter port and k'th receiving antenna port and $\underline{h}(\tau,t)$ is the vector of impulse responses. For a time invariant channel the impulse response is independent of t . The delay power impulse response for a time invariant set of channels is a matrix with elements $Q_{k\ell}(\tau)$, where

$$Q_{k\ell}(\tau)\; \delta(\tau-\nu) \;=\; E\left[h_k(\tau)\, h_\ell^*(\nu)\right] \;\; .$$

Since the impulse responses for different receiving ports are correlated it is necessary to specify all the N^2 function $Q_{k\ell}(\tau)$, $k,\ell = 1, 2, \ldots, N$. The definitions of multipath spread and coherence bandwidth for a single channel do not generalize to the multichannel case. However, for any linear combination of the receiving ports, e.g.,

TABLE 2-1

COMPARISON OF DELAY SPREAD DEFINITIONS

$Q(\tau)$	RECTANGLE WIDTH	2σ WIDTH	99% WIDTH
1 for $0 < \tau < T$ 0 otherwise	T	$T/\sqrt{3}$	$0.99\ T$
$\tau^n e^{-\alpha\tau/T}$, $\alpha = n!e^n/n^n$	T	$2T\ \dfrac{\sqrt{n+1}}{\alpha}$, or $n=0$: 2 T $n=1$: 1.04 T $n=2$: 0.94 T $n\to\infty$: 0.80 T	 $n=0$: 4.6 T $n=1$: 2.4 T $n\to\infty$: 2.1 T
$\dfrac{1}{1+\left(\frac{\pi\tau}{2T}\right)^2}$	T	∞	$40.5\ T$

$$r(t) = \sum_{n=1}^{N} w_n r_n(t)$$

the multipath spread and coherence bandwidth can be defined as before.

2.1.3 Doppler Smear

The fading of the received signal is caused by the wind moving the scatterers, thus changing the relative phase of the different scattered signal components. The time varying channel is characterized by the correlation function

$$E\{h(\tau,t_1) h^*(\nu,t_2)\} = Q(\tau,t_1-t_2) \delta(\tau-\nu) \quad .$$

where $Q(\tau,0)$ is the delay impulse response defined earlier. This definition assumes both uncorrelated scattering and wide sense stationary channel fading. For multiple channels Q is a matrix as before. It is generally reasonable to assume that the troposcatter channel is Wide Sense Stationary and Uncorrelated Scatterer (WSSUS). Stationarity is a particularly good assumption while the uncorrelated scatterer assumption can break down for systems with extremely wide bandwidth. This question will be discussed later.

For a single channel, or a linear combination of several channels, we can define the coherence time, T_c, and Doppler spread, B_d. The coherence time is the width of the temporal correlation function defined as

$$b(t_1 - t_2) = \int Q(\tau, t_1 - t_2) d\tau \quad .$$

The Doppler spread B_d is the width of the Fourier transform of $b(t_1 - t_2)$, so

$$B_d \sim \frac{1}{T_c} \quad .$$

Another common characterization of the troposcatter channel is the scattering function:

$$S(\tau, f) = \int dt \, Q(\tau, t) e^{-j2\pi ft} \quad .$$

The width of the scattering function in the τ direction is the multipath spread, while the f-dependence displays the Doppler spread. The convenience of using the scattering function is a result of the two basic assumptions: uncorrelated scattering, and stationary fading.

2.2   PHYSICAL MODEL OF TROPOSCATTER EFFECTS

The previous section dealt with a mathematical description of the received troposcatter signal. In this section we discuss the relationship between the various parameters which characterize the received signal and the physics of the troposcatter medium. This is important because any investigation of adaptive troposcatter techniques must incorporate the effects of the tro-

poscatter medium in a realistic manner. In particular we must establish a relationship between the average received signal power of the output of each receiving antenna element and their correlations as well as the matrix delay power impulse response $Q(\tau)$ (or its width - the delay spread) and the parameters which describe the physics of the troposcatter medium. The average received signal power is needed to determine the average signal-to-noise ratio of the system whose performance is to be evaluated while the delay power impulse response is needed if we are dealing with wideband systems. In addition, when the receiving system consists of an array of receiving apertures we also need to determine the correlation between the signals received at each aperture.

2.2.1 Average Received Signal Level

The average received signal level in a troposcatter link depends on the path geometry as well as the distribution and 'strength' of turbulence of scatterers in the atmosphere. A measure of the distribution and strength of the turbulent scatter is given by the wavenumber spectrum $\Phi(\kappa)$ where the wavenumber κ is related to the size of the scatterer, ℓ, by $\kappa = 2\pi/\ell$. The functional dependence of Φ on κ can be found either by measurement or from theoretical considerations. The dependence of the average received power on the wavenumber spectrum depends on the scattering mechanism. Tatarskii [2] has shown that troposcatter is of the Bragg scatter type so that the average received power is given by

$$P_R = P_T G_T G_R \frac{\pi k^2}{2} \int_V d^3\underline{r} \; \frac{|g_T(\underline{r})|^2 \; |g_R(\underline{r})|^2}{R_T^2(\underline{r}) \; R_R^2(\underline{r})} \; \Phi\left(2k \; \sin\left(\frac{\Theta(\underline{r})}{2}\right)\right) \quad (2.1)$$

where

P_R, P_T are the received and transmitted power levels.

G_T, G_R are the transmitter and receiver antenna gains.

g_T, g_R are the voltage gains relative to boresight of the transmitter and receiver antennas, in the direction of the point $\underline{r}$ of scattering volume.

R_T, R_R are the distances from the point $\underline{r}$ in the common volume V to the transmitter and receiver antennas.

$k = 2\pi/\lambda = 2\pi f/c$ is the wavenumber.

θ is the scattering angle, i.e., the angle between the lines from the transmitter and receiver terminals to the point $\underline{r}$ in the common volume.

$\phi(\ )$ is the wavenumber spectrum of the turbulence, or the three dimensional Fourier transform of the spatial correlation function.

The common scattering volume V is determined by the antenna patterns g_T, g_R.

The above expression is valid in most cases of interest. The assumptions made in arriving at it are

1. the scattering volume must be large compared to the correlation distance of the turbulence L_0. This limits the antenna gain that is practical. The condition is

$$R_R \delta_R, \ R_T \delta_T \gg L_0$$

where

δ_T, δ_R = beamwidths of transmitter and receiver, respectively

and

L_0 = outer scale of turbulence.

2. The Fresnel zone condition

$$2L_0^3/\lambda < R_T^2, \ R_R^2 \ .$$

Both of these conditions put an upper limit on usable frequencies for troposcatter. The condition in 2. (derived by Parl and Malaga [3]) represents an improvement on the condition derived by Tatarskii.

Assuming a worst case situation where $R_T = R_R = 25$ km and $L_0 = 100$ meters (pessimistic), then condition 2. states that

$\lambda > .0032$ meters

or

$f < 93$ GHz.

Equation (2.1) is generally accepted as the basis of all models of scatter from turbulence. However, many different models for the turbulence spectrum have been proposed. Booker and Gordon [4] based their model on an exponential correlation function, leading to the scattering cross section dependency on θ as θ^{-4}. Other models proposed in the 1950's showed a scattering angle dependence of θ^{-5} [5,6] or $\theta^{-13/3}$ [7]. Based on approximate agreement with troposcatter experiments in the 40-1000 MHz range the θ^{-5} was selected as the basis for the NBS method [8]. However, the model originally developed by Obukhov [9] and Kolmogorov [10] is the model which is now generally accepted by atmospheric physicists. It predicts a scattering angle dependence of $\theta^{-11/3}$. The main reason that this theory was not adopted for tropospheric scatter is that many measurements at frequencies below 1GHz revealed layer or feuillet reflections in addition to the scatter from turbulence, and the θ^{-5} dependence was selected by NBS as the best overall fit to the data base.

The Kolmogorov-Obukhov theory considers the turbulence as the result of breaking up of eddies into progressively smaller and smaller eddies. The size of the largest eddies contributing to the turbulence is the outer scale L_0 of the turbulence. L_0 is also a good measure of the correlation distance. The smallest eddy size, ℓ_0 is called the inner scale. Turbulence of a scale smaller than ℓ_0 is dissipated rapidly. The range of turbulence

$$2\pi/L_0 < k < 2\pi/\ell_0$$

is called the inertial subrange. In this range the Kolmogorov-Obukhov theory predicts a wavenumber spectrum of the form

$$\Phi(\kappa) = 0.033C_n^2 \kappa^{-11/3} \tag{2.2}$$

where C_n^2 is a measure of the strength of the turbulence.

Based on this, and the approximate behavior in the equilibrium range $(k < 2\pi/L_0)$ and in the dissipative range $(k > 2\pi/\ell_0)$ the following expression is often used to represent the entire spectrum:

$$\Phi(\kappa) = \Phi(\underline{r}, \kappa) = 0.033C_n^2(\underline{r})\left[\kappa^2 + (2\pi/L_0)^2\right]^{-11/6} \exp\left[-\left(\frac{\kappa\ell_0}{2\pi}\right)^2\right] \tag{2.3}$$

where C_n^2, L_0 and ℓ_0 are functions of climate, time, and height above ground. The problem of predicting the performance of a troposcatter link is therefore reduced to predicting these parameters. Typical values of L_0 are in the range of 1-100 meters while ℓ_0 is typically 1 mm. Most troposcatter links can be assumed to interact with turbulence in the inertial subrange.

Take, for instance, a typical scatter angle of 2° and inner and outer scales of 0.001 and 10 meters, respectively. Then the condition for being in the inertial subrange is

$$\frac{1}{L_0} < \frac{\theta}{\lambda} < \frac{1}{\ell_0}$$

or

$$0.9 \text{ GHz} < f < 900 \text{ GHz} .$$

Hence it is realistic to use the simpler form (2.2) at the higher microwave frequencies.

The model used in SIGNATRON's troposcatter computer program [11, 12] assumes a general spectrum of the Von Karman type,

$$\Phi(\kappa) = \frac{\Gamma(m/2)}{\pi^{3/2} \Gamma(\frac{m-3}{2})} \frac{\sigma_n^2 r_0^3}{(1+\kappa^2 r_0^2)^{m/2}}$$

where σ_n^2 is the measure of the refractive index variance, $r_0 = L_0/2\pi$ and m is called the spectrum slope. It reduces to (2.3) when $m = 11/3$. The generality of the form above is convenient since it allows the inclusion of the NBS model by simply setting $m=5$.

The structure constant C_n^2 will be used extensively instead of the variance σ_n^2. The two parameters are related by

$$C_n^2 = 2\sigma_n^2 \Gamma(\frac{5-m}{2}) / [\Gamma(\frac{m-1}{2}) (2r_0)^{m-3}]$$

or, for $m = 11/3$,

$$c_n^2 = 1.911 \ \sigma_n^2 \ r_0^{-2/3} \ .$$

2.2.2 Spatial Correlation

In order to evaluate the performance of troposcatter systems employing an array of receiving apertures one must be able to calculate the correlation between the signals received by each aperture. If the spacing between each aperture is small compared to the distance from the receiving array to the scattering volume, then all apertures in the receiving array have the same common volume. Decorrelation between the signals received by each aperture results then strictly from the difference in path length from each scatterer to each of the receiving apertures. The correlation between the signals received by any two apertures is then obtained as follows.

Let r_1 and r_2 be the signals received by apertures 1 and 2. If the apertures have equal dimensions, then the average power received by each aperture is the same and given by

$$P_r = E(|r_1|^2) = E(|r_2|^2)$$

where P_r was defined in equation (2.1).

Since the received signal is Rayleigh fading, it has zero mean, and therefore the correlation coefficient between the signals received by the two apertures is given by

$$\rho_{12} = \frac{E(r_1 r_2^*)}{P_r} \tag{2.4}$$

where

$$E(r_1 r_2^*) = C \iiint_V \frac{|g_T|^2 \; |g_R|^2}{R_T^2(\underline{r}) \; R_R^2(\underline{r})} \; \Phi(\kappa\Theta(\underline{r})) \; \exp[-j\kappa\delta(\underline{r})]d^3r \qquad (2.5)$$

where $\delta(\underline{r})$ is the difference in path length from a point $\underline{r}$ in the scattering volume to the two receiving apertures, and $C = P_T G_T G_R \pi \kappa^2 / 2$.

2.2.3 Angle Diversity Correlation

In an angle diversity system the apertures are in the same location so $\delta(\underline{r})$ is zero. However, the gain patterns, $g_{R1}(\Theta,\phi)$ and $g_{R2}(\Theta,\phi)$, are different. So the correlation is given by (2.5) with $\delta(r)=0$ and $|g_R|^2$ replaced by $g_{R1}(\Theta,\phi) \; g^*_{R2}(\Theta,\phi)$ where * denotes complex conjugate.

2.2.4 Delay Power Impulse Response

The delay power impulse response $Q(t)$ which characterizes the received power per unit delay can be calculated by subdividing the common volume into small cells. The power received in the delay interval $(\tau, \tau + \delta\tau)$ can then be calculated by adding the contributions from all these cells for which the relationship

$$\tau = \frac{R_T + R_R}{c} \qquad (2.6)$$

is satisfied, where c is the speed of light and R_T and R_R are the distances from the cell to the transmitting and receiving apertures, respectively. The 2σ delay spread of the channel which is inversely proportional to the coherence bandwidth (maximum frequency separation for which the fading is correlated) is then found from the second central moment of the power impulse response, i.e.,

$$\tau_{2\sigma}^2 = \frac{4 \int_{-\infty}^{\infty} (\tau - \tau_{AV})^2 Q(\tau) d\tau}{P_r}$$

where

$$\tau_{AV} = \frac{\int_{-\infty}^{\infty} \tau Q(\tau) d\tau}{P_r} \quad .$$

2.2.5 Condition for Uncorrelated Scatterers

The validity of the uncorrelated scatter model presumes that resolvable delay cells are small compared to the correlation distance of the turbulence. Consider a link with slant range d_0 and the angles α, β as defined in Figure 2-1. The scattering angle is θ_0. For this link it can be shown [Monsen et al, 1981] that the relative delay is

$$\tau = \frac{1}{c} \left(r_1 + r_2 - d_0 \right) = 2 \frac{d_0}{c} \frac{\sin \frac{\alpha}{2} \sin \frac{\beta}{2}}{\cos \frac{\alpha+\beta}{2}} \quad .$$

Differentiating this expression yields

$$\frac{\Delta\tau}{\Delta\alpha} = \frac{d_0 \sin \beta}{2c \cos^2(\frac{\alpha+\beta}{2})} \quad .$$

The change in height, $\Delta\ell$, with a change in the angle α by $\Delta\alpha$ is given by

$$\frac{\Delta\ell}{\Delta\alpha} = d_0 \left[\frac{\sin \frac{\beta}{2}}{\sin(\alpha+\beta)} \right]^2 \quad .$$
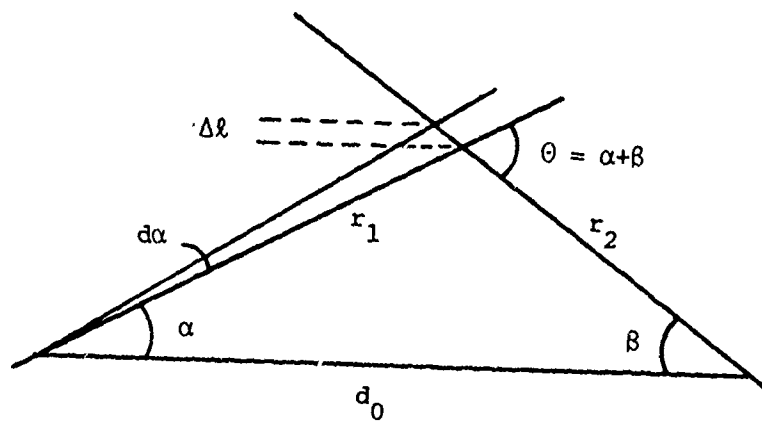
Figure 2-1   Geometry for Determination of the Uncorrelated
            Scatter Condition

Hence if $\Delta\ell = L_0$, the vertical correlation distance of the turbulence, we get

$$\Delta\tau = \frac{L_0}{2c} \frac{\sin^2(\alpha+\beta)}{\sin\beta \cos(\frac{\alpha+\beta}{2})} \sim \frac{L_0}{2c} \frac{\theta^2}{\beta} \; .$$

The condition for uncorrelated scatter is

$$\Delta\tau \ll 1/W$$

where W is the bandwidth. Since $\theta/2\beta$ is on the order of one we get the condition

$$WL_0\theta/c \ll 1 \; .$$

This condition is almost always satisfied. As an example take $L_0 = 70$ m and $\theta = 12$ mrad (corresponding to a 100 km link). Then the condition is

$$W \ll 350 \text{ MHz} \; .$$

2.2.6 Doppler Spread

The Doppler spread, i.e., the inverse of the coherence time, is another important parameter, particularly for a realistic evaluation of adaptive troposcatter techniques. In order for the adaptive loops to opera : the channel coherence time must be longer than the time consta of the loops. In other words, the channel must be essentially time invariant long enough to allow a reliable measurement of the channel.

The Doppler spread is found from the refractive index spectrum using Taylor's hypothesis of frozen turbulence. The received spectrum is then

$$S_R(f) = \int_V d^3\underline{r}\ H(\underline{r})\ S_T\big(f - (\underline{e}_T - \underline{e}_R) \cdot \underline{u}/\lambda\big)$$

where

$\underline{e}_T, \underline{e}_R$ =   direction vectors of the incident and scattered fields

$S_T(f)$ =   spectrum of the transmitted waveform, normalized to unit power,

$\underline{u}$ =   wind velocity vector,

$H(\underline{r})$ =   integrand in (2.1)

$$= P_T G_T G_R \cdot 0.0518\ k^{-5/3}\ C_n^2\ \frac{g_T^2 g_R^2}{R_R^2 R_T^2}\ \theta^{-11/3} \quad .$$

The ℓ'th moment μ_ℓ of the Doppler spectrum is then found from

$$\mu_\ell = \int_V d^3\underline{r}\ H(\underline{r})\ \big((\underline{e}_T - \underline{e}_R) \cdot \underline{u}/\lambda\big)^\ell \quad .$$

The Doppler spread is defined from

$$\sigma_{Doppler}^2 = (\mu_0 \mu_2 - \mu_1^2)/\mu_0^2 \quad .$$

2.3 THE CONCEPT OF APERTURE-TO-MEDIUM COUPLING LOSS

2.3.1 Introduction

It was recognized early that troposcatter links do not realize the full antenna gain for very large apertures. The difference between the total terminal antenna gains and the actually realized gains is called the aperture-to-medium coupling loss. The physical basis for the loss can be explained either in terms of antenna beamwidth or in terms of spatial decorrelation. Since the concept of the aperture-to-medium coupling loss is often misunderstood it may be helpful to view this concept from both the spatial and angular viewpoint. It must first be pointed out, however, that the coupling loss discussed here pertains to a specific model of the scattering mechanism. Part of the confusion about coupling loss is caused by the comparison of coupling loss for different scattering models. Different models may yield different values for the coupling loss but still be correct. The concept of coupling loss is only to be considered as a tool in the evaluation of the total path loss and as long as the path loss is correct, differences in coupling loss predictions are immaterial. The theoretically calculated coupling loss is again different from the coupling loss that is measured by adding a small aperture (wide beamwidth) to an existing high gain aperture system. In this case the coupling loss depends not only on the atmospheric structure inside the common volume of the high gain antennas, but also on the atmosphere outside that common volume. It can therefore experience large long-term variations which are completely independent of what happens in the common volume, i.e., what affects the total path loss. The fact that the measured coupling loss can vary, even if the measured path loss does not, indicates that the concept of aperture-to-medium coupling loss should be used with caution. We now discuss the coupling loss concept from two points of view in order to clarify these ideas.

2.3.2 The Definition of Coupling Loss in Beam Space

A heuristic explanation is simplified by assuming

(1) Ideal beam shape (zero gain outside the beam, constant inside)

(2) A volume of scatterers of finite extent.

Figure 2-2 illustrates the situation where the antenna beams are so large that the common volume illuminated by the antennas encompasses all the scatterers. With the idealized assumptions above it is convenient to define

Common Volume:
: The volume in space which is illuminated by both the transmitter beam and the receiver beam.

Scattering Volume:
: The part of the common volume which contains scatterers.

Volume of Scatterers:
: The total volume containing scatterers.

When the common volume is larger than the volume of scatterers then all scatterers contribute to the received field and there is no coupling loss. This is illustrated in Figure 2-2. When the beams are narrower (Figure 2-3) only a fraction of the scatterers are illuminated by both apertures and the received field does not include contributions from all scatterers. This lack of scattering contribution reduces the total realized antenna gain. This is the coupling loss. We now see how the coupling loss arises naturally from the integration formulas developed earlier.

Common
Volume

Volume of
Scatterers

Transmitter
Beam

Receiver beam

Transmitter

Receiver
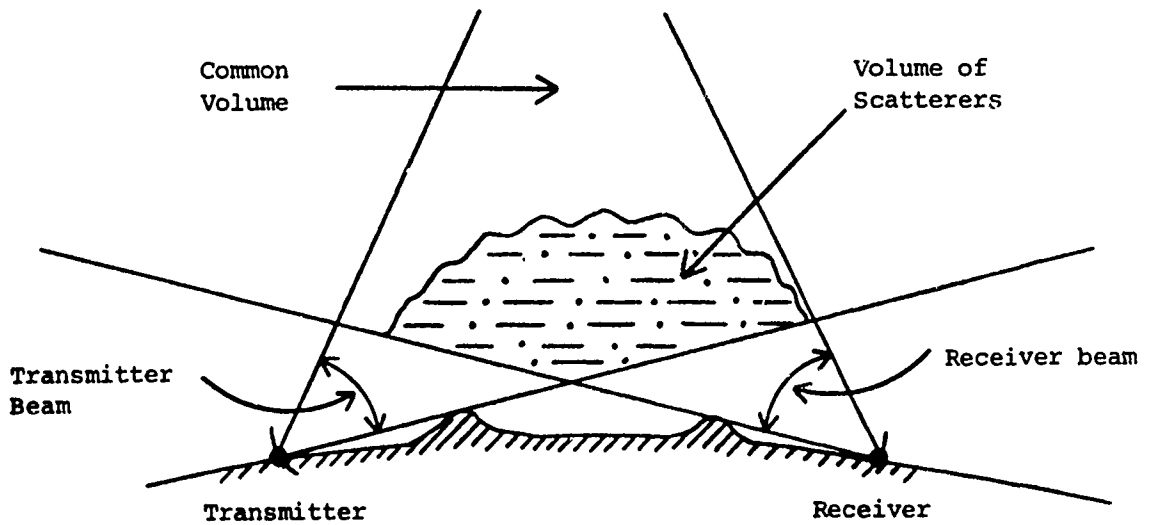
Figure 2-2 Link With No Coupling Loss:
The common volume contains all
scatterers.
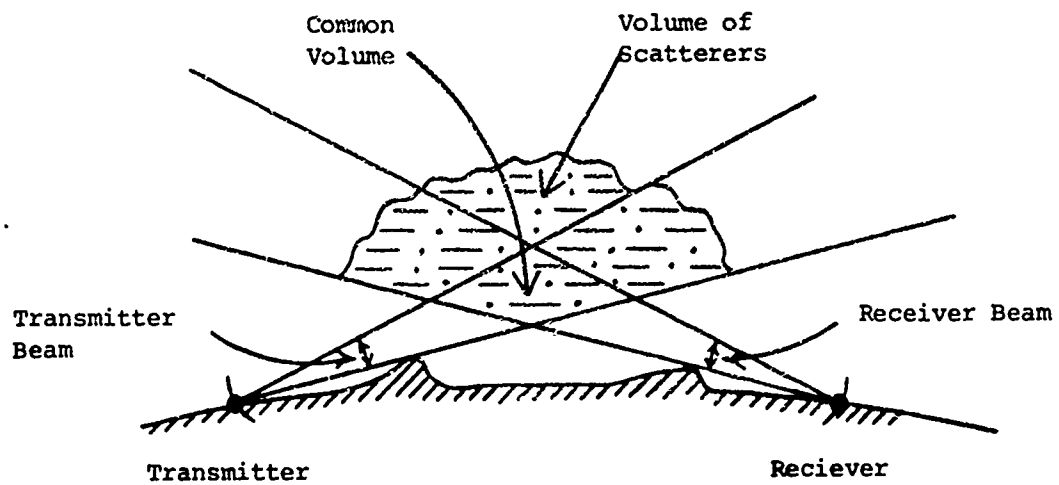
Figure 2-3   Link With Significant Coupling Loss:
The common volume contains only a
fraction of the scatterers.

The aperture-to-medium coupling loss is the loss incurred due to the fact antennas with non-isotropic radiation patterns do not illuminate all of the turbulent atmosphere and hence do not receive all of the scattered energy. Thus if we define the path loss L as

$$\frac{1}{L} = \frac{P_R}{P_T G_T G_R} = 0.0518 \, k^{-5/3} \int_V d^3\underline{r} \; c_n^2(\underline{r}) \; \left|\frac{g_T g_R}{R_T R_R}\right|^2 \theta^{-11/3}(\underline{r}) \; , \quad (2.7)$$

where use of the Kolmogorov wavenumber spectrum has been substituted for $\Phi(\;)$ in (2.1), then the basic path loss L_b is defined as the loss when the radiation patterns g_T and g_R are isotropic. If c_n^2 is constant (i.e., not a function of $\underline{r}$), then (2.7) can be integrated analytically for the case of isotropic radiation patterns. The basic path loss is then given by [13],

$$\frac{1}{L_b} = \frac{P_R}{P_T G_T G_R} = 0.0196 c_n^2 (k\theta_S)^{-5/3}/D \; . \quad (2.8)$$

where θ_S is the minimum scattering angle in the common volume.

The aperture-to-medium coupling loss is then the difference (in dB) between the actual path loss and the basic path loss, i.e.,

$$10 \, \text{Log} \, L_C = 10 \, \log L - 10 \, \log L_b \quad (2.9)$$

From (2.7) and the definition of basic path loss it should be clear that one can reduce the aperture-to-medium coupling loss by reducing the aperture size of the transmitting and receiving antennas since their radiation patterns would then become

'fatter' approaching the radiation pattern of isotropic radiators. This can be seen from Figure 2-4 (solid line) where we have plotted the asymptotic aperture-to-medium coupling loss as a function of antenna diameter (transmit and receive) for narrow beamwidths. However a reduction in antenna size also results in a reduction in antenna gain G_T, G_R , as seen from the dashed line in Figure 2-4. In fact if we double the transmit and receive antenna diameter, G_T and G_R increase by 6 dB each while the aperture-to-medium coupling loss increases by 9 dB which is less than the 12 dB increase in antenna gain. The net result is a higher received signal level and hence a larger system signal-to-noise ratio (SNR).

Let us see what happens asymptotically as one or both beams become narrower. If the transmitter beam is fixed and the receiver beam is much smaller, the receiver beam will cut out a narrow cone segment from the volume of scatterers. The length of the segment is determined by the transmitter beamwidth and therefore fixed. As the receiver beam is narrowed by a factor of two the receiver antenna gain is increased by 6 dB. However, the common volume is reduced by a factor of two. Asymptotically for small beamwidths the scatterers are uniformly distributed in the scattering volume so the scattered power is also reduced by 6 dB. The net effect is then that the path loss is the same, but the received signal is composed of fewer independently scattered signals. If the transmitter beam is then narrowed by a factor of two the antenna gain increases by 6 dB while scattered power is reduced by 3 dB since the scattering volume is reduced by a factor of two. Hence the path loss is always reduced by using narrower beams at both ends of the link.

Suppose that the receiver beam is replaced by two beams illuminating separate halves of the original scattering volume. The two received signals have different amplitudes and phases.
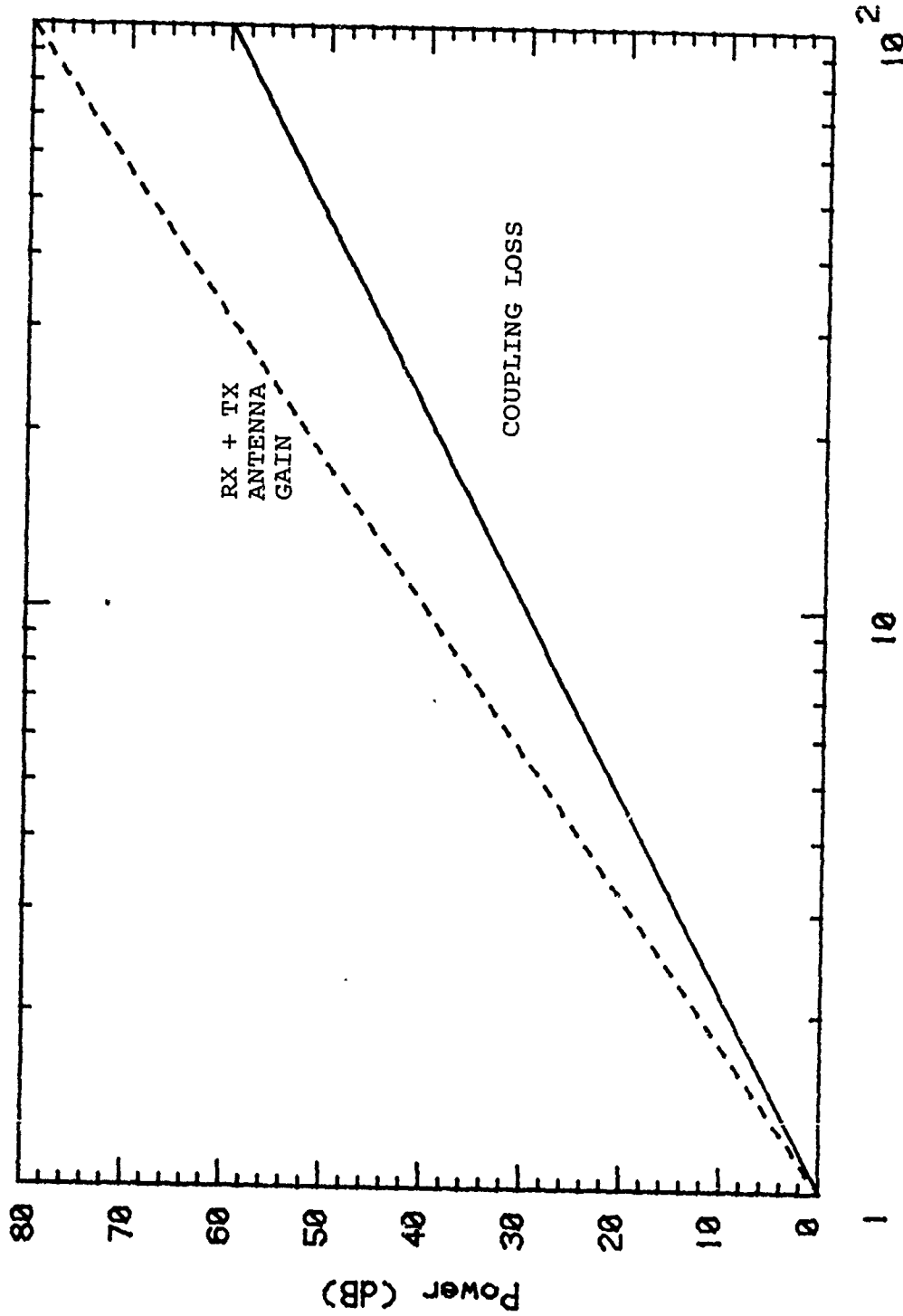
RX-TX Antenna dimension

Figure 2-4 Comparison of Antenna Gain (from both receiver and transmitter antennas) to Coupling loss. Receive and Transmit Antennas are Square Arrays of the Same Size. Values are Normalized to 0dB for Dimension 1.

The sum of these two complex signals is equivalent to the signal received on the original single beam. The phases are random and therefore the amplitudes can add destructively. The key feature of adaptive troposcatter is that the received signals can be added in phase and with optimal amplitude weightings. This advantage is achieved by splitting a beam, which may represent no coupling loss, into two beams each of which have a significant coupling loss. The adaptive combining not only overcomes the coupling loss of each beam, but actually improves on the performance of the single beam system with no coupling loss.

2.3.3 Coupling Loss in Terms of Spatial Correlation

Assume a relatively wide-beam transmitter. At the site of the receiver, the field received at different points of a given aperture will not be perfectly correlated since the signal is arriving from many directions. In other words, the wavefront at the receiver exhibits random fluctuations. A correlation function can be defined in the plane of the aperture. If u and v are coordinates in this aperture the correlation function is

$$\rho(u_1 - u_2, v_1 - v_2) = E[z(u_1, v_1)z^*(u_2, v_2)]$$

where $z(u,v)$ is the field at the point u,v. The total received field over the aperture A is

$$r = \frac{1}{A} \iint_A du\ dv\ z(u,v)$$

and the received power is

$$P = E[|r|^2] = \frac{1}{A^2} \iint_A du_1 dv_1 \iint_A du_2 dv_2\, \rho(u_1-u_2, v_1-v_2)$$

For small apertures ρ is constant for any pair of points and

$$P = \rho(0,0) \ .$$

In this case there is no coupling loss. If the aperture is larger the decorrelation between widely spaced points on the aperture results in a lower received power. This is the coupling loss, which can therefore be defined also as

$$L_C = \rho(0,0)/[\frac{1}{A^2} \iint_A du_1 dv_1 \iint_A du_2 dv_2\, \rho(u_1-u_2, v_1-v_2)] \ .$$

It is not difficult to show directly that the two coupling loss definitions are identical, but we shall not do so here. Previous SIGNATRON reports [11,12,13] have presented analytical expressions for the coupling loss as well as the horizontal and vertical correlation distances.

SECTION 3
THE USE OF DIVERSITY

3.1 DIVERSITY TECHNIQUES

In the previous section it was shown that the system SNR can be improved by increasing the size of the transmitting and receiving apertures. However this is often impractical. A substantial improvement in system SNR can be achieved if we use multiple smaller apertures and combine the signals received with each aperture in an optimum manner. This is commonly referred to as space diversity and the order of diversity is determined by the number of apertures. Thus a system employing one transmit antenna and four receiving apertures is said to employ quadruple space diversity. A multi-element receiving array whose outputs are weighted and combined in an optimum manner is a particular implementation of a space diversity system.

Space diversity improves the effective SNR of the system because the multiple scattered waves which make up the received troposcatter signal combine in a different manner at two spaced receiving locations and therefore fade in an uncorrelated manner. Given N uncorrelated fading signals, the diversity receiver combines them in some manner designed to improve the system SNR and hence system performance.

In addition to space diversity, multiple uncorrelated fading signals can be obtained by other means: namely

(a) Frequency diversity, i.e., a system which employs multiple frequencies (channels) to transmit the same information. The fading at two frequencies is uncorrelated if the frequency separation is greater than the coherence bandwidth of the channel.

(b) Space/Polarization diversity, i.e., a system which transmits the same signal on two orthogonal polarizations and uses multiple spaced antennas to receive both polarizations. A fourth order diversity system which uses two transmitting antennas, one for each polarization, and which receives both polarizations on two spaced antennas is shown in Figure 3-1. Decorrelation between the four signals (4 different paths) is achieved solely from the spacing between the two transmit and two receive antennas and not from the use of orthogonal polarizations.

(c) Angle diversity, i.e., a system which employs a single receiving aperture and multiple feeds to generate multiple beams which illuminate different portions of the scattering volume and hence fade in an uncorrelated manner. One specific example of an angle diversity system is one which employs a single dish receiving antenna with two offset feed-horns. Another example is a receiving array, the outputs of which are fed by means of a Butler matrix which generates the multiple beams to scan different parts of the common volume.

Another type of diversity available on broadband systems is implicit diversity. When the bandwidth is wide enough to permit resolution of different segments of the power impulse response, then a tapped delay line equalizer can exploit the independent fading on the different segments.
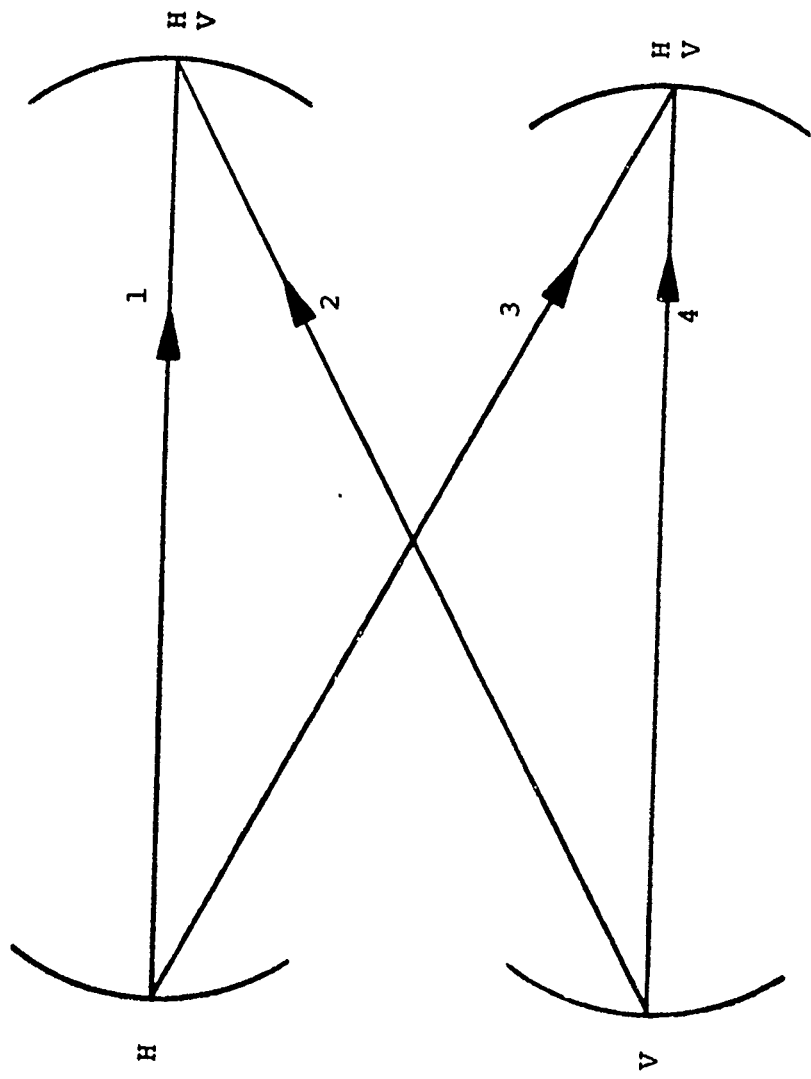
Figure 3-1 2S/2P Diversity Configuration

3.2 PERFORMANCE MEASURE

Any of the diversity systems described can be analyzed by considering a general N-port diversity combiner. The receiver combines the N diversity outputs to form an estimate of the transmitted signal. The optimum combiner is a maximal ratio combiner, which scales each output by its conjugate (i.e., the conjugate of the channel gain) and then sums them. We define a performance criterion for diversity systems in terms of this optimum combiner. In this way the potential gains from diversity may be examined directly without regard to the actual implementation.

The transmitter sends a sequence of pulses of the form

$$z(t) = \sum_k b_k p_k(t)$$

where $b_k = \pm 1$, is the polarity of each pulse and p_k is the shape of the pulse.

It is assumed that a small percentage of these pulses are transmitted with a polarity that is known to the receiver so that they can be used to measure the channel. Appendix C derives the performance including the effect of errors in the channel measurements. These effects are also discussed further in Section 7. For simplicity we assume here that the measurement errors are negligible.

At the receiving array output we have available a number of noisy replicas of the transmitted signal, which can be modelled as

$$z_n(t) = G_n z(t) + v_n(t)$$

where G_n is the complex fading introduced by the troposcatter channel and v_n is the n'th receiver thermal noise. We have re-

moved the explicit dependence of G_n on t because we are interested in observation intervals short enough so that the channel gains can be assumed to be essentially constant. The values of G_n in this expression can arise from individual elements of the array, from beamformer outputs, or from subarrays that are nonadaptively steered. In any case, the receiver then samples each $Z_n(t)$ by correlating it with every $p_k(t)$ to produce the sampled-data outputs

$$Z_{n,k} = G_n b_k + v_{n,k} .$$

These samples are weighted by the complex conjugate of the G_n and a linear combination of them (sum over $n = 1, N$) is used to determine the polarity b_k of the transmitted pulses according to some decision rule. The error rate, i.e., fraction of pulses whose polarity is not determined correctly, is a measure of the performance of the array as a diversity combiner. The error rate depends on the correlation between the gains G_n, and the receiver noise power in a 1 Hz bandwidth (noise spectral density) N_0, assumed to be identical for all N output ports. We assume that the channel is 'Frozen' so that G_n is known to the receiver.

Let m_{ij} be the cross correlation between the channel gains for the i'th and j'th output ports, i.e., $m_{ij} = E(G_i G_j^*)$, and define M_G as the covariance matrix whose elements are the m_{ij}. Note that the diagonal elements of M_G represent the average received power at each array output port while the off-diagonal elements represent the correlation between the signal components at two different ports.

An upper bound ϕ_0 to the error rate (Chernoff bound) can be written as (See Appendix C)

$$\phi_0 = \frac{1}{|I_N + N_0^{-1} M_G|}$$

where

$$I_N = \text{(NxN) identity matrix,}$$

or as

$$\phi_0 = \prod_{n=1}^{N} \left(1 + \lambda_n/N_0\right)^{-1}$$

where $\{\lambda_n\}$ are the eigenvalues of the covariance matrix M_G.

The smaller the error bound ϕ_0 is, the better the array performs. Since ϕ_0 decreases as the eigenvalues increase, the problem of evaluating the performance of a receiving array then consists of determining the eigenvalues of the array and the conditions under which these eigenvalues result in a small error rate. With DPSK the error rate is BER = $\phi_0/2$.

The performance measure we use in comparing the different diversity configurations is the signal-to-noise ratio (SNR) required at the receiver to set the Chernoff bound on the bit error rate equal to 10^{-4}. The SNR is not clearly defined for a system with a number of receiver ports since in general each port sees a different signal power. So we define the SNR to be that which would be present on a system without diversity. Because of this normalization the SNR required by the system without diversity is determined entirely by the desired BER bound ϕ_0. For instance, if $\phi_0 = 10^{-4}$ then the SNR required by a no diversity system is 40 dB.

3-6

A simple bound on the benefit of various orders of diversity may be derived as follows. If $\{\lambda_n: i = 1,\ldots,N\}$ are the eigenvalues of the covariance matrix M_G (normalized to the noise power), then the BER bound is

$$\phi_0 = \prod_{n=1}^{N} \frac{1}{1 + \lambda_n} \quad .$$

Suppose λ is the eigenvalue for a single diversity system with a given aperture size. (For a single diversity system λ is also the SNR.) The power received by each of the n ports of a diversity system consisting of n single diversity systems equals λ. The eigenvalues cannot exceed λ so the BER bound for an n-th order system is bounded by

$$\phi_0 > \left(\frac{1}{1+\lambda}\right)^n \quad .$$

This implies

$$\lambda > \left(\frac{1}{\phi_0}\right)^{1/n} - 1 \quad .$$

This final inequality bounds the SNR required to achieve a given BER bound. Note that λ is the SNR derived from a single diversity system as previously defined. Table 3-1 contains values of this bound for various n.

If the various diversity ports have equal power and are independent then this bound may be achieved. This is the case

TABLE 3-1

Lower Bounds on the Required SNR to Achieve BER Bound $\phi_0 = 10^{-4}$
for Various Orders of Diversity

Order of Diversity	SNR Bound Fixed Element Aperture
1	40.0
2	20.0
3	12.1
4	9.5
5	7.3
6	5.6
7	4.4
8	3.4
9	2.5
10	1.8
11	1.2
12	.62

with space (and polarization) diversity if the antennas are sufficiently separated and for frequency diversity if the two frequencies ~? far enough apart. For angle diversity, however, the bound is ot generally achievable because the extent of the common volume is limited and so additional beams receive less power than the first. If the beams are narrow and the scatter angle is large then the bound may be approached.

The bound clearly demonstrates that diminishing returns are seen with increasing diversity. This conclusion does not depend on any particular geometry or diversity type.

3.3   DIVERSITY FROM ARRAY ANTENNAS

3.3.1 Phased Array

High order diversity systems are of interest because of the great diversity gains possible. The cost of high order diversity systems using traditional diversity types, such as space, polarization, and frequency, is prohibitive. Phased arrays offer potentially high diversity at reasonable cost; hence it is of interest to examine how much diversity may be derived from a given phase array.

A general discussion of phased arrays and their gain patterns is given in Appendix D.

3.3.2 Beam Transformation

Different diversity ports may be formed by dividing the array into subarrays. The outputs of these subarrays may then be combined adaptively. Increases in diversity may then be accomplished by subdividing the array further.

If the array is divided into equal subsections then each section has the same gain pattern and common volume and so each section receives the same power. The effective order of diver-

sity (i.e., the number of significant eigenvalues in the signal covariance matrix) is determined by the correlations between subsections. The degree of correlation between subarrays is not intuitively obvious and so it is difficult to see the effect on performance of further subdivision of the array. It is much easier to see the possible diversity gains from a phased array through a beam transformation.

A beam transformation takes the outputs from a uniform array of antennas which have the same gain pattern (i.e., same gain for each pair of elevation and azimuth angles), and forms a set of beams which point in different directions. The beams are orthogonal and the maximum gain for each beam is at a null of all other beams. The transformation is invertible and lossless, hence the system performance is not affected by it. The total number of beams formed is the same as the number of antennas in the array. The performance of various orders of diversity for this array may then be evaluated simply by combining different subsets of these beams. (In an actual system not all of the beams would be formed.)

Since the beams point in different directions they have different common volumes, and so the signals on the beams are largely uncorrelated. In addition the power received by the various beams is different, so it is easy to estimate how much a given beam may affect the system performance. A beam which points away from the atmospheric volume illuminated by the transmitter receives very little power, hence it cannot greatly affect performance.

Another advantage to the beam transformation is that the correlations between ports are real. This simplifies the computation of the eigenvalues of the covariance matrix.

If the phased array is rectangular then the beams from a rectangular set, so there are a number of beams in azimuth and a

number of beams in elevation. The total number of beams is the product of these two numbers. In azimuth the common volume is chiefly limited by the transmitter beamwidth. A dual azimuth diversity system is not greatly affected by broadening the transmitter beam, but higher order azimuth diversity systems generally improve when the transmit beam is broadened even though this reduces the boresight gain of the array. These effects are considered in greater detail in Section 5.

The number of elevation beams which may be used is determined by the minimum scattering angle and the spacing between beams. Higher elevation beams receive less power and eventually their contribution becomes negligible. The transmitter beamwidth does not limit elevation diversity since different elevation beams always intersect the transmitter beam.

Consider a linear array with N elements. If the outputs are summed using equal gains and with linear phasing (i.e., the n-th element is phase-shifted by $n\alpha$) then the one-dimensional amplitude pattern which results is

$$A(\theta) = \frac{\sin\left[\frac{N}{2}\left(\frac{2\pi}{\lambda}d\,\sin\theta - \alpha\right)\right]}{\sin\left[\frac{1}{2}\left(\frac{2\pi}{\lambda}d\,\sin\theta - \alpha\right)\right]} \, g_e(\theta)$$

where $g_e(\theta)$ is the element gain pattern, d is the element spacing, θ is the off-boresight angle, and α is the phase shift between adjacent elements. For the derivation of this equation see Appendix D. A Butler matrix transformation forms a set of N beams where the m-th beam has

$$\alpha = \frac{(2m-1)\pi}{N} \quad .$$

3-11

These beams are orthogonal, and the peak (or peaks) of each beam falls at nulls of all other beams.

If the number of elements is large and the element spacing small then each beam has a single mainlobe and the beams cover all of visible space. For our purposes only the beams which are relatively near boresight are of any consequence.

An example of the beams which results from a Butler matrix transformation is given in Figure 3-2a. The array is linear and consists of four elements. The element gain pattern is the envelope of the four beam patterns.

A slight modification to the beam transformation is necessary to allow an odd number of beams to be used when the number of array elements along a given dimension is even (or an even number of beams when the number of elements is odd). Consider a linear phased array. If the number of elements in the array is even then none of the beams formed by a beam transformation has a boresight which is perpendicular to the array. However, if we wish to use an odd number of these beams in a system then the set of beams should be symmetric about a line perpendicular to the array, hence the center beam of the set should be perpendicular to the array. This difficulty may be overcome by modifying the definition of the beam transformation so that the beams are shifted by 1/2 the separation between adjacent beams. The last beam in the set then becomes a "difference beam". For this beam the phase shifts applied to the outputs of adjacent elements differ by 180°, so its gain pattern has two lobes with equal gain which occur outside the other beams. This is illustrated in Figure 3-2 for a linear array of four elements. If two beams are desired then the center two beams which result from the usual beam transformation may be used (Figure 3-2a). If one or three
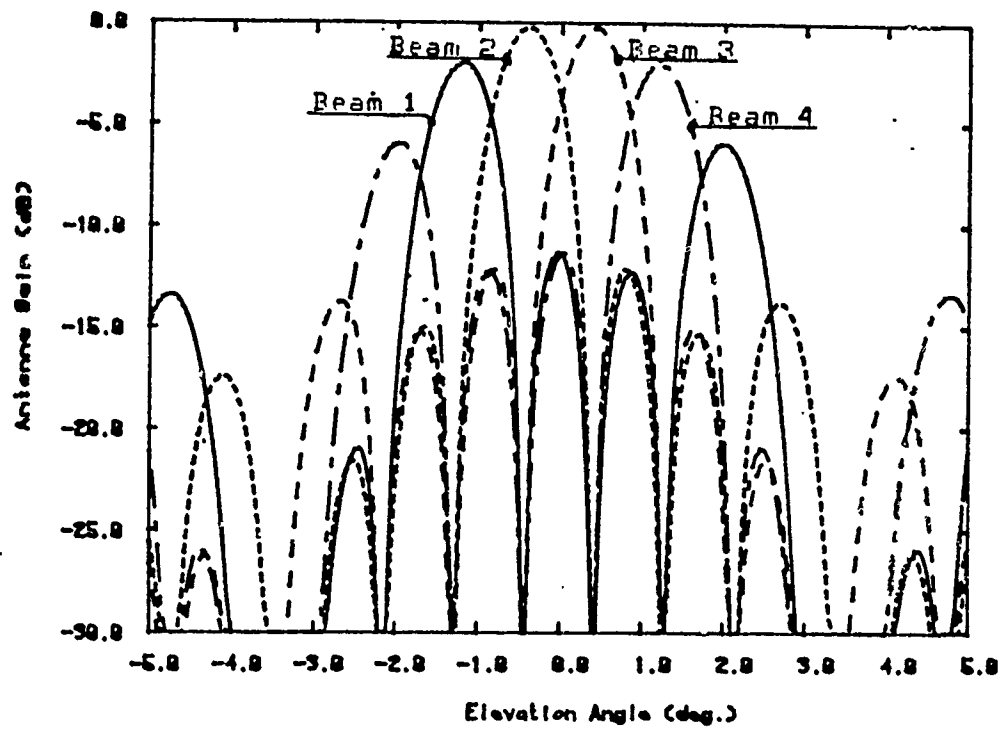
a) Normal Beam Transformation
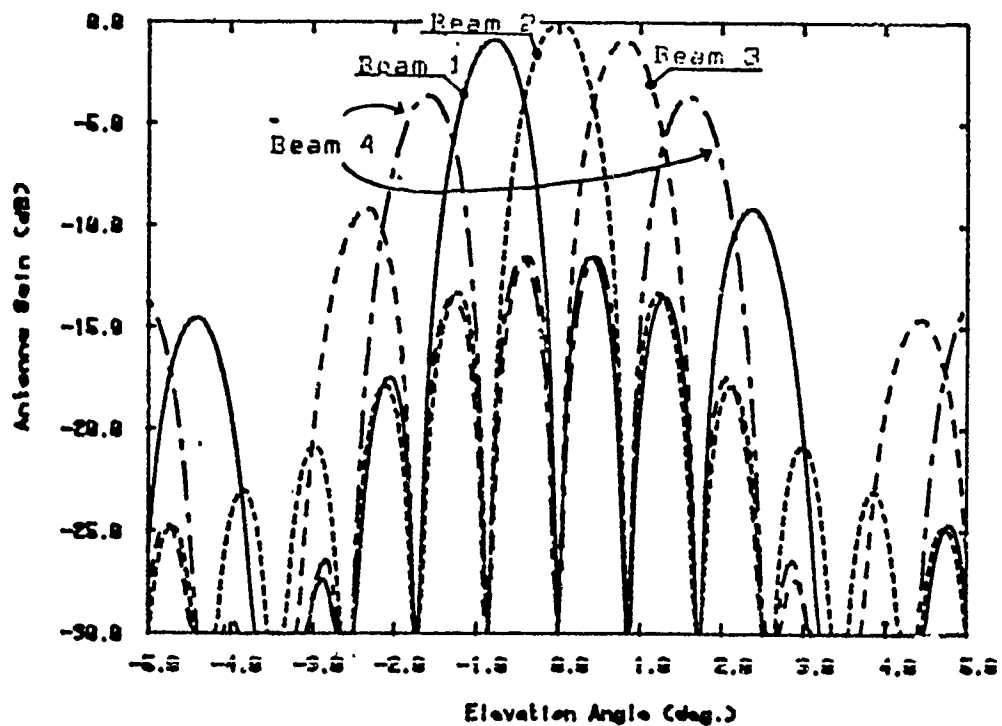
b) Modified Beam Transformation

Figure 3-2   Beam Patterns of a Four Element Array. The pattern in (a)
is Used if 2 or 4 Beams are Required. The Pattern in (b)
is for 1 or 3 Beams.

beams are desired the transformation of Figure 3-2b is used. Either set of beams may be derived from the other so no loss of information is involved. This idea may be applied for both dimensions of a two-dimensional array to allow even or odd numbers of beams to be selected in either direction.

SECTION 4
COMPUTED PERFORMANCE OF A PHASED ARRAY

The short-term performance of a number of different orders of diversity has been evaluated using the TROPO program for a few typical troposcatter links. The transmit and receive antennas are single phased arrays. The arrays are rectangular and are oriented with one axis horizontal. The boresight of both arrays lie in the great circle plane (i.e., the azimuth angle is zero for both arrays). No polarization diversity is employed. The transmit beam is generated from the entire array with no phasing of the elements. For most of the results the receiver ports consist of sets of beams which are derived from the element outputs through a beam transformation. The elements are assumed to be small enough that their gain is the same over the entire common volume. This assumption is made to prevent the gain pattern of the elements from affecting the diversity performance. The beams form a rectangular set; that is, the number of receiver ports is the product of the number of beams in azimuth and the number of beams in elevation.

For a given minimum scattering angle, the link distance has no effect on diversity gains. The link distance does affect the path loss. The path losses which are presented in this section assume a 100 km path length. The _changes_ in path loss due to scatter angle and antenna beamwidth are also unaffected by link distance. So the results which follow apply to any link with the given minimum scatter angles.

The carrier frequency affects the diversity gains only through the antenna beamwidths. So the results apply to any combination of carrier frequency and antenna size which give the specified beamwidth. For path loss calculations the beamwidth is assumed to be 5GHz, but as with link distance this has no bearing on changes in path loss.

4-1

Thus, the diversity results derived in this section are generally applicable to any link with the specified beamwidth and scatter angle, and are not limited to the specific link distance and carrier frequency which are used to determine the path loss.

4.1   ELEVATION DIVERSITY

We first examine diversity systems with a number of beams which differ only in elevation.   All of the beams have zero azimuth angles, i.e., they are pointed directly toward the transmitter beam.   The lowest elevation beam has its lower 3 dB point at the horizon, so its boresight is roughly one-half the 3 dB beamwidth above the horizon.   The other beams have boresights at increments of half the null beamwidth above the first beam. Adjacent beams cross over at the $2/\pi$ level (-3.9 dB).

The first link we consider has horizon angles of .25° at both the transmitter and the receiver.   This results in a minimum scattering angle of 1.20°.   The antenna apertures are square and measure 3 meters along each side, so the half-power beamwidth of the arrays is 1.0°.   Table 4-1 presents the SNR's required to make the BER bound $\phi_0 = 10^{-4}$ for various orders of elevation diversity.

The bound on diversity gain derived in Section 3.2 is included for comparison.   The dual elevation diversity system is only 3.3 dB above the bound, but after third order diversity, additional elevation beams improve performance very little.   The basic reason for this effect is that the power on the upper elevation beams is very low due to the large scatter angle.   To further investigate this effect we have examined the performance of one, two, and three beam elevation diversity systems for different minimum scatter angles and beamwidths.   The aperture sizes are 1.5m x 1.5m,   3m x 3m, and 6m x 6m which result in beamwidths of 2°, 1°, and .5° respectively.   The minimum scatter angles considered are .7°, 1.2°, and 1.7°.   The results are presented in Table 4-2.

Table 4-1

Elevation Diversity Performance --
Required SNR for Chernoff bound on BER = .0001
(1.2° Minimum Scatter Angle, 1° Beamwidth, Square Array)

Number of Elevation Beams*	Required SNR (dB)	
	Elevation Diversity	Lower Bound (Equal Power, Independent)
1	40.0	40.0
2	23.3	20.0
3	19.3	13.1
4	18.1	9.5
5	17.5	7.3

* NOTE: The elevation beams are formed by phasing the elements of the array as described in Section 3.3.

Table 4-2

Comparison of elevation diversity gain for different antenna sizes and minimum scattering angles. (Antenna sizes 1.5m, 3m, 6m. Minimum scattering angles .7°, 1.2°, 1.7°.)

a. 1.5m by 1.5m Antennas

Order of Diversity	Required SNR		
	.7°	1.2°	1.7°
1	40.0	40.0	40.0
2	25.6	24.5	23.9
3	23.2	21.5	20.4

b. 3m by 3m Antennas

Order of Diversity	Required SNR		
	.7°	1.2°	1.7°
1	40.0	40.0	40.0
2	24.3	23.3	22.6
3	21.1	19.3	18.3

c. 6m by 6m Antennas

Order of Diversity	Required SNR		
	.7°	1.2°	1.7°
1	40.0	40.0	40.0
2	23.1	22.3	21.8
3	18.9	17.5	16.7

Increasing the beamwidth and decreasing the scatter angle both decrease the diversity gains. The boresight of the first beam is usually at about $\theta_{min} + \frac{1}{2}\beta$ where θ_{min} is the minimum scatter angle and β is the beam separation (1/2 the null beamwidth). Additional beams have boresights at increments of β above the first. If we define a parameter

$$\gamma = \frac{\beta}{\theta_{min} + \frac{1}{2}\beta}$$

then we may compare results for different beamwidths and scatter angles on a single plot. The result is given in Figure 4-1. Note that ordering using α leads to fairly smooth curves.

An approximation to the performance of elevation diversity systems may be derived as follows. Assume that the signals on each port are independent and that the losses in power on the upper elevation beams are determined solely by the scatter angle at their respective boresights. This determines a sequence of eigenvalues, which may be used to find the required SNR for a given bit-error-rate.

The scatter angle of the boresight of the i-th beam is

$$\theta_i = \theta_{min} + \frac{1}{2}\beta + (i-1)\beta$$

where $i = 1, 2, \ldots, N$, θ_{min} is the minimum scattering angle and β is the beam spacing. For relatively narrow beams, the power on the i-th beam is proportional to
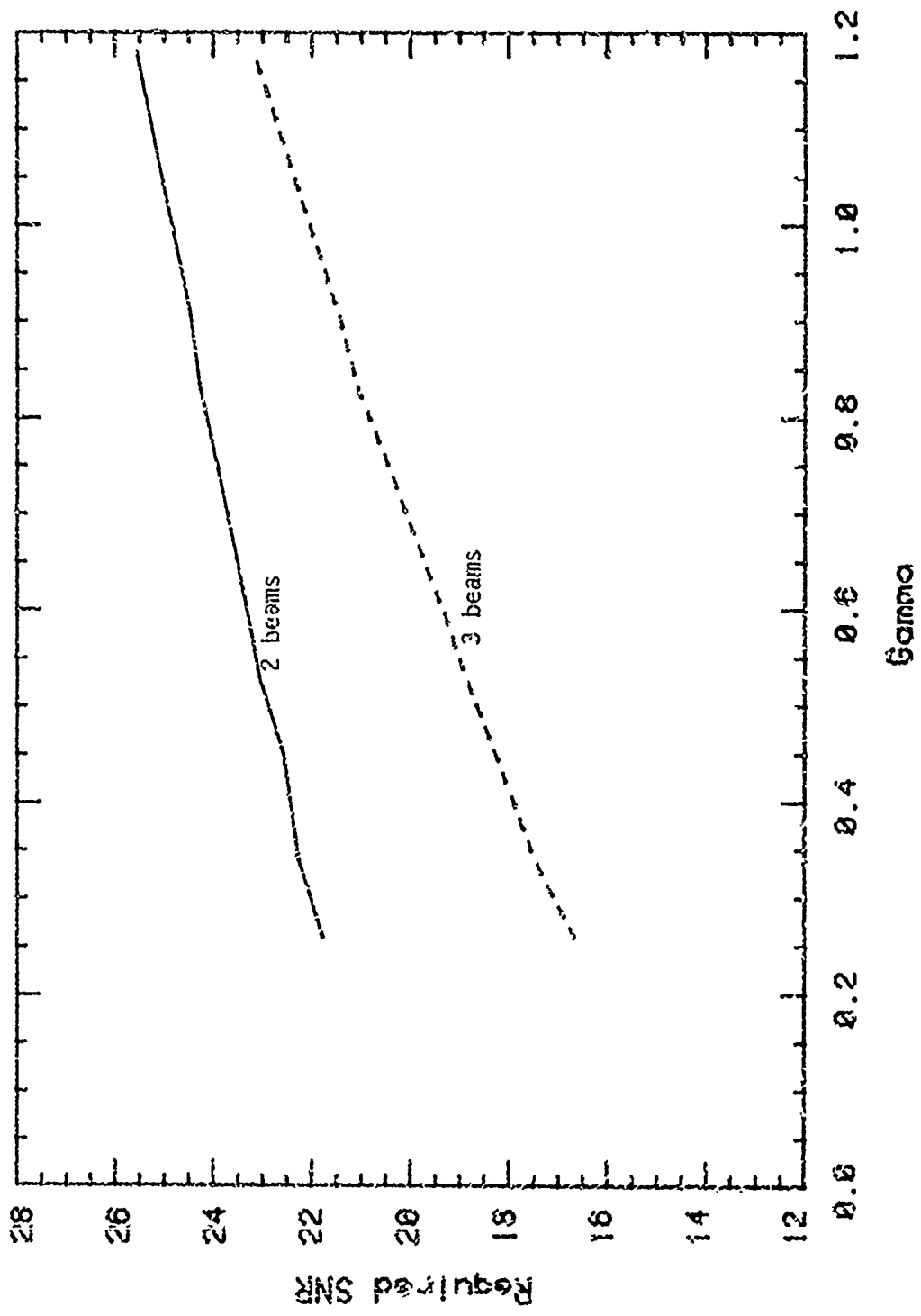
Figure 4-1. Required SNR vs γ for elevation diversity. γ is the ratio of the beam spacing to the lowest beam scatter angle at boresight. Link distance 100 km, 5 GHz, various scatter angles and antenna sizes.

$$\lambda_i = \left(\frac{\theta_i}{\theta_1}\right)^{-11/3}$$

$$= \left(1+(i-1)\frac{\beta}{\theta_1}\right)^{-11/3}$$

$$= \left(1+(i-1)\gamma\right)^{-11/3}$$

where

$$\gamma = \frac{\beta}{\theta_{min} + \frac{1}{2}\beta}$$

is the ratio of the beam spacing to the scatter angle of the lowest elevation beam boresight. The Chernoff bound on the bit-error-rate is

$$BER = \prod_{i=1}^{n} \frac{1}{1+\sigma[1+(i-1)\gamma]^{-11/3}}$$

where σ is the required SNR.

In Figure 4-2 the required SNR from the approximation (dashed lines) is compared with actual computed values for 2 and 3 beams. The curves agree to within about .5 dB in all cases. The main source of error here is the effect of horizon blockage, which is greatest with dual diversity and large beamwidths. Table 4-3 compares the actual performance of 2,3,4, and 5 beam systems (from Table 4-1) with the approximation. Note that the values for the four and five beam systems agree very well.
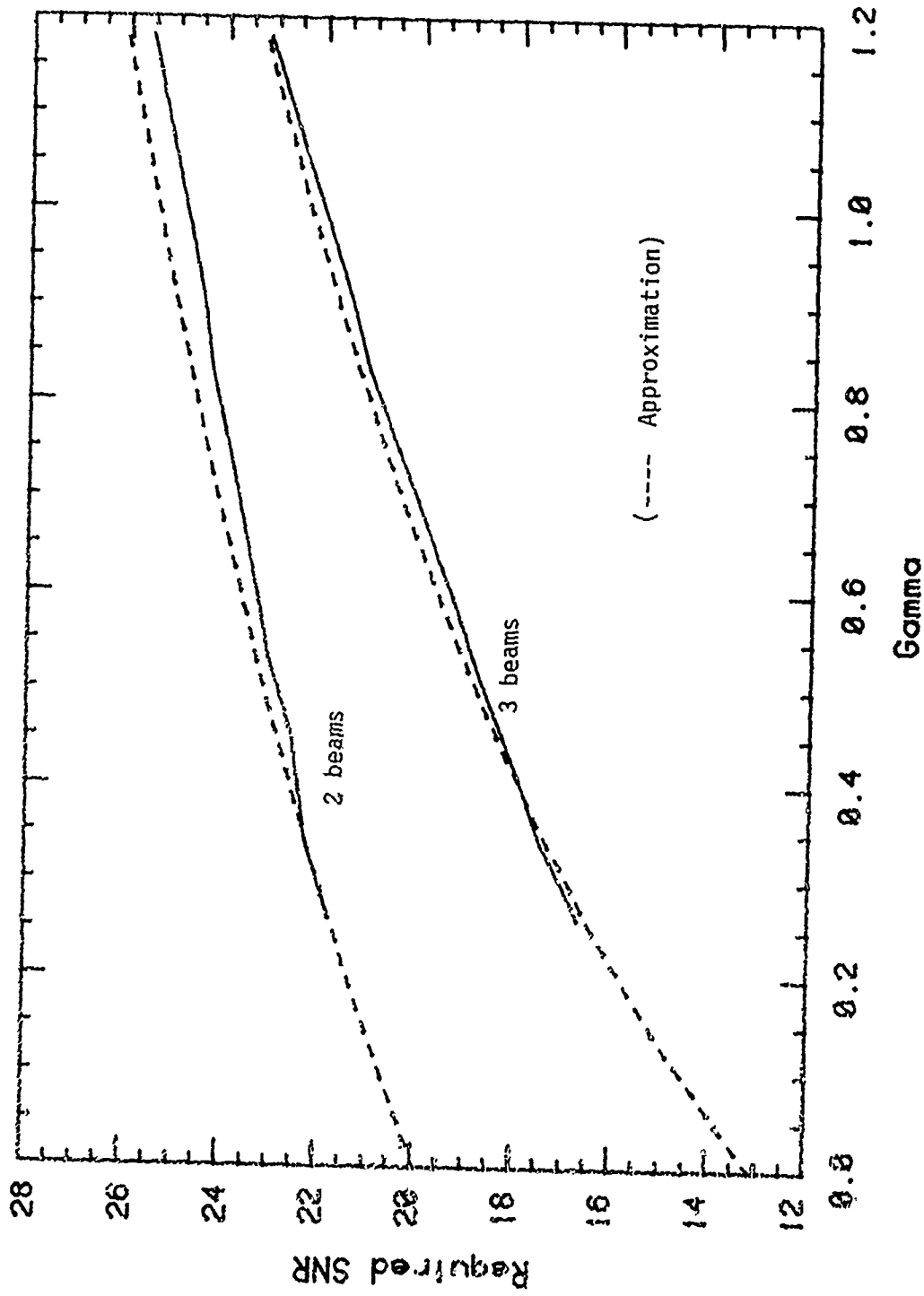
Figure 4-2 Comparison of elevation diversity performance with approximation.

Table 4-3

Comparison of Elevation Diversity Performance
With the Approximation
(Min. Scat. Angle 1.2°, 3m x 3m Antennas, 100 km link, 5 GHz)

| Order of Diversity | Required SNR (for BER = .0001 | |
	Actual (dB)	Approximation (dB)
1	40	40
2	23.3	23.6
3	19.3	19.6
4	18.1	18.1
5	17.5	17.5

Figure 4-3 presents more approximate results for 2nd through 6th order diversity. With very narrow beams ($\gamma = 0$) the performance approaches the bound derived in Section 3.2 under the assumption of equal power and independent ports. These curves, although not exact, give a rough idea of the beamwidths and scatter angles necessary to make third or fourth order elevation diversity worth while. For instance at $\theta_{min} = \beta = 1^0$ the gain from adding a fourth beam to a three beam system is only 1.4 dB whereas the gain with independent equal power diversities ($\alpha = 0$) is 3.6 dB.

Thus far we have been concerned only with the effect of scatter angle and beamwidth on diversity gain. These factors also change the antenna gain and aperture-to-medium coupling loss, generally by more than they affect the diversity gains. So the diversity gains alone cannot be used to determine the antenna dimensions, for example, since the dimensions also affect the required transmiter power. Path loss calculations are always necessary to determine these factors.

4.2 AZIMUTH DIVERSITY

Under the assumption that the receiver and transmitter antennas have the same dimensions, an azimuth diversity system cannot achieve the bound on diversity gains of the previous section. The reason is that if we transmit with the entire aperture then the common volume is limited in azimuth by the transmitter beamwidth. Since the receiver beams have the same beamwidth, additional azimuth beams (that is, beams with non-zero azimuth angles) receive power through sidelobes even if the beamwidths are very narrow. In order to illuminate a number of azimuth beams with the mainbeam of the transmitter the aperture must be under-illuminated, which decreases the boresight gain of
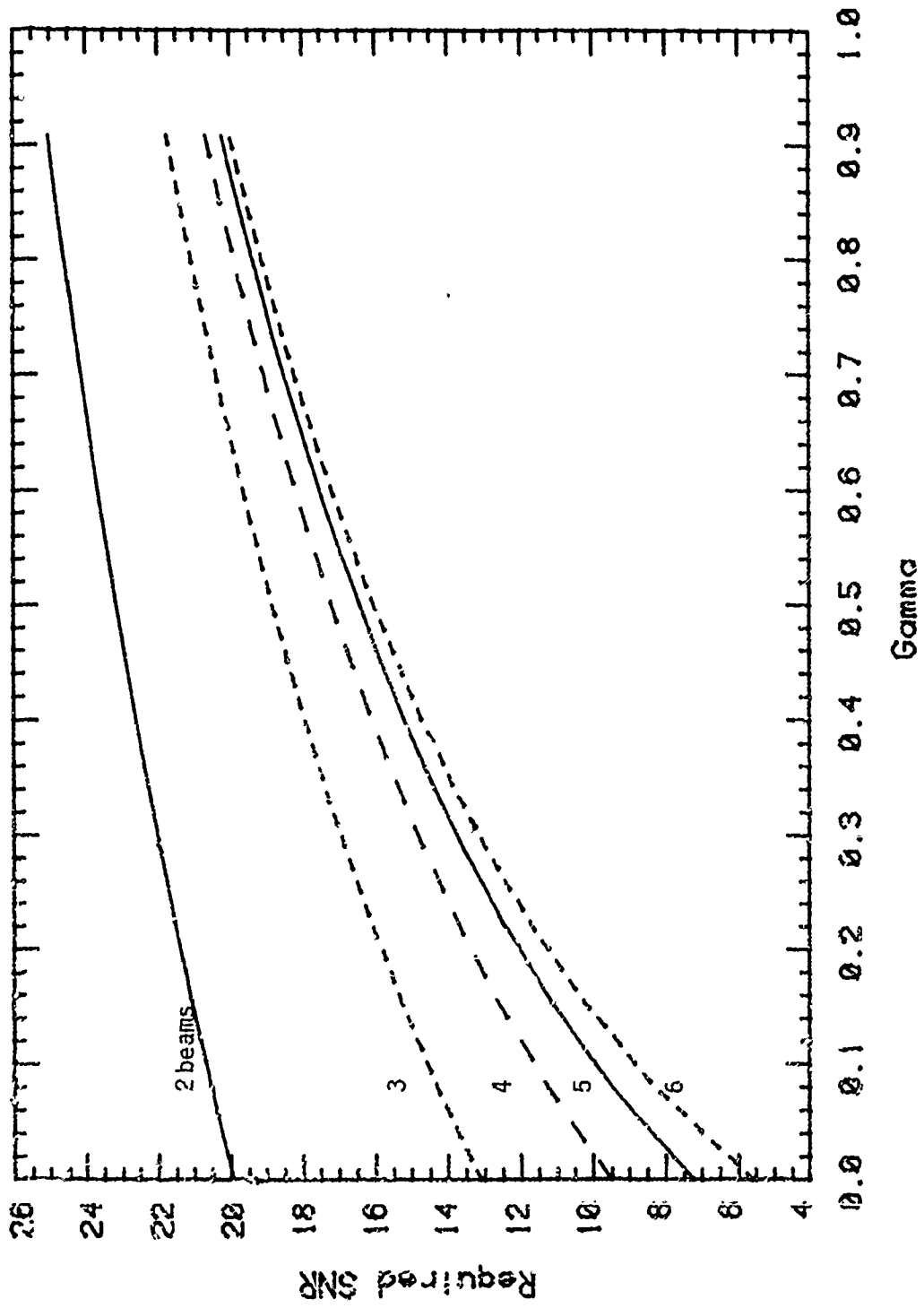
Figure 4-3   Approximate elevation diversity performance for 2nd through 6th order diversity. γ is the ratio of the beam spacing to the lowest beam scatter angle (at boresight).

the antenna. So additional azimuth beams cannot have the same power as the first beam. Either power is lost on the outside beams due to the transmitter beam pattern or power is lost on all beams due to a decrease i‍ boresight gain.

A bound on azimuth diversity performance may be derived as follows. Assume that the scatter angle is large relative to the beamwidth so that additional azimuth beams are not affected by increasing scatter angle. Under this assumption only a one-dimensional integration (in azimuth) is necessary since all beams have the same elevation behavior. The covariance matrix is thus determined by the transmitter and receiver beam patterns. So with rectangular apertures the transmitter gain pattern is

$$g_T(\alpha, x) = \sqrt{\alpha} \; \frac{\sin \alpha x}{\alpha x}$$

where α is varied to change the boresight gain and the beamwidth, and the receiver beam patterns are

$$g_{R_i}(x) = \frac{\sin[x-(i-n/2 + 1/2)\pi]}{x-(i-n/2 + 1/2)\pi} \quad ,$$

where $x = \dfrac{L_H}{\lambda \sin\Theta}$, and L_H is the width of the array. The ij-th element of the signal covariance matrix is

$$C_{ij}(\alpha) = \int_{-\infty}^{\infty} g_T^2(\alpha, x) g_{R_i}(x) g_{R_j}(x) \, dx \; .$$

The results of this procedure are given in Figure 4-4. Here we graph the SNR required to achieve a BER of 10^{-4} versus the parameter α. (α is proportional to the boresight gain at the transmitter antenna, and $1/\alpha$ is proportional to the transmit beamwidth.) As the order of diversity increases the optimum transmit beamwidth also increases. In Table 4-4 we give the required SNR for the best transmitter beamwidth along with the value of α which gives this beamwidth ($\alpha = .5$ means that the transmitter beamwidth is double the receiver beamwidth), and the dB loss incurred if full illumination is employed.

Note that a dual azimuth diversity system loses only .2 dB if the transmit beamwidth is not increased, but that higher order diversity systems lose 2 or 3 dB. The potential gains from azimuth diversity are much lower than those possible with elevation diversity (cf. Table 4-3). With third order diversity the difference between the bounds is 4.3 dB, and with fourth order diversity the difference is 5.5 dB.

We next present computed results for various azimuth diversity systems. The link used is 100 km with 3m x 3m antennas ($1°$ beamwidth) and a minimum scatter angle of $1.2°$. The carrier frequency is 5 GHz. The optimum transmit beamwidth is used with each order of diversity. In Table 4-5 we compare the azimuth diversity performance with elevation diversity performance. Also included for reference is the transmitter azimuth beamwidth (for the azimuth diversity systems). Elevation diversity is always better than azimuth diversity for this link.

If the scatter angle is small and the beamwidth is large, then a dual azimuth diversity system may perform slightly better than a dual elevation diversity system. For example, if the antenna dimensions are 1.5m x 1.5m instead of 3m x 3m for the

4-13
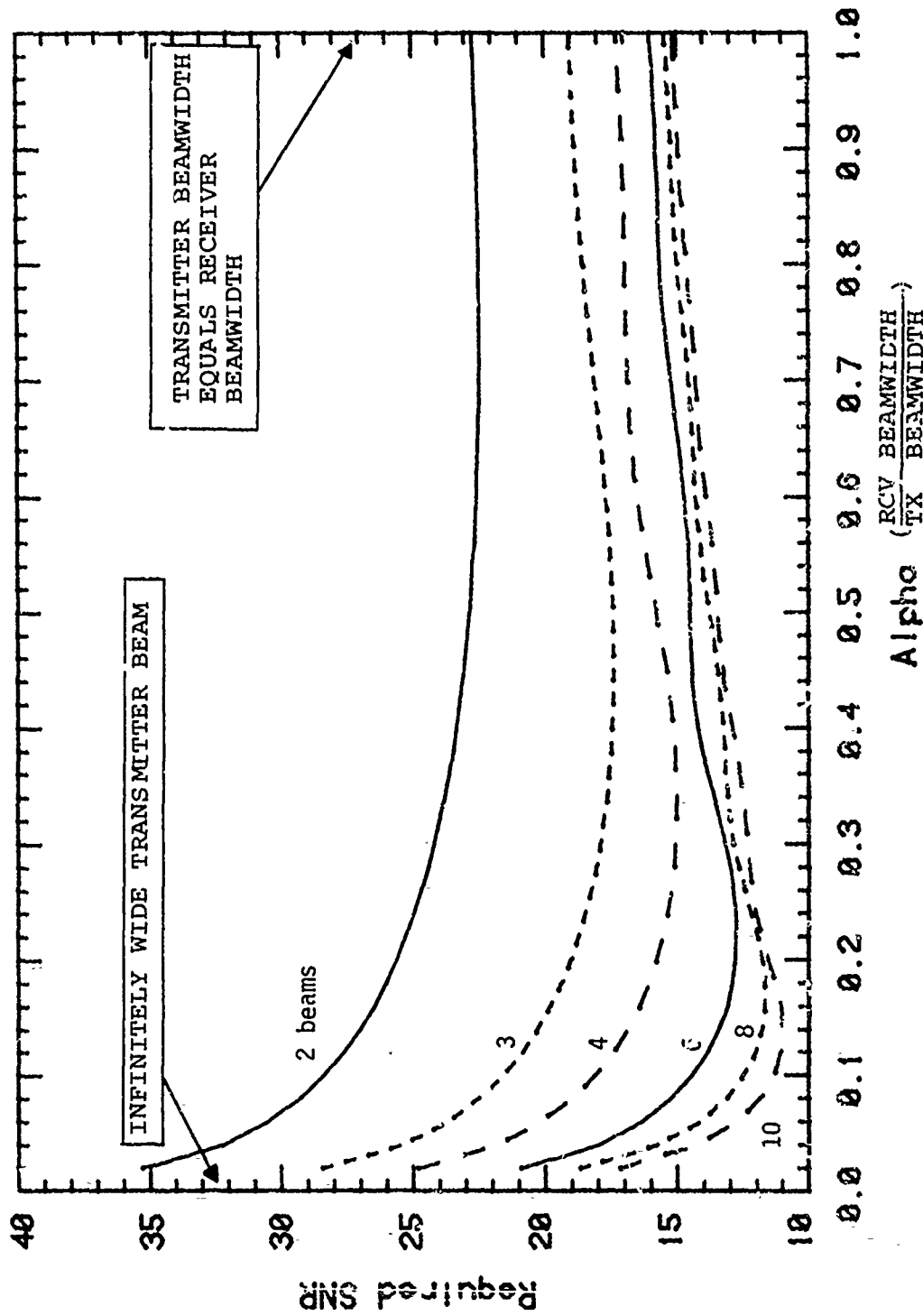
Figure 4-4 Effect of transmitter antenna beamwidth on azimuth diversity systems. Orders of diversity 2, 3, 4, 6, 8, 10. α is proportional to the TX boresight gain, 1/α is proportional to the TX beamwidth.

Table 4-4

Bound on Azimuth Diversity Gains

(1/α is proportional to the transmitter beamwidth. α = 1 corresponds to identical transmitter and receiver bandwidths)

Order of Diversity	Azimuth Diversity Required SNR Bound (dB)	α	Loss at α = 1 (dB) (Full Illumination)	Elevation Diversity SNR Bound (dB)
1	40.0	1	0	40.0
2	22.5	.73	.2	20.9
3	17.4	.45	1.5	13.1
4	15.0	.34	2.3	9.5
5	13.7	.26	3.0	7.3
6	12.8	.22	3.2	5.6
7	12.1	.20	3.7	4.4
8	11.7	.16	3.8	3.4
9	11.3	.16	4.1	2.5
10	11.0	.14	4.2	1.8

Table 4-5

Comparison of Azimuth and Elevation Diversity
100 km Link, 3m x 3m Antenna, 1.2° Scattering Angle

Order of Diversity	Required SNR		Transmit Azimuth Beamwidth (Azimuth Diversity Systems (Elevation Beamwidth = 1.0°)
	Azimuth	Elevation	
1	40.0	40.0	1.0°
2	23.5	23.3	1.0°
3	20.2	19.3	1.4°
4	19.5	18.1	1.7°
5	19.2	17.5	2.0°

above link, then the required SNR is 24.5 dB with elevation diversity and 24.3 dB with azimuth diversity. With higher order diversity this almost never occurs since the transmitter beamwidth must be increased significantly, causing a loss in antenna gain.

We may conclude that in general azimuth diversity is not as effective as other diversity types. Dual azimuth diversity, however, is often almost as good as elevation diversity and sometimes slightly better. Further, dual azimuth diversity may be combined with elevation diversity for higher order angle diversity systems.

4.3 COMBINED AZIMUTH AND ELEVATION DIVERSITY

We next consider combined elevation and azimuth diversity systems of various orders. As before the link we consider has horizon angles of .25° at both the transmitter and the receiver. This results in a minimum scattering angle of 1.20°. The antenna apertures are square and measure 3 meters along each side, so the half-power beamwidth of the arrays is 1.0°. Table 4-6 presents the SNR's required to make the BER bound $\phi_0 = 10^{-4}$ for various orders of diversity. The diversity systems are specified by the number of beams in azimuth and the number in elevation. The bound derived in Section 3.2 is included for comparison. Note that the gains achieved by the system are within a few dB of the bound for small n. The larger the aperture the closer the results will approach the bound.

Different systems which have the same order of diversity are compared. For example, if four beams are desired then a square set (two beams in azimuth and two in elevation) or a set of four beams with different elevations but the same azimuth may be used. In general more than two beams in azimuth result in little gain. For instance a 6th order system with three beams in

4-17

Table 4-6

Required SNR for BER Bound $\phi_0 = 10^{-4}$
(Minimum Scattering Angle 1.2°, Antennas 3m by 3m. Beamwidth 1°, Square Aperture)

Order of Diversity	No. of Beams in Elevation	No. of Beams in Azimuth	Required SNR	Lower Bound on Required SNR (cf. Table 2-1)
1*	1	1	40.0	40.0
2*	2	1	23.3	20.0
2	1	2	23.5	20.0
3*	3	1	19.3	13.1
3	1	3	20.4	13.1
4	4	1	18.1	9.5
4*	2	2	15.4	9.5
4	1	4	20.0	9.5
6*	3	2	13.6	5.6
6	2	3	14.3	5.6
8*	4	2	13.0	3.4
9*	3	3	12.5	2.5
12*	4	3	12.0	.6

* Optimum Diversity Configuration

azimuth and two in elevation is only 1.1 dB better than a 4th order system with two beams in both azimuth and elevation.

We next consider the effect of antenna aperture size on diversity gains. Table 4-7 contains the SNR required for the same link as above for square arrays with dimensions 1.5 m or 6m. In all cases the transmit and receive antennas are the same size. The values for 3m arrays are included for comparison. The diversity gains are not greatly affected. In general the larger antenna has better diversity gain but only by one or two dB. These differences are much smaller than the changes in path loss and antenna gain. The path loss is smaller for small antennas due to a decrease in the aperture-to-medium coupling loss, but this is more than offset by the decrease in antenna gain. (These values are also presented in Table 2-4.)

The transmitter and receiver horizon angles also affect diversity gains. In general diversity gain decreases as the horizon angle decreases. This effect is due to the scattered power dependence on the scatter angle θ. As θ decreases, a larger fraction of the received power comes from the lowest section of the common volume. This effect is illustrated in Table 4-8. Minimum scattering angles of .7° and 1.7° are compared with the original case of 1.2° for 3m antennas. The diversity gain is less for small horizon angles, but this effect is small compared to the decrease in path loss. Figure 4-5 graphs these points with values computed for 1.5m and 6m antennas.

4.4 DECREASED COMPLEXITY USING SUBARRAYS

A diversity system with beams derived from the element outputs may be too complex. If the array has N elements and m beams are desired then mN phase shifts are required if m is less than $\log_2 N$. (All N beams may be formed with $N\log_2 N$ phase shifts.) A great reduction in the number of phase shifts may be achieved by

Table 4-7

Comparison of systems which employ square antennas of different sizes (1.5m, 3m, 6m)

a. Half Power Beamwidths and Path Losses

	Antenna Size		
	1.5m	3m	6m
Half Power Beamwidth	2°	1°	0.5°
Boresight Antenna Gain	39.0 dB	45.0 dB	51.0 dB
Path Loss	259.1 dB	262.6 dB	267.4 dB

b. Diversity Gains

Order of Diversity	Elevation Beams	Azimuth Beams	Required SNR		
			1.5m	3m	6m
1	1	1	40.0	40.0	40.0
2	2	1	24.5	23.3	22.3
2	1	2	24.3	23.5	23.0
3	3	1	21.5	19.3	17.5
4	2	2	17.2	15.4	14.2
6	3	2	15.9	13.6	11.8
8	4	2	15.5	13.0	10.8

Table 4-8

Comparison of system performance on links with different minimum scattering angles. (100 km Link, Minimum Scattering Angles .7°, 1.2°, 1.7°, Antenna Size 3m).

a. Path Losses

	Scattering Angle		
	.7°	1.2°	1.7°
Path Loss	254.6 dB	262.6 dB	268.1 dB

b. Diversity Performance

Order of Diversity	Elevation Beams	Azimuth Beams	Required SNR		
			.7°	1.2°	1.7°
1	1	1	40.0	40.0	40.0
2	2	1	24.3	23.3	22.6
2	1	2	24.1	23.5	23.2
3	3	1	21.1	19.3	18.3
4	2	2	16.8	15.4	14.6
6	3	2	15.4	13.6	12.5
8	4	2	15.0	13.0	11.9

a) 1.5 by 1.5 Antenna
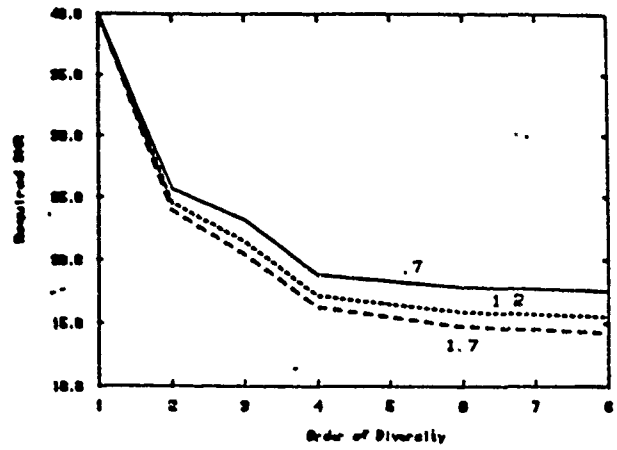
b) 3m by 3m Antenna
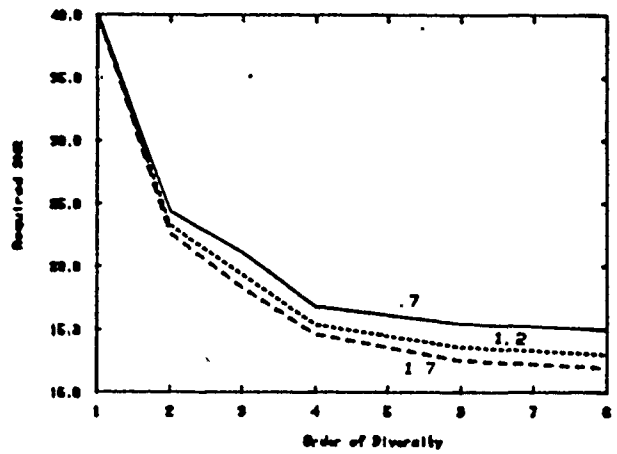
c) 6m by 6m Antenna
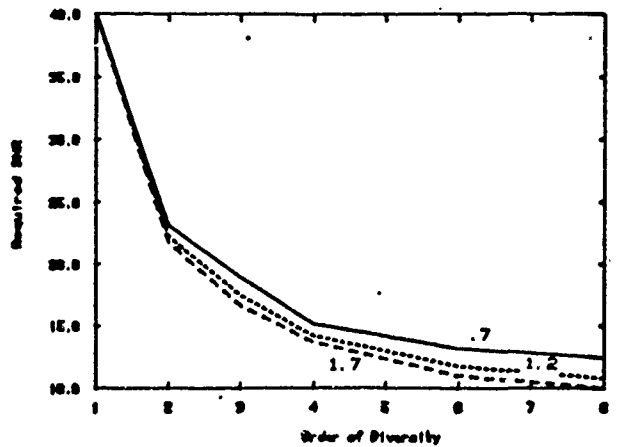
Figure 4-5   Diversity Performance of Different Aperture Sizes.   Each Plot
Contains Curves for Minimum Scattering Angles of .7°, 1.2°,
and 1.7°.

4-22

subdivision of the array. The element outputs within each subarray are summed and phase shifts applied to each subarray. The number of subdivisions in a given dimension must be at least as large as the number of beams desired. For instance, if three beams with different boresight elevations are desired then the array must be divided into three sections which are spaced vertically.

Subdivision of the array causes performance to degrade because the element outputs within each subarray are not exactly in phase. Hence when they are summed some loss in power occurs. This decreases the boresight gain of the beams which are not perpendicular to the array. In Figure 4-6 this effect is illustrated for a 3 beam system. Note that the main lobes of the beams formed by subarrays have lower gain than those formed by the array elements. The sidelobes of the gain patterns formed from subarrays are much higher than those formed by the elements. This effect is due to the small number of subarrays. These sidelobes may make a system employing subarrays more susceptible to jamming. So greater subdivision of the array or tapering of the subarrays may be important to improve ECCM capabilities.

For most of the results here we consider the diversity performance of arrays which are not subdivided. In this way the benefit of diversity alone is determined without effects due to implementation.

The performance of systems employing subdivision of the receiver array has been evaluated for 3m x 3m antennas with transmitter and receiver horizon angles of .25°. For each system the arrays are divided into the minimum number of subarrays permissible for the beams desired. The results are presented in Table 4-9 along with the values for undivided arrays. The path loss is determined by the case without diversity so it is the same for divided and undivided array systems. As expected the subdivided

4-23
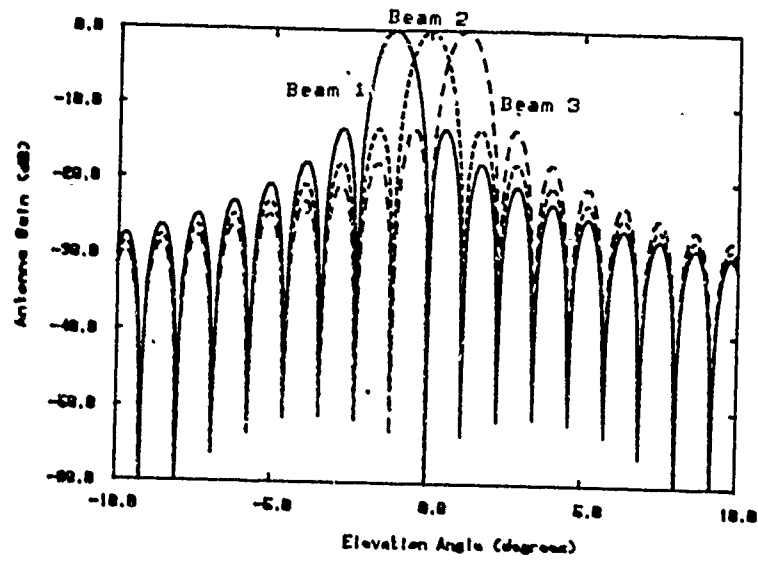
(a) undivided array
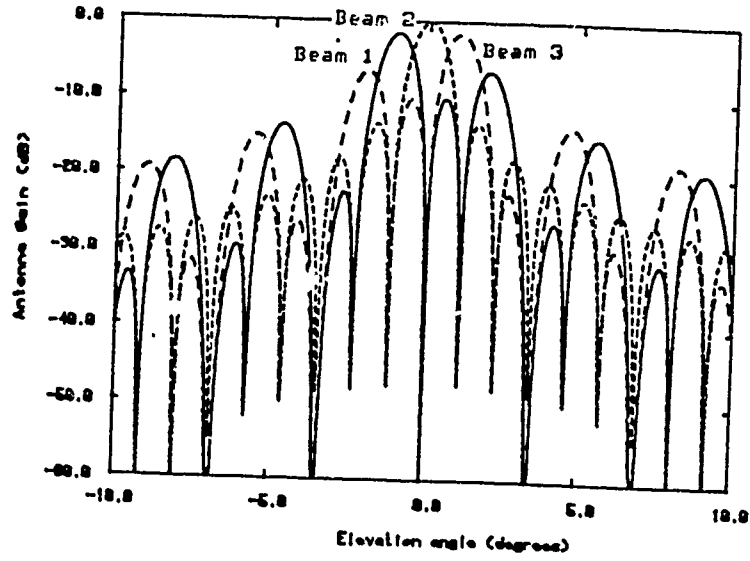
(b) array divided into three subarrays

Figure 4-6   Comparison of Three Elevation Beams Formed by (a) Applying
Phase Shifts to Element Outputs (No Subdivision of Array),
(b) Dividing the Array into Three Subarrays whose Outputs
are Shifted to Form Beams.

Table 4-9

Diversity Performance when the array is divided into subarrays. (The largest possible subarrays are used for each diversity type.) Link distance 100 km, scattering angle 1.2°, 3m antennas.

Order of Diversity	Elevation Beams	Azimuth Beams	Required SNR (dB)		Loss Due to Use of Subarrays
			Subarrays	No Subarrays	
1	1	1	40.0	40.0	--
2	2	1	23.6	23.3	.3 dB
2	1	2	23.7	23.5	.2 dB
3	3	1	19.8	19.3	.5 dB
4	2	2	15.9	15.4	.5 dB
6	3	2	14.3	13.6	.7 dB
8	4	2	13.8	13.0	.8 dB

arrays do not perform as well. However the performance loss is very small relative to the reduction in complexity. If a more complex system is permissible then a greater improvement in required SNR results from increasing the order of diversity rather than increasing the number of subarrays.

4.5   EFFECTS OF ELEVATION ANGLES

The results of previous sections are derived under the assumption that the antenna elevation angles above the horizon are chosen optimally. This is not possible in practice since atmospheric changes affect the radio horizon, and in addition small pertubations are present due to wind and other factors. The robustness of a system against these problems may be examined by varying the elevation angle. Figure 4-7 is a graph of required SNR vs. elevation angle for some different diversity systems. (The SNR is that which would be observed by a single diversity system with the optimum elevation.) The elevation angles of the transmitter and receiver antennas vary together. This data is for a 100 km link, 6m by 6m antennas and 1.7° scattering angle.

The systems degrade in roughly the same manner as the elevation angle varies about its optimum point. Systems with more elevation beams are affected somewhat less, e.g., a pertubation of $\pm$ .2° degrades a system with three azimuth beams by 1.5 dB and the degradation for three elevation beams is only 1dB. Overall this effect is small compared to the diversity gains.

4.6   EFFECT OF APERTURE SHAPE

The common volume is affected by the shapes of the antenna beams, and these are determined by the shapes of the antenna apertures. To determine the significance of this effect we have determined the performance of a number of rectangular apertures
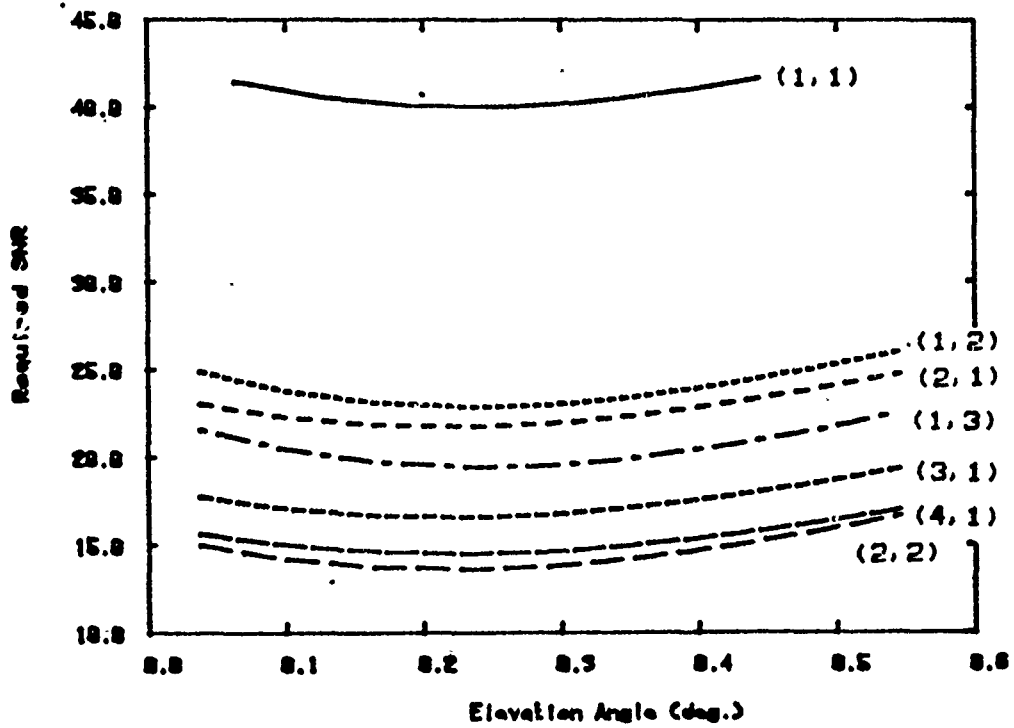
Figure 4-7   The Effect of Antenna Elevation Angles Above the
            Horizon for Various Diversity Systems. Diversity
            specified by (# of Elevation Beams, # of Azimuth
            Beams). (The product of these two numbers is the
            order of diversity.)
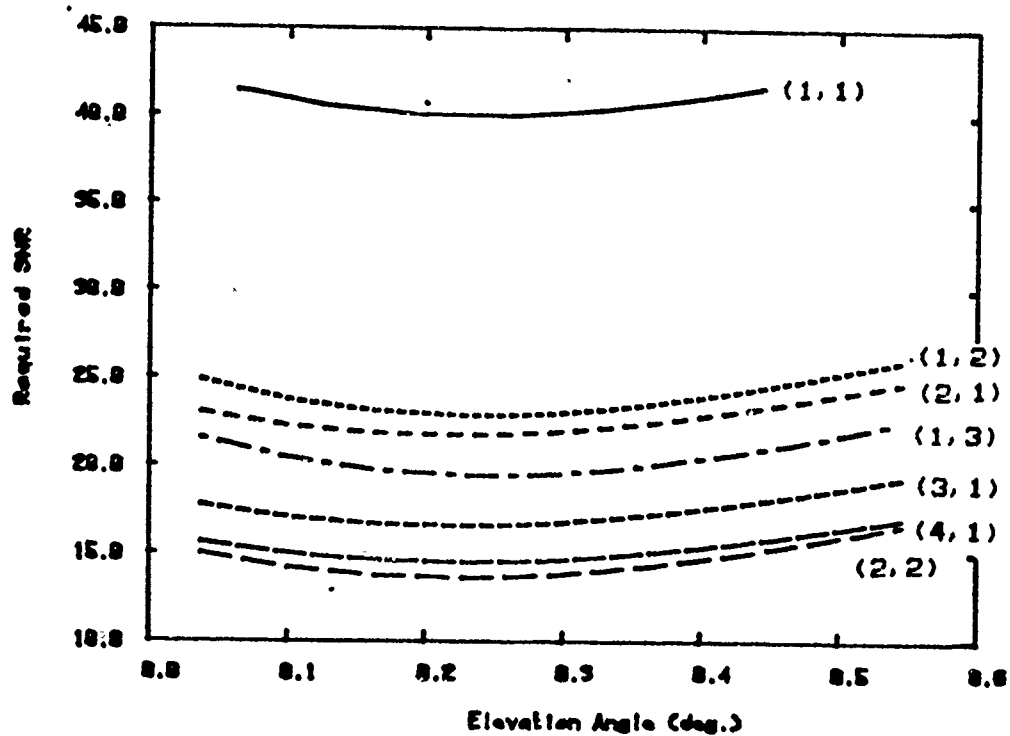
Figure 4-7   The Effect of Antenna Elevation Angles Above the
              Horizon for Various Diversity Systems.   Diversity
              specified by (# of Elevation Beams, # of Azimuth
              Beams).   (The product of these two numbers is the
              order of diversity.)

with different horizontal and vertical dimensions. The area of the arrays is fixed, so the boresight gain is the same for all cases. We define an asymmetry parameter

$$\zeta = \log\left(\frac{L_v}{L_h}\right)$$

where L_v and L_h are the vertical and horizontal array dimensions of the transmit and receive antennas. (The area, $L_v L_h$, is fixed.)

As L_v increases the antenna beams become narrow in elevation and broad in azimuth. The two factors which determine the best ratio of L_v to L_h are the scattering angle and the size of the common volume. As the beam becomes narrow the common volume increases. For example if L_h is doubled and L_v halved for both antennas then the area of the common volume which intersects the great circle plane increases by a factor of four. The extent of the common volume in azimuth (i.e., perpendicular to the great circle plane) is only halved so the common volume increases by a factor of two. This effect is offset because the additional common volume elements have larger scattering angles and the common volume integral includes a factor of $\theta^{-11/3}$ where θ is the scattering angle. The scattering angle does not increase as rapidly with increasing azimuth angles.

Figure 4-8 illustrates the effect of asymmetry on the required SNR (for $\phi_0 = 10^{-4}$) for a number of diversity systems. The link distance is 100 km, the antennas have areas of 36 m^2, and the scattering angle is 1.7°. The receiver and transmitter antennas have the same shape. The SNR here is that which would be measured by a single diversity system employing a square array. The effect of asymmetry is relatively small compared with
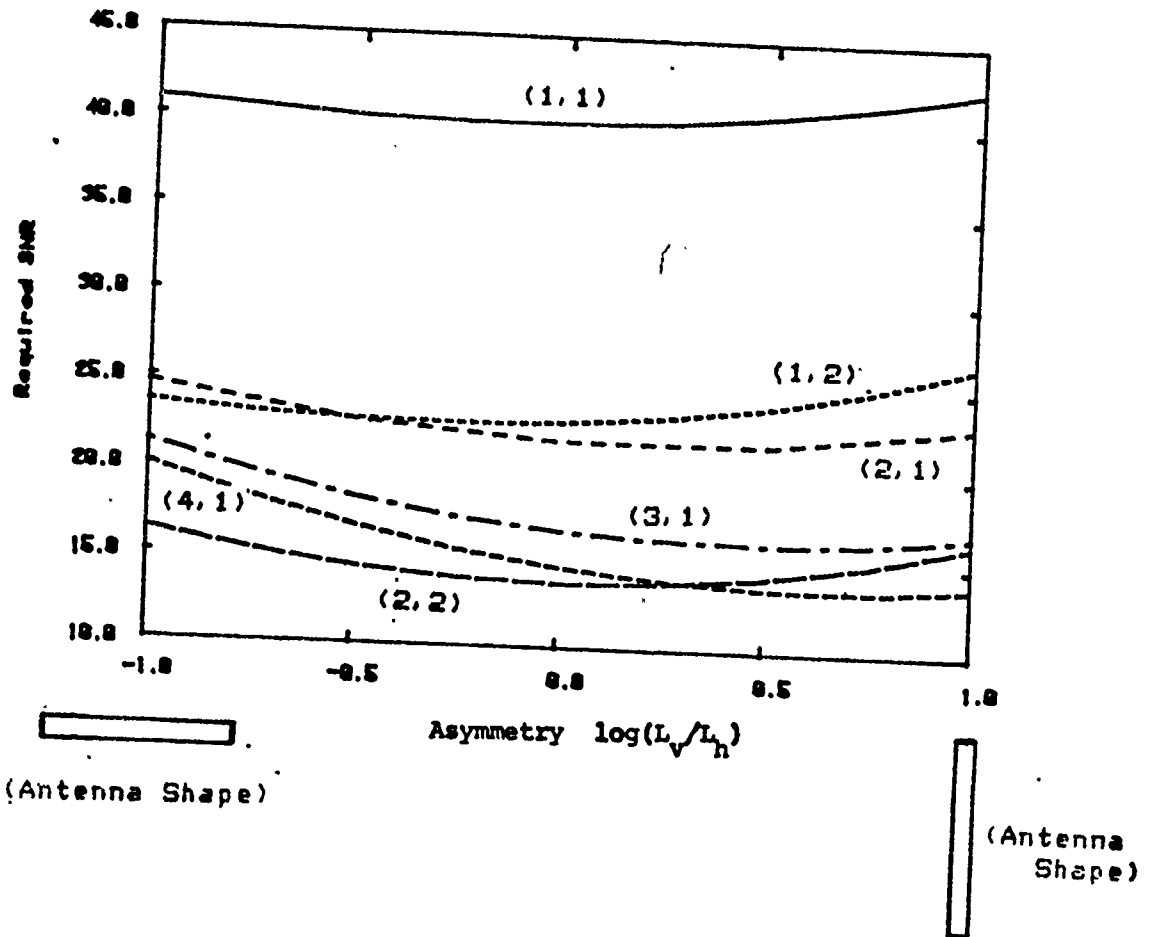
Figure 4-8   Effect of Asymmetry on Various Diversity Systems.
Diversity Specified by (# of Elevation Beams,
# of Azimuth Beams).

diversity gains. Systems with many elevation beams tend to perform better with wide azimuth beams (positive asymmetry), whereas azimuth diversity systems are better with narrow azimuth beams. In both cases the atmospheric volume illuminated by the various receiver beams is roughly square.

If we consider the systems in terms of the largest subarrays which give the same basic beam patterns (under a Butler matrix transformation) then the resultant subarrays are nearly square. Thus, an optimum diversity system should be formed by arranging the desired number of square subarrays.

SECTION 5
COMPARISON OF DIVERSITY COMBINERS

5.1   INTRODUCTION

Thus far we have compared diversity systems under the assumption that the signals on the diversity branches are combined optimally using a maximal-ratio combiner.   It is of interest to examine the effect of sub-optimal combining techniques on diversity gains both to allow comparison with existing systems and also to see if less complex combiners may be used with little loss in performance.   We assume that the signals on the diversity branches are independent and have equal power. This assumption is conservative since with unequal powers on diversity ports the difference between various combining techniques is generally less.

As previously mentioned the optimal combiner is a maximal-ratio combiner.   This combiner multiplies each fading signal by its complex conjugate so the signals are added in-phase and the larger ones have bigger weights.   One sub-optimal combiner is selection diversity where the strongest of the N fading signals is selected.   Another sub-optimal combiner selects the strongest K of the N signals and combines these using a maximal-ratio combiner.   The final method which we consider is the equal-gain combiner where the signals are added in-phase but with the same gains.

For the first three combiners we compute the exact probability of error expression (DPSK modulation).   Note that selection diversity and maximal ratio combining are special cases of "K of N" combining, with $K=1$ and $K=N$.   The exact performance of the equal gain combiner is difficult to compute.   However, a simple approximation may be derived for low error rates.

The results of these calculations are presented in Table 5-1 for a bit-error rate of 10^{-4}. Selection (or switch) diversity is 1.5 dB worse than maximal-ratio combining for dual diversity and is 4.5 dB worse at sixth order. This is a significant loss since the difference between an optimal fourth order system and an optimal sixth order system is only 3.7 dB. Choosing the best 2 of N is about 2 or 2.5 dB better than selection diversity so for a fourth order system choosing the best 2 is only 1.0 dB worse than combining all four. Similarly if the best 4 of 8 ports are combined the required SNR is only 1 dB above the optimum. Equal gain combining performs almost as well as maximal ratio combining. Even at 12th order diversity the difference is only 1.2 dB. This is an important result since phased arrays already have variable phase shifters in order to steer the beam. So an equal gain combiner might be significantly simpler to implement with a phased array.

5.2 MAXIMAL RATIO DIVERSITY COMBINING

The output of any combiner is a linear combination of the N diversity signals, so that the signal-to-noise ratio at the output of the combiner is of the form

$$\rho = \frac{\left| \sum_{i}^{N} W_i A_i e^{j\phi_i} \right|^2}{\sum_{i}^{N} W_i^2 \overline{n_i^2}}$$

where A_i is the amplitude of the i'th signal, ϕ_i is its phase, $\overline{n_i^2}$ is the average noise power in the i'th diversity branch and W_i is a proportionality constant (weight) to be determined so as to maximize ρ. It should be clear that for any choice of the magnitude of the W_i's, ρ will be maximum when all N signals are combined in phase. Furthermore from the Schwartz inequality we know that

Table 5-1

Comparison of Required SNR for BER = .0001
(DPSK Modulation) for Various Combining Techniques

Order of Diversity (N)	Required SNR for Maximal-Ratio Combiner (dB)	Loss Relative to Maximal-Ratio Combiner (dB)			
		Switch Diversity	Best 2 Of N	Best 4 Of N	Equal Gain Combiner (Approximate)
1	37.0	0	--	--	0
2	18.4	1.5	0	--	0.6
3	12.1	2.5	0.6	--	0.9
4	8.7	3.4	1.0	0	1.0
5	6.5	4.1	1.7	0.2	1.0
6	5.0	4.5	2.1	0.4	1.1
8	2.8	5.4	2.9	1.0	1.2
10	1.3	6.1	3.5	1.4	1.2
12	0.1	6.7	4.1	1.9	1.2

$$\rho = \frac{(\sum_i W_i A_i)^2}{\sum_i W_i^2 \overline{n_i^2}} \quad < \quad \sum_i \frac{A_i^2}{\overline{n_i^2}}$$

with equality occurring when $W_i = k\, A_i/\overline{n_i^2}$ where k is an arbitrary constant. Therefore the signal-to-noise ratio at the output of the combiner is maximum when the W_i are chosen as indicated above and the optimum signal-to-noise ratio ρ_{opt} is given by

$$\rho_{opt} = \sum_i \frac{A_i^2}{\overline{n_i^2}} = \sum_{i=1}^{N} \rho_i$$

i.e., it is the sum of the SNR in each diversity branch. Since the ρ_i are independent and exponentially distributed, the probability density of ρ_{opt} is given by

$$P(\rho_{opt}) = \frac{1}{\rho} \left(\frac{\rho_{opt}}{\rho}\right)^{N-1} \frac{e^{-\rho_{opt}/\rho}}{(N-1)!} \quad , \quad 0 < \rho_{opt} < \infty .$$

5.3 TRADEOFFS BETWEEN MAXIMAL-RATIO COMBINING AND SWITCH DIVERSITY

Consider a system with N diversity ports. The optimum receiver does maximal-ratio combining of all of the N outputs. One suboptimal combining method is to take the best K (K<N) of the diversity ports and combine these optimally. The best subset of the N ports changes as the channel fades. We assume here that the fading process is slow relative to the time necessary to select the best K ports. In an actual implementation the receiver might consist of K receivers which may be connected to any of the N ports using RF switching, and a measurement receiver

5-4

which examines the power on the other ports. When the power on one of the unused ports becomes greater than the smallest of the K currently being combined, the receiver on the lowest power port is switched over to the new port. The weight used for the new port in the maximal-ratio combiner is initially zero so that it adapts slowly without affecting the system performance.

In this subsection we compare the performance of systems for various N and K. We assume that the N diversity ports have equal power and fade independently. The delay spread of the channel is assumed to be small relative to the system signaling interval so that the signals are well described by a Rayleigh fading model.

The modulation is assumed to be DPSK so the error rate is

$$P_e = \frac{1}{2} e^{-\alpha}$$

where α is the signal-to-noise ratio. The distribution of the SNR thus determines the average bit-error-rate and the outage probability for any given theshold. The SNR distribution may be derived as follows.

The system SNR is simply the sum of the K largest powers of the N diversity branches (maximal-ratio combining). The power on each diversity branch is exponentially distributed. Let $\{Z_i,$ $i=1, \ldots, N\}$ be the powers on the N branches. The (N-K)th smallest of the Z_i is denoted $Z_{(N-K)}$ (that is, the largest one not combined). It has the density function [14]

$$q_{N-K}(x) = \frac{N!}{K!(N-K-1)!} (1-e^{-x})^{N-K-1}(e^{-x})^{K+1}$$

and the cumulative distribution function

$$Q_{N-K}(x) = \sum_{i=N-K}^{N} \binom{N}{i}(1-e^{-x})^{i}(e^{-x})^{n-i}.$$

This is the $(N-K)$th order statistic. (For simplicity we assume that the Z_i have unit power. They may be scaled later by their actual power.) Since the Z_i are exponentially distributed the difference between one of the K largest and $Z_{(N-K)}$ is also exponentially distributed with unit variance and is independent of $Z_{(N-K)}$. Thus, the sum of the K largest has the same distribution as

$$Z \overset{\Delta}{=} KZ_{(N-K)} + \sum_{i=1}^{K} Y_i$$

where the Y_i are independent unit-variance exponentially distributed random variables. The probability density function of $Y \overset{\Delta}{=} \sum_{i=1}^{K} Y_i$ is

$$p_Y(x) = \frac{x^{K-1}}{(K-1)!} e^{-x}$$

so the density of Z is the convolution of q_{N-K} and p_Y; that is

$$f_{N,K}(\alpha) = \int_0^\alpha q_{N-K}\left(\frac{x}{K}\right)p_Y(\alpha-x)\ dx.$$

5.3.1 Average Bit-Error-Rate

The average bit-error-rate is

$$\text{ABER} = \int_0^\infty P[\text{SNR}=\alpha]P[\text{Error}|\text{SNR}=\alpha]\ d\alpha.$$

For DPSK, we have

$$P[\text{Error}|\text{SNR}=\alpha] = \frac{1}{2}e^{-\alpha\sigma},$$

where σ is the average SNR per diversity branch, and

$$P[\text{SNR}=\alpha] = f_{N,K}(\alpha)\ .$$

So

$$\text{ABER}(N,K,\sigma) = \frac{1}{2}\int_0^\infty f_{N,K}(\alpha)e^{-\alpha\sigma}\ d\alpha$$

$$= \frac{1}{2}\int_0^\infty \int_0^\alpha q_{N,K}\left(\frac{x}{K}\right)p_\gamma(\alpha-x)dx\ e^{-\alpha\sigma}\ d\alpha$$

$$= \frac{1}{2}\int_0^\infty q_{N,K}\left(\frac{x}{K}\right)\int_x^\infty e^{-\alpha\sigma}\ p_\gamma(\alpha-x)d\alpha\ dx$$

where the last step follows by interchanging the order of integration. These integrals may be computed directly. The result is

$$ABER(N, K, \sigma) = \frac{1}{2} \frac{1}{(\sigma+1)^K} \cdot \frac{1}{1+\frac{K\sigma}{K+1}} \cdot \frac{1}{1+\frac{K\sigma}{K+2}} \cdots \frac{1}{1+\frac{K\sigma}{N}} .$$

The loss due to combining the best K of N ports relative to combining all N ports may be seen directly from this formula. The slope of the BER for large σ is the same since the denominator increases as σ^N. The first K factors in the expression are the same as those for maximal-ratio-combining (N=K). The factors after these K have their SNRs reduced by increasing amounts. The (K+1)st one is reduced by $\frac{K}{K+1}$, the next by $\frac{K}{K+2}$, etc. For large SNR the required increase in SNR for the same BER if we combine only K of the ports is approximately

$$\frac{\sigma_{K,N}}{\sigma_{MRC}} \approx \left(\frac{N!}{K!} K^{N-K}\right)^{1/N} .$$

We have computed the required input SNR (i.e., the required σ) to give an ABER of 10^{-4} for a number of different N and K. The results are presented in Table 5-2 and Figure 5-1. The results show that a significant reduction in complexity may be realized with only a small loss in performance. For instance, the required SNR for 8th order maximal-ratio combining (N=8, K=8) is 2.8 dB. If the best 4 of the 8 ports are used (N=8, K=4) then the required SNR increases by only 1 dB. These factors are almost exactly the same as those given by the asymptotic formula above for large SNR.

Table 5-2

Required Input SNR to Achieve ABER=10^{-4} (BPSK) for Various N and K.
(N is the number of diversity ports, the best K of which are combined optimally.)

K (# of ports combined optimally)

N (# of ports)	1	2	3	4	5	6	7	8	9	10	11	12
1	37.0											
2	19.9	18.4										
3	14.6	12.7	12.1									
4	12.1	9.7	9.0	8.7								
5	10.6	8.2	7.2	6.7	6.5							
6	9.5	7.1	6.0	5.4	5.1	5.0						
7	8.8	6.3	5.1	4.5	4.1	3.9	3.8					
8	8.2	5.7	4.5	3.8	3.3	3.0	2.9	2.8				
9	7.8	5.2	4.0	3.2	2.7	2.4	2.2	2.0	2.0			
10	7.4	4.8	3.5	2.7	2.2	1.8	1.6	1.4	1.3	1.3		
11	7.1	4.5	3.2	2.4	1.8	1.4	1.1	0.9	0.8	0.7	0.7	
12	6.8	4.2	2.9	2.0	1.5	1.0	0.7	0.5	0.3	0.2	0.2	0.1
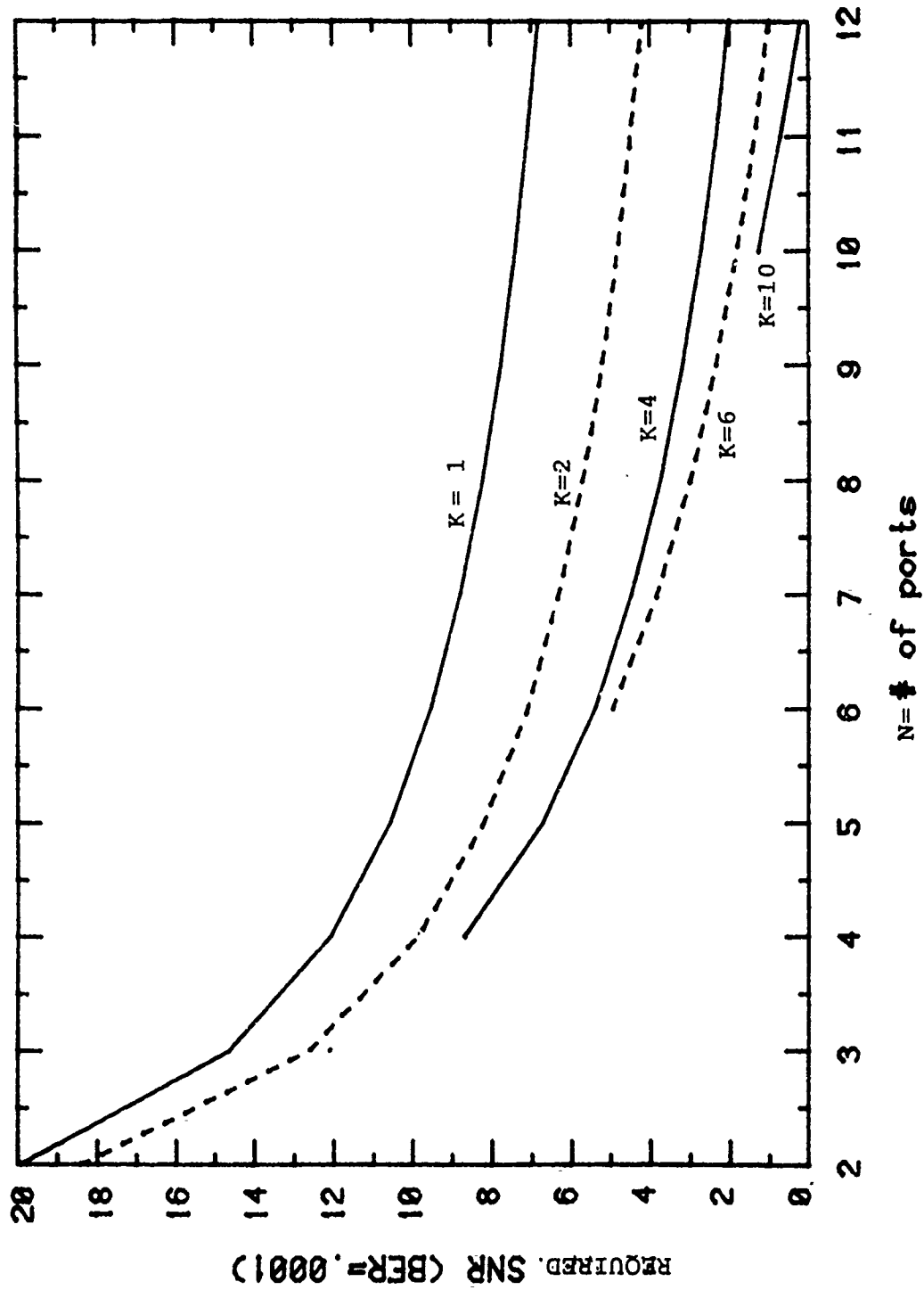
Figure 5-1 Required SNR to achieve ABER = 10^{-4} for various N and K.

The results also show that maximal ratio combining of a few of the ports is significantly better than switch diversity. A 4th order system with K=2 performs as well as a 6th order switch diversity system (K=1). Also, a 5th order system with K=2 performs better than a 4th order maximal-ratio combining system.

If the cost of a system is proportional to (N+K) then a combination of switch diversity and maximal-ratio combining is the most economical solution. If, on the other hand, the cost of diversity branches (antennas, etc.) is significantly greater than the down converters and combiner, i.e., cost proportional to N+γK, where γ is small, then maximal-ratio combining should be used. If the cost imbalance is reversed then switch diversity is the most economical solution. In general, if the cost goes as N+Kγ then the best system may be chosen by comparing the required SNR's for various N and K which have the same cost. For example, if the cost is N+K, then for cost=6, we may choose [N=5, K=1], [N=4, K=2], or [N=3, K=3]. Since the required SNR's are 10.6, 9.7, and 12.1 respectively (from Table 5-2), we see that [N=4, K=2] is best.

5.3.2 Outage Probability Calculation

The outage probability, that is, the probability that the SNR falls below a threshold, is determined by the cumulative distribution of the SNR. This cumulative distribution is most easily derived by convolving the cumulative distribution of $Z_{(N-K)}$ with the density of Y. That is,

$$F_{N,K}(\alpha) \triangleq P[Z < \alpha]$$

$$= \int_0^\alpha Q_{N-K}\left(\frac{x}{K}\right) p_Y(\alpha - x) dx.$$

The result of this integral is

$$F_{N,K}(\alpha) = \sum_{i=N-K}^{N} \binom{N}{i} e^{-\alpha} \sum_{j=0}^{i} \binom{i}{j} G(N,K,i,j,\alpha)$$

where

$$G(N,K,i,j,\alpha) \triangleq \begin{cases} e^{-\alpha\gamma}\gamma^{-K} - \displaystyle\sum_{\ell=0}^{K-1} \frac{\alpha^{K-1-\ell}}{(K-1-\ell)!\,\gamma^{\ell+1}} & ; \quad \gamma \neq 0 \\ \\ \dfrac{1}{K!}\,\alpha^{K} & ; \quad \gamma = 0 \end{cases}$$

and

$$\gamma \triangleq \frac{K-N+i-j}{K} \; .$$

This expression may be used directly to calculate outage probabilities for any given threshold. If the threshold is λ and the average SNR on each diversity branch is σ then the outage probability is $F_{N,K}(\frac{\lambda}{\sigma})$. The threshold is divided by σ because $F_{N,K}$ is derived assuming unit variance exponential random variables.

5.4 EQUAL GAIN DIVERSITY COMBINING

The SNR at the output of an equal gain combiner is

$$\rho = \frac{\left(\displaystyle\sum_{i=1}^{N} A_i\right)^2}{N\,\overline{n^2}}$$

where A_i is the amplitude of the i-th signal and $\overline{n^2}$ is the average noise power. The amplitude A_i is Rayleigh distributed, i.e., its density is

$$p_{A_i}(x) = \frac{2x}{\alpha}\, e^{-x^2/\alpha}\, ,$$

where $\alpha/\overline{n^2}$ is the SNR on each diversity branch. If

$$Z \triangleq \sum_{i=1}^{N} A_i$$

then for small arguments the density of Z is

$$p_Z(x) \approx \frac{2^N\, x^{2N-1}}{(2N-1)!\ \alpha^N}\, .$$

Similarly if W is the output of a maximal ratio combiner we have

$$p_W(x) = \frac{x^{N-1}}{(N-1)!\ \alpha^N}\, e^{-x/\alpha}$$

$$\approx \frac{x^{N-1}}{(N-1)!\ \alpha^N}$$

for small x.

The outage probability, i.e., the probability that the gain falls below a fixed level ρ_0) for the equal gain combiner is

$$P_{out} = P\left[\rho < \rho_0\right]$$

$$= P\left[Z < N\,\overline{n^2}\,\rho_0\right]$$

$$= \int_0^{N\,\overline{n^2}\,\rho_0} p_Z(x)\,dx$$

$$\approx \frac{2^N(N\,\overline{n^2}\,\rho_0)^N}{(2N)!\;\alpha^N} \quad .$$

Similarly, for the maximal-ratio combiner

$$P_{out} \approx \frac{(\overline{n^2}\,\rho_0)^N}{\alpha^N\,N!} \quad .$$

So the ratio of the equal-gain combiner input SNR's $\left(\alpha/\overline{n^2}\right)$ to that of the maximal-ratio combiner is

$$\frac{\alpha_{EGC}}{\alpha_{MRC}} = \frac{2N}{(2N)!^{1/N}}\,(N!)^{1/N} \quad .$$

Since this ratio does not depend on the threshold ρ_0 the same ratio applies if the performance criterion is the average bit-error rate.

As a check on the accuracy of this approximation the same procedure may be applied to selection diversity. With selection diversity the output SNR is

$$\rho = \max_{i} \frac{A_i^2}{\overline{n^2}}$$

and

$$P_E = P\left[\rho < \rho_0\right]$$

$$= \left(1 - e^{-\rho_0/\alpha}\right)^N$$

so we have

$$\frac{\alpha_{SEL}}{\alpha_{MRC}} = (N!)^{1/N} .$$

Table 5-3 presents the approximate increase in required SNR for both equal-gain and selection combiners at low error rates and the actual increase for selection combiners at BER = 10^{-4} from the previous section. The equal-gain combiner performs only slightly worse than the maximal-ratio combiner. Selection diversity is significantly worse than equal-gain combining. Although these results are for asymptotically low error rates the actual values for BER = .0001 are within .2 dB for N < 5 and within .5 dB for N < 12. So even at an error rate of .0001 the approximation is good.

Table 5-3

Increase in required SNR at a given error rate if equal-gain or selection combining is used instead of maximal-ratio combining. Approximation is accurate for asymptotically small error rates.

Order of Diversity	Additional SNR required (relative to maximal-ratio combiner)		
	Equal Gain Combiner (Approximate)	Selection Diversity	
		Approximate	Actual BER = .0001
1	0	0	0
2	.62	1.5	1.5
3	.85	2.6	2.5
4	.97	3.5	3.4
5	1.04	4.2	4.1
6	1.09	4.8	4.5
7	1.12	5.3	5.0
8	1.15	5.8	5.4
9	1.17	6.2	5.8
10	1.18	6.6	6.1
11	1.20	6.9	6.4
12	1.21	7.2	6.7

SECTION 6
EFFECTS OF TIME-VARYING PARAMETERS

We show in this section that wideband systems are not severely limited by typical troposcatter fade rates. The loss caused by inaccurate channel measurements can be held to less than 0.5 dB for a 1 Mbps system. In Section 6.3, the optimum use of diversity on a fading channel is derived and it is shown that diversities with SNR below a critical value, ϕ_A, are not used by the optimum combiner; ϕ_A depends on data rate, channel fade rate, and SNR.

6.1   FADE RATE LIMITATION ON CHANNEL GAIN MEASUREMENT

Thus far we have assumed that the channel gains vary so slowly that they may be measured exactly by the receiver. In this section we instead assume that estimates of the channel gains are made by averaging K reference pulses. The number K is determined by the channel coherence time, the data rate, and the percentage of reference pulses.

We consider a combiner which weights each of the diversity branch outputs by the conjugate of its estimated channel gain. This combiner is not optimum, since the channel gains are not known exactly, but as K becomes large its performance approaches that of a maximal-ratio combiner.

In Appendix C, an upper bound ϕ_0 on the error rate for this combiner is shown to be

$$\phi_0 = \left| f(K)I_N + g(K)M_G/N_0 \right|^{-1}$$

6-1

where M_G is the covariance matrix of the channel gains,

$$f(K) = \frac{K+1+1/K}{K+2+1/K}$$

$$g(K) = \frac{1}{1+1/K}$$

$$I_N = (NxN) \text{ identity matrix,}$$

and N_0 is the noise spectral density.
Equivalently we may write

$$\phi_0 = \prod_{i=1}^{N} \left[f(K) + g(K)\lambda_i/N_0 \right]^{-1}$$

where $\{\lambda_i\}$ are the eigenvalues of M_G. As K increases $f(K)$ and $g(K)$ approach 1, and the BER bound is the same as that for maximal-ratio combining.

6.2 PERFORMANCE DEGRADATION

Since the formulas for the performance criterion include the effective number of reference pulses K used in the measurement, it is helpful to have quantitative estimates of this number.

Typical troposcatter circuits can be assumed to communicate at least 1 Megabit/second in the absence of AJ protection. Data rates as high as 12 Mbit/sec are seen on some circuits. A transmission using 10% of the transmitted bits for reference is a plausible value, although possibly slightly excessive. This yields a rate of transmission of reference pulses of at least 10^5 bits/second for a 1 Mbit/sec data rate.

The number of reference pulses must be equivalent to the coherence time of the channel, i.e., the time interval over which the gains G_n (fading) remain constant. With typical troposcatter fade rates of a few Hz, a measurement bandwidth of a few tens of Hz is more than adequate to track the fading. A measurement duration of 10^{-2} seconds is therefore reasonable in the absence of airplane flutter or other high fluctuation rate effects. We conclude that if measurements can be made continuously on each port of the antenna system, then

$$K = 10^3$$

is reasonable for a 1 Mbit/sec system.

The value $K = 10^3$ in the formulas for the performance criterion will obviously give superb performance even with a very large number of adaptively controlled ports. We can overbound ϕ_0 by

$$\phi_0 \;<\; (1+1/K)^N \;\prod_{n=1}^{N}\; \left(1+\lambda_n/N_0\right)^{-1} \;.$$

For $K=1000$ a value of $N=100$ only results in a 10% increase in the error probability bound, and this is negligibly small. The weakness in this line of argument, however, lies in the implicit assumption that it is possible to measure the reference signal on each antenna port continuously and with the full SNR available from that port. This implicit assumption is only valid if there is separate RF amplification for every antenna port.

If it is desired to achieve adaptation on a large number of antenna ports, it is probably necessary to assume that a single "measurement receiver" is time-multiplexed among the outputs of directional couplers connected to the ports. If we make a real-

istic assumption that 10 dB couplers are used in this configuration, then the effective value of K is reduced by 10 because of the coupler loss. The multiplexing of the measurement among N ports then results in a further division of K by N, and the result is that we must use the value

$$K = 100/N$$

for the multiplexed measurement. If we then rewrite the bound

$$\phi_0 \quad < \quad (1+1/K)^N \prod_{n=1}^{N} \left(1+\lambda_n/N_0\right)^{-1}$$

to display its dependence on N, we have

$$\phi_0 \quad < \quad (1+N/100)^N \prod_{n=1}^{N} \left(1+\lambda_n/N_0\right)^{-1} \quad .$$

Let σ be the factor by which the eigenvalues must be increased to maintain the same error rate bound. Then we have

$$\prod_{n=1}^{N} \left(1+\lambda_n/N_0\right)^{-1} = (1+N/100)^N \prod_{n=1}^{N} \left(1+\sigma\lambda_n/N_0\right)^{-1} \quad .$$

If λ_n/N_0 is the same for all n, then

$$\sigma \approx 1+(N/100)\left(1+N_0/\lambda\right) \quad .$$

If $\lambda/N_0 = 1$ (0 dB input SNR per diversity branch) then with 6th order diversity this is a loss of .5 dB, and even with 25th order diversity the loss is only 1.8 dB. These losses are small compared to the diversity gains. If λ_n/N_0 is larger then the losses are even less. Significant losses occur only for

$$N > \min\left(1, \frac{\lambda}{N_0}\right) \cdot \frac{R}{B} \delta$$

where

    W =   data rate

    B =   Doppler spread

    δ =   duty factor for reference and measurement

We have assumed that all eigenvalues are the same, but if some are very small then the effective order of diversity is smaller than N and so the order of the system should be reduced. We conclude that channel measurement inaccuracy need not be a severe problem on most troposcatter systems. The next section shows that advanced processing can further reduce the limitations imposed by the channel fading.

6.3 OPTIMUM COMBINING WITH MEASUREMENT INACCURACIES

It is now shown with an optimum orthogonalizing transformation that only some of the diversity branches (eigenvalue) should be used by the optimum combiner. An example of the number of required measurements is evaluated.

6.3.1 Accessibility of Independent Fading Components

The following discussion is in the nature of determining theoretical limitations rather than defining practical implementations.

The basic scheme assumes that we have access to noisy fading replicas of the transmitted signal in the form

$$S_n(t) = G_n(t)z(t) + \nu_n(t)$$

either from the original array ports or from the output ports of a fixed linear transformation on the array ports. From these replicas we form the diversity-combined output

$$C(t) = \Sigma W_n(t) S_n(t)$$

where the $\{W_n(t)\}$ are adaptively computed from known reference pulses imbedded in $z(t)$.

In the previous section it was assumed that the measurements were performed on the individual $\{S_n(t)\}$, possibly by a multiplexed measurement. We also assumed that this might be done using an auxiliary measurement receiver that was connected to, say, directional couplers on each of the ports. We now describe a way in which the entire measurement procedure can <u>theoretically</u> be improved, and a consequent improvement that can be achieved in the diversity combining.

First of all, we observe that even with a fairly noisy measurement it is possible to "measure" the covariance matrix of the fading, which we recall was defined as

$$M_G = E\left(\overline{G}G'\right) .$$

Although this covariance matrix is not fixed for all time, its variations will tend to be at the slow rate associated with changing atmospheric conditions rather than the several Hz fluctuating rate of G . We therefore can theoretically compute the unitary matrix Q which diagonalizes M_G

$$Q' \, M_G \, \overline{Q} = \Lambda \, .$$

We next observe that since the diversity combining network can form $C(t)$ as a weighted combination of the $S_n(t)$, it can theoretically use different weights during the reference pulses, and form a linear combination

$$C(t) = \sum_n w_n \, S_n(t) \, .$$

In fact, it can use N different sets of weights and form N different linear combinations during N successive measurements to create a set of measurable signals

$$s_m(t) = \sum_n P_{mn} S_n(t)$$

which can be expressed more compactly in matrix form as

$$s(t) = P \, S(t)$$

where P is the $(N \times N)$ matrix with entries $\{P_{mn}\}$. Now, the covariance matrix of s is

$$M_s = E(\overline{s} s')$$

$$= E(\overline{P} \, \overline{S} \, S' P')$$

$$= \overline{P} \, E(\overline{S} S') P'$$

$$= \overline{P}(M_G + I_N) P' \, .$$

6-7

Consequently, if we choose P to be the previously calculated unitary matrix Q,

$$P = Q, P' = Q' = \overline{Q} ,$$

we have

$$M_S = \Lambda + I_N$$

so that we can display the independently fading components of S(t) in the measurement.

We note that this structure also implies that it is unnecessary to use an auxiliary receiver for measurement with its directional coupler loss. [Nevertheless it might be desirable to use such an approach from practical considerations.]

6.3.2 Improved Diversity Combining for Finite Measurement Time

Appendix D defines the performance criterion

$$\phi_0 = \underset{t>0}{\text{Minimum}} \quad \phi(t)$$

where

$$\phi(t) = 1/\underset{n}{\Pi} D_n(t)$$

with

$$D_n(t) = 1 + 2\lambda_n t - N_0 \left[\lambda_n (1+1/K) + N_0/K \right] t^2 .$$

We pointed out that, in general, the maximum of each $D_n(t)$ occurs at a different value of t and therefore it is not possible to evaluate the minimum explicitly.

This difficulty is a reflection of the fact that with noisy measurements, the fading components with very low SNR should be partially or completely suppressed in the combining algorithm. In the original problem formulation this was not possible because we didn't have access to these components. With the conceptual modification used here this restriction no longer applies, and it can be assumed that an additional (optimum) weighting is applied to the coherently weighted components before combining them. With that change, we can write the performance criterion as

$$\phi_0 = 1/\Pi_n \left[\underset{0 < t}{\text{Maximum}} \; D_n(t) \right]$$

to obtain

$$\phi_0 = 1/\Pi_n \left[1 + \frac{\rho_n}{1+1/K + 1/(K\rho_n)} \right]$$

where

$$\rho_n = \lambda_n/N_0 \; .$$

The expression can also be written as

$$\phi_0 = \Pi_n \frac{1 + (1+K)\rho_n}{1 + (1+K)\rho_n + K\rho_n^2} \; .$$

6.3.3 Apportionment of Measurement Times

The preceding results assume that the same measurement time is used for tracking each independently fading component. That

6-9

is, a fixed value of K is used for all components. The next level of generalization is to allow different values of K for each fading component. This leads to the performance criterion

$$\phi_0 = \prod_n \frac{1 + (1+K_n)\rho_n}{1 + (1+K_n)\rho_n + K_n\rho_n^2} \; .$$

This immediately suggests the variational problem of choosing the K_n to minimize ϕ_0 given a constraint on the total measurement time. The solution to this problem is

$$K_n = \begin{cases} 1/\rho_A - 1/\rho_n \; , & \rho_n > \rho_A \\ \\ 0 & , \quad \text{otherwise} \end{cases}$$

where the value of ρ_A is determined by the constraint. With this dependence of K_n on ρ_n we then have

$$K_{TOTAL} = \sum_{n:\rho_n>\rho_A} \left[\frac{1}{\rho_A} - \frac{1}{\rho_n} \right] \; ,$$

which implicitly defines ρ_A, and the diversity branches that should be included. The error bound is

$$\phi_0 = \prod_{n:\rho_n>\rho_A} \frac{1 + \rho_A}{1 + \rho_n} \; .$$

6-10

6.3.4 Error Probability in Terms of the Performance Criterion

The performance criterion we are using is a bound on the saddle-point integral that defines the error probability. Although there is not a one-to-one relation between the values of the bound and the exact error probability, it is possible to arrive at approximate relations that are sufficiently accurate for most system performance predictions. The most useful approximation of this sort is

$$\text{Prob(error)} \approx \frac{\phi_0}{[4+\pi b]^{1/2} + [\pi b]^{1/2}}$$

where

$$b = \frac{1}{2} s_0^2 L''(s_0)$$

and

$$s_0 = \text{value of } s \text{ that minimizes } \phi(s) \text{ ,}$$

$$L(s) = \log[\phi(s)] \text{ .}$$

Now, in many circumstances it is sufficiently accurate to approximate the logarithm of the moment-generating function by a parabola:

$$L(s) \approx -2C_1 s + C_2 s^2 \ .$$

The minimum of this is at

$$s_0 = C_1/C_2 \ .$$

where

$$L(s_0) = -C_1{}^2/C_2 \ .$$

Since

$$L''(s_0) = 2C_2$$

we then have

$$b = \frac{1}{2} (-C_1/C_2)^2 (2C_2)$$

$$= C_1{}^2/C_2$$

$$= -L(s_0)$$

$$= -\log(\phi_0) \ .$$

This leads to the approximation

$$P_e \approx \frac{\phi_0}{[4-\pi\log(\phi_0)]^{1/2} + [-\pi\log(\phi_0)]^{1/2}} \ .$$

It must be cautioned that this formula tends to underestimate the error probability at very large SNR when the number of eigenvalues is small.

SECTION 7
DIVERSITY PERFORMANCE OF WIDEBAND SYSTEMS

INTRODUCTION

Angle diversity improves troposcatter system performance because the signals from different sections of the common volume fade independently. The difference in angle of arrival of these signals makes different beams of an angle diversity antenna some-what uncorrelated.

Similarly, the spatial separation of scatterers leads to delay differences in signals received from the common volume. If the signals at different delays could be added coherently, then great gains in SNR could be achieved. Hence there is a potential for diversity to improve system performance. Such diversity is often called implicit since it is implicit in the received wave-form. The delay spreads seen on most troposcatter links typically range from 30 to 200 nsec. This corresponds to coher-ence bandwidths of 5 to 30 MHz. Frequencies separated by more than the coherence bandwidth fade independently while frequencies separated by an amount less than the coherence bandwidth fade in phase (correlated fading). That is, the implicit diversity in the channel may not be exploited if the signal bandwidth is much less than the channel coherence bandwidth because all frequency components in the signal will fade in a correlated manner. This is analogous to angle diversity systems, where very little diver-sity gain is possible if the antenna beamwidth is very large.

If the transmitted signal is wideband then it is possible to improve performance by utilization of the implicit channel diversity. A tapped delay line combiner may be used to ac-complish this task. It forms the weighted sum of signals at various delays. The weights are chosen adaptively in the same

manner as the weights of a maximal-ratio combiner are adjusted to combine the outputs of different antenna ports.

Because of the implicit diversity, a wideband system with equalization may perform better than a narrowband system. However, the channel also introduces distortion (intersymbol interference) which degrades the SNR relative to that of a narrowband system. Hence equalization is necessary in many cases to remove distortion. Since we are chiefly interested in diversity gains, we do not consider the problem of removing distortion. In particular, for the digital systems considered here we do not consider intersymbol interference (ISI). Although it may be difficult to remove ISI, it is possible via Viterbi decoding so this assumption is not unreasonable. All of the results which are presented here are for the one-shot case; that is, only a single pulse is transmitted.

One key difference between combining the signals from different antenna ports and combining delayed versions of the same signal is that in the former case the noise components are independent whereas in the latter case noise is correlated. The autocorrelation function of the noise is determined by the receiver filter. This generally reduces the effectiveness of delay combining since it is likely that the noise on two delay taps can be large at the same time.

To illustrate the effectiveness of implicit diversity, we present in Figure 7-1 the SNR gains of implicit diversity for various signal bandwidths and delay combiners. The results are graphed vs. σ/T for various numbers of taps, where σ is the channel delay spread, and T is the duration of the transmitted symbol. The SNR gain is relative to a narrowband system on the same link.

As σ/T increases the implicit diversity gains increase initially, but then decrease. The initial benefit is due to
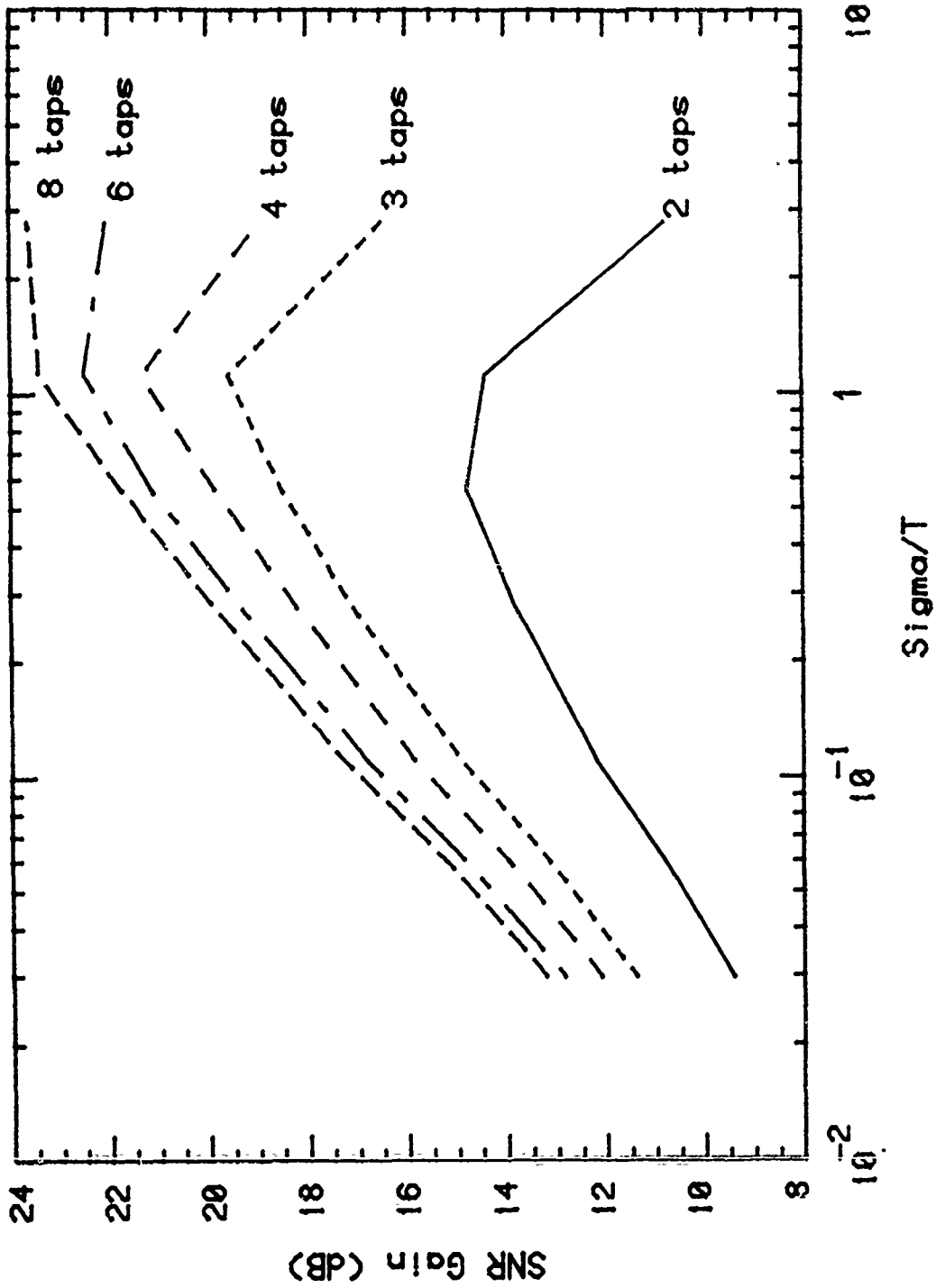
Figure 7-1 Time Diversity Gain vs. Channel-Delay-Spread-to-Pulse-Duration Ratio. (SNR for bit-error-rate = 0.0001.)

increased diversity. Eventually, however, the loss of signal power due to the spreading of the transmitted symbol offsets the diversity gain and the SNR gain decreases. The gain begins to decrease at higher σ/T as the number of taps increases.

The link used as an example is 100 km long and has a minimum scatter angle of 1.7°. The receiver and transmitter antenna apertures are 3 m. square and are aimed one quarter beamwidth above the horizon. This results in a delay profile with a 2σ delay spread of 56 nsec. The shape of the channel delay profile is insensitive to variations in the link parameters. The major effect of changing link distance or scatter angle is to change the delay spread. If the pulse durations are changed in a similar manner then the same results are observed. So σ/T, the ratio of the pulse duration to the channel delay spread determines the benefit of diversity for a particular system and link.

In Section 7.1 we discuss the wideband troposcatter channel model. In Section 7.2, the wideband system model and the performance measure are considered. Section 7.3 contains calculated results for delay combining of systems with and without explicit diversity.

The results may be summarized as follows: Equalization yields significant gains for wideband systems without diversity. (We call a system "wideband" if the pulse duration is not much greater than the channel delay spread.) For wideband systems with diversity a two-tap delay combiner (i.e., "dual implicit-diversity") can improve performance significantly. In fact a dual angle diversity system with two delay taps on each port performs nearly as well as a fourth-order angle diversity system. In general, more than two taps are of little help for wideband systems with explicit diversity. While implicit diversity is helpful in many situations, the gains are not as large as those for angle diversity.

7.1 TROPOSCATTER CHANNEL MODEL FOR WIDEBAND SIGNALS

In a troposcatter system the received signal is the sum of a large number of scattered signals. These scattered signals arrive at the receiver with small relative delays, so the channel impulse response is spread over some time interval. For a narrowband system the transmitted waveform changes very little over this interval so the channel statistics are given by Rayleigh fading. The transmitted waveform changes slowly enough that the channel impulse response does not affect the shape of the waveform but only its amplitude. With wideband signals, however, the relative delays of the scattered signals must be taken into account. The symbol duration is short enough that the channel causes significant distortion.

Consider a system without explicit diversity. If s(t) is the transmitted signal then the received signal r(t) is

$$r(t) = \int_{-\infty}^{\infty} s(\tau)h(t-\tau)d\tau$$

where the channel impulse response, h(t), is a zero-mean random process with complex Gaussian statistics. The impulse response at two different times is independent, and it is non-zero only in an interval $[0, \tau_m]$, where τ_m is the maximum difference in delays of signals from the common volume. So the channel statistics are completely determined by the second moment of h(t)

$$E[h(t)h^*(\tau)] = \delta(t-\tau)Q(t).$$

(The real and imaginary parts of h(t) are independent and identically distributed.) The function $Q(t)$ specifies the incremental power which arrives in the time interval $[t,t+dt]$, hence it is called the delay-power profile. The TROPO computer program computes a discrete approximation to $Q(t)$ by determining the relative delay of each element of the common volume and adding the signal from the element to a particular delay cell of the profile.

In Figure 7-2a an example of a delay-power profile is given. This profile is for a 100 km link with a 1.7° scattering angle and has 2σ delay spread of 56 nsec. Figure 7-2b and 7-2c are possible impulse responses which correspond to this delay profile. These curves are actually discrete approximations to the channel impulse response, but for transmitted signals which vary little from sample to sample the approximation is adequate to characterize the channel. Each point of the impulse response curves is a Gaussian random variable with variance given by the value of the delay profile.

Next, consider systems with N explicit diversity ports. If $r_k(t)$ is the k-th received signal, then

$$r_k(t) = \int_{-\infty}^{\infty} s(t)h_k(t-\tau)dt$$

where $h_k(t-\tau)$, the impulse response of the channel between the transmitter and the k-th receiver, is a complex Gaussian process. The impulse responses $h_k(\tau)$ and $h_\ell(\tau)$ are correlated for all k and ℓ since they are derived from the same scatterers, whereas $h_k(t)$ and $h_k(\tau)$ are independent for $\tau \neq t$. So the channel statistics are specified by the second order statistics of $\{h_k(t), k=1,\ldots N\}$,
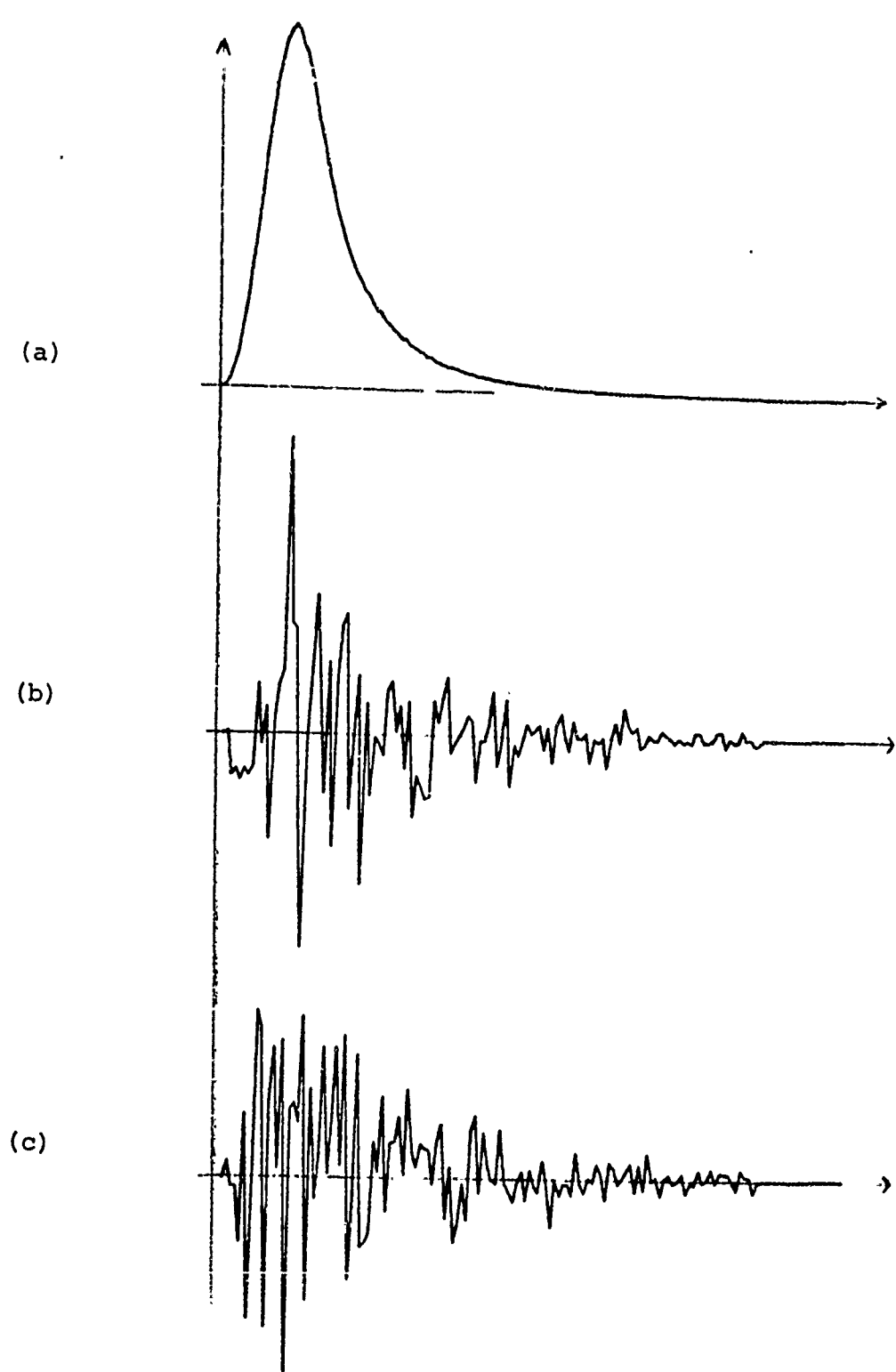
Figure 7-2   Troposcatter Channel Response; (a) delay-power profile,
(b) and (c) Possible Impulse Responses

$$E\left[h_k(\tau)h_\ell^*(t)\right] = \delta(t-\tau)Q_{k\ell}(t)$$

If $k=\ell$ we refer to $Q_{k\ell}(\cdot)$ as a delay-power profile, for $k \neq \ell$ it is called a cross correlation profile. Note that

$$Q_{k\ell}(\tau) = Q_{\ell k}^*(\tau)$$

where x^* denotes the conjugate of a complex number x.

On space diversity paths the crosscorrelation $Q_{\ell k}(\tau)$ can depend on frequency. This dependence can be ignored for most practical systems where the fractional bandwidth is significantly smaller than the ratio of aperture size to aperture separation.

7.2   WIDEBAND SYSTEM DESCRIPTION

The system is digital and employs a linear modulation technique, so the baseband-equivalent transmitted signal is

$$s(t) = \sum a_i p(t-iT) \tag{7.1}$$

where $p(t)$ is the transmitted pulse shape, T is the signaling interval and $\alpha_i = \pm 1$ is the i-th data sample. (The actual transmitted signal is the RF carrier f_c modulated by $s(t)$.) The system transmits one data sample each T seconds. The transmitted pulse shape is determined by the transmitter filter response. (The transmitter filter serves to limit the bandwidth of the transmitted signal.) The receiver consists of a filter and a

7-8

tapped delay line equalizer. The filter is matched to the transmitted waveform (i.e., the filter impulse response is the transmitted pulse shape) and the equalizer compensates for channel-introduced distortion.

In a narrowband system $p(t)$ changes very little in time τ_c, where τ_c is the interval over which the channel impulse response $h(t)$ is non-zero. Figure 7-3 illustrates the effect of a troposcatter channel on a narrowband system where the transmitted pulse is rectangular. Figure 7-3a is a discrete approximation to a possible channel impulse response. The impulse response is random, so this function is one of the random ensemble of functions with a given delay-power profile $Q(t)$. Figure 7-3b and 7-3c show the transmitted and received pulse shapes. The received pulse shape is somewhat distorted, but after the receiver filter, the shape is nearly triangular (Figure 7-3d). (The matched filter output for a rectangular pulse is triangular.)

Now consider a wideband system with a rectangular pulse shape. Figure 7-4 illustrates the effect of the same impulse response on a wideband signal. Note that the received pulse shape differs greatly from the transmitted pulse shape. After filtering the pulse bears no resemblence to the triangular waveform of Figure 7-3d. In systems without delay combining the receiver is simply matched to the transmitted waveform. Such a system may be severely degraded by channel distortion. However, the received waveform actually has more energy in the wideband case than in the narrowband case (assuming the same energy per pulse). So if the system were matched to the received waveform, the wideband system would perform better.

(a)

(b)

(c)

(d)
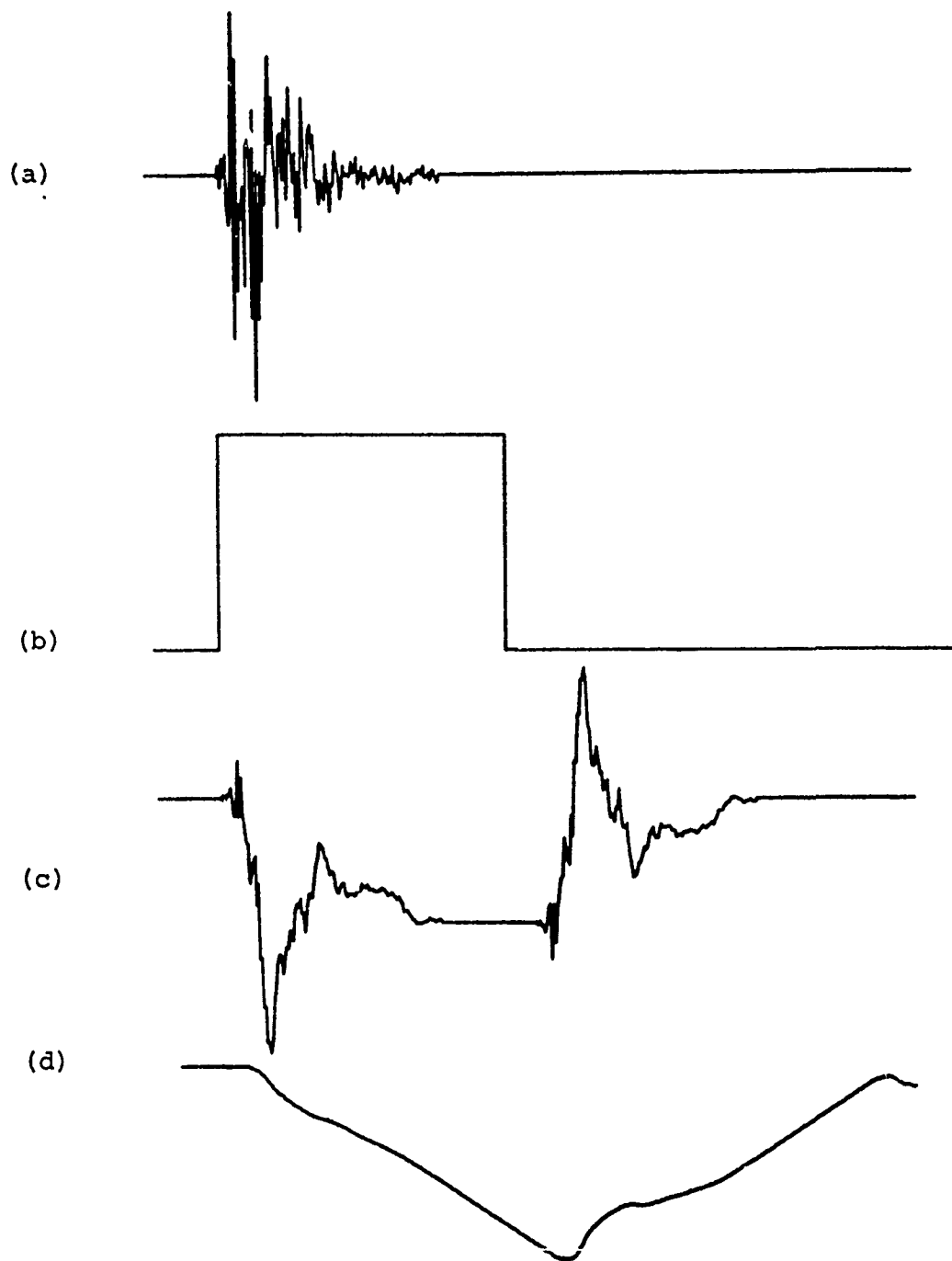
Figure 7-3 Troposcatter Channel Effect on Narrowband System:
(a) Channel Impulse Response, (b) Transmitted
Pulse, (c) Received Pulse, (d) Received Pulse
After Filtering.

(a)

(b)

(c)

(d)
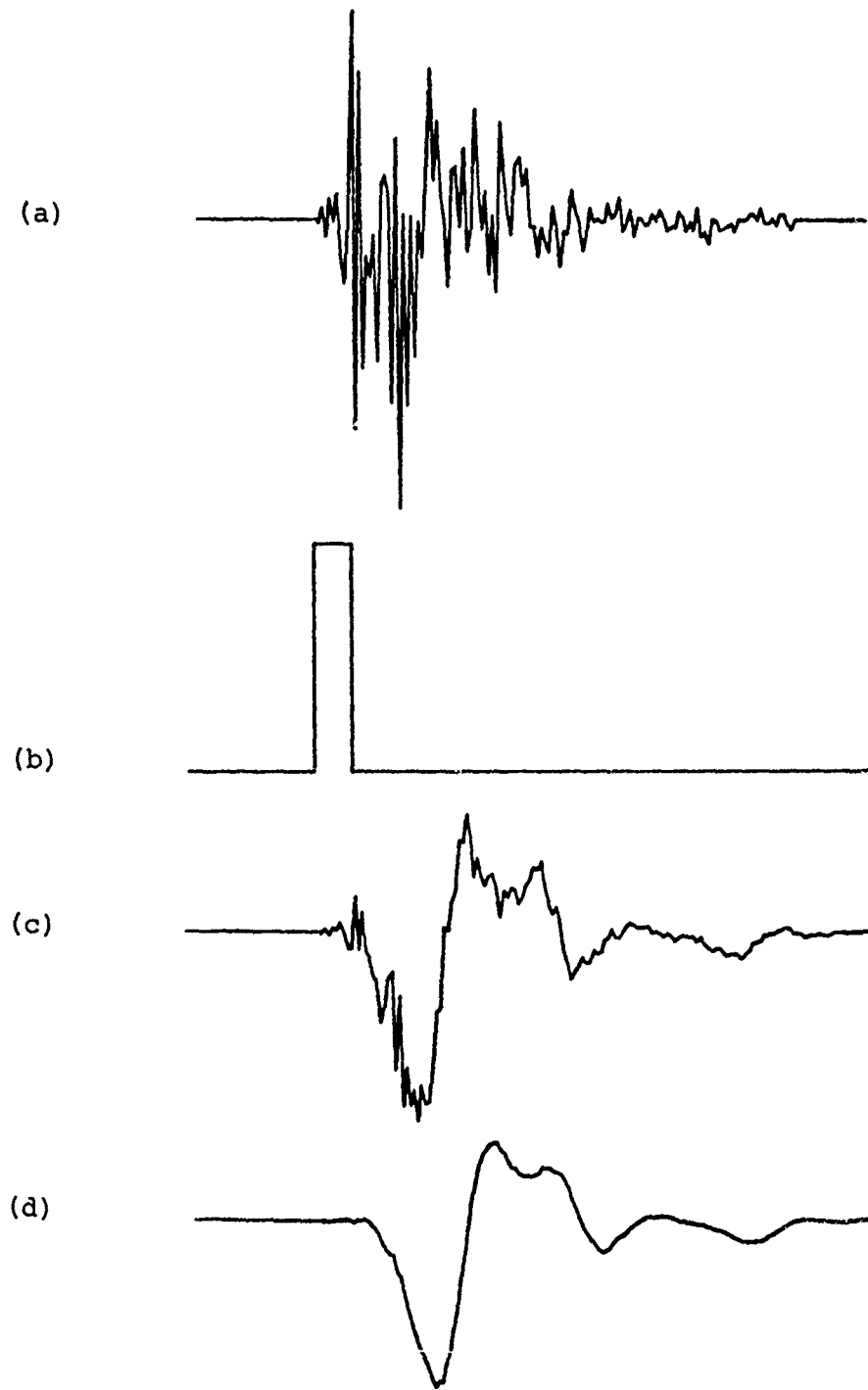
Figure 7-4   Troposcatter Channel Effect on Wideband System:
(a) Channel Impulse Response, (b) Transmitted
Pulse, (c) and (d) Received Pulse Before and
After Filtering.

7-11

Just as the spatial separation of the scatterers allows angle diversity to be used, the relative delays of the signals from different scatterers allows implicit diversity to improve performance. If the receiver were matched to the received waveform, then the maximum possible gain from implicit diversity would be achieved. (This corresponds to infinite subdivision of the receiver aperture in angle diversity.) A tapped delay-line combiner, whose weights adapt as the channel changes, may be used to approximate this optimum system. The number of taps corresponds roughly to the order of diversity. As the number of taps increases the complexity of the system increases, and as with the angle diversity systems, the decrease in the required SNR becomes less.

In addition to the delay combiner a filter is necessary in the receiver in order to limit the thermal noise. The thermal noise on different taps of the combiner is correlated because of this receiver filter, and the correlation between the noise on different taps is given by the autocorrelation function of the receiver filter. That is, if we define

$$R(\tau) = \int_{-\infty}^{\infty} f_R(t) f_R(t+\tau) dt, \qquad (7.2)$$

where $f_R(\cdot)$ is the RX filter impulse response, then the correlation between the noise on two taps separated by τ seconds is

$$E\left[n(t)n(t+\tau)\right] = N_0 R(\tau)$$

where N_0 is the noise variance and $f_R(\cdot)$ is normalized to unit energy, i.e., $R(0)=1$. This is a key difference between angle or space diversity and implicit diversity. In the former case the noise on different diversities is uncorrelated, whereas in the latter case this is not true.

Figure 7-5 illustrates the wideband system model which incorporates the above-mentioned features. The transmitted signal is s(t) as defined in (7.1). The received signal is

$$y(t) = \int_0^{\tau_c} s(\tau-t)h(\tau)dt + \hat{n}(t) . \qquad (7.3)$$

where $h(\cdot)$ is the channel impulse response (non-zero only on an interval $[0,\tau_c]$) and $\hat{n}(t)$ is a white Gaussian noise process. After the receiver filter the waveform is

$$r(t) = x(t) + n(t) \qquad (7.4)$$

where

$$x(t) = \int_{-\infty}^{\infty} y(\tau-t)f_R(\tau)d\tau, \qquad (7.5)$$

and n(t) is a Gaussian process whose autocorrelation is given by (7.2). The combiner forms an estimate of the i-th transmitted symbol by sampling r(t) at times $iT+\tau_1$, $iT+\tau_2,\ldots,$ $iT+\tau_M$, weighting these and summing. That is, the estimate of the i-th symbol is
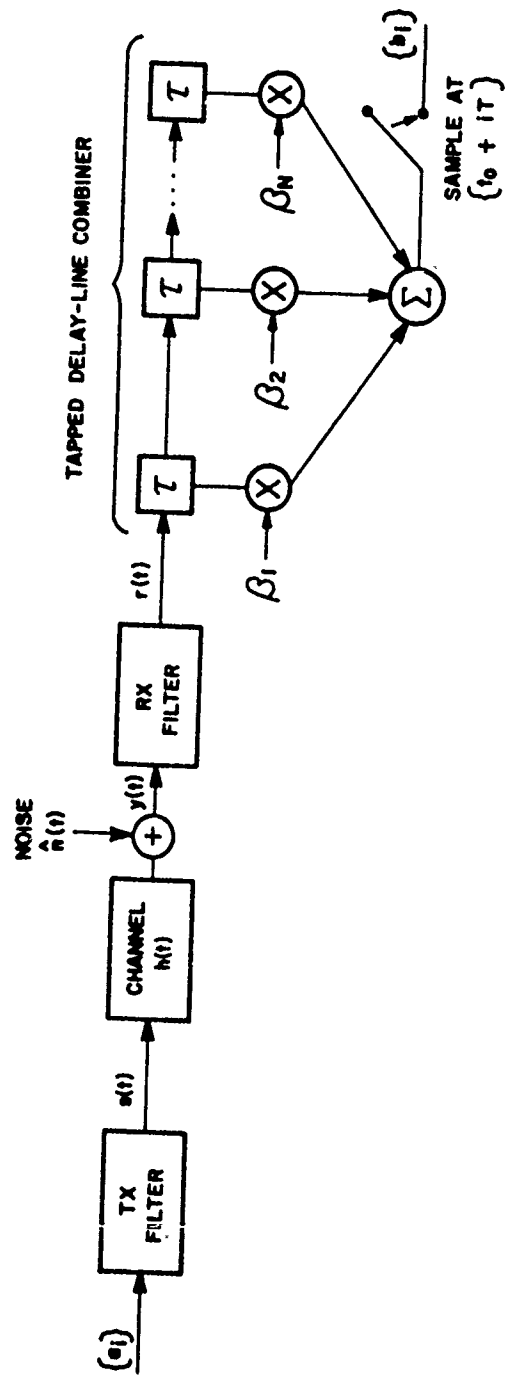
Figure 7-5   Wideband System Model (Single Antenna Beam)

$$b_i = \sum_{j=1}^{M} \beta_j r(iT+\tau_j) \qquad (7.6)$$

where the weights β_j are selected adaptively to maximize the SNR.

In vector form we may write (7.6) as

$$b_i = \underline{\beta}\underline{r}$$
$$= \underline{\beta}(\underline{x} + \underline{n}) \qquad (7.7)$$

where $\beta = \{\underline{\beta}_1, \ldots, \beta_M\}$ is the vector of tap weights, $\underline{r} = r(iT+\tau_1)$, $r(iT+\tau_2), \ldots, r(iT+\tau_M)$ is the vector of tap outputs and $\underline{x}$ and $\underline{n}$ are the signal and noise components of $\underline{r}$.

The system performance depends on the distribution of b_i. Without loss of generality we assume $i=0$. From Equations (7.3)-(7.5) we see that both the signal and noise components of the sampled signal, $\underline{r}$, are random. The thermal noise is a stationary Gaussian process with autocorrelation given by RX filter autocorrelation $R(\tau)$, so $\underline{n}$ is a zero-mean Gaussian vector with covariance matrix $R_n = \{\gamma_{kj}; k=1, \ldots, M, j=1, \ldots M\}$, where γ_{kj} is the correlation between the k-th and l-th taps, that is,

$$\gamma_{kj} = R(\tau_k - \tau_j) . \qquad (7.8)$$

7-15

The signal component is a non-stationary Gaussian process whose autocorrelation is determined by the delay power profile $Q(t)$ and the TX and RX Filters, $f_T(t)$ and $f_R(t)$. The signal vector $\underline{x}$ has covariance matrix $R_S = \{\lambda_{kj}; k=1,\ldots,M, j=1,\ldots,M\}$ where

$$\lambda_{kj} = E\left[x(\tau_j)x(\tau_k)\right]$$

$$= E\left[\int_{-\infty}^{\infty}\int_0^{\tau_c} h(u)s(u-\nu+\tau_j)f_R(\nu)\,du\,d\nu\right.$$

$$\left. \times \int_{-\infty}^{\infty}\int_0^{\tau_c} h(u)s(u-\nu-\tau_k)f_R(\nu)\,du\,d\nu\right]$$

$$= \int_{-\infty}^{\infty}\int_{-\infty}^{\infty}\int_0^{\tau_c} Q(u)f_R(\nu_1)f_R(\nu_2)s(u-\nu_1-\tau_k)s(u-\nu_2-\tau_j)\,du\,d\nu_1\,d\nu_2.$$

$$(7.9)$$

We assume that no intersymbol interference (ISI) is present so that the tap outputs for the zero-th symbol depend only on a_0. This assumption is made because we wish to examine the gains which are theoretically possible through time diversity and ISI may be removed by Viterbi decoding (although at some cost in complexity). Under this assumption $s(t)$ in (7.9) may be replaced by $a_0 f_T(t)$. The signal covariance matrix may thus be computed. The signal and noise components are independent so the system performance is determined by the two covariance matrices R_N and R_S. Again the only difference between the implicit-diversity and angle diversity cases is that in the angle diversity case the matrix R_n is diagonal since the noise components are independent.

This analysis generalizes trivially to include a combination of explicit and implicit diversity. In this case we have one received waveform for each of N antenna ports, so we have $r_1(t), r_2(t), \ldots, r_N(t)$. These are defined as in (7.3)-(7.5) except that each port sees a different channel so $h(t)$ in (7.3) becomes $h_i(t), i=1, \ldots, N$. The properties of $h_i(t)$ are given by

$$E[h_i(t) h_j(\tau)] = Q_{ij}(t) \delta(t-\tau) \qquad (7.10)$$

where $Q_{ij}(t)$ is the ij-th cross-correlation profile. If each port has an M-tap delay line then the total number of samples to be combined is NM, so (7.6) is replaced by

$$b_0 = \sum_{k=1}^{N} \sum_{j=1}^{M} \beta_{kj} r_k(\tau_j) \qquad (7.11)$$

$$= \underline{\beta} \underline{r}$$

where $\underline{\beta} = \{\beta_{11}, \beta_{12}, \ldots, \beta_{1M}, \beta_{21}, \beta_{22}, \ldots, \beta_{NM}\}$ and $\underline{r}$ is defined similarly. The signal covariance matrix is also NMxNM and consists of N^2 blocks of size MxM, each of which is determined by Equation (7.9) with $Q(\cdot)$ replaced by $Q_{kj}(\cdot)$, $k=1, \ldots, N, j=1, \ldots, N$. Each port sees an independent noise process $n_j(t), j=1, 2, \ldots, N$, so the noise covariance matrix R_n is block diagonal. Each MxM diagonal block corresponds to the taps of one equalizer.

The performance criterion used for narrowband systems is the Chernoff bound on the bit-error-rate. This criterion also applies to the wideband system of Figure 7-5. So we have P{Error} < ϕ_0, where ϕ_0 is given by [15],

$$\phi_0 = \frac{1}{\left| I_L + R_S R_n^{-1} \right|} \, ,$$

L=MN is the order of the system, I_L is the LxL identity matrix, and R_S and R_n are the signal and noise covariance matrices. Note that if R_n is replaced by $N_0 I_L$ (N_0 is the noise variance), which corresponds to independent noise components, then this is exactly the same as the narrowband performance measure.

7.3 COMPUTED PERFORMANCE OF WIDEBAND SYSTEMS

The tapped delay-line combiners are assumed to have uniform tap spacing. The spacing of the taps and the first tap position are chosen optimally by numerical means. In general, as the number of taps increases the tap spacing decreases, but the spacing between the first and last taps increases.

The receiver filter is assumed to be matched to the transmitted waveform. Thus, if the transmitted pulse is rectangular, the receiver filter impulse response is also rectangular and of the same duration. In this way the combiner compensates for the channel and not the transmitted waveform.

We consider two types of transmitted pulses; rectangular pulses and sinc (($\sin \pi t)/\pi t$) pulses. Rectangular pulses have no intersymbol interference (ISI) but have too large a bandwidth to be used in a practical system. Sinc pulses are completely band-limited, but have unbounded ISI if any perturbation occurs. So although neither of these pulses would be used in an actual sys-

tem, they are limiting cases and the behaviour of actual pulses will be similar. Sections 7.3.1 - 7.3.3 consider rectangular pulses. Section 7.3.4 contains similar results for sinc pulses.

The noise autocorrelation function for the rectangular pulse case is triangular. The autocorrelation for the sinc pulse is also a sinc pulse.

The link used as an example is 100 km long with a scattering angle of 1.7° (as previously mentioned). The transmitter and receiver antennas are 3m square and the channel 2σ delay spread on a system without explicit diversity is 56 nsec. For clarity we use the pulse duration to characterize the different systems. However, if we instead used the ratio of the pulse duration to the delay spread then the results would apply to links with different delay spreads as well.

7.3.1 Effect of Pulse Duration

We first examine the effect of equalization for different pulse durations. The pulses are rectangular, and the system has only a single antenna port (no explicit diversity). Figure 7-6 contains results for pulse widths of 2000, 500, 100, and 20 nsec with equalizers of up to 8 taps. The SNR's are those required for a bit error rate of 10^{-4}, and they are normalized such that 40 dB is the required SNR for a system with a very long pulse duration.

For narrow pulse widths (wideband systems) the channel lengthens the pulse considerably so that a single tap system performs poorly. The wideband system benefits most from large numbers of taps, however, since the implicit diversity of the channel may be exploited. The behaviour of the narrowband systems is the opposite. The performance of a single tap system is better because the channel spreads the transmitted pulses only a little, but the gains from additional taps are less.
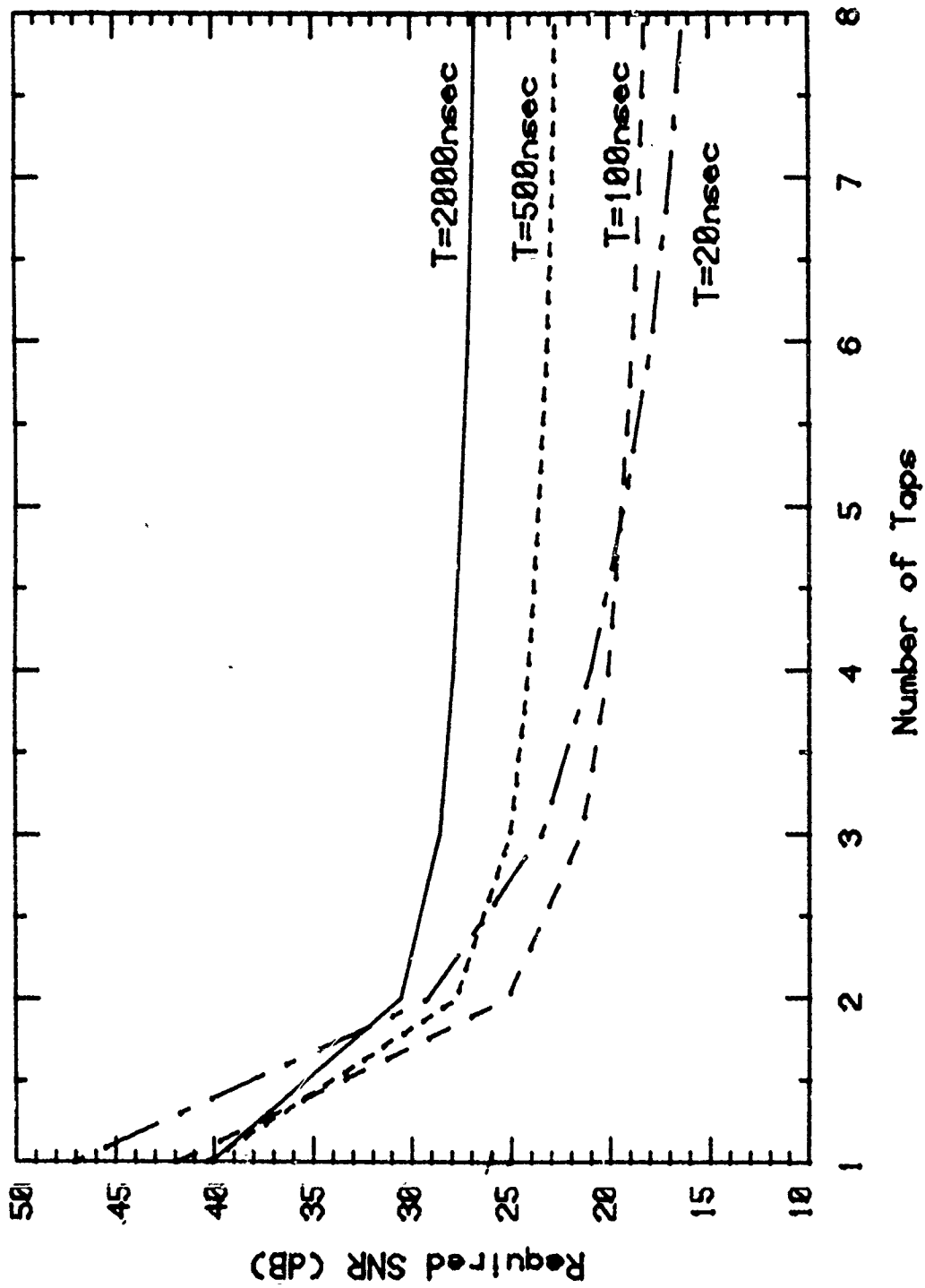
Figure 7-6 Required SNR (BER = 0.0001) vs. Number of Taps for Various Rectangular Pulses.

As with angle and space diversity the gains from delay com-
bining decrease as the number of taps increase.

The comparison of various pulse durations is not a compari-
son of alternative systems, since the system bandwidth is fixed
by other considerations. Rather the results illustrate what
improvement may be provided by diversity for various bandwidth
systems.

7.3.2 Equalization of Diversity Systems

We next consider the use of delay combining on systems
which have a number of antenna beams. Since the antenna beams
are not orthogonal the combiner weights for a given antenna beam
depend on the other beams. Due to the complexity of having a
number of tapped delay lines, an explicit function is used to
determine the tap positions for each profile. These tap posi-
tions are not optimal, but are close enough so that there is
little effect in required SNR.

Figure 7-7 graphs the required SNR (for BER=10^{-4}) vs.
number of taps for a single beam system (1) and for systems with
two azimuth beams (1,2), two elevation beams (2,1), three eleva-
tion beams (3,1), and four beams with two elevation and two azi-
muth (2,2). The pulses are rectangular and of duration 100 nsec.
(The 2σ delay spread of the channel is 56 nsec.) The benefit of
delay combining is much less for higher order diversity systems,
even for relatively high bandwidth systems. (Equalization to
remove ISI would still be necessary for these systems even though
delay combining is of little benefit.) Figure 7-8 presents the
same results for 2000 nsec rectangular pulses. These results
show that for the narrowband case, very little is to be gained
from delay combining.

Figure 7-7 Required SNR (BER = 0.0001) vs. Number of Taps for Various Orders of Diversity (Rect., T = 100 nsec)
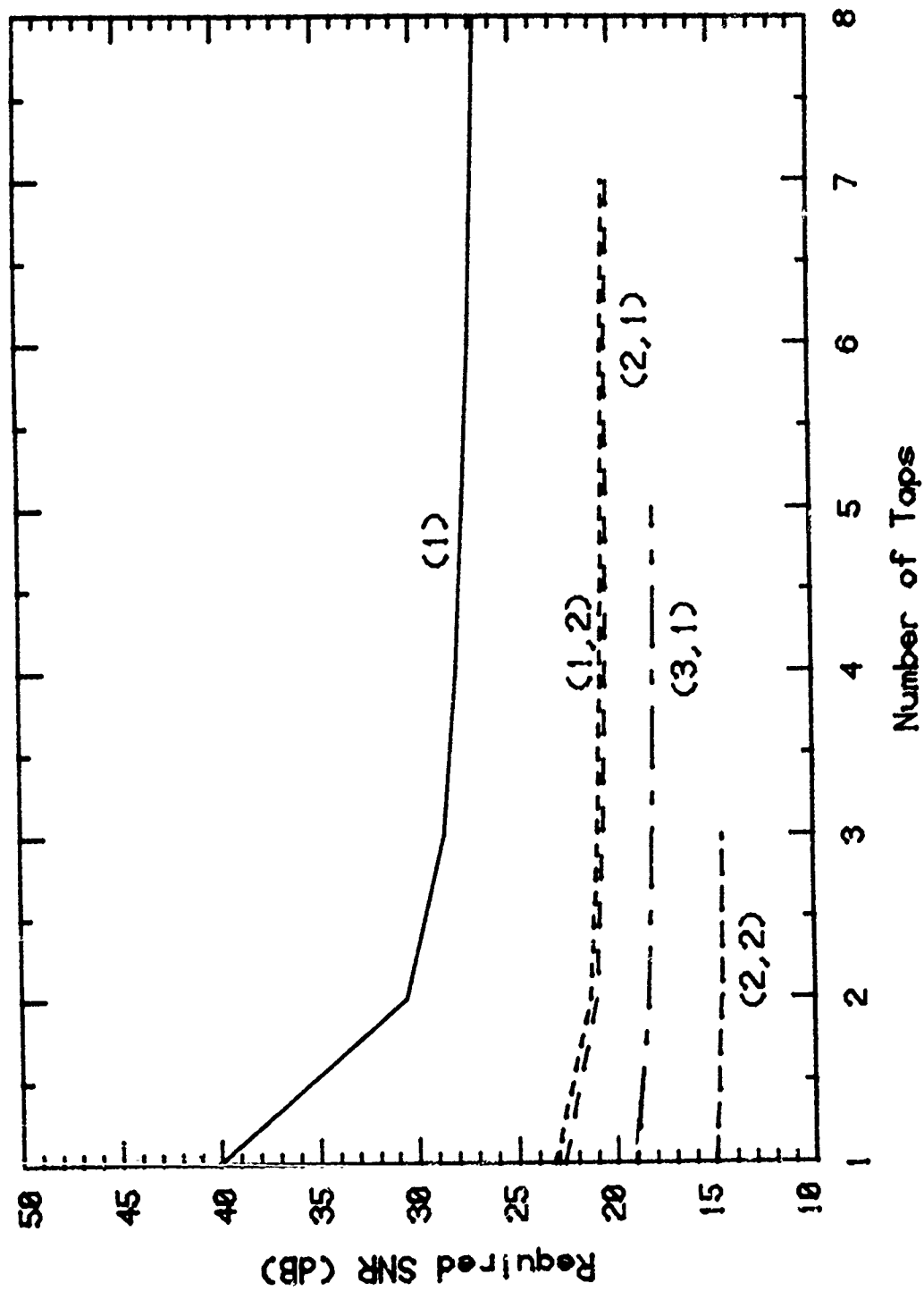
Figure 7-8 Required SNR (BER = 0.0001) vs. Number of Taps for Various Orders of Diversity (Rect., T = 2000 nsec).

7.3.3 Tradeoffs in Implicit and Angle Diversity

The number of weights which must be adaptively adjusted in an angle diversity system which also has time diversity is the number of delay taps times the number of antenna ports. The tradeoffs between the number of antenna ports and the number of taps is an important consideration.

Figures 7-9 and 7-10 graph the same data as Figures 7-7 and 7-8 but with the order of diversity (i.e., number of weights) as the x-axis. For the short pulse duration, 100 nsec, a single beam system with a 2-tap delay combiner performs only 0.5 dB worse than a dual angle diversity system. Similarly, a dual elevation diversity system with two delay taps on each port is only 1dB worse than the quad angle diversity system.

For the narrowband system, (2000 nsec pulse duration), the angle diversity systems perform significantly better than implicit diversity systems of the same order of diversity.

7.3.4 Results for Sinc Pulses

Sinc pulses are entirely band-limited and so they are not time-limited. For this reason we consider systems by various bandwidths rather than pulse durations. A sinc pulse of bandwidth W is given by $\text{sinc}(2Wt) = \frac{\sin(2\pi Wt)}{2\pi Wt}$. To allow comparison with the results for rectangular pulses the bandwidths used give filtered waveforms which are similar to those for rectangular pulses (in the absence of channel delay spread). The bandwidths which correspond to 2000, 500, 100, and 20 nsec pulse durations are 500 kHz, 2 MHz, 10 MHz, and 50 MHz. In Figure 7-11 we compare a duration T rectangular pulse (after filtering) and a 1/T bandwidth sinc pulse. The mainlobe of the sinc pulse coincides with the triangular waveform which results when the rectangular pulse passes through a matched filter.

Figure 7-9 Required SNR (BER = 0.0001) vs. Order of Diversity for Angle
Diversity Systems (Rect., T = 100 nsec)
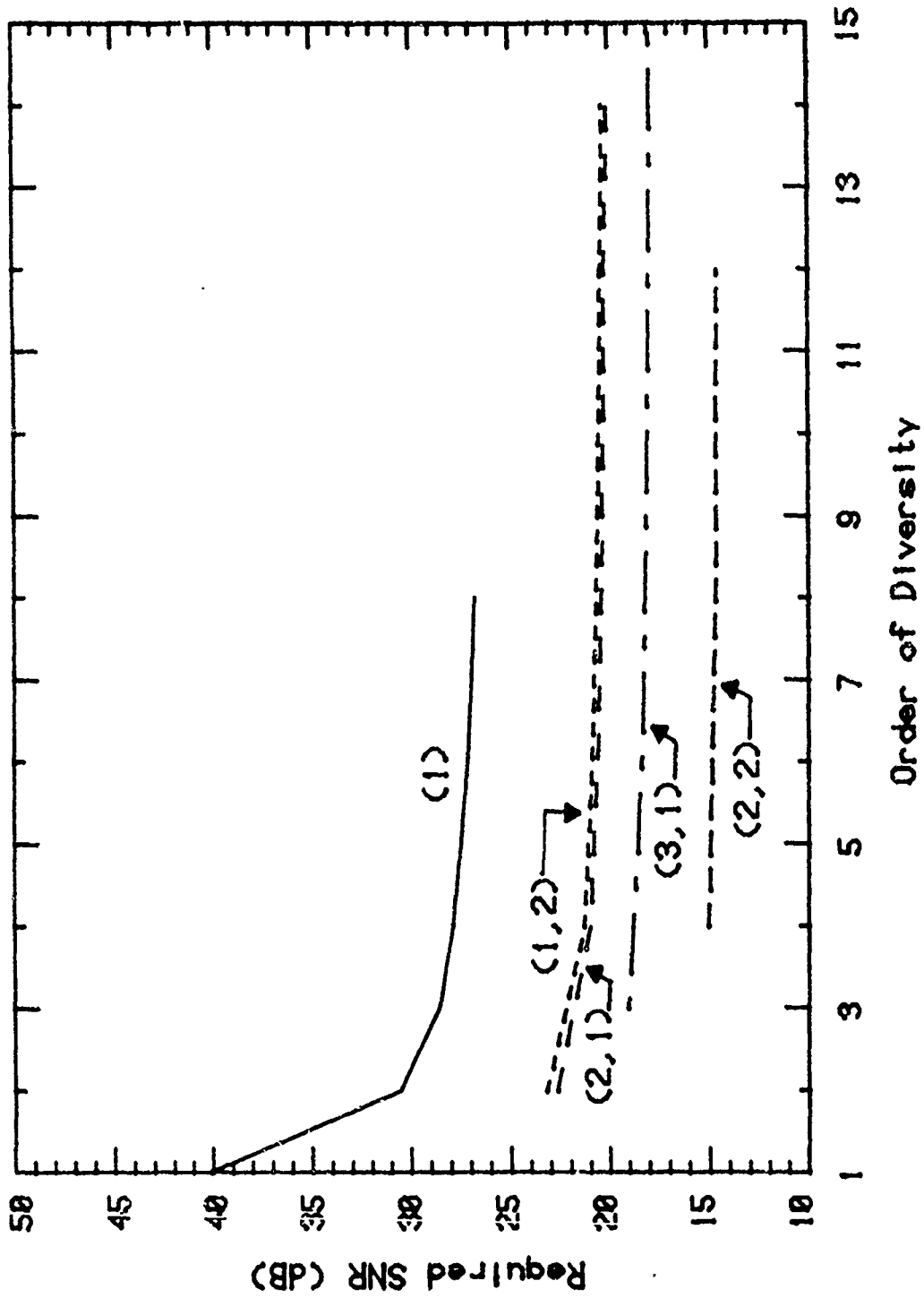
Figure 7-10 Required SNR (BER = 0.0001) vs. Order of Diversity for Angle
Diversity Systems (Rect., T = 2000 nsec).
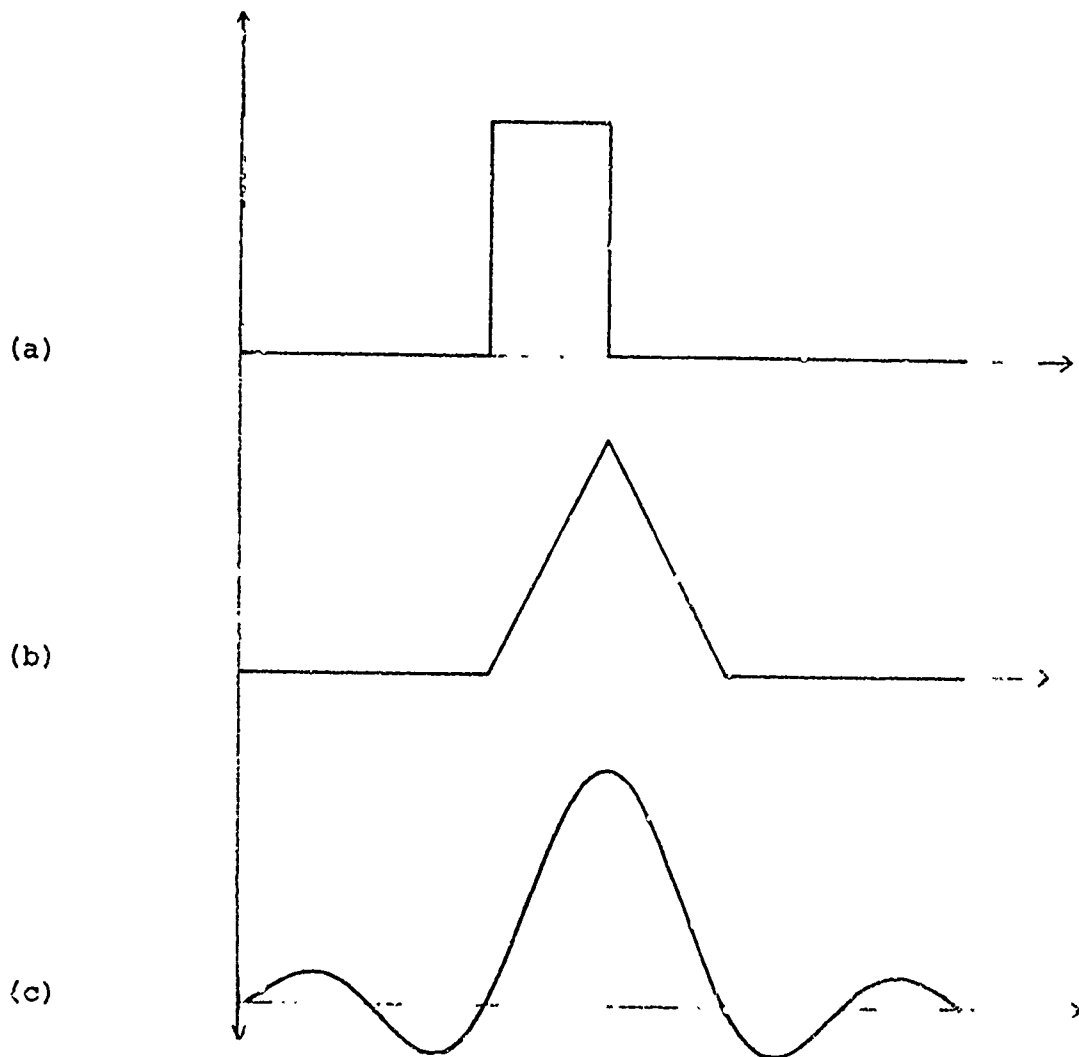
Figure 7-11   Comparison of Sinc and Rectangular Pulses:
              (a) Rectangular Pulse Duration T, (b) Filtered
              Rectangular Pulse, (c) Sinc Pulse of Bandwidth
              1/T. (Sinc Pulse is the Same Before and
              After Filtering.).

7-27

The required SNR for BER=10^{-4} is given in Figure 7-12 for the various bandwidth pulses. As with rectangular pulses (Figure 7-6) the gains from delay combining decrease as the number of taps increase. For narrowband systems the curves saturate more rapidly than the corresponding curves for rectangular pulses. This occurs because the rectangular pulses have energy over a wider band in frequency. For very wideband systems this is no longer a factor, and so the two types of pulses perform about the same.

Figures 7-13 and 7-14 present the effect of implicit diversity on higher order diversity systems. As with rectangular pulses, even with a 10 MHz bandwidth higher order systems gain relatively little from implicit diversity. The narrowband systems gain practically nothing.

Figures 7-15 and 7-16 contain the same points graphed vs. order of diversity. Wideband systems with 2-tap delay combiners perform nearly as well as systems with twice as many angle diversity ports, however, additional taps are not very beneficial.
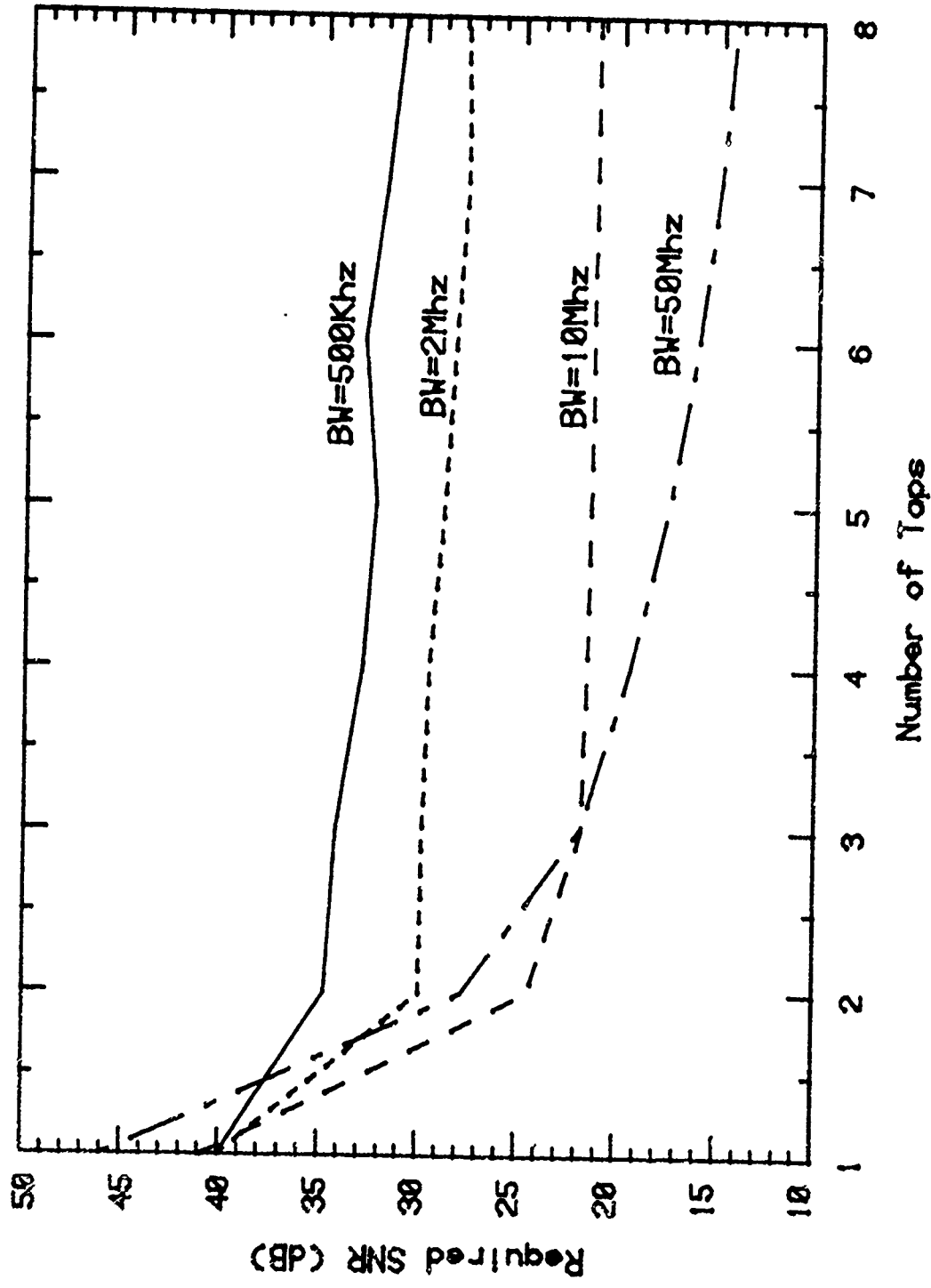
Figure 7-12 Required SNR (BER = 0.001) vs. Number of Taps for Various Bandwidth Sinc Pulses.
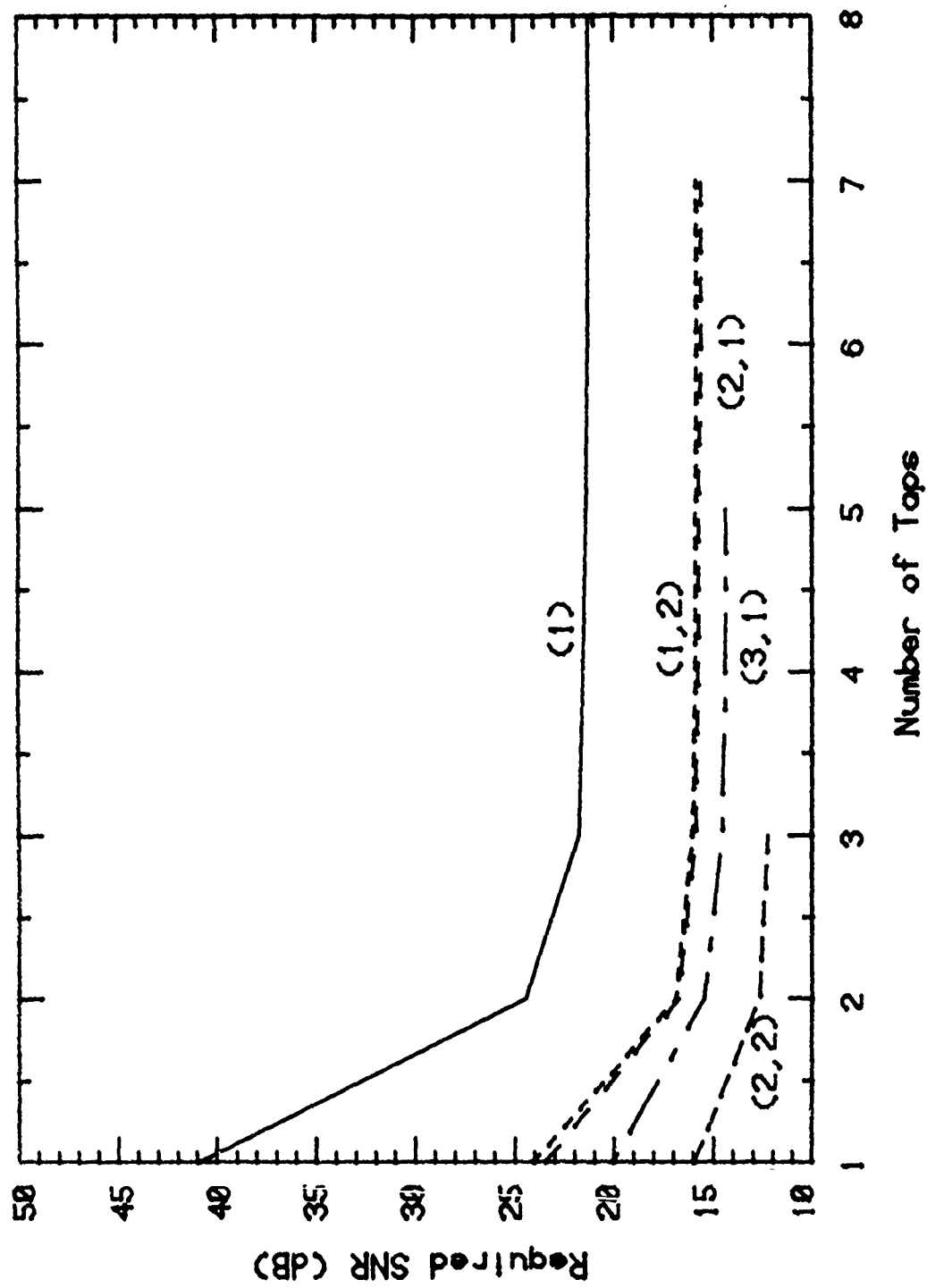
Figure 7-13 Required SNR (BER = 0.0001) vs. Number of Taps for Various
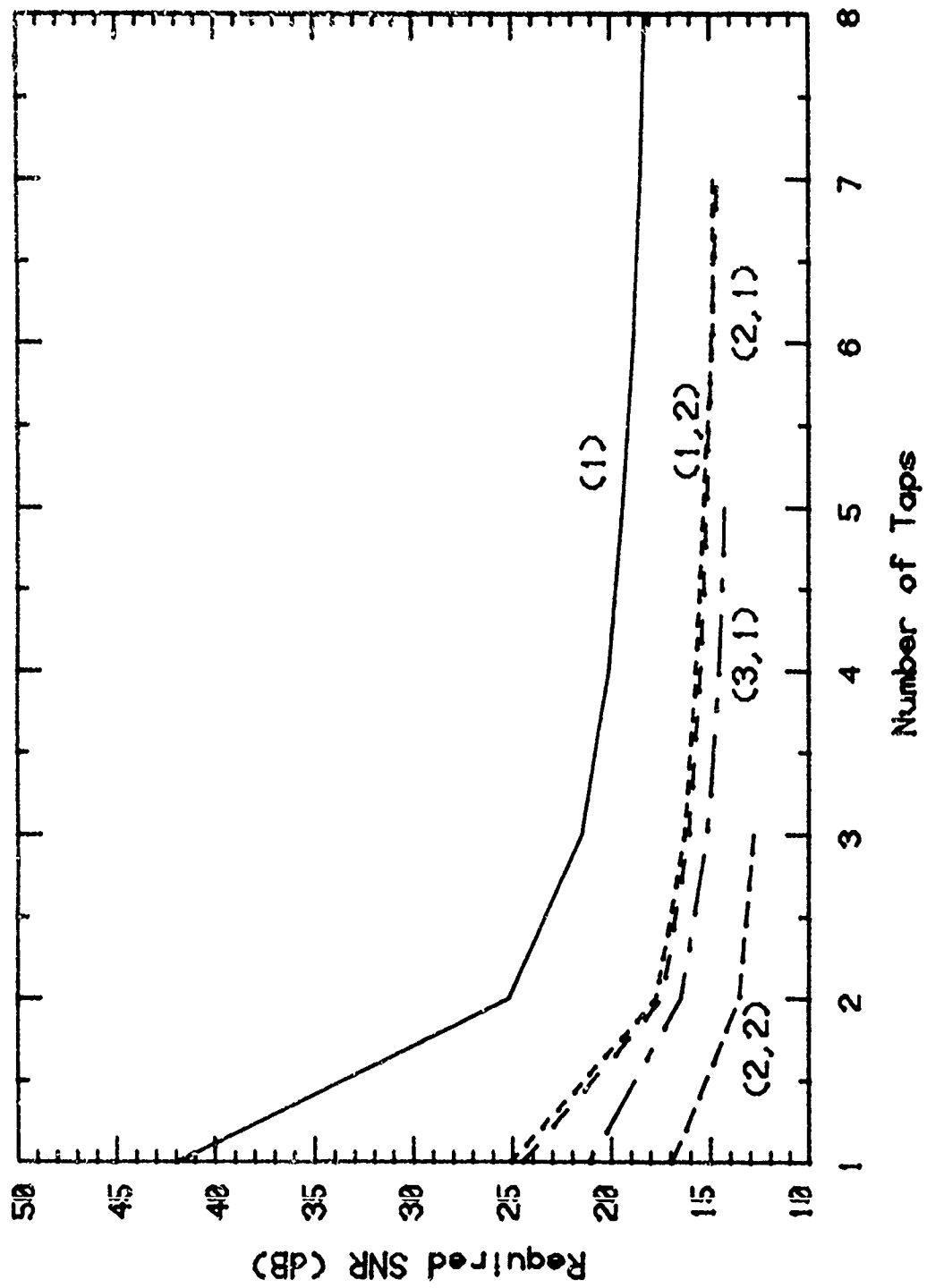of Diversity (Sing. BW = 10 MHz).
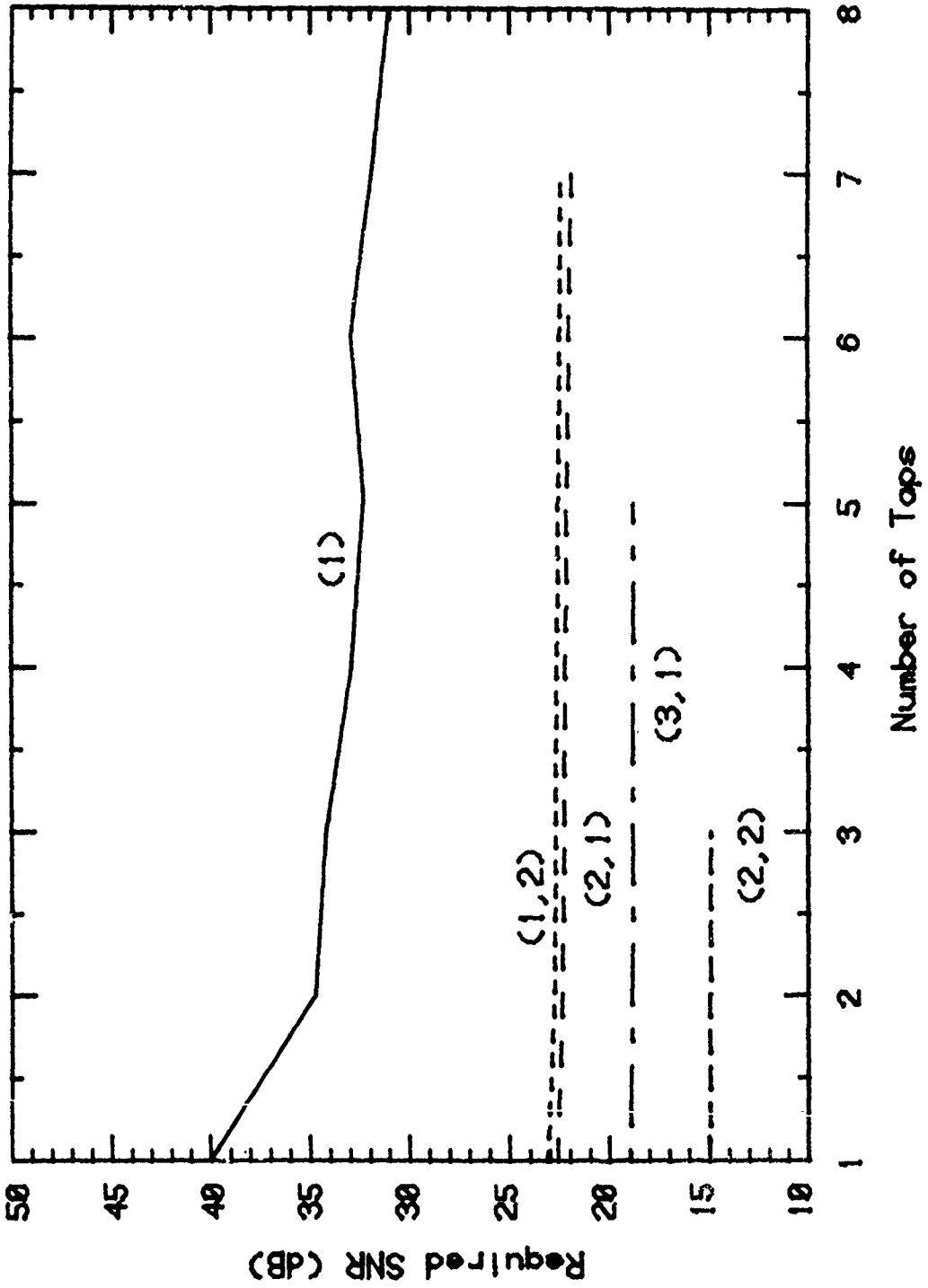
Figure 7-14   Required SNR (BER = 0.0001) vs. Number of Taps for Various
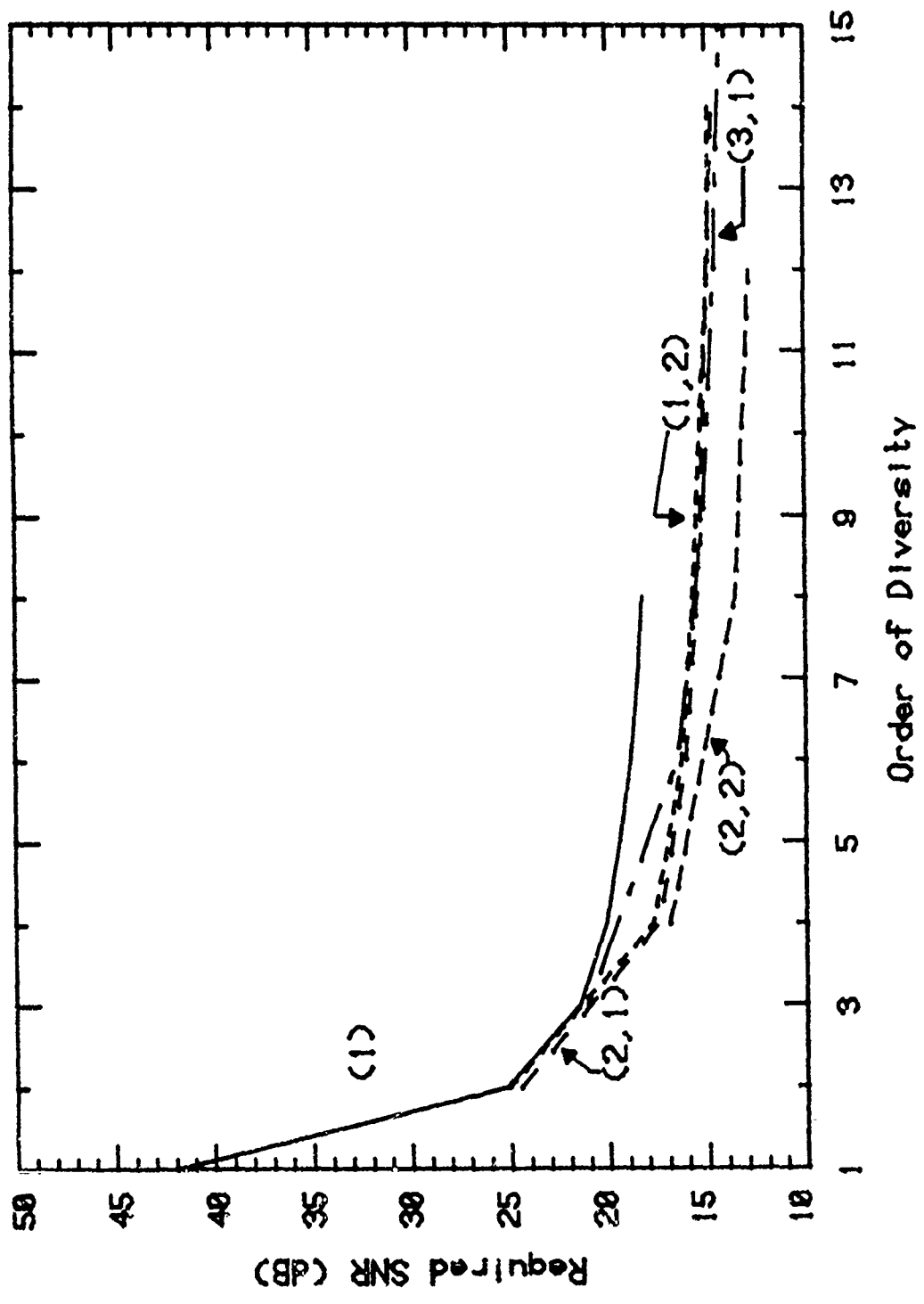Orders of Diversity (Sinc, BW = 500 KHz).
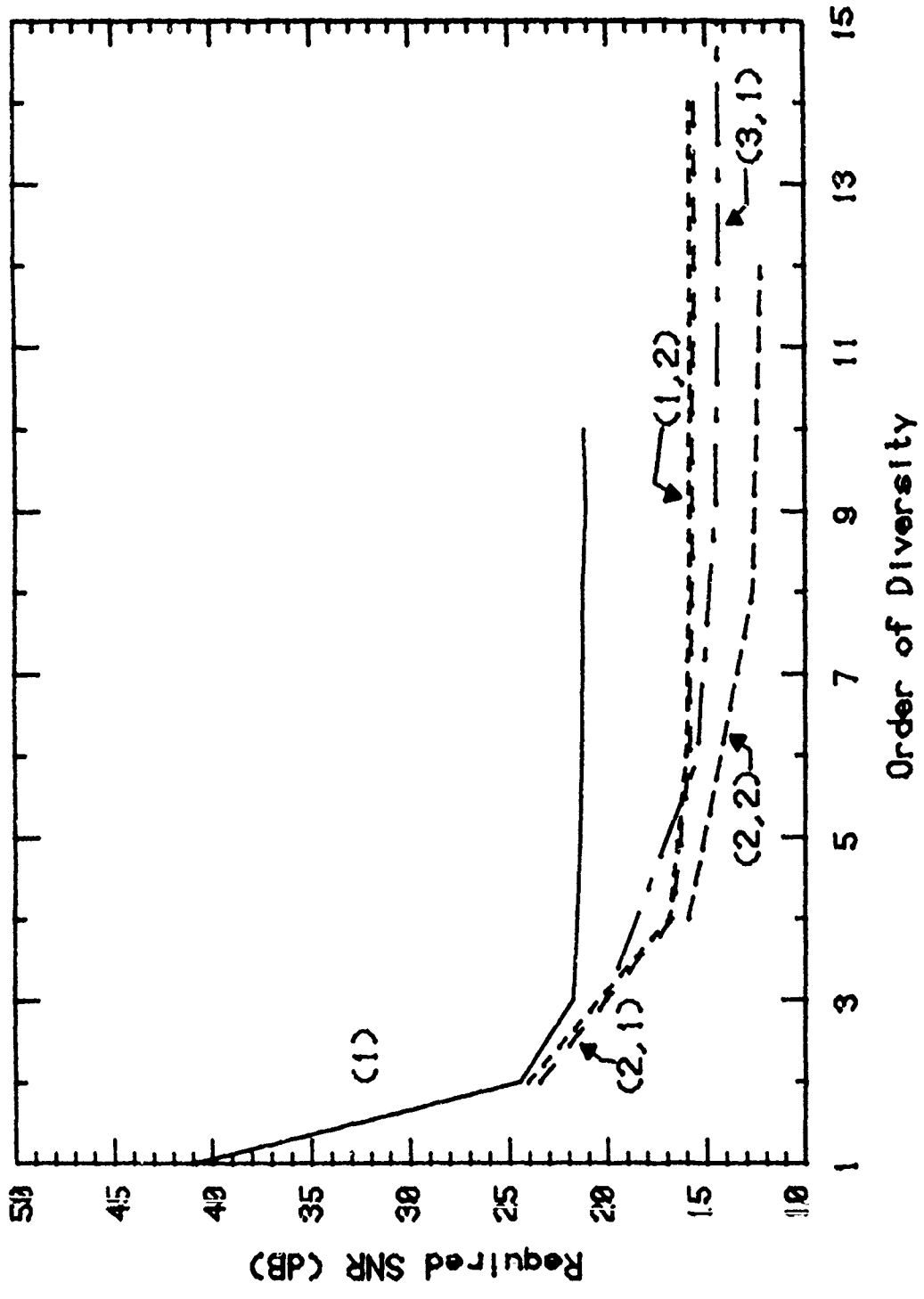
Figure 7-15   Required SNR (BER = 0.0001) vs. Order of Diversity for Angle Diversity Systems (Sinc, BW = 10 MHz)
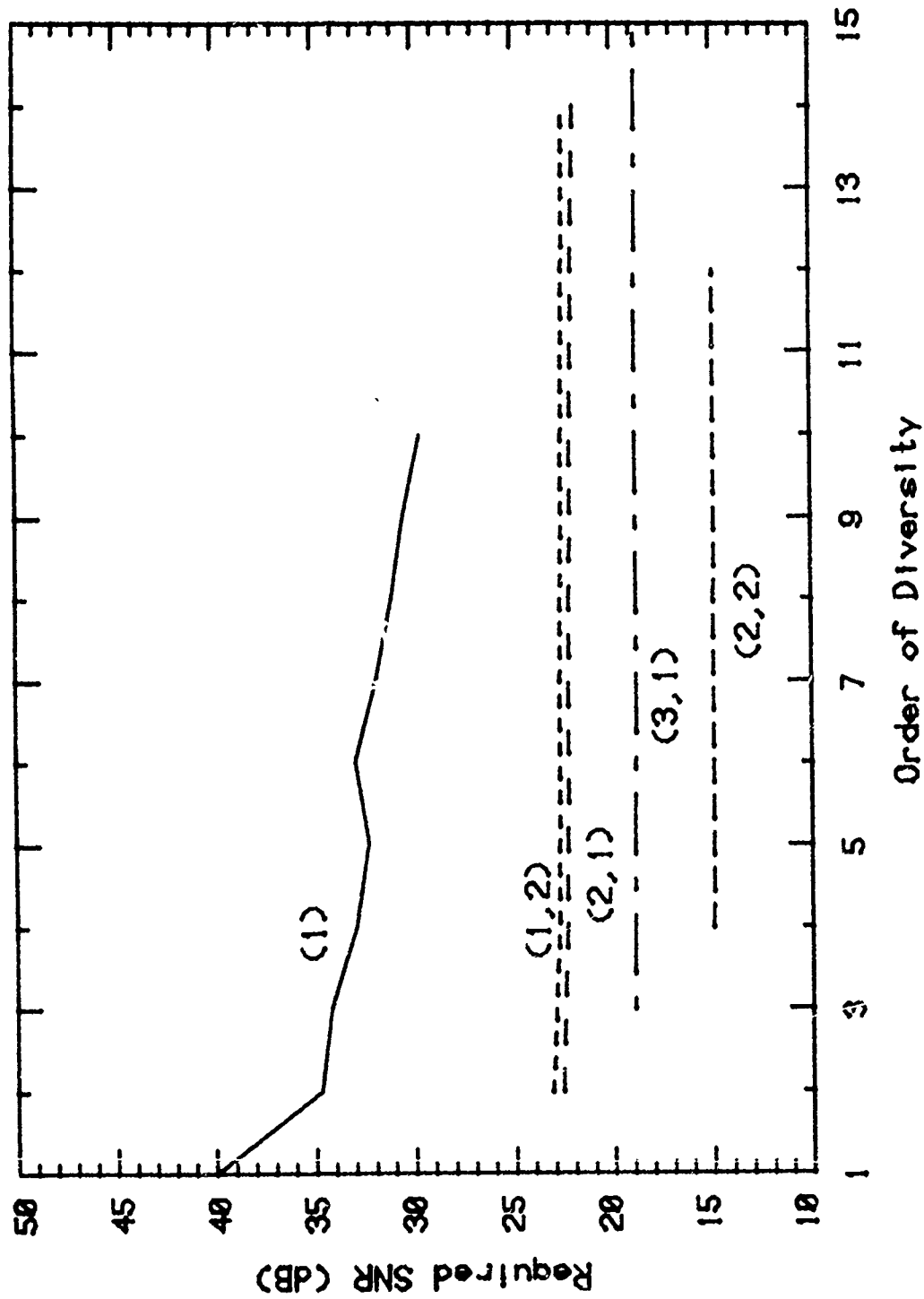
Figure 7-16 Required SNR (BER = 0.0001) vs. Order of Diversity for Angle
Diversity Systems (Sinc, BW = 500 KHz)

SECTION 8
A PROPOSED ADAPTIVE TROPOSCATTER EXPERIMENT

8.1 OBJECTIVES

The diversity results defined in this report rely on a few simplifying assumptions: 1) no diffraction or layer reflection; and 2) specific C_n^2 profile. An experiment verifying the diversity gains must also be able to determine to what degree these assumptions are satisfied. The experiment should cover several diversity configurations, diversity combining techniques, and performance measures. This high degree of flexibility requires recording of the received signals so that the same measured data can be used for different applications.

The basic requirements of the experiment are:
1. distinguish between troposcatter and diffraction
2. performance evaluation of the key arrays considered in Section 4
3. Determine diversity gain
4. evaluate fade rate limitation
5. resolve long term atmospheric layering.

Only narrowband diversity performance will be considered here, i.e., the results in Section 7 cannot be validated with the proposed experiment. However the proposed system can probe the channel accurately enough to permit analytical estimates of the wideband performance.

8.2 EXPERIMENT CONFIGURATIONS

A reasonable experiment would consist of seven separate antennas with downconverters, as shown in Figure 8-1. A study of the cost complexity tradeoffs has shown that an X-band experiment

8-1
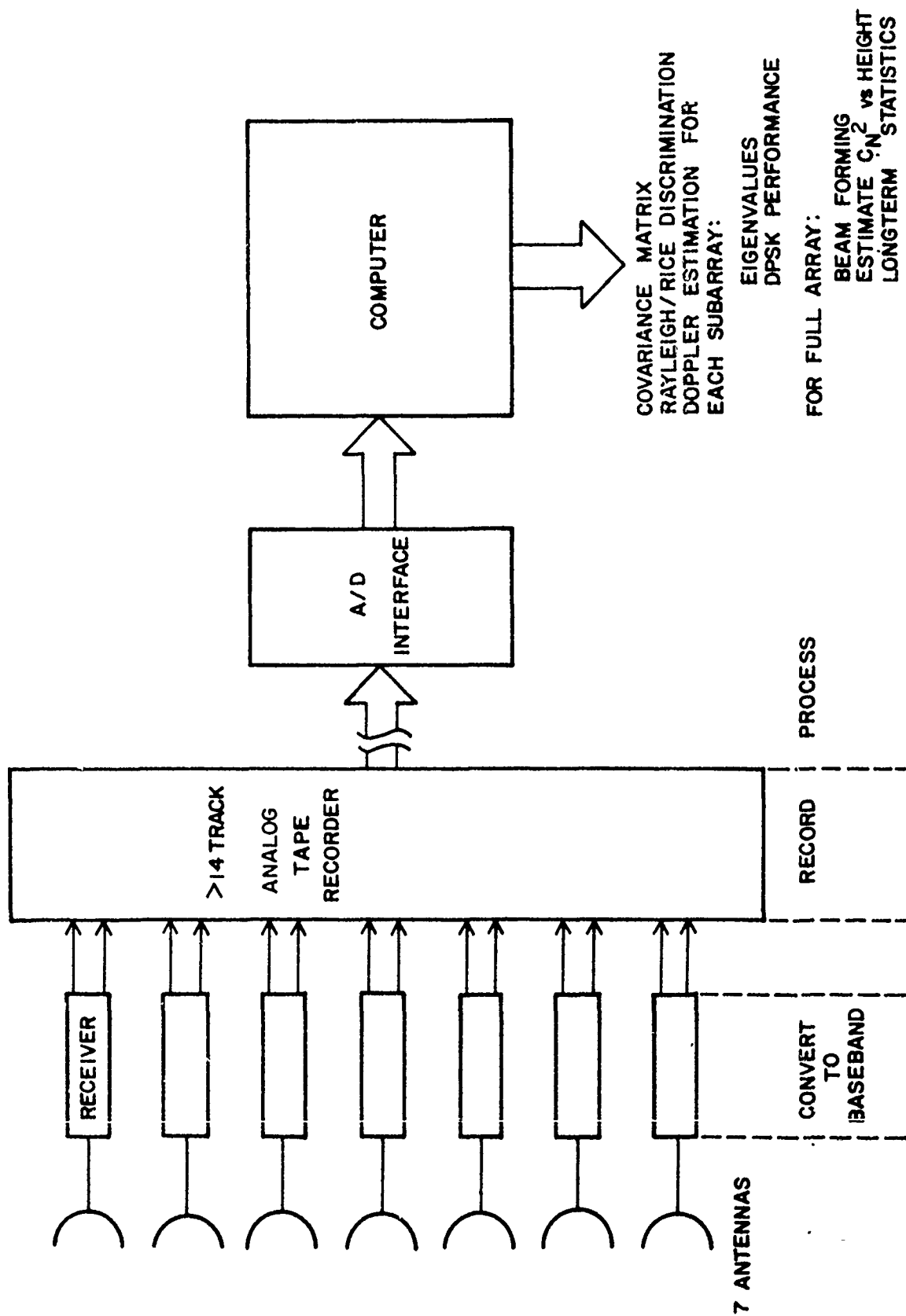
Figure 8-1 Receive Array Processing, Non-Real Time

with 2'-3' parabolic antennas is the most cost effective configuration. At lower frequencies, the larger antennas, waveguide, masts, etc. increase the cost while at high frequencies the component cost is excessive. From the point of view of mobility it is desirable to use a high frequency so that the resolution can be achieved with smaller antennas.

The transmitter will be a separate aperture, either small (2'-3') to test the diversity effects of broad transmitter beams, or large (10'-15') to evaluate the effect of a narrow transmitter beam with horizontal or vertical diversity. Only a CW tone need to be transmitted.

The narrowband receivers convert to baseband and either record the analog signals or sample at a rate of approximately 200 Hz and perform near real time processing.

The least costly system uses the analog tape recording with off-site, non-real-time data processing. This approach is also very flexible, the same tape can be used over and over to calculate different system parameters.

A more sophisticated approach is on-site, real-time processing, recording only the pertinent data such as periodic covariance matrix estimates, coherence time. Real time processing is then possible using an array processor such as the Floating Point Systems Model AP-120B with an analog interface. Such a system is shown in Figure 8-2. This approach is more expensive but is actually cost effective in the long run when a lot of different data (arrays, technical sites, etc.) are to be evaluated. It obviates the need for the enormous task of processing the large amount of analog tapes.

The proposed configuration is similar in many respects to the experiment of Waterman, et al. [17]. They use 12 antennas on a tower at 3 GHz while we propose 7 antennas at 8 GHz that can be reconfigured to several types, e.g., linear array, sparse array,

8-3
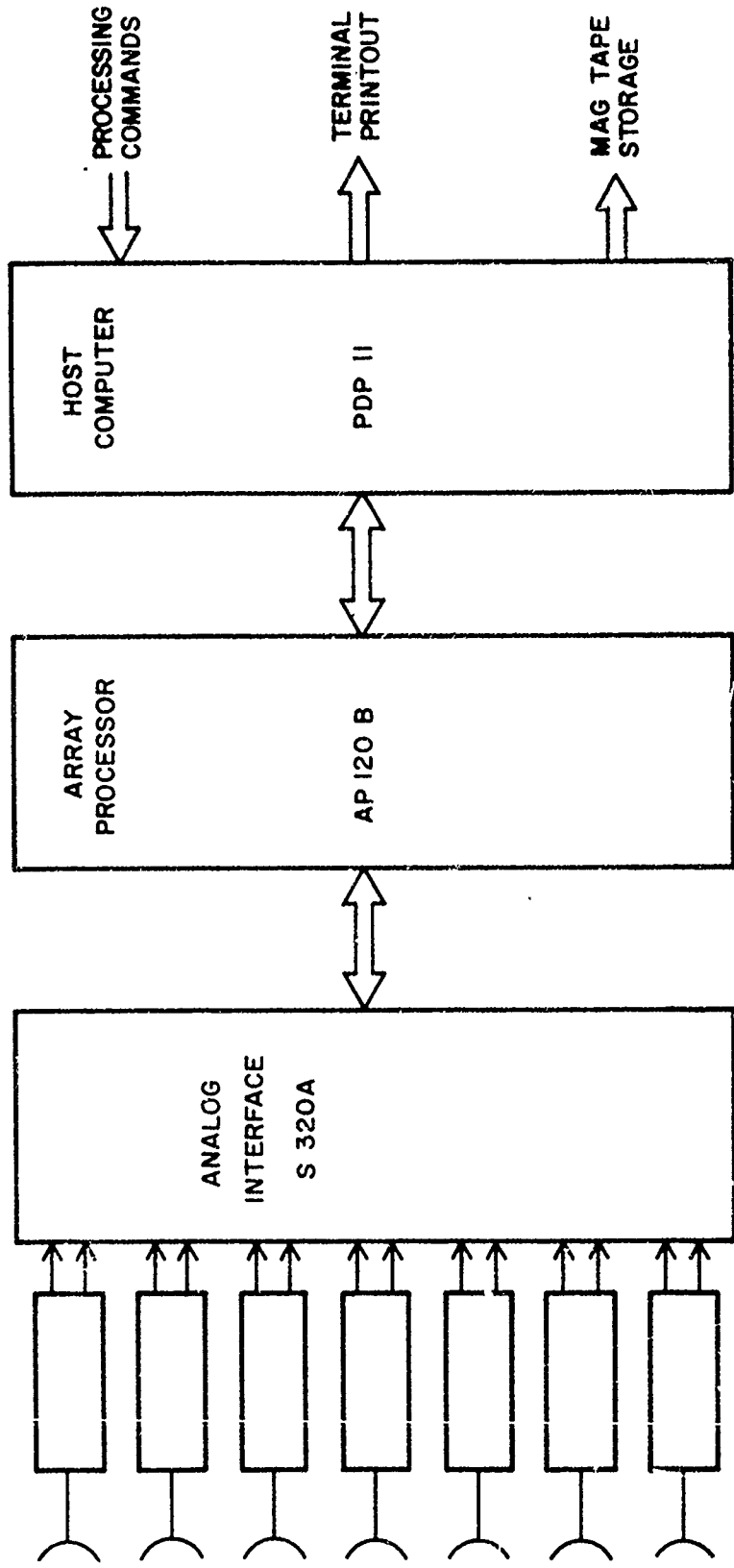
Figure 8-2 Alternate Real Time Processing

and rectangular array. They use an LOS reference to compensate for array motion, and the proposed system would do that as well. The key new features of the proposed system are:

1. flexible array configuration and portability
2. Rice/Rayleigh discrimination
3. diversity performance.

This is achieved by the signal processing shown in Figure 8-3. This processing can be done in real-time with the system in Figure 8-2, but requires later computer processing with the system in Figure 8-1 (doubling the required man-hours for the experiment). The diversity performance in the presence of specular components, although not considered in this report, can be calculated as well.

8.3 ARRAY CONFIGURATIONS

The antenna elements can be arranged in a number of configurations. A very interesting configuration is a sparse linear array in elevation which would allow a much better resolution than previous measurements. It would be possible to study details of the structure of the atmosphere that are not presently known, even though it is known that such effects, e.g., turbulence layers, strongly affect the long term performance of troposcatter systems. By estimating the turbulence (C_n^2 profile) it would be possible to estimate the delay spread as well by using the computer program described in Section 9. Thus, we would be able to get wideband performance estimates even though only probing the channel with a CW signal. The profile measurements would be made with either the linear array of the sparse array shown in Figure 8-4.
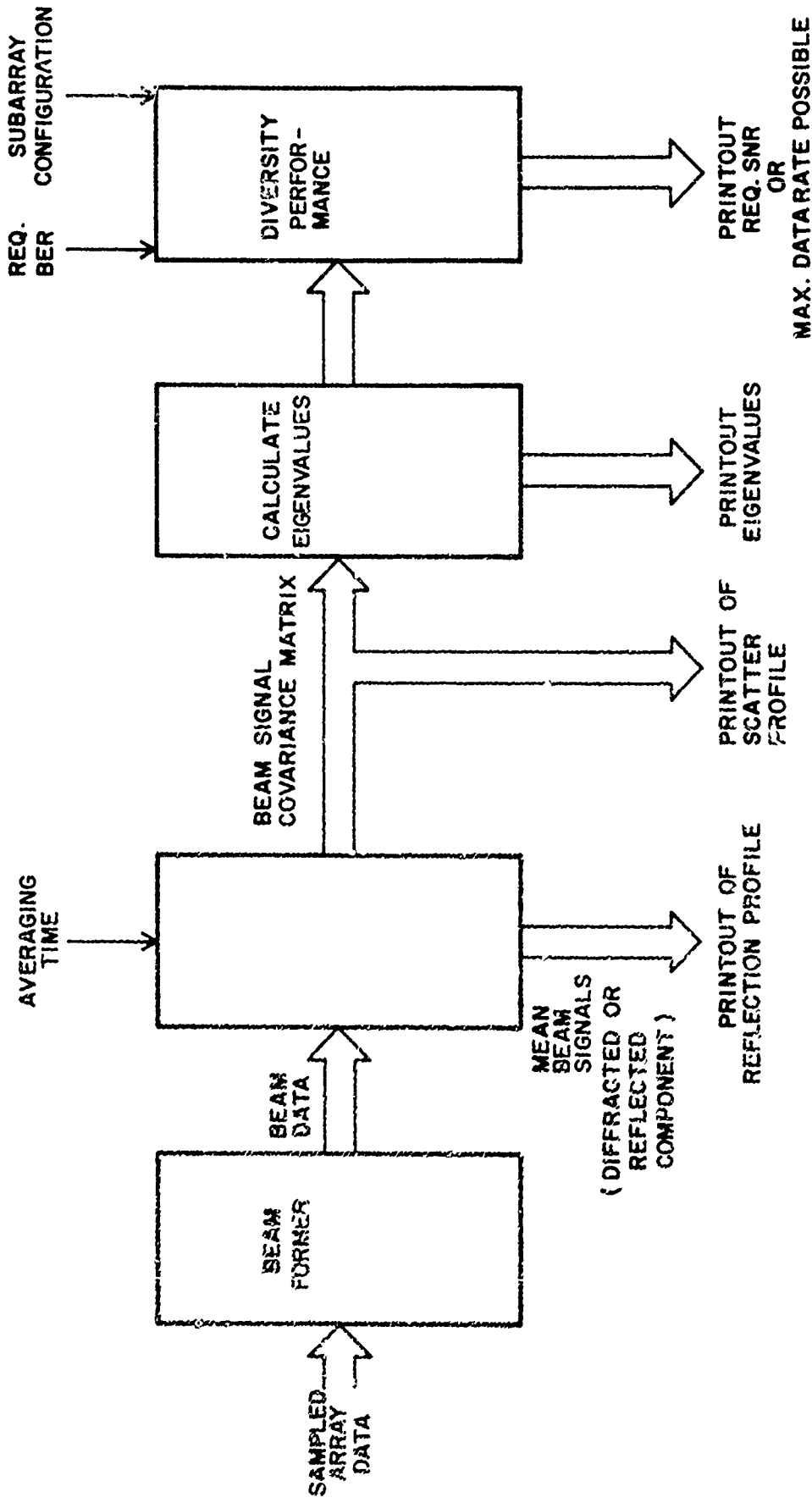
Figure 8-3   Functional Diagram of the Signal Processing

Linear Array (Horizontal or Vertical on Tower)

$\bullet_1\bullet_1\bullet_1\bullet_1\bullet_1\bullet_1\bullet$

Diversity Performance For:

AZ: (7,1),(6,1),(5,1),..,(2,1)

EL: (1,7),(1,6),(1,5),..,(1,2)

Sparse Array (Vertical only of Interest)

$\bullet_1\bullet_1\bullet$ 4 $\bullet$ 4 $\bullet$ 4 $\bullet$ 3 $\bullet$

Diversity Performance For: (1,18),(1,17),...(1,2)

L-shaped Array

```
      •
   1
      •
   1
      •
   1
   •₁ •₁ •₁ ∘
```

Diversity Performance For:

(4,4),(4,3),(4,2),(4,1)

(3,4), ..., (3,1)

.
.
.

(1,4), ..., (1,2)

Figure 8·4   Some possible array configurations and the (AZ, EL) dimension arrays for which performance can be calculated.

Most of the diversity results in this report can be verified by measurement on the L-shaped array shown in Figure 8-4. Instead of a 4x4 array as shown, a 5x3 or a 6x2 array can be used. Note how the flexible rearrangement of the array allows us to calculate a large number of different systems.

8.4   TYPICAL PRINTOUT RESULTS

For each link where the measurement system is set-up an initial receiver calibration is performed and then the system is started. Assuming real time processing as in Figure 8-2, we can get the following results printed out once a minute.

<u>Mean (Diffraction/Reflection) and Variance (Scatter):</u>

BEAM NO.	SPECULAR COMPONENT	SCATTER
1	...	...
2	...	...
.		
.		
.		
N	...	..

<u>Diversity Configuration (AZ, EL):</u>

		Tropo Only	Total Rician Signal
Eigenvalues:	...		
Required SNR		...	...
Maximum Data Rate		...	...

The last part would be repeated for each diversity configuration requested by the operator. The only limitation would be the speed of the printing terminal. This system could be used to assess the potential digital performance of all existing DCS troposcatter links, for instance.

SECTION 9

DESCRIPTION OF TROPOSCATTER PROPAGATION PARAMETER COMPUTATION

9.1   INTRODUCTION

The computer program determines the propagation parameters of a troposcatter link for general antenna configurations. The inputs to the program are:

- link parameters (distance, elevations, etc.)
- system parameters (frequency, power)
- diversity antenna configuration parameters
- antenna parameters.

The program allows arbitrary diversity configuration (no particular symmetry is required) and three basic types of antennas. The antenna types are

1)   parabolic reflectors,

2)   phased arrays of parabolic reflectors, and

3)   phased arrays of sub arrays,

where each subarray is a phased array of parabolic reflectors.

A diagram of a troposcatter link is given in Figure 9-1. The parameters which are necessary to define the link are the link distance, the antenna elevations (above sea level), and the horizon elevation angles. These parameters are used (along with the atmospheric parameters which determine the earth radius transformation) to determine the distance D' and the angles α_0 and β_0 (which determine the lower boundary of the common volume) in Figure 9-2. Each scatterer in the common volume is specified by a vector $\underline{v} = (\alpha, \beta, \gamma)$ which consists of the transmitter and receiver elevation angles and the distance γ perpendicular to the great circle plane (i.e., the plane of the paper).
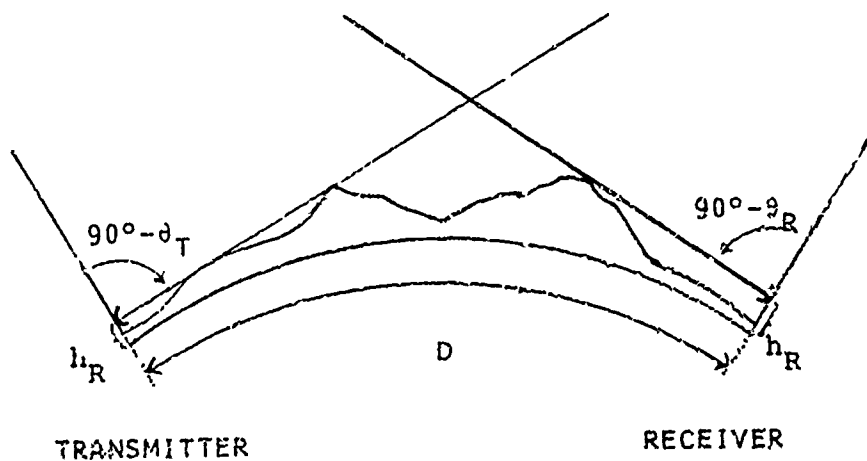
Figure 9-1. Physical Parameters Which Define A Troposcatter
Link; Link Distance D, Terminal Elevations Above
Sea Level h_T, h_R, Horizon Elevation Angles θ_T, θ_R.
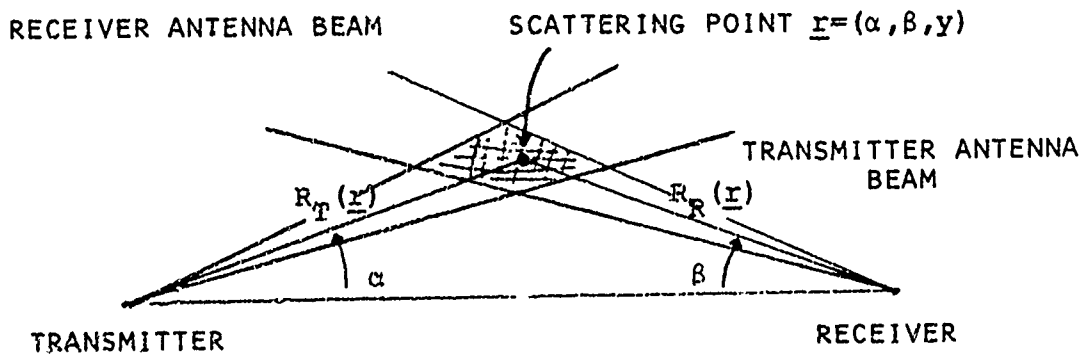
Figure 9-2 Link Parameters Used In Integration Over The Common Volume.

The program determines the correlation between signals at the various receiver ports. In the narrowband case this correlation is given by an integral over the common volume. Specifically, the correlation between receiver ports 1 and 2 is

$$\delta_{12} = \int \frac{\left|g_T(\underline{r})\right|^2 g_{R_1}(\underline{r}) \; g_{R_2}^*(\underline{r})}{R_T^2(\underline{r}) \quad R_R^2(\underline{r})} \; \theta^{-m} \; \underline{dr}$$

where $R_T(\underline{r})$ and $R_R(\underline{r})$ are the distances to the scattering point $\underline{r}$ from the receiver and transmitter respectively, θ is the scattering angle, $g_T(\underline{r})$ is the transmitter antenna gain in direction $\underline{r}$, and $g_{R_1}(\underline{r})$ and $g_{R_2}(\underline{r})$ are the (complex) receiver antenna gains. The integral is performed numerically, so the common volume is divided into cells which are small enough that the integrand may be approximated by a constant over the cell. In the wideband case for each delay the integral is performed over all cells with that delay (delay is proportional to $R_T(\underline{r})+R_R(\underline{r})$). The outputs of the program are the power vs. delay profiles and the cross-correlation profiles which are defined in what follows.

The value of the channel impulse response at a given time is a zero-mean Gaussian random variable. The scatterers are assumed independent so the values of impulse response at two different times are independent. A power vs. delay profile is the variance of the channel impulse response for a given antenna. The cross-correlation profiles determine the correlation between different antennas as a function of time. Different antennas are correlated in general because for a given delay the scatterers are the same for all antennas. (This assumption is not valid if the antennas are very far apart, but it represents a good approximation in practical systems.)

9-4

These profiles give all the necessary propagation information to compute the performance of a combiner or modem. If the symbol duration is long compared to the delay spread of the channel (i.e., narrowband), then only the integrals of the profiles are necessary. The intersymbol interference due to "smearing" of the source symbols by the channel is not significant. For the wideband case the entire profile is necessary to determine the system performance. Intersymbol interference is important here, and equalization may be necessary.

The major steps involved in the computation of the propagation parameters are given in Figure 9-3.

9.2 BRIEF DESCRIPTION OF STEPS IN PROPAGATION CALCULATIONS

We next describe the function of the modules in the flowchart of Figure 8-3.

9.2.1 Earth Radius Transformation

A modified form of the effective Earth's radius transformation is performed in subroutine TRANSF. When the surface refractivity is not specified (SURFN = 0), the effective radius factor ERFAC in the input data is used; otherwise ERFAC is calculated from the surface refractivity SURFN and this value of ERFAC is used instead of the value in the input file. This accounts for the mean curvature of the beams due to atmospheric refraction. In the transformed coordinate system, the beams follow straight lines, simplifying the calculation of various distances and angles which are necessary to determine the profiles.

9.2.2 Antenna Gains and Parameters

As previously mentioned the program allows antennas of three types; parabolic reflectors, phased arrays of parabolic reflectors, and phased arrays whose elements are also phased
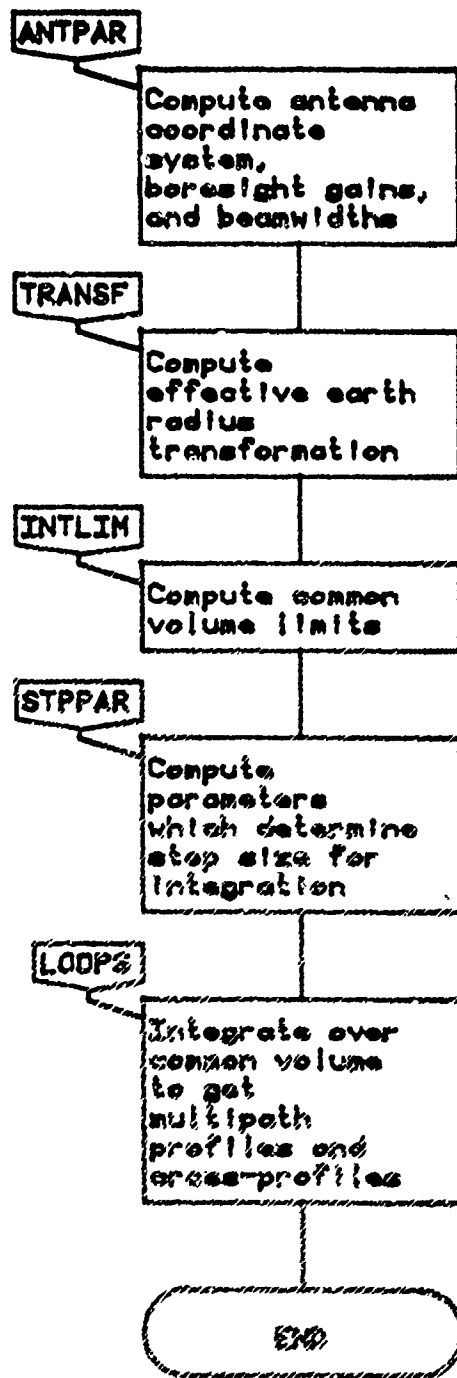
Figure 9-3 Flowchart of Propagation Section of Program.

9-6

arrays. To implement these antennas we note that the first two types are special cases of the third. That is, if a phased array has only a single element then it is a simple antenna. So the parameters in the program are set up for the most general type.

The phased arrays are rectangular planar arrays of elementary antennas as shown in Figure 9-4. The parameters necessary to define such a phased array include the gain of the elements, the number of elements along each axis, and their spacing. In addition a relative phase shift is applied between adjacent elements which changes the direction of maximum gain of the antenna. Two phase shifts are specified; one between vertically adjacent elements and one between horizontally adjacent elements. The elements of the array are identical and have boresight normal to the plane of the array.

The gain patterns of the receiver and transmitter arrays are given by functions RGAIN and TGAIN respectively. The arguments of these functions are the antenna index, the off-boresight angle, and the azimuth angle. (The boresight of a phased array is perpendicular to the plane of the array, not necessarily the direction of maximum gain.) Two angles are necessary because the gain patterns of the arrays are not radially symmetric. The azimuth angle must be measured relative to some reference vector in the plane of the array. For this reason an antenna coordinate system is defined (in subroutine ANTPAR). One unit vector of the system is the boresight. The other two vectors are roughly vertical and horizontal. See Figure 9-5. A detailed description of the definition of the coordinates is given in Appendices A and B.

Subroutine ANTPAR computes the horizontal and vertical half-power beamwidths of the receiver and transmitter arrays and subarrays. The beamwidths are computed with no phase shifts between elements of the arrays, so that the direction of maximum gain of the antenna is normal to the array plane. The boresight
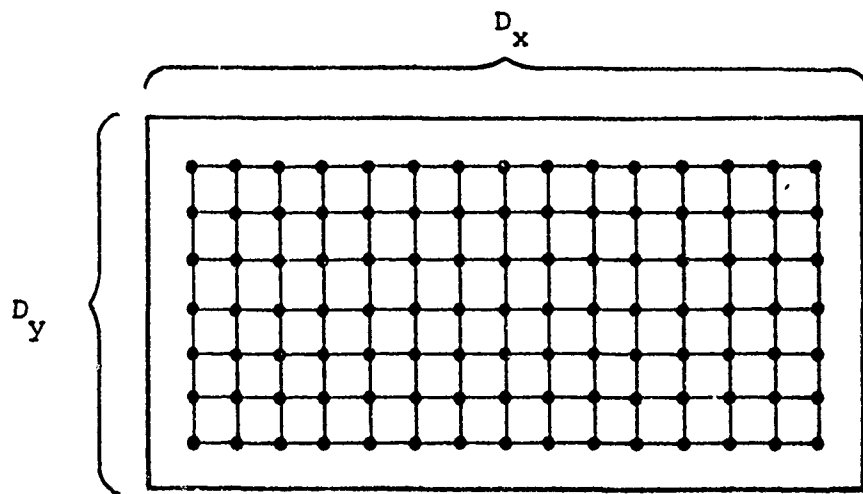
Figure 9-4   A Planar Array Antenna
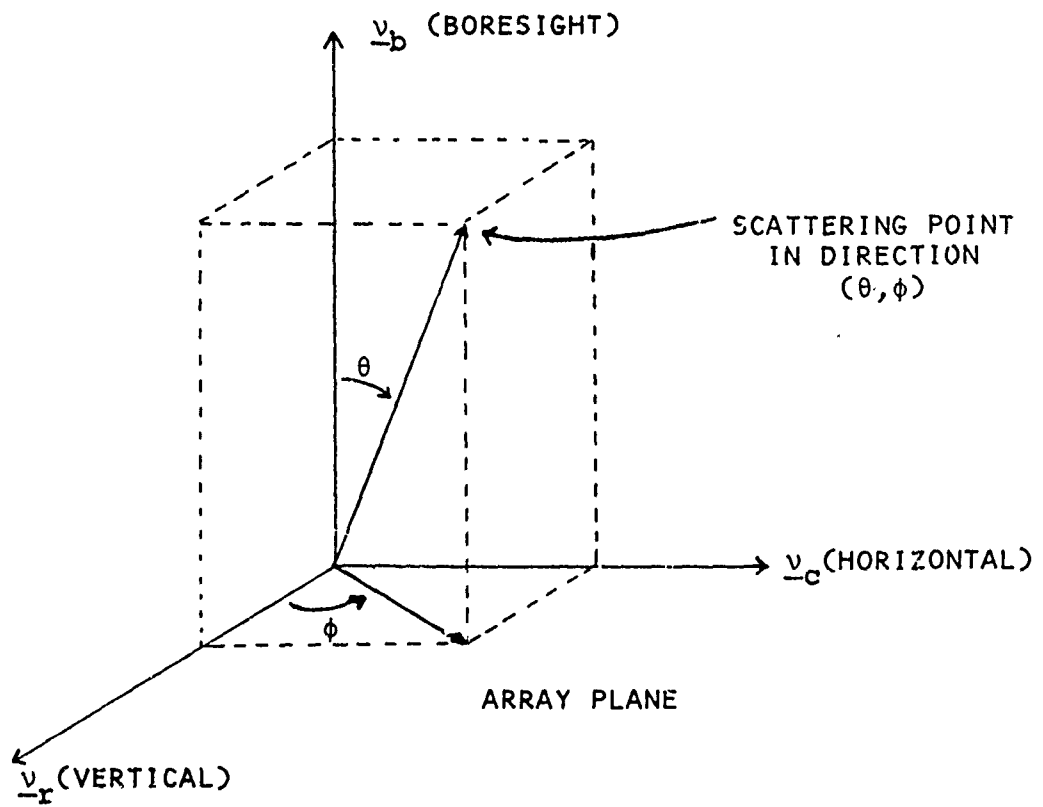
Figure 9-5   Antenna Coordinate System and Angles Used
To Define Directions of Scattering Points
for the Antenna Patterns.

9-9

gains of the antennas are also computed (with no phase shifts). The functions RGAIN and TGAIN give the antenna gain patterns relative to these values.

9.2.3 Common Volume Integration Limits

Subroutine INTLIM determines lower bounds on the limits of integration for the common volume. The beamwidths of the subarrays and the scattering parameter are used to determine these bounds. The actual region of integration may be larger than the region determined by INTLIM as the integration does not terminate until the contributions to the delay profiles become small. These bounds ensure that the integration does not terminate before a sufficient volume has been integrated. In addition the estimate of the common volume is used to determine the size and number of delay cells to be used in the profiles. An input parameter ERR is used in determining the limits. Small values of ERR increase the size of the region.

9.2.4 Common Volume Integration

Subroutine LOOPS performs a numerical integration over the common volume to determine the power vs. delay and cross-correlation profiles. Each scattering point in the common volume is specified by the transmit and receive elevation angles α, β (measured relative to a straight line between the receiver and transmitter in transformed earth coordinates) and the distance y perpendicular to the great circle plane. The great circle plane contains the nominal receiver and transmitter locations and the center of the earth.

For each scattering point r, the program computes the distances from the transmitter to r and from r to the receiver (slightly different for each receiver location), the angles of r relative to the transmitter and receiver antenna patterns, and

the scattering angle. The net received power from this single scattering element at vector location $\underline{r}$ for transmitter ᵀ and receiver R is

$$P(\underline{r}) = P_T C \; dV \; \frac{g_T(\underline{r})^2 \; g_R(\underline{r})^2}{R_T(\underline{r})^2 \; R_R(\underline{r})^2} \; \theta^{-m}$$

where

P_T	=	transmitted power
$g_T(\underline{r})$	=	gain of the transmit antenna in the direction of $\underline{r}$
$g_R(\underline{r})$	=	gain for the receive antenna
$R_R(\underline{r}), R_T(\underline{r})$	=	distances from $\underline{r}$ to receiver and transmitter, respectively.
C	=	a factor depending on wavelength and height above sea level
dV	=	Volume of infinitesimal scatterer at $\underline{r}$.
θ	=	scattering angle, i.e. angle by which waves from transmitting antenna must be deflected at the scattering point $\underline{r}$ to reach the receiver antennas.
m	=	spectrum slope of refractive index (m controls rate of fall-off of scattering coefficient with scattering angle).

The antenna gain patterns in this equation are, of course, expressed as dimensionless ratios (not dB).

The delay profiles are generated by computing the delay for each scatterer and adding the value of the power $P(\underline{r})$ for that scatterer to the corresponding delay all in the profile. The integral of the profile determines the total path loss.

The cross correlation profiles between different receiver ports are obtained similarly, except that the receiver antenna power gain $\left|g_R(\underline{r})\right|^2$ is replaced by $g_{R_1}(\underline{r})g^*_{R_2}(\underline{r})$, the product of one receiver voltage gain with the conjugate of the other. Each voltage gain is a complex quantity with a phase angle determined by the RF phase shift from the scatterer to the receiver. If receivers R_1 and R_2 have the same location (i.e., angle diversity) then these phase shifts are the same and $g_{R_1}(\underline{r})g^*_{R_2}(\underline{r})$ is real. So the phase shift has an effect only when the receivers are in different locations. In addition if the receivers are for different polarizations then the RF phase shifts from the transmitters to the scattering point are included. The different phase shifts for scatterers over the common volume cause decorrelation of the signals at two space diversity receivers.

9.2.5 Step Size Parameters

Subroutine STPPAR determines a number of parameters which are used to determine the step sizes in the integration over the common volume. The step sizes must be selected such that the contribution of scatterers to the profiles does not change too much from one scatterer to the next. To accomplish this, the variations of all of the parameters which determine this contribution are considered. The dominant effects are given by the gain patterns of the receiver and transmitter antennas, the scattering angle, and the phase shifts for space diversity antennas.

9.3 VARIABLE DIMENSIONING PARAMETERS IN TROPO

Many of the arrays used in TROPO have variable dimensions. These distances are specified in parameter statements. These parameters are:

NTMX	Maximum number of distinct transmitter ports
NRMX	Maximum number of distinct receiver ports
NRLMX	Maximum number of distinct receiver locations
NRBMX	Maximum number of distinct receiver beams
NRAMX	Maximum number of distinct receiver physical antennas
NSTMX	Maximum number of different subarray types
NPOWMX	Maximum number of receiver ports for which the power may be computed
NCORMX	Maximum number of cross-correlations between receiver ports which may be computed
NQMX	Total number of samples in all delay profiles
NCN2	Maximum number of samples in C_n^2 profile.

9.4 INPUT FILE FORMAT

The inputs for the TROPO program are taken from a file called TROPO.INP. In the input file the line before a data line begins with '*'. Any number of comment lines beginning with 'C' may be included before the line which begins with '*'.

The inputs are divided into five basic sections:

1. Unit specifications
2. System parameters
3. Path geometry
4. Propagation and control parameters
5. Diversity input.

9.4.1 Parameters Which Determine Units

DISTU   Distance units specification, (FORTRAN A4 format, left justified): SMI, KM, or NMI. All parameters designated below as having units in smi/nmi/km will be interpreted according to the setting of DISTU, as follows:

    SMI   Statute Miles
    NMI   Nautical Miles
    KM   Kilometers

HDU   Height and diameter units specification (FORTRAN A4 format, left justified): FT or M, standing for feet or meters, respectiv ly. All parameters designated below as being in units of ft/m will be interpreted according to the setting of HDU.

ANGU   Angle units specification, (FORTRAN A4 format, left justified): DEG or MRAD. All parameters representing angles will be interpreted according to the setting of ANGU, as follows:

    DEG   all angles are in degrees
    MRAD   all angles are in milliradians,
             i.e. 1000 mrad = 1 radian.

FRU   Frequency units specification, (FORTRAN A4 format, left justified): MHZ or GHZ. All frequency units will be interpreted according to the setting of FRU, unless otherwise noted.

9.4.2 Transmitter and Receiver Parameters

PXMIT   Rated transmitter power in dBm. (Default = 70 dBm). If PXMIT is input as 0, it is computed from WLT as $10 \, \mathrm{Log}_{10}(\mathrm{WLT}) + 30$.

WLT   Rated transmitter power in Watts. If WLT is zero then WLT is computed as $10(\mathrm{PXMIT} - 30)/10$. The input value of WLT is ignored in this case.

F   Carrier Frequency

TLL   Transmitter line loss in dB. Default = 0dB.

RLL   Receiver line loss in dB. Default = 0dB.

PNOISE   Noise power in dBm.

9.4.3 Path Geometry

D	Great circle distance (measured at sea level) between transmitter and receiver (km, smi, nmi)
HTN,HRN	Elevation of transmit and receiver nominal antenna locations above sea level (meters or feet)
ITOFF	control indicator for entry or calculation of transmit/receive radio horizon angles THET, THER. Use as follows:

0 = user specifies radio horizon angles THET,THER.

2 = radio horizon angles THET,THER are calculated in program using the horizon distance (DLT,DLR) and horizon elevations (HLT,HLR).

THET,THER	radio horizon elevation angles at transmit and receiver sites in degrees or mrad. (Ignored if ITOFF≠0.)
DLT,DLR	distance to radio horizon from transmitter and receiver respectively (km, smi, nmi). (Ignored if ITOFF=0.)
HLT,HLR	transmit and receive radio horizon elevation above sea level (meters or feet). (Ignored if ITOFF=0.)

9.4.4   Propagation and Control Parameters

IHFLG	profile type: 0 for delay, 1 for height (default = 0)
SEAN	surface refractivity at sea level (default = 0)
ERFAC	effective earth radius factor (default = 1.333)
SCPARM	wavenumber spectrum slope parameter m (default = 3.666)
NACCU	integration accuracy parameter (default = 40)

ERR   termination parameter (default = .001)

KPROF   number of c_n^2 samples

DELH   distance between samples

CN2(1:KPROF) c_n^2 profile

9.4.5 Diversity Input

9.4.5.1 Transmitter Parameters

NT   Number of transmit ports (NT < 2)

PSITEO(NT) Antenna boresight elevation above the hori-
            zontal (deg/mrad). (Boresight is defined as
            perpendicular to the plane of a phased array.)

PSITAO(NT) Transmit antenna boresight azimuth, relative
            to the great circle plane containing the re-
            ceive and transmit sites. Positive counter-
            clockwise (deg/mrad).

IPOLT(NT)   Transmit antenna polarizations. The integer
            values 0 and 1 represent any two orthogonal
            polarizations. These may, for example, rep-
            resent horizontal and vertical polarization.

UTH(i_T) Horizontal, vertical, and longitudinal
UTV(i_T) location of transmitting antenna i_T
UTL(i_T) relative to the nominal position where i_T=1,
            ..., NT (ft/m)

NRLOC   Number of distinct receiver locations

Note: For these coordinates, the longitudinal axis
            is taken to be horizontal and in the great
            circle plane containing the transmit and
            receive sites. The positive longitudinal
            direction is from the transmitter to the
            receiver site. Up is positive in the vertical
            direction and left is positive in the horizon-
            tal direction, as seen looking from transmit-
            ter to receiver.

ITSAT(1:NT) index of the subarray type for each antenna

NTVPA(1:NT) # of subarrays in vertical direction

NTHPA(1:NT) # of subarrays in horizontal direction

DTVPA(1:NT)	distance between vertically adjacent subarrays
DTHPA(1:NT)	distance between horizontally adjacent sub-arrays
PTVPA(1:NT)	phase shift between vertically adjacent sub-arrays
PTHPA(1:NT)	phase shift between horizontally adjacent sub-arrays
GDBTX(1:NT)	boresight gain of transmit antenna (computed if entered as 0).

9.4.5.2 Receiver Parameters

Due to space limitations a number of pointers are used in specifying the receiver ports. These pointers are illustrated in Figure 9-6. For each of the NR ports, IRLOC specifies the location index (i.e., the i-th port has horizontal offset URH(IRLOC(i)), IRBEAM specifies the beam (which phasing of which array), and IRPOL specifies the polarization (0 or 1).

Similarly, IRANT(i) is the physical antenna index for the i-th beam. So, for example, the elevation angle of the i-th beam is PSIRE0(IRANT(i)).

Definition of Variables

NR	number of ports
NRLOC	number of locations
NRBEAM	number of beams
NRANT	number of antennas
NSAT	number of subarray types
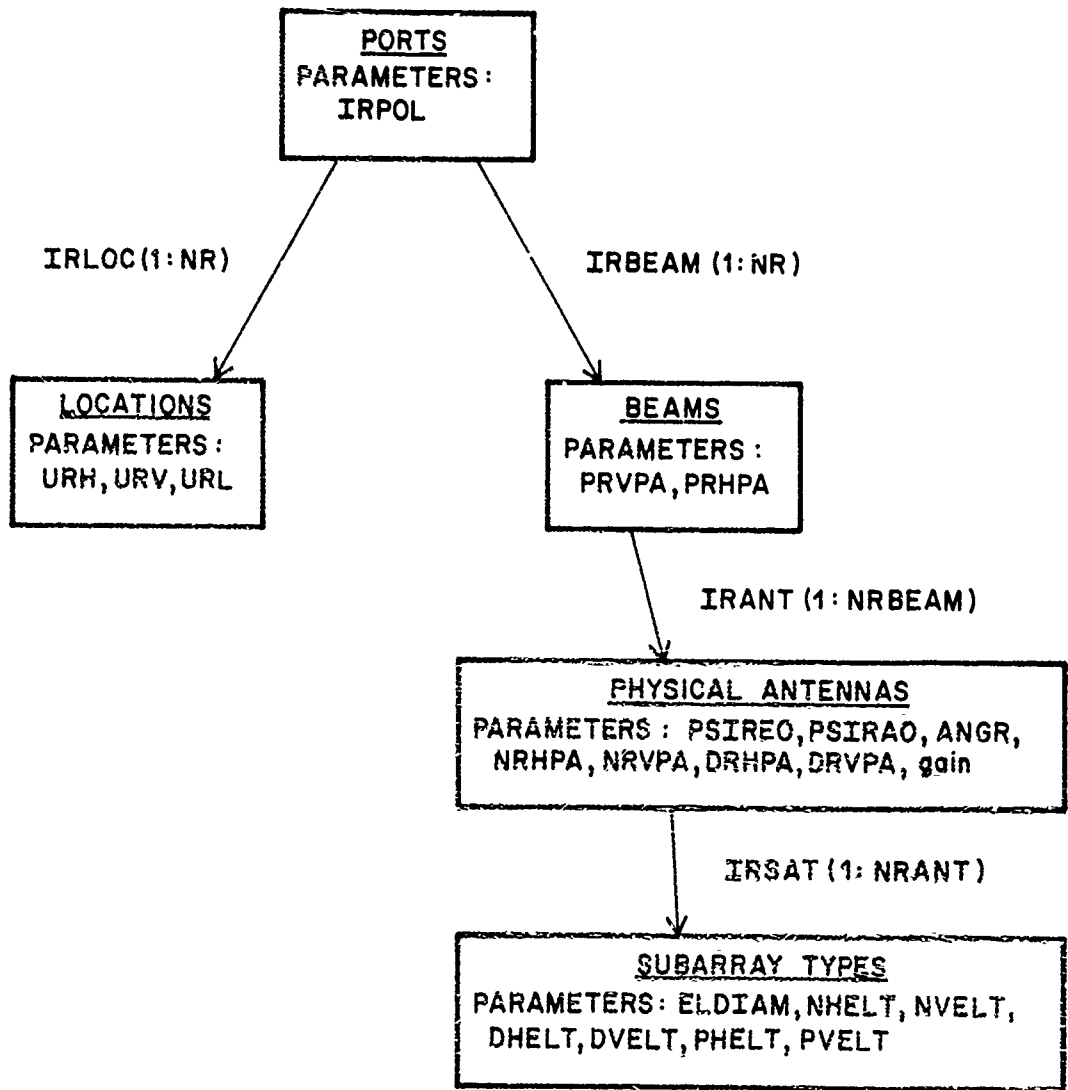
Figure 9-6   Receiver Port Definition

Port Parameters (arrays with NR elements)

IRPOL( )	polarization
IRLOC( )	location index
IRBEAM( )	number of subarray types

Location Parameters (NRLOC elements)

URV( )	horizontal offset
URV( )	vertical offset
URL( )	longitudinal offset (positive towards transmitter)

Beam Parameters (NRBEAM elements)

PRHPA ( )	phase shift between horizontally adjacent elements
PRVPA( )	phase shift between vertically adjacent elements
IRANT( )	index of physical antenna type

Physical Antenna Parameters (NRANT elements)

PSITE0( )	elevation angle above horizon
PSITA0( )	azimuth angle (= 0 if pointed at transmitter)
ANGR( )	rotation of array with respect to horizontal
NRHPA( )	number of subarrays in horizontal direction
NRVPA( )	number of subarrays in vertical direction (NRVPA(i)*NRHPA(i) = total number of subarrays)
DRHPA( )	distance between horizontally adjacent subarrays
DRVPA( )	distance between vertically adjacent subarrays
GDBRX( )	boresight gain (computed if input as 0)
IRSAT( )	index of subarray type.

9.4.5.3 Subarray Parameters

NSAT   # of subarray types (default 1)

ELDIAM(1:NSAT) element dimension for each subarray type
          (elements assumed to be circular)

NVELT(1:NSAT) # of elements in vertical direction for each
          subarray

NHELT(1:NSAT) # of elements in horizontal direction for
          each subarray

DVELT(1:NSAT) distance between vertically adjacent
          elements (Default: element dimension)

DHELT(1:NSAT) distance between horizontally adjacent ele-
          ments (Default: element dimension)

PVELT(1:NSAT) phase shift between vertically adjacent ele-
          ments (Default 0)

PHELT(1:NSAT) phase shift between horizontally adjacent
          elements (Default 0)

9.4.5.4 Selection of Correlations Desired

IPROF   1 if profiles desired, 0 if not

NPOW   number of power profiles

IPOW(1:NPOW) indices of power profiles (i.e., which
          ports)

(I1CORR(1:NCORR), pairs of indices for correlation profiles
I2CORR(1:NCORR))

REFERENCES

[1]   Beckman, P. (1967), Probability in Communication Engineering, Haycourt, Bruce, and World, Inc., New York.

[2]   Tatarski, V.I. (1971), The Effects of the Turbulent Atmosphere on Wave Propagation, U.S. Department of Commerce, NTIS, Springfield, VA.

[3]   Parl, S.A. and A. Malaga, (1981), "Theoretical Analysis of Microwave Propagation: Interim Report", SIGNATRON Report for RADC/ESD, Contract F19628-80-C-0106.

[4]   Booker, H.G. and W.E. Gordon (1950), "A Theory of Radio Scattering in the Troposphere", Proc. IRE, Vol. 38, pp. 401-402.

[5]   Booker, H.G., and J.T. DeBettencourt (1955), "Theory of radio transmission by tropospheric scattering using very narrow beams", Proc IRE, V. 43, pp. 281-290.

[6]   Villars, F. and V.F. Weisskopf (1955), "On the Scattering of Radio Waves by Turbulent Fluctuations of the Atmosphere", Proc. IRE, Vol. 43, No. 10, pp. 1232-1239.

[7]   Megaw, E.C.S. (1950), "Scattering of Electromagnetic Waves by Atmospheric Turbulence", Nature, Vol. 166, pp. 1100-1104.

[8]   Rice, P.L., A.G. Longley, K.A. Norton, and A.P. Barsis (1965, Rev. 1967), "Transmission Loss Predictions for Tropospheric Communications Circuits" N.B.S. Tech. Note 101.

[9]   Obukhov, A.M. (1941), "On the Distribution of Energy in the Spectrum of Turbulent Flow", Bull. Acad. Sci. USSR Geo. and Geophys. Ser. 4-5, 453. See also Comptes Rendus (Doklady) L'Academie des Sciences de L'USSR Vo. 32, No. 1.

[10] Kolmogoroff, A.N. (1943), "Dissipation of energy in Locally Isotropic Turbulence", Complete Rendus (Doklady) de l'Acadamie des Sciences de l'USSR, Vol. 32, No. 1, pp. 16-18.

[11] Monsen, P. and S.A. Parl (1978), "Adaptive Antenna Control 2nd Interim Report for U.S. Army ECOM, Report No. ECOM-76-8085-2, October 1977.

REFERENCES (Con't)

[12]   Monsen, P. and S.A. Parl (1980), _Final Report, Adaptive Antenna Control (AAC) Program_, CSA-76-8085-6, for U.S. Army, Ft. Monmouth, N.J., March 1980.

[13]   Parl, S.A. (1979), "New Formulas for Tropospheric Scatter Path Loss", _Radio Science_, Vol. 14, No. 1, pp. 49-57.

[14]   David, H.A., _Order Statistics_, 2nd Edition 1981, Wiley, New York.

[15]   Monsen, P., "Theoretical and Measured Performance of a DFE Modem on a Fading Multipath Channel", _IEEE Transactions on Communications_, Vol. COM-25, No. 10, October 1977, pp. 1144-1153.

[16]   Brennan, L.E., "The Maximum Signal-to-Noise Ratio Realizable from Several Noisy Signals", _Proc. IRE_, Vol. 43, pp. 1530, October 1955.

[17]   Cox, D.C. and A.T. Waterman, Jr. (1967), "A Data-Gathering Antenna Array for Transmission Propagation Research", _IEEE Trans. Antenna Prop._, Vol. AP-17, pp. 69-77, January 1967.

APPENDIX A

DEFINITION OF MATHEMATICAL AND COMPUTER PROGRAM SYMBOLS
USED IN TROPOSCATTER PROPAGATION MODEL

This appendix contains the mathematical symbols used and the corresponding computer program parameters. The symbols are described in the context of the COMMON statement in which they appear in the computer program. In what follows, the symbols used in the computer code are listed in square brackets.

A.1 PATH GEOMETRY

Figure A-1 shows the geometry of the path as seen in the plane of the great circle through the nominal antenna locations. Figure A-2 shows a top view of a path with horizontally spaced antennas. The parameters in Figure A-1 are those used in most troposcatter calculations. In addition to these parameters we must also consider:

1. location of space diversity antennas relative to the nominal terminal location,

2. angle diversity beams,

3. phased array parameters.

Scatter Volume
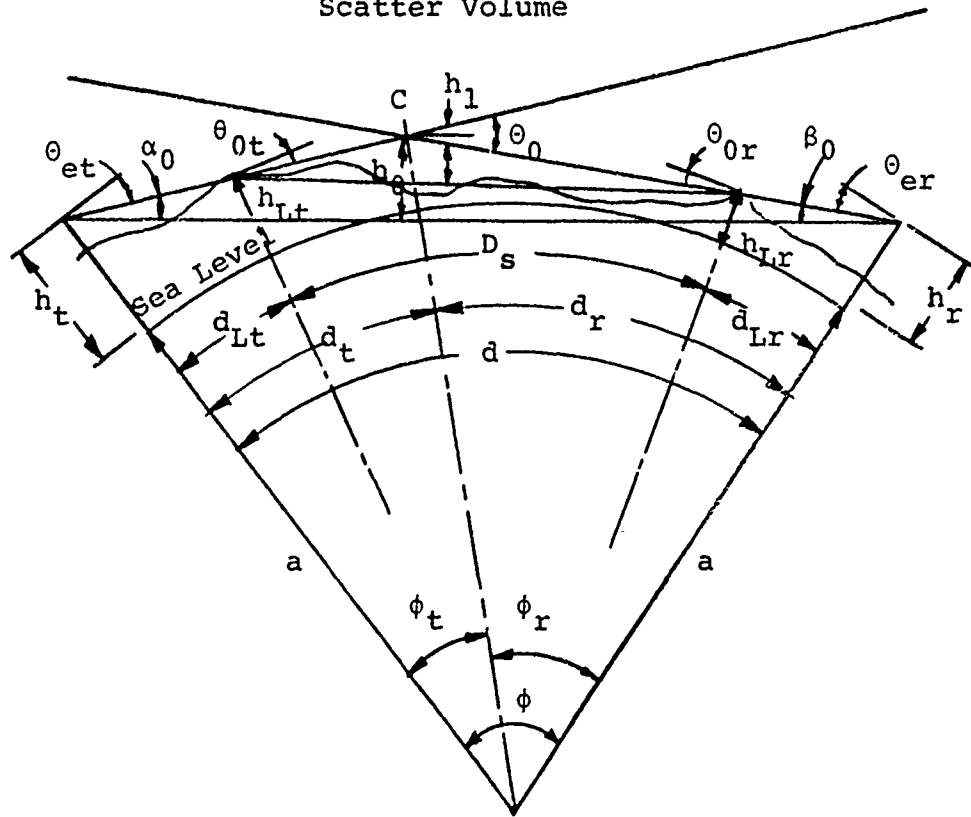
$$\theta_2 = \frac{d}{a} + \theta_{et} + \theta_{er}$$

FIGURE A-1   PATH GEOMETRY - GREAT CIRCLE VIEW

A-2
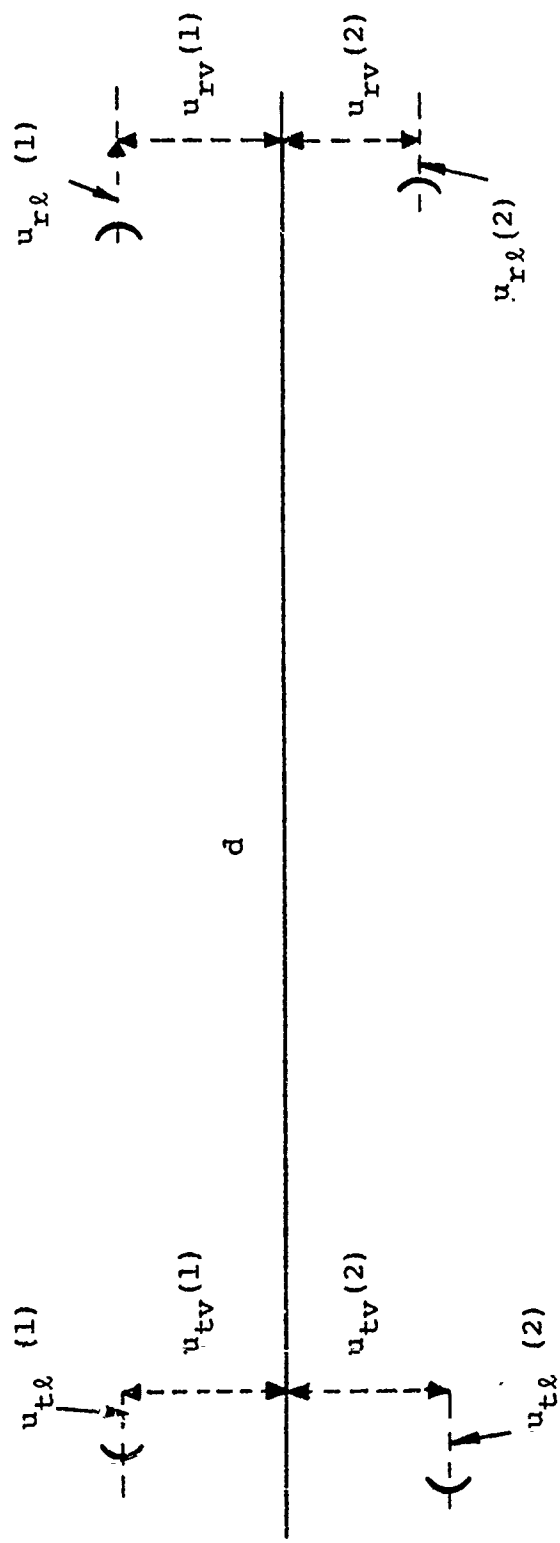
FIGURE A-2 PATH GEOMETRY – TOP VIEW

The key TROPO program parameters including the effective earth radius transformation are listed below.

     TROPO SYMBOL

NBS TECH. NOTE SYMBOL	TROPO SYMBOL	
a_0	[A0]	Earth radius.
a	[A]	Effective earth radius.
d	[D]	Distance between nominal terminal locations.
d_{Lt}	[DLT]	Distance to horizon from the transmitter, measured at sea level.
d_{Lr}	[DLR]	Distance to horizon from the receiver (measured at sea level).
d_t	[DT]	Sea level distance to the scattering point from the nominal transmitter location.
d_r	[DR]	Sea level distance to the scattering point from the nominal receiver location.
h_{tn}	[HTN]	Height above the sea level of the nominal transmitter location.
h_{rn}	[HRN]	Height above the sea level of the nominal receiver location.
$u_{th}, u_{tv}, u_{t\ell}(i_t)$	[UTH(I), UTV(I) I ≤ NTMX]	Horizontal, vertical, and longitudinal location of transmitting antenna number i_t relative to the nominal position (site ground level mid way between antennas) (counted positive up, into the paper, and from the transmitter to receiver respectively).

u_{rh}, u_{rv} $u_{r\ell}(i_r)$	[URH(I), URV(I), URL(I), I $\leqslant$ NRMX]	Horizontal, vertical and longitudinal location of receiving antenna no. i_r relative to the nominal position (site ground level mid way between antennas).
$h_t(i_t)$	[HT]	Height above the sea level of the center of transmit antenna no. i_t, $(=h_{tn} + u_{th}(i_t))$.
$h_r(i_r)$	[HR]	Height above the sea level of the center of receive antenna no. i_r, $(=h_{rn} + u_{rh}(i_r))$.
S	[S]	Asymmetry parameter α_0/β_0.
S_1	[S1]	Asymmetry parameter $(\alpha_0-\beta_0)/\theta_0$ $= (1-S)/(1+S)$.
h_{Lt}, h_{Lr}	[HLT,HLR]	Height above the sea level of the transmit (receive) horizon obstacle.
h_0	[HCOM]	Height of lowest scattering point above sea level.
α_0	[ALFA0]	Angle at the nominal transmitter between the horizon ray and the ray to the receiver.
β_0	[BETA0]	Angle at the nominal receiver between the horizon ray and the ray to the nominal transmitter.
θ_0	[THETA0]	Scattering angle of horizon rays.
ϕ_t	[PHIT]	d_t/a.
ϕ_r	[PHIR]	d_r/a.
θ_{et}	[THET]	Transmitter horizon elevation angle.
θ_{er}	[THER]	Receiver horizon elevation angle.

A.2 ANTENNA PARAMETERS

Parameters relating to the transmitter and receiver antennas are defined. Antenna location parameters are described in A.1.

$g_t(i_t, \theta, \psi)$	[TGAIN]	Directive gain pattern of the transmitting aperture no. i_t. θ is the off-boresight angle, ϕ is the azimuth angle. TGAIN is a function subroutine.
$g_r(i_r, \theta, \psi)$	[RGAIN]	Receiver gain patterns.
$G_t(i_t)$	[GDBTX(I)],	Boresight transmitter antenna gains.
$G_r(i_r)$	[GDBRX(I), I $\leqslant$ NR]	Boresight receiver antenna gains.
$\psi_{te0}(i_t)$	[PSITE0(I) I $\leqslant$ NT]	Antenna boresight elevation above the horizon for each transmit antenna.
$\psi_{re0}(i_t)$	[PSIRE0(I) I $\leqslant$ NR]	Same for receive antennas.
$\psi_{ta0}(i_t)$	[PSITA0(I) I $\leqslant$ NT]	Transmit antenna boresight azimuth, defines the angle to the great-circle plane. Positive counter clockwise.
$\psi_{ra0}(i_r,$	[PSIRA0(I) I $\leqslant$ NR]	Same for receiver, but positive clockwise.
N_t	[NT]	No. of distinct transmit ports.
N_r	[NR]	No. of distinct receive ports.

PROPAGATION PARAMETERS

AA	[AA]	Atmospheric dB attenuation.
K	[ERFAC]	Effective earth radius factor.
M	[SCPARM]	Wavenumber spectrum slope parameter.

N_s	[SEAN]	Minimum monthly median value of sea level surface refractivity.
$C_n^2(ih)$	[CN2(I), I ≤ NPROF]	Atmospheric structure constant profile.
Δ_h	[DELH]	Interval of sampled C_n^2.

SYSTEM TRANSMISSION PARAMETERS

$W_{\ell t}$	[WLT]	Transmitted power.
W_t	[WT]	Radiated power.
W_r	[WR]	Available power at receiver input.
f	[F]	Frequency.
λ	[WAVLEN]	Wavelength.

APPENDIX B

DESCRIPTION OF MATHEMATICAL RESULTS USED IN
THE TROPOSCATTER PREDICTION PROGRAM

This appendix contains the mathematical results used in the coding of the common volume integration routine. The correspondence of symbols to the variable names in the computer program are found in Appendix A.

B.1 THE EARTH RADIUS TRANSFORMATION

We use the well known effective earth radius concept in a way that allows an exact transformation.

Let a_0 be the actual earth radius (measured at sea level) and let r_0 be the distance from the center of the earth to any point on or above the surface of the earth. Propagation in a spherically stratified atmosphere is guided by the following equation

$$r_0 n(r_0) \sin \Theta_0(r_0) = a_0 n(a_0) \sin \Theta_0(a_0) \quad \text{(Snell's Law)} \qquad \text{(B.1)}$$

and

$$r_0 d\phi_0 = \tan \Theta_0(r_0) dr_0 \qquad \text{(B.2)}$$

where (see Figure B-1)

$$\theta_0(r_0) = \text{zenith angle of ray at distance } r_0$$

$$\phi_0(r_0) = \text{angle from start of path } (\text{at } r_0 = a)$$

to a variable point on the path.

We now assume a special form of height variation of the refractive index,

$$n(r_0) = n_0(a_0/r_0)^\gamma \quad . \tag{B.3}$$

The refractive index varies according to a power law. Near the surface of the earth the gradient is nearly constant. The refractive index varies with height in a way similar to that of the exponential model although the fall-off with increasing height is slower than for the exponential model. However the model in (B.3) is a better approximation than the linear gradient often assumed. The parameter γ is related to the gradient of the coefficient of refraction (expressed in N-units) by

$$\frac{\Delta N}{\text{N-units/km}} = -\gamma \cdot 10^9 \frac{n(a_0)}{a_0/[1m]} \quad . \tag{B.4}$$
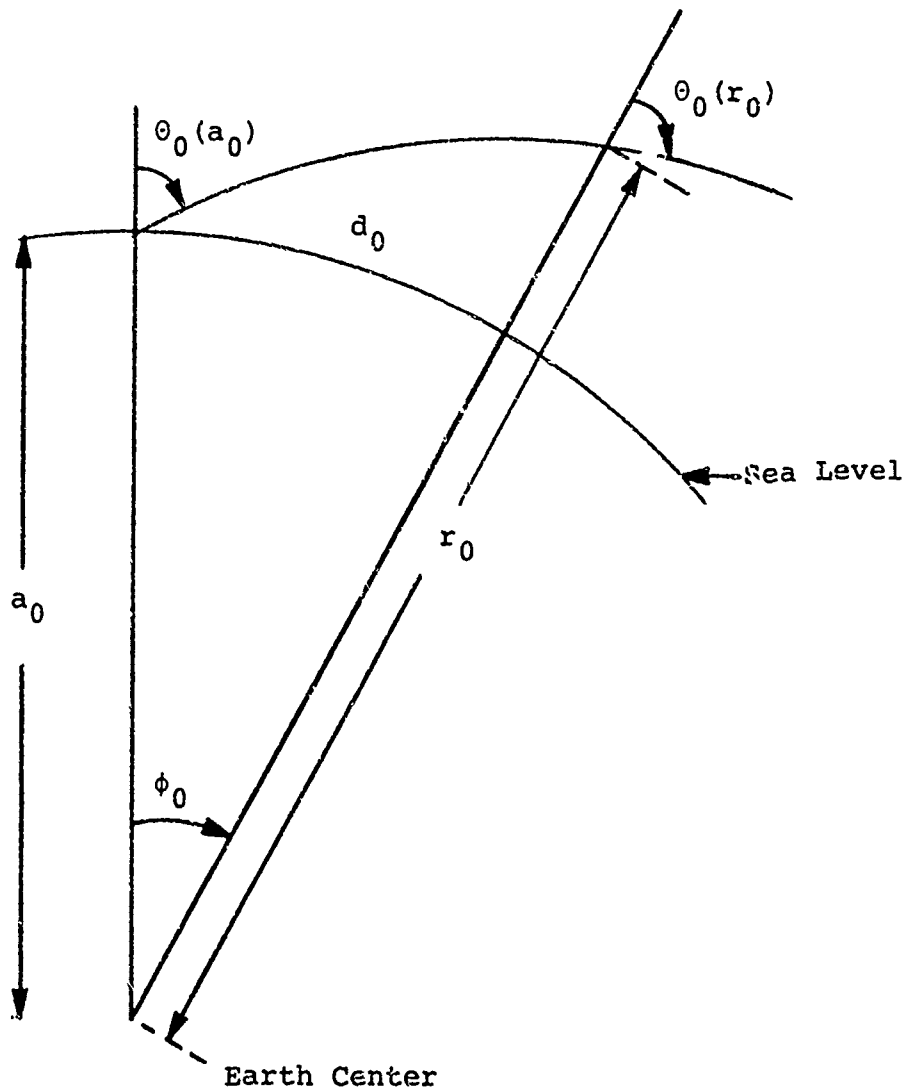
Fig. B-1   Path Geometry for Refractive Path

For the standard atmosphere we have $\gamma = 0.25$. The form of the refractive index in (B.3) allows us to transform the coordinates so that the electromagnetic waves propagate in straight lines in the transformed coordinate system. Define in the great circle plane

$$r = r(r_0) = \frac{1}{1-\gamma} \, a_0^{\gamma} \, r_0^{1-\gamma}$$

$$d = d_0 \ . \tag{B.5}$$

This transformation preserves distance along the surface of the earth, but the new earth center distance r is different. In particular the new effective earth radius is

$$a = r(a_0) = a_0/(1-\gamma) \ . \tag{B.6}$$

The angular distance ϕ_0 is transformed into

$$\phi = \delta_0(1-\gamma) \ . \tag{B.7}$$

The angles Θ are preserved in the transformation,

$$\Theta(r,\phi) = \Theta_0(r_0,\phi_0) \ . \tag{B.8}$$

The transformation (B.5) when inserted into (B.1) and (B.2) shows that a path in the transformed coordinates satisfies

$$r \sin \Theta(r) = a \sin \Theta(a) \qquad \text{(B.1a)}$$

$$r \, d\phi = \tan \Theta(r) dr \qquad \text{(B.2a)}$$

which represents the equations for a straight line. Heights above the nominal sea level are transformed according to

$$a + h = \frac{1}{1-\gamma} a_0^{\gamma} (a_0 + h_0)^{1-\gamma}$$

or

$$h \approx h_0 - \frac{\gamma}{2} \frac{h_0^2}{a_0} + \frac{\gamma(\gamma+1)}{3!} \frac{h_0^3}{a_0^2} \dots \qquad \text{(B.9)}$$

This formula describes the height reduction effect in a near linear profile of the refractive index. In practice only the first two terms are needed.

B.2 CALCULATION OF SCATTERING POINT

The geometry for calculating the distances to and the height of the scattering point is shown in Figure B-2. The distances a_t is given by $a + h_{te}$, where h_{te} is the effective transmitter height. Let us place a coordinate system with origin at the center C and with X-axis along the line CR. Express in vector coordinates the equation
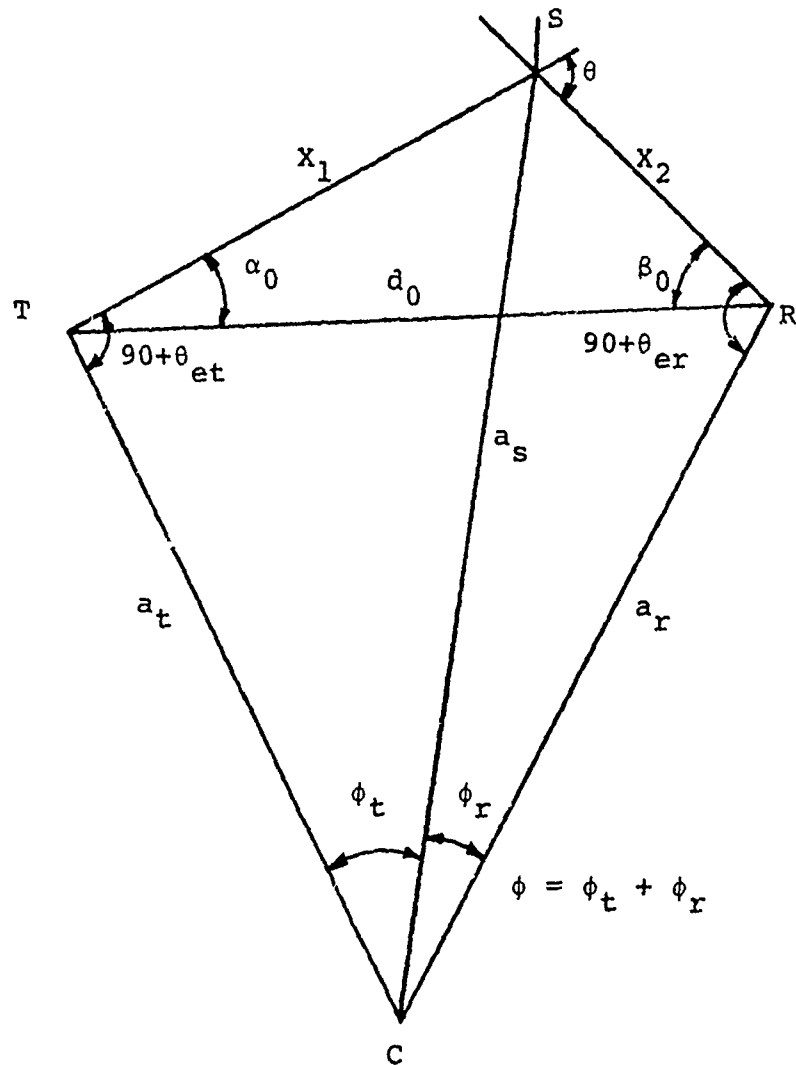
FIGURE B-2

$$\underline{CT} + \underline{TS} = \underline{CR} + \underline{RS} \ ,$$

$$(a_t \cos \phi, \ a_t \sin \phi) + X_1 (\cos(\phi - 90^0 + \Theta_{et}), \ \sin(\phi - 90^0 + \Theta_{et}))$$

$$= (a_r, 0) + X_2 (\cos(90^0 - \Theta_{er}), \ \sin(90^0 - \Theta_{er}))$$

where X_1 and X_2 are unknowns. Solving for X_1 and X_2 we get

$$X_1 = [a_r \cos \Theta_{er} - a_t \cos(\phi + \Theta_{er})]/\sin \Theta$$

$$X_2 = [a_t \cos \Theta_{et} - a_r \cos(\phi + \Theta_{et})]/\sin \Theta \ .$$

These numbers should be positive if the input parameters are correct. The angle ϕ_r is determined from

$$\tan \phi_r = \frac{X_2 \cos \Theta_{er}}{a_r + X_2 \sin \Theta_{er}} \quad X_2/a_r \ .$$

ϕ_t is calculated from $\phi_t = \phi - \phi_r$. The signs of ϕ_t and ϕ_r are checked. a_s is calculated from

$$(a_s - a_r) \cos \phi_r = 2a_r \sin^2(\phi_r/2) + X_2 \sin \Theta_{er} \ .$$

B-7

The slant range d_0 between the terminals is given by

$$d_0^2 = a_t^2 + a_r^2 - 2a_t a_r \cos \phi$$

$$= (a_t - a_r)^2 + 4a_t a_r \sin^2(\phi/2) \quad .$$

The angles α_0 and β_0 are then given by

$$\sin \alpha_0 = \frac{x_2}{d_0} \sin \theta_0$$

$$\sin \beta_0 = \frac{x_1}{d_0} \sin \theta_0$$

$$\alpha_0 + \beta_0 = \theta_0 \quad .$$

B.3 COMMON VOLUME CALCULATIONS

The size of the common volume is limited by the antenna size, pointing angles, scattering angle, and atmospheric structure constant. We have already determined the minimum angles α_0, β_0 of the angle α and β (see Figure B-3). The integration is performed by integrating over α, β, and the distance y perpendicular to the great circle plane. It is assumed that all antenna transmitter beams are essentially pointed at the horizons. Let β_c be the β-angle corresponding to the boresight of the most elevated receiving beam. and let α_c, θ_c be the corresponding transmitter and scatter angles. We have

B-8
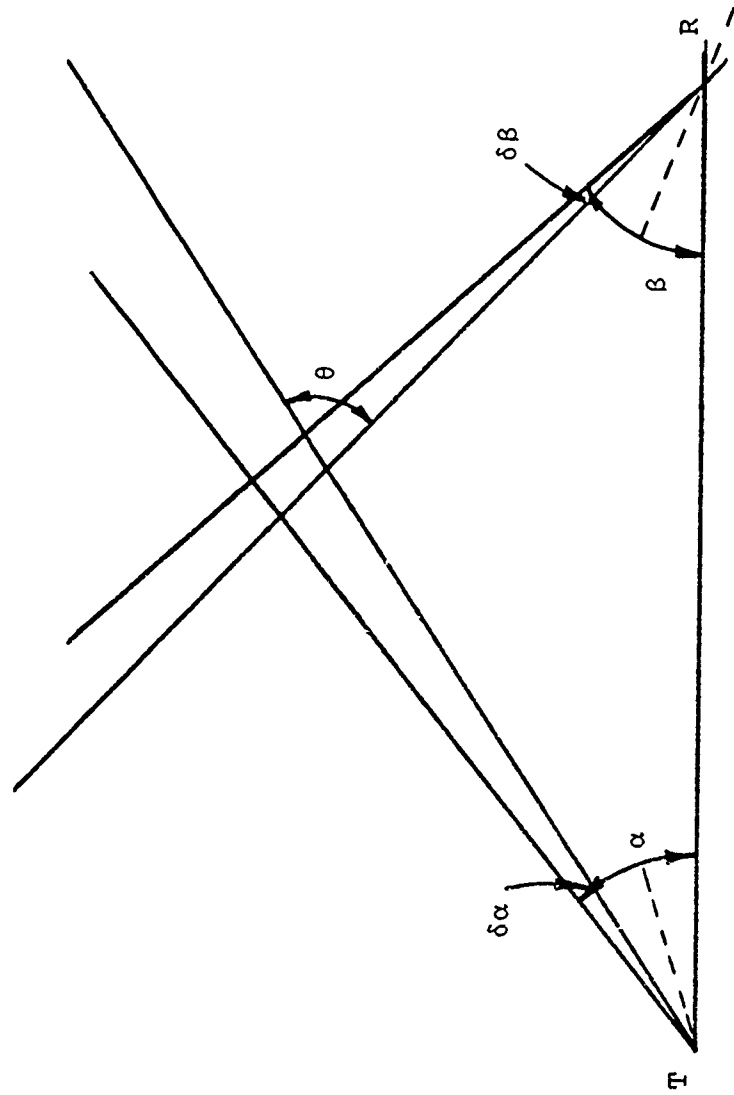
FIGURE B-3 COMMON VOLUME INTEGRATION IN THE GREAT CIRCLE PLANE

$$\alpha_1 - \alpha_c > \delta_{vte} \qquad\qquad\qquad (\text{B.10})$$

where $2\delta_v$te is the maximum vertical 3dB beamwidth of the transmitter elements. Similarly

$$\beta_1 - \beta_c > \delta_{vre} . \qquad\qquad\qquad (\text{B.11})$$

We also need not consider angles where the contribution to the integral is less than ϵ, where ϵ is a program controllable accuracy parameter. Using the results of [Equation 8 in Parl, 1979] we get

$$\left(\alpha_1 + \beta_1\right)^{2-m} < \epsilon_1 \left(\alpha_c + \beta_c\right)^{2-m}$$

or

$$\alpha_1 + \beta_1 > \epsilon_1^{\frac{1}{m-2}} \left(\alpha_c + \beta_c\right) .$$

A weaker bound is then

$$\alpha_1 > \epsilon_1^{-1/(m-2)}\left(\alpha_c + \beta_c\right) - \beta_m \qquad (B.12)$$

$$\beta_1 > \epsilon_1^{-1/(m-2)}\left(\alpha_c + \beta_c\right) - \alpha_m \qquad (B.13)$$

(B.10) through (B.13) determine the minimum and maximum angles. The value of ϵ_1 used is min $(0.2, 50\epsilon)$.

Now consider the integration in the y-axis direction perpendicular to the great circle plane. Let $\pm y_1$ be the extreme values of the integration. We must have

$$y_1 > \max\left(d_t \delta_{hte}, d_r \delta_{hre}\right) \quad, \qquad (B.17)$$

where δ_{hte} and δ_{hre} are the horizontal semi-beamwidths of the transmitter and receiver array elements respectively. The maximum y-values may also be limited by the scattering angles. We assume here that the horizons are straight horizontal obstacles so that α_{min} and β_{min} are unchanged for off-centerplane scattering. For present purposes we can use the following approximation to the scattering angle Θ,

$$\Theta^2(\alpha, \beta, y) = \Theta^2(\alpha, \beta, 0) + \left(y/R_0\right)^2 \quad,$$

where

$$R_0 = \frac{d_t d_r}{d_t + d_r} \ .$$

If we require that

$$\Theta^{-m}(\alpha, \beta, y) < \varepsilon \ \Theta^{-m}(\alpha, \beta, 0),$$

we get

$$|y_1| > R_0 \Theta(\alpha, \beta, 0)[\varepsilon^{-2/m} - 1]^{1/2} \ . \tag{B.18}$$

B.4 STEP SIZE PARAMETERS

The step size in the integration is affected by the antenna patterns and scattering angle. In addition changes the phase difference between space diversity antennas limits the step size. Let $\delta\alpha$, $\delta\beta$ and δy be the step sizes for α, β and y respectively. We set

$$\delta\alpha < K\delta_{vt}$$

$$\delta\beta < K\delta_{vr}$$

where δ_{rt} and δ_{vr} are the minimum vertical half-power semi-beam-widths for the transmitter and receiver, and K is a constant generally not more than .2. In the program we set

$$K = \min(.5,\ 200 \times ERR)$$

where ERR is an input parameter. Similarly we have

$$\delta y < K \min(d_t \delta_{ht},\ d_r \delta_{hr})$$

where δ_{hr} and δ_{hr} are the minimum horizontal half-power semi-beamwidths.

The scattering angle imposes the limitation

$$(\theta + \delta\alpha)^{-m} > (1-K)\theta^{-m}\ .$$

This limitation is the same for both α and β so we use

$$\delta\alpha,\ \ \delta\beta < \theta[(1-K)^{-1/m} - 1]\ .$$

The step size in the y direction is limited by

$$\theta^{-m}(\alpha, \beta, y+dy) > (1-K)\theta^{-m}(\alpha, \beta, y)$$

or equivalently,

$$\delta y < [A^2 + y^2]^{1/2} - y$$

where

$$A = \theta(\alpha, \beta, y) \, R_0 \quad (1-K)^{-2/m} - 1 \, .$$

The limitations imposed by the scattering angle allow dynamic step size calculations since $\theta(\alpha, \beta, y)$ depends on the scattering point.

In computing the cross-correlation between space diversity antennas there is a constraint on the step size due to the phase difference between antennas. The y step size must be refined for horizontal space diversity at either the transmitter or the receiver, the α step size for vertical space diversity at the transmitter, and the β step size for vertical space diversity at the receiver. Consider horizontal space diversity at the transmitter. Let Δ_{ht} be the horizontal spacing of the transmit antennas. If a step δy is made the <u>change</u> in the phase difference between the antennas is approximately

$$\delta\phi \approx \frac{\delta y \, \Delta_{ht}}{d_t} \, \frac{2\pi}{\lambda}$$

(under the far field assumption), where d_t is the distance from the transmitter to the scatterer. Since d_t is roughly the same for all scatterers, for step size calculation we replace d_t by d_{Lt}, the distance to the scatterer at $(\alpha_0, \beta_0, 0)$. So to limit the phase change to $\delta\phi$ we set

$$\delta y < \delta\phi \frac{\lambda}{2\pi} \, \frac{d_{Lt}}{\Delta_{ht}} \, .$$

To decide on a value for $\delta\phi$ which yields the same accuracy as that chosen due to the beamwidths we examine a beam transformation. Let the two space diversity beam patterns be $g(\underline{r})$ and $g(\underline{r}) \, e^{j\phi(\underline{r})}$ where $g(\underline{r})$ is real and $\phi(\underline{r})$ is the phase difference. A beam transformation yields two <u>real</u> patterns $g(\underline{r})\cos(\phi(\underline{r})/2)$ and $g(\underline{r})\sin(\phi(\underline{r})/2)$. The 3dB point for these patterns (without considering $g(\underline{r})$) is at $\phi(\underline{r}) = \pi/2$. So we set $\delta\phi = K\pi/2$.

Similarly, we have

$$\delta y < \frac{K\lambda}{4} \frac{d_{Lr}}{\Delta_{hr}} ,$$

and if Δ_{vt} and Δ_{vr} are the maximum transmitter and receiver horizontal separations we have

$$\delta\alpha < \frac{K\lambda}{4} \frac{1}{\Delta_{vt}}$$

and

$$\delta\beta < \frac{K\lambda}{4} \frac{1}{\Delta_{vr}} .$$

B.5   CALCULATION OF DISTANCES TO THE SCATTERING POINT

The distances are required to calculate the delay associated with each scattering point. In addition, they are needed to evaluate the cross correlations for space diversity antennas. For the latter application high accuracy is needed. Define a coordinate system centered at the nominal transmitter, X-axis along the line to the nominal receiver location, Z-axis up, and Y-axis perpendicular to the great circle plane. The transmitter, receiver, and scatterer (X,Y,Z) coordinates are

B-15

$$\underline{T} = (u_{t\ell}, \ u_{th}, \ u_{tv})$$

$$\underline{R} = (d_0 + u_{r\ell}, \ u_{rh}, \ u_{rv})$$

$$\underline{S} = (R_{0t} \cos \alpha, \ y, \ R_{0t} \sin \alpha)$$

$$= (d_0, \ 0, \ 0)$$

$$+ (-R_{0R} \cos \beta, \ y, \ R_{0R} \sin \beta)$$

where d_0 is the distance between nominal transmitter and receiver locations,

$$R_{0T} = d_0 \sin \beta / \sin \Theta_1$$

$$R_{0R} = d_0 \sin \alpha / \sin \Theta_1 \ ,$$

$(\Theta_1 = \alpha + \beta)$, and the scattering point is determined by (α, β, y). The geometry is shown in Figure B-4. We wish to calculate the distances r_{ts}, r_{rs} to the scattering point with sufficient accuracy so that the variation of the differences in

$$\frac{2\pi}{\lambda} (r_{rsa} - r_{rsb}) \quad \text{or} \quad \frac{2\pi}{\lambda} (r_{tsa} - r_{tsb})$$

B-16
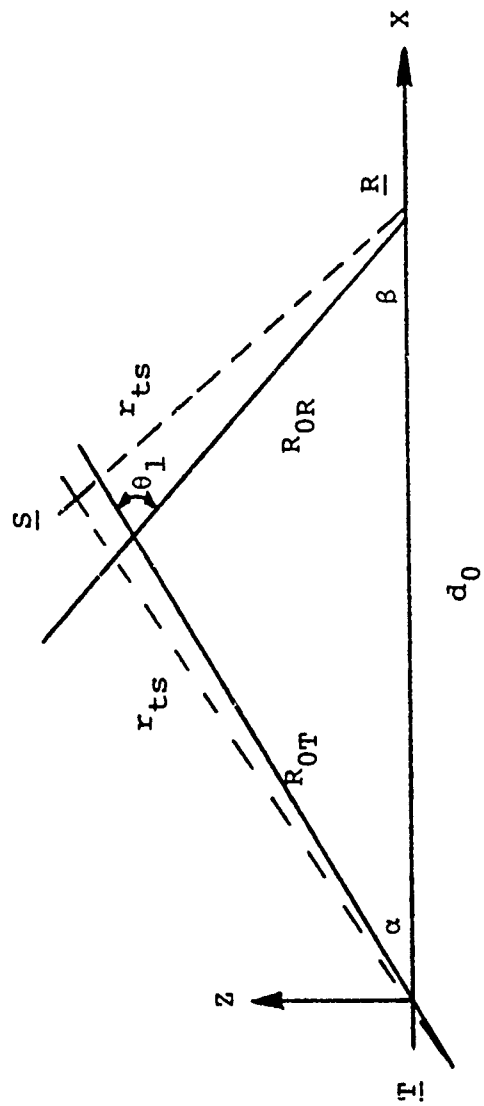
FIGURE B-4 GEOMETRY FOR DISTANCE CALCULATION

is much less than unity for two spaced antennas a and b. Write the vector $\underline{v}_{ts} = \underline{T}\,\underline{S}$ as

$$\underline{v}_{ts} = \underline{v}_{ts1} + \underline{u}_{ts1} \quad ,$$

where

$$\underline{v}_{ts1} = \left(R_{0t} \cos \alpha, \, 0R_{0t} \sin \alpha \right)$$

$$\underline{u}_{ts1} = \left(-u_{t\ell y}, \, y - u_{th}, \, -u_{tv} \right) \quad .$$

Then, if

$$r_{ts} = \left| \underline{v}_{ts} \right| \quad , \quad r_{ts1} = \left| \underline{v}_{ts1} \right| \quad ,$$

$$r_{ts} - r_{ts1} = \frac{r_{ts}^2 - r_{ts1}^2}{r_{ts} + r_{ts1}} = \frac{2\underline{v}_{ts1}\,\underline{u}_{ts1} + \left| \underline{u}_{ts1} \right|^2}{\left| \underline{v}_{ts1} + \underline{u}_{ts1} \right| + \left| \underline{v}_{ts1} \right|} \quad . \quad \text{(B.20)}$$

Calculation of r_{ts} relative to r_{ts1} in this way is much less susceptible to round off errors than a direct calculation of r_{ts}. This assumes that r_{ts1} is known with sufficient accuracy. At this point we note that the accuracy is actually required for the total path delay, and that we can write

$$r_{ts1} + r_{rs1} = d_0 + 2d_0 \frac{\sin\alpha/2 \, \sin\beta/2}{\cos(\alpha+\beta)/2} \quad . \qquad (B.21)$$

Since the first term only contributes a constant delay it need not be evaluated. The overall path length is then described accurately by the sum of (B.21), (B.20), and the term analogous to (B.20) for the receiver.

For use in scattering angle calculations the distances r_{ts}, r_{rs} can be evaluated with sufficient accuracy using

$$r_{ts1} = d_0 \frac{\sin\beta}{\sin(\alpha+\beta)} \quad .$$

B.6 CALCULATION OF SCATTERING ANGLE

It is assumed that, for each point in the scattering volume, the scattering angle to any pair of transmitter and receiver terminals is essentially the same. The scattering angle calculations here therefore refer to nominal transmit and receive antennas located in the great circle plane.

A point in the scattering volume is given by the coordinates (α, β, y). The scattering angle is the angle between the vectors TS (transmitter-to-scatterer) and the vector SR (scatterer-to-receiver). The length of these vectors are denoted r_{ts} and r_{rs}, respectively. The scattering angle Θ is evaluated from

$$\sin^2\Theta = 1 - \frac{(TS \cdot RS)^2}{r_{ts}^2 \, r_{rs}^2}$$

B-19

this is found to reduce to

$$\sin^2\Theta = \frac{(\sin^2\Theta_1 + Q_\beta^2 - Q_\alpha^2 + 2\cos\Theta_1 Q_\alpha Q_\beta)}{(1 + Q_\alpha^2)(1 + Q_\beta^2)}$$

where

$$\Theta_1 = \alpha + \beta$$

$$Q_\alpha = \frac{y \sin\Theta_1}{d_0 \sin\alpha} = y/R_{0R}$$

and

$$Q_\beta = \frac{y \sin\Theta_1}{d_0 \sin\beta} = y/R_{0T} \quad .$$

B.7   CALCULATION OF OFF-BORESIGHT ANGLES

Considering a scattering point (α, β, y) and a transmitter antenna with

$$\psi_{te0} = \text{elevation above horizon}$$

$$\psi_{ta0} = \text{azimuth angle} \quad .$$

For coordinate system centered at the transmitter the vector to the scattering point is

$$\underline{v}_{ts} = \left(R_{0T} \cos, y, R_{0T} \sin \alpha\right) \quad ,$$

where

$$R_{0T} = d_0 \sin \beta / \sin (\alpha + \beta) \quad .$$

The unit vector in the direction of the antenna beam is

$$\underline{v}_b = \left(\cos \psi_{ta0} \cos \alpha_A, \sin \psi_{ta0}, \cos \psi_{ta0} \sin \alpha_A\right)$$

where

$$\alpha_A = \alpha_0 + \psi_{te0} \quad .$$

The angle ν_t that the line to the scattering point makes with the antenna boresight is given by

$$\sin^2 \nu_T = 1 - \frac{\left| \underline{v}_{ts} \cdot \underline{v}_b \right|^2}{\left| \underline{v}_{ts} \right|^2}$$

$$= 1 - \frac{\left(R_{0T} \cos \psi_{ta0} \cos(\alpha - \alpha_A) + y \sin \psi_{ta0} \right)^2}{R_{0T}^2 + y^2}$$

$$= \left[\sin^2 \psi_{ta0} + \sin^2(\alpha - \alpha_A) \cos^2 \psi_{ta0} \right.$$

$$+ \left(y/R_{0T} \right)^2 \cos^2 \psi_{ta0}$$

$$\left. - 2(y/R_{0T}) \cos(\alpha - \alpha_A) \cos \psi_{ta0} \sin \psi_{ta0} \right]$$

$$/\left[1 + (y/R_{0T})^2 \right] \quad .$$

For the purpose of antenna gain calculation the following approximation is adequate:

$$\sin^2 \nu_T = \left[\sin^2(\alpha - \alpha_A) + (\sin \psi_{ta0} - y/R_{0T})^2 \right]/\left(1 + (y/R_{0T})^2\right) \quad .$$

Similarly, for the receiver,

$$\sin^2 \nu_R \; = \; [\sin^2(\beta - \beta_A) + (\sin\psi_{ra0} - y/R_{0R})^2]/(1 + y/R_{0R})^2)$$

where

$$\beta_A \; = \; \beta_0 + \psi_{re0}$$

and

$$R_{0R} \; = \; \frac{d_0 \sin \alpha}{\sin(\alpha + \beta)} \; .$$

B.8   DEFINITION OF ANTENNA COORDINATES AND AZIMUTH ANGLES

To determine the gain of an antenna which is not circularly symmetric two angles are required; the off-boresight angle and the azimuth angle. (The off-boresight angle is defined in the previous section.) Let the plane perpendicular to the boresight be called the antenna plane. The azimuth for a given vector is the angle between the projection of the vector into the antenna plane and a reference vector in the plane. So a reference vector must be selected in order to determine the azimuth. Basically we choose a vector which is approximately vertical. Specifically we use the following three conditions to determine this reference vector (See Figure B-5.):
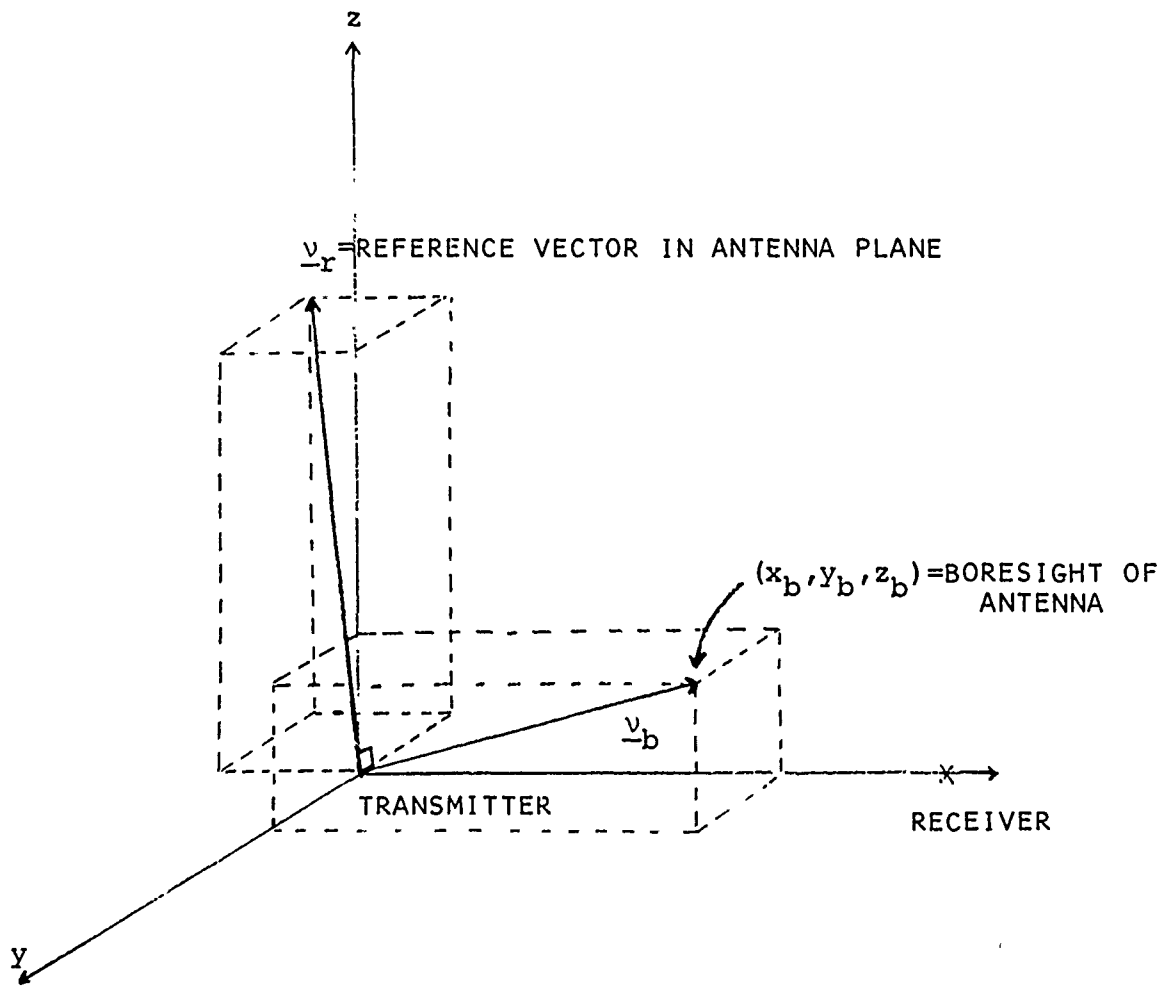
B-23

FIGURE B-5 DEFINITION OF THE TRANSMITTER REFERENCE
VECTOR FOR AZIMUTH ANGLE CALCULATIONS.
THE xz-PLANE IS THE GREAT CIRCLE PLANE.

1. The reference vector is perpendicular to the boresight.

2. Let the boresight have coordinates (x_b, y_b, z_b) in a coordinate system centered on the antenna with the x-axis pointing toward the other terminal and the z-axis pointing up in the great circle plane. Then the reference vector is in the plane determined by (x_b, y_b, z_b), $(x_b, y_b, 0)$ and $(0,0,0)$.

3. A sign ambiguity remains. This is resolved by requiring the x-component of the reference vector to have the opposite sign of z_b, the z-component of the boresight. (If z_b is zero then $\underline{v}_r = (0,0,1)$.)

These three conditions give the reference vector $\underline{v}_r$ uniquely as

$$\underline{v}_r = (-x_b z_b, \; -y_b z_b, \; x^2_b + y^2_b)/A$$

where A is the magnitude of the numerator. To resolve the question of which direction to measure the azimuth angle we define the cross product at the beamsight and the reference vector, i.e. we define $\underline{v}_c = \underline{v}_b \times \underline{v}_r$, where $\underline{v}_b$ is the boresight. (The computation of the reference vectors and cross products is done in subroutine ANTASM.)

The azimuth angle for a vector $\underline{u}$ is then defined as arctan (a/b) where $a = \underline{u} \cdot \underline{v}_c$ and $b = \underline{u} \cdot \underline{v}_r$. This angle is computed in subroutine LOOPS and used as an argument for the antenna gain subroutines. The antenna gain subroutines are written such that the azimuth angle is measured relative to the same reference vector as is computed here.

B.9 CALCULATION OF RECEIVED POWER AND CORRELATIONS

The received power on a troposcatter link is

$$P_R = P_T G_T G_R C \iiint \frac{|g_T(\underline{r})|^2 \; |g_R(\underline{r})|^2}{R_R^2(\underline{r}) \; R_T^2(\underline{r})} \; \Theta(\underline{r})^{-m} \; d^3\underline{r} \qquad (B.22)$$

where

$G_T(G_R)$	=	the transmitter (receiver) boresight gain.
P_T	=	transmitted power.
C	=	$\sigma_n^2 r_0^{\,3-m} \, k^{2-m} \Gamma(\tfrac{m}{2})/[2\sqrt{\pi} \; \Gamma(\tfrac{m-3}{2})]$
$g_T(r)(g_R(r))$	=	voltage gain relative to boresight for transmitter (receiver).
$R_T(R_R)$	=	distance from scattering point to transmitter (receiver).
Θ	=	scattering angle.
m	=	spectrum slope of the refractive index.
σ_n^2	=	variance of the refractive index.
k	=	$2\pi/\lambda$ = wavenumber of the frequency of interest.
r_0	=	correlation distance of the turbulent scatter.

For the Kolmogorov-Obukhov turbulence theory, the spectrum slope m is 11/3. In that case, it is customary to define the structure constant C_n^2 ,

$$C_n^2 = \sigma_n^2 r_0^{-2/3} 2^{1/3} \frac{\Gamma(2/3)}{\Gamma(4/3)} \quad .$$

The constant C is then

$$C = C_n^2 k^{-5/3} \Gamma(m-1) \sin \frac{\pi(m-3)}{2} / (8\pi)$$

$$= 0.0518 k^{-5/3} C_n^2 \quad . \tag{B.23}$$

The constant C_n^2 is often measured as a function of height. For m = 11/3 the received power is

$$P_R = P_T G_T G_R \ 0.0518 k^{-5/3} C_n^2 \iiint \frac{|g_T|^2 \ |g_R|^2}{R_R^2 \ R_T^2} \theta^{-11/3} d^3 \underline{r} \quad . \tag{B.24}$$

Observed values of m range from 2 to 5, but the mechanisms which causes values of m different from the 3.67 predicted by the turbulent scatter theory are not completely understood. It is generally assumed to be due to atmospheric layering and other nonhomogeneous or nonisotropic of effects. The NBS method uses m=5, based on a large number of empirical results at lower frequencies. We wish to match the model to the NBS model for m=5, assuming nearly symmetrical paths. For $\theta d < 10$ and for a surface refractivity $N_S \stackrel{\bullet}{-} 301$ the basic transmitter loss is

$$L_b = 135.8 + 30 \log \frac{f}{1 \text{ MHz}} + 30 \log \theta + 10 \log \frac{d}{1 \text{km}} + \frac{d\theta}{1 \text{km}} \qquad (B.25)$$

$$= -74.2 + 30 \log f + 30 \log \theta + 10 \log d + \theta + 0.332 \cdot 10^{-3} \theta d .$$

The basic loss for m=5 is derived in Parl [1979],

$$(B.26)$$

$$L_p(m=5) = -10 \log (Cf^3) + 9.5 + 30 \log f + 30 \log \theta + 10 \log d$$

The two expressions match when

$$-10 \log (Cf^3) = -83.7 + 0.332 \cdot 10^{-3} \theta d .$$

The θd dependence can be attributed to the height dependence of the refractive index. For small take-off angles, we have

$$h \sim \frac{1}{8} d\theta .$$

Define

$$C_5 = k^3 C(m=5) .$$

We then get

$$C_5 = \left(\frac{2\pi}{c}\right)^3 f^3 C = 2.15 \cdot 10^{-3} e^{-h/1635} \qquad (B.27)$$

For the turbulent scatter model (m=11/3) we use the Fried model for the height dependence of C_n^2 or equivalently σ_n^2, but point out that there is a considerable variance in the observed profiles. For the Fried model we have

$$\sigma_n^2 = 6.7 \cdot 10^{-14} \exp(-h/3200)$$

and

$$r_0 = 2\sqrt{h} .$$

Define now $C_{11/3}$ in the same way as above

$$C_{11/3} = k^{5/3} C(m=11/3)$$

$$= 0.0518 C_n^2$$

$$= 0.0990 \, \sigma_n^2 \, r_0^{-2/3}$$

$$= 4.18 \cdot 10^{-15} \, h^{-1/3} \exp(-h/3200). \qquad (B.28)$$

The constant C can then be determined from (B.28) for $C_{11/3}$, and for m=5 it deviates by less than 1dB from the NBS model, i.e., (B.27); for 500m < h < 3000 m. The correlation between two receiving beams is

$$P_{12} = P_T G_T G_R C \iiint \frac{|g_T|^2 g_{R1} g_{R2}'}{R_R^2 R_T^2} \theta^{-m} d^3 \underline{r}$$

where g_{R1} and g_{R2} are the two beam patterns. For space of polarization diversity paths, it is necessary to include in the integral the phase difference from a scatterer to different terminals. When the profile C_n^2 is given (m=11/3 or m=5) then (B.23) must be used while keeping C_n^2 inside the integral. The computer program is designed to take this into account when indicated by the input data.

B.10   ANTENNA GAIN PATTERNS

The gain of a phased array antenna in direction (θ, ϕ), where θ is the off-boresight angle and ϕ is the azimuth angle, is determined as follows. The phase difference between vertically adjacent elements of an array is

$$p_v = \frac{2\pi}{\lambda} d_v \sin\theta \cos\phi - \gamma_v$$

where λ is the wavelength, d_v is the vertical spacing of the elements, and γ_v is the phase shift between vertically adjacent elements. Similarly the phase difference between horizontally adjacent elements is

$$p_h = \frac{2\pi}{\lambda} d_h \sin\theta \sin\phi - \gamma_h \quad .$$

The voltage gain is then given by

$$g(\theta,\phi) = \frac{\sin(.5 n_h p_h)}{\sqrt{n_h} \sin(.5 p_h)} \quad \times \quad \frac{\sin(.5 n_v p_v)}{\sqrt{n_v} \sin(.5 p_v)} \quad \times \quad g_e(\theta,\phi)$$

where n_v and n_h are the numbers of elements in the vertical and horizontal directions and $g_e(\theta,\phi)$ is the gain pattern of the elements. If the elements are subarrays then $g_e(\theta,\phi)$ is determined in the same way as $g(\theta,\phi)$. If the elements are parabolic then $g_e(\theta,\phi)$ is the gain pattern of a dish with 55% area efficiency. (In this case $g_e(\theta,\phi)$ does not depend on ϕ.)

These equations are implemented in the program by functions RGAIN, TGAIN and PHARGN.

B.11 PARABOLIC DISH ANTENNA PATTERN AND GAIN

The default antenna patterns assume a parabolic dish with a 55% area efficiency. Let D be the diameter of the circular aperture. The boresight gain of a parabolic dish with diameter D is

$$G = \frac{6.4 D^2}{\lambda^2} \quad .$$

The voltage beam pattern is given by

$$g(\theta) = \frac{2J_1\left(\frac{\pi D_e}{\lambda}\sin\theta\right)}{\frac{\pi D_e}{\lambda}\sin\theta} \ .$$

where

$$D_e = D/1.2$$

and θ is the off boresight angle. To simplify the integration the antenna pattern is truncated beyond the first sidelobe.

B.12   DELAY RESOLUTION

The delay between consecutive elements of the channel profile is chosen to be about the variation in delay within a cell at the horizon. Let $d\alpha$ and $d\beta$ be the step sizes for a cell located at $(\alpha, \beta, y) = (\alpha_0, \beta_0, 0)$. Then the delay variation is roughly

$$\Delta\tau \simeq \frac{d_0}{2_0}\left(\beta_0 \ d\alpha + \alpha_0 \ d\beta\right) \ .$$

This value is used for the delay resolution DELPB.

APPENDIX C
PERFORMANCE CRITERION

We use as our performance criterion an approximation to the error probability of a hypothetical digital communication modem connected to the array.

Model of the Communication Modem

The basic modulation in the hypothetical system is phase-reversal keying of Nyquist pulses

$$p_k(t) = \frac{\sin\left[\pi B(t-k/B)\right]}{\pi B^{1/2}(t-k/B)} \, .$$

[The normalization is chosen so that the pulses form a set of orthogonal unit-energy waveforms.] The transmitted sequence is then of the form

$$z(t) = \sum b_k p_k(t)$$

where $b_k = \pm 1$.

It will be assumed that a small percentage of these pulses are transmitted with a polarity that is known to the receiver. This is a common practice where the receiver may have to contend with interference which might capture the tracking loops of the measurement circuitry. The percentage of the pulses used for this reference signal might typically be 10%. This results in an effective loss of about 0.5 dB from the energy devoted to transmitting information.

At the array output we have available a number of noisy replicas of the transmitted signal, which can be modelled as

$$Z_n(t) = G_n z(t) + \nu_n(t) \; .$$

We have removed the explicity dependence of G_n on t because we are interested in observation intervals short enough so that the channel gains can be assumed to be essentially constant. The values of G_n in this expression can arise from individual elements of the array, from beamformer outputs, or from subarrays that are nonadaptively steered. In any case, the receiver then samples each $Z_n(t)$ by correlating it with every $p_k(t)$ to produce the sampled-data outputs

$$Z_{n,k} = G_n b_k + \nu_{n,k} \; .$$

We now consider the problem of deciding on the polarity of a single one of these pulses, say b_0. In order to make this decision the receiver will form an estimate of G_n by averaging a specific number of reference pulses preceding b_0. We will denote this estimate by H_n, and write it as

$$H_n = G_n + \frac{1}{K} \sum_{k=-K}^{-1} \nu_{n,k} \; .$$

(We take the liberty of pretending that the reference pulses are consecutive.) The overall performance is sensitive to the value of K which is limited by the coherence time of the channel (reci-

procal of the fade rate) and the actual implementation. It would be inappropriate here to dwell on the details of determining the effective value of K.

Having estimated the channel gain, the receiver uses this estimate in an approximation to a maximal ratio combiner by forming

$$Z = \prod_n \overline{H}_n Z_{n,0} \quad .$$

Under ideal conditions this will be proportional to the value of b_0, and the receiver correspondingly takes as its estimate of b_0 the quantity

$$\hat{b}_0 = \left\{ \begin{array}{ll} 1 & \text{if } \text{Real}(Z) > 0 \\ -1 & \text{if } \text{Real}(Z) < 0 \end{array} \right\} \quad .$$

Demodulator Statistics

Let G be the column vector with entries $G_1, \ldots, G_N$; similarly, let H be a column vector with entries $H_1, \ldots, H_N$. We next define the noise components

$$U_n = \frac{1}{K} \sum_{k=-K}^{-1} \nu_{n,k} \quad .$$

These noise components are independent complex Gaussian variables with variance N_0/K. We can then let U be the column vector with coordinates $\{U_n\}$, and write H as

$$H = G + U .$$

It will be noted that G is also a vector of complex Gaussian numbers with zero mean; the covariance matrix of G will be denoted by M_G :

$$M_G = E[G'\overline{G}] ,$$

where the prime is used to indicate the transposed (row) matrix and the overbar again indicates complex conjuguate. The components of M_G are determined by the array and scattering geometries.

We next let X be the column matrix whose entries are

$$X_n = Z_{n,0} , \quad 1 < n < N .$$

We let V_n be the noise component of $Z_{n,0}$,

$$V_n = v_{n,0} ,$$

and let V be the column matrix with entries $\{V_n\}$. These coordinates are independent and have variance N_0. It should be noted that V is also independent of U. We then express X as

$$X = b_0 G + V \ .$$

Z is then expressed as

$$Z = X'\overline{H} \ .$$

The last step of the initial development is to define the demodulator output

$$\beta = 2 \text{ Real Part of } Z \ .$$

This can be written as

$$\beta = X'\overline{H} + H'\overline{X} \ .$$

However, we will want to express β in a slightly more complicated way to facilitate subsequent averaging. To this end we define the concatenated row matrix

$$Y' = (X',H')$$

and write β as

$$\beta = Y' R \overline{Y}$$

where R is a (2N x 2N) matrix with entries

$$R_{mn} = 1 \text{ if } m-n = \pm N \text{ ,}$$

$$R_{mn} = 0 \text{ otherwise.}$$

That is, R can be written in partitioned form as

$$R = \begin{bmatrix} O_N & I_N \\ I_N & O_N \end{bmatrix}$$

where O_N is the (NxN) null matrix and I_N is the (NxN) identify matrix.

We now write the demodulator error probability as

$$P(\text{error}) = \Gamma(\beta > \quad | b_0 = -1) \text{ .}$$

C-6

This can also be expressed in terms of the conditional density of β as

$$P(\text{error}) = \int_0^\infty f_\beta(\beta \mid b_0 = -1) \, d\beta .$$

Rather than leaping into the problem of determining this density function directly we will look instead at its <u>moment-generating function</u>

$$\phi(s) = \int_{-\infty}^\infty f_\beta(\beta \mid b_0 = -1) \, e^{s\beta} d\beta$$

which can also be written as the conditional expectation

$$\phi(s) = E(e^{s\beta} \mid b_0 = -1) .$$

If we substitute the definition of β as a matrix product this can be written as

$$\phi(s) = E[e^{sY'R\overline{Y}} \mid b_0 = -1] .$$

The next steps are simple arithmetic. Let M_Y be the conditional covariance of Y;

$$M_Y = E(\overline{Y}Y' \mid b_0 = -1) .$$

C-7

Then the (conditional) density of Y is

$$f_Y(y|b_0 = -1) = \pi^{-N} |M_Y|^{-1} \exp(-y'M_Y^{-1}\bar{y}) \, ,$$

and the moment-generating function is

$$\phi(s) = \int f_Y(y|b_0 = -1)e^{sy'R\bar{y}}dy \quad .$$

[The integral in this expression is a 4N-dimensional integration over the real and imaginary parts of the 2N coordinates of y.] For values of s with sufficiently small real parts the integrand is well behaved and we have

$$\phi(s) = \frac{1}{|I_{2N} - s\,M_YR|} \, ,$$

where I_{2N} is the (2N x 2N) identity matrix. The region of validity is simply

$$\text{Real } s \; < \; \frac{1}{\text{largest eigenvalue of } M_YR} \quad .$$

The last step in the evaluation of $\phi(s)$ is to express M_Y in terms of M_G. We have, when $b_0 = -1$,

$$Y = \begin{bmatrix} X \\ H \end{bmatrix} = \begin{bmatrix} -G + V \\ G + U \end{bmatrix}$$

and

$$M_Y = E \begin{bmatrix} -\overline{G} + \overline{V} \\ \overline{G} + \overline{U} \end{bmatrix} \begin{bmatrix} -G' + V' & , & G' + U' \end{bmatrix}$$

$$= \begin{bmatrix} M_G + N_0 I_N & -M_G \\ -M_G & M_G + (N_0/K)I_N \end{bmatrix} .$$

It will be a notational convenience to write

$$M_R = M_Y R$$

so that we have

$$\phi(s) = \frac{1}{|I_{2N} - sM_R|} .$$

C-9

The entries in M_R are easily evaluated as

$$M_R = \begin{bmatrix} -M_G & M_G + N_0 I_N \\ M_G + (N_0/K)I_N & -M_G \end{bmatrix} .$$

Error Probability and Performance Criterion

The density function $f_\beta(\beta)$ is recoverable from the moment-generating function as

$$f_\beta(\beta) = \frac{1}{j2\pi} \int_{c-j\infty}^{c+j\infty} e^{-\beta s} \phi(s) ds .$$

This function involves at most polynomials and exponentials of β since $\phi(s)$ is the reciprocal of a polynomial in s. Consequently it is theoretically straightforward to evaluate the integral of $f_\beta(\beta)$ on the half-line $\beta > 0$. As a practical matter, however, this is a computationally difficult way to solve for the error probability, and it is much better to do the integration on β first and evaluate the resulting integral by numerical saddle-point methods.

There is a somewhat more straightforward way of arriving at a figure-of-merit for the diversity combining algorithm, via the Chernoff bound. We have

$$\text{Prob(Error)} \quad = \quad \int_0^\infty f_\beta(\beta)\, d\beta$$

$$< \quad \int_0^\infty f_\beta(\beta) e^{t\beta} \quad \text{if } t > 0$$

$$= \quad \phi(t) \quad ,$$

and therefore we can write

$$\text{Prob(Error)} \quad < \quad \phi_0$$

where

$$\phi_0 \quad = \quad \underset{0 < t < t_{max}}{\text{Minimum}} \quad \phi(t) \quad .$$

The real t that minimizes $\phi(t)$ is, in fact, the location of the saddlepoint integration path as it crosses the real axis, and it is possible to develop excellent approximations to the error probability that depend only on ϕ_0. Since all of these approximations are monotonic in ϕ_0, it is sufficient to use ϕ_0 itself as the performance criterion, and we will do this in most of the evaluations in the text.

The Determinant in Terms of the Eigenvalues of M_G

Since the covariance matrix M_G is Hermitian, we can find a unitary matrix Q for which

$$Q'\overline{Q} = I_N \, ,$$

and

$$Q'M_G\overline{Q} = \Lambda$$

where Λ is the diagonal matrix of the eigenvalues of M_G:

$$\Lambda_{nm} = 0 \quad \text{if } n \neq m \, .$$

Let S be the $(2N \times 2N)$ matrix consisting of 2 copies of Q :

$$S = \begin{bmatrix} Q & O_N \\ O_N & Q \end{bmatrix} \, .$$

Clearly,

$$S'S = I_{2N}$$

C-12

and

$$|S| = 1 \ .$$

Therefore

$$\left|S'\left(I_{2N} - sM_R\right)\overline{S}\right| = \left|I_{2N} - sM_R\right| = 1/\phi(s) \ .$$

The left side of this is readily evaluated by multiplying the partitioned matrices, and we have

$$1/\phi(s) = \begin{vmatrix} I_N + s\Lambda & -s\Lambda - sN_0 I_N \\ -s\Lambda - s(N_0/K)I_N & I_N + s\Lambda \end{vmatrix} \ .$$

The matrix in this determinant has mostly zero values in it, and a simple permutation permits the determinant to be written as

$$1/\phi(s) = \prod_{n=1}^{N} D_n$$

where

$$D_n = \begin{vmatrix} 1 + s\lambda_n & -s\lambda_n - sN_0 \\ -s\lambda_n - sN_0/K & 1 + s\lambda_n \end{vmatrix}$$

$$= 1 + 2\lambda_n s - [\lambda_n N_0 (K+1)/K + N_0^2/K]s^2$$

The Special Case of Large K

In many troposcatter applications the coherence time of the channel is so large that we can assume that

$$K \approx \infty$$

even if the measurement of channel gains has to be multiplexed among the array ports. In this special case

$$D_n = 1 + 2\lambda_n s - \lambda_n N_0 s^2$$

$$= 1 + \lambda_n/N_0 - \lambda_n N_0 (s - 1/N_0)^2 \quad .$$

In this form we see that the maximum of every D_n occurs at $s = 1/N_0$. Consequently the minimum of $\phi(t)$ occurs there also, and

$$\phi_0 = \Pi \left(1 + \lambda_n/N_0\right)^{-1} \quad .$$

It is not even necessary to determine the eigenvalues of M_G in this case since the last equation can be written as

$$\phi_0 = \frac{1}{|I_N + M_G/N_0|} \quad .$$

A Rough Approximation for Moderate K

The value of t that minimizes the individual terms $\{D_n\}$ is

$$t = \frac{\lambda_n}{N_0\left[\lambda_n(1 + 1/K) + N_0/K\right]}$$

which can be written as

$$t = \frac{1}{N_0} \cdot \frac{1}{1 + 1/K + N_0/(K\lambda_n)} \quad .$$

Even if K is not large we can assume that the location of the minimum of $\phi(t)$ is approximately at

$$t = \frac{1}{N_0} \cdot \frac{1}{1 + 1/K}$$

as long as there are not too many terms for which

$$N_0/K\lambda_n > 1 \quad .$$

It is worthwhile using this value of t in the general case even when it is not terribly accurate. This is justifiable since the minimum of $\phi(t)$ will be fairly broad anyway; in addition, the use of this value only weakens the bound on error probability, and is therefore conservative.

We thus substitute

$$s = \frac{1}{N_0} \frac{1}{1 + 1/K}$$

in the expression for D_n to obtain

$$D_n = 1 + \frac{2\lambda_n/N_0}{1 + 1/K} - \frac{\lambda_n/N_0}{1 + 1/K} - \frac{1}{K(1 + 1/K)^2}$$

C-16

or

$$D_n = \frac{K + 1 + 1/K}{K + 2 + 1/K} + \frac{\lambda_n/N_0}{1 + 1/K} \; .$$

Again, we can express the result directly in terms of M_G as

$$\phi_0 = \frac{1}{\frac{K + 1 + 1/K}{K + 2 + 1/K} \; I_N + M_G/N_0(1 + 1/K)} \; .$$

APPENDIX D
PHASED ARRAY ANTENNAS

D.1   INTRODUCTION

The purpose of this appendix is to establish the array antenna background for the adaptive Troposcatter program. We will discuss the principles of and problems involved in the design of phased array antennas for this application, leaving for other sections the detailed discussion of the adaptive algorithms.

D.1.1 Array Theory

A planar array antenna is a two dimensional set of elementary antennas, as shown in Figure D-1. The figure shows the elementary antennas separated by a distance d_x in the X direction (azimuth) and d_y in the Y direction (elevation), with an overall array size of D_x and D_y. It will be shown that in general, $d_x = d_y$, that is, the element spacing is the same in the azimuth and elevation directions. There is no underlying reason, however, to have $D_x = D_y$, and their ratio is one of the design tradeoffs affecting troposcatter performance.

Before continuing with the analysis of the planar array, let us first examine the simpler case of the linear array, as shown in Figure D-2. Here we have assumed a uniform spacing d_x, and an incident plane wave at an angle θ from broadside. Thus, $\theta=90°$ is broadside, while the endfire condition is for $\theta = 0°$ and $180°$. The phase difference between the wavefront at successive antenna elements is

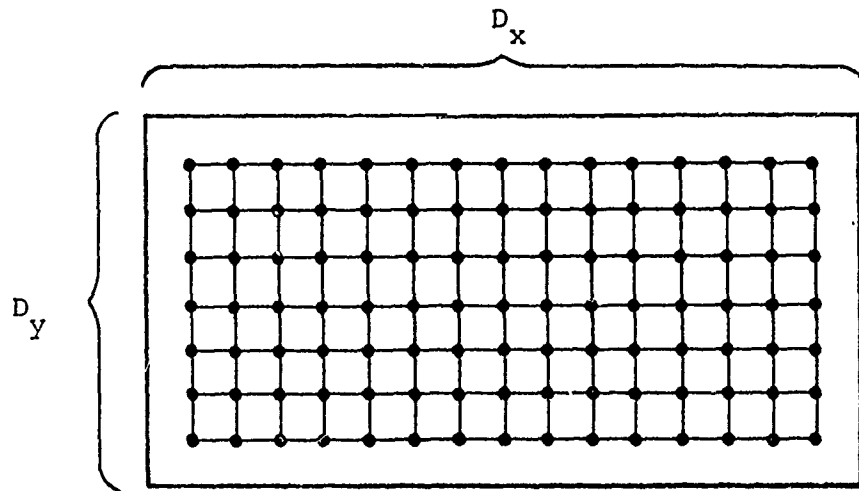$$\Delta \phi = \frac{2 \pi d_x}{\lambda} \cos \theta .\qquad (D.1)$$

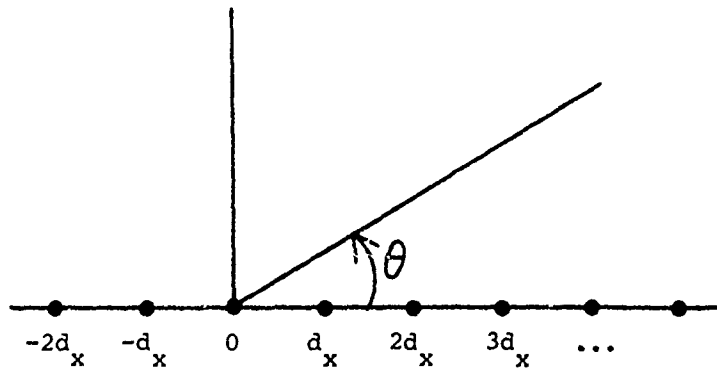Figure D-1 A Planar Array Antenna

Figure D-2 Linear Array Phasing

If there are $2N + 1$ elements in the linear array, then the far field amplitude array factor is

$$A(\theta) = \sum_{n=-N}^{N} I_n e^{j\left(\frac{n2\pi d_x}{\lambda} \cos \theta\right)}, \qquad (D.2)$$

where I_n is the complex amplitude weighting on the array elements. If the weighting is uniform, then $|I_n| = 1$, and the phasing is the only antenna control. If the phasing is uniform, that is the phase shift applied to the n-th element is $n\alpha$, then,

$$A(\theta) = \sum_{n=-N}^{N} e^{jn\left(\frac{2\pi d_x}{\lambda} \cos \theta - \alpha\right)}. \qquad (D.3)$$

The array factor in units of power, $S(\theta)$, is the magnitude-squared of the amplitude array factor,

$$S(\theta) = |A(\theta)|^2$$

$$= \frac{\sin^2\left[\frac{1}{2} (2N+1)\left(\frac{2\pi d_x}{\lambda} \cos \theta - \alpha\right)\right]}{\sin^2\left[\frac{1}{2} \left(\frac{2\pi d_x}{\lambda} \cos \theta - \alpha\right)\right]} \qquad (D.4)$$

D-3

Equation (D.4) shows the following factors involved in array antennas.

1. The array factor has, in cos θ space, periodically spaced nulls, at values of θ given by the zeros of the numerator of Eq. (D.4):

$$\frac{1}{2}(2N+1)\left(\frac{2\pi d_x}{\lambda}\cos\theta - \alpha\right) = k\pi; \qquad k=0, \pm1, \ldots$$

$$\theta = \cos^{-1}\left\{\left(\frac{2k\pi}{2N+1} + \alpha\right)\frac{\lambda}{2\pi d_x}\right\} \tag{D.5}$$

2. The array factor has, in cos θ space, periodically spaced maxima, of value $(2N+1)^2$, given by the simultaneous zeros of the numerator and denominator of Eq. (D.4):

$$\frac{1}{2}\left(\frac{2\pi d_x}{\lambda}\cos\theta - \alpha\right) = k\pi; \quad k=0, \pm1, \ldots$$

$$\theta = \cos^{-1}\left\{(2k\pi + \alpha)\frac{\lambda}{2\pi d_x}\right\} \quad . \tag{D.6}$$

Equation (D.6) will always have one solution in visible space at the value k=0, such that:

$$\alpha = \frac{2\pi d_x}{\lambda}\cos\theta \; . \tag{D.7}$$

Figure D-2 shows that this value of α points the antenna in the direction of the incoming wavefront. Additional maxima, or grating lobes, are given by solutions of Eq. (D.6) for $k \neq 0$. The first grating lobe occurs at

$$\cos \theta = (\alpha \pm 2\pi) \frac{\lambda}{2\pi d_x}$$

$$= \cos \theta_0 \pm \frac{\lambda}{d_x} \tag{D.8}$$

where θ_0 is given by $\cos \theta_0 = \lambda\alpha/2\pi d_x$. Thus, to avoid grating lobes, the antenna elements must be spaced such that:

$$\frac{\lambda}{d_x} > 1 + |\cos \theta_0| , \tag{D.9}$$

e.g., if the antenna is to be steered through all visible space, the element spacing must be a half wavelength.

3. The array factor has secondary maxima located between the pattern nulls of Eq. (D.5). These maxima are approximately located when the numerator of Eq. (D.4) is unity, that is

$$\frac{1}{2} (2N+1) \left(\frac{2\pi d_x}{\lambda} \cos \theta - \alpha \right) = \pm\left(\frac{2m+1}{2} \right)\pi; \quad m=0,1,\ldots$$

$$\theta = \cos^{-1} \left\{ \left(\pm\left(\frac{2m+1}{2N+1} \right)\pi + \alpha \right) \frac{\lambda}{2\pi d_x} \right\} . \tag{D.10}$$

These maxima and their adjacent minima define the array antenna's sidelobes.

4. The beam widths between nulls of a main lobe steered to angle θ_0 is:

(D.11)

$$\text{Null Beamwidth} = \cos^{-1}\left\{\cos\theta_0 - \frac{1}{2N+1}\frac{\lambda}{d_x}\right\} - \cos^{-1}\left\{\cos\theta_0 + \frac{1}{2N+1}\frac{\lambda}{d_x}\right\}$$

At Broadside, $\theta_0 = \pi/2$, and

$$\text{Null Beamwidth} \cong \frac{1}{2N+1}\frac{2\lambda}{d_x} = 2\frac{\lambda}{L} \qquad \text{(D.11a)}$$

where L is the array length. The null separation on sidelobes is half of Eq. (D.11a), or λ/L radians.

The 3dB beamwidth is given by

$$\text{Half Power Beamwidth} = \cos^{-1}\left\{\cos\theta_0 - 0.886\frac{1}{2N+1}\frac{\lambda}{2d_x}\right\} \qquad \text{(D.12)}$$

$$- \cos^{-1}\left\{\cos\theta_0 + 0.886\frac{1}{2N+1}\frac{\lambda}{2d_x}\right\},$$

and at broadside:

$$\text{Half Power Beamwidth} \cong 0.886\frac{1}{(2N+1)}\frac{\lambda}{d_x} = 0.886\frac{\lambda}{L}. \qquad \text{(D.12a)}$$

Equations (D.11) and (D.12) show that the antenna beamwidth is a function of the length of the antenna, $(2N+1)d_x$, while Eq. (D.6) shows that the grating-lobe spacing is a function of the element separation d_x.

D-6

Up to this point, the discussion has been devoted to a uniform linear array of isotropic elements. Eq. (D.4) shows that the resulting antenna pattern has a $(\sin x/x)^2$ behavior. The first sidelobes of this pattern are 13.5 dB below the main lobe. Tapering of the array can reduce the sidelobes, but will broaden the main lobe. In addition, if the elements are not isotropic, the pattern of the resulting antenna is the product of the element and array patterns.

The linear array theory extends directly to planar arrays. Figure D-3 shows the coordinate system of a planar array. The array is in the X-Y plane, ϕ is the angle from the X axis to the projection of the r vector in the X-Y plane, and θ is the polar angle. As with the linear array we denote the element weighting by I_{mn}, where the index m is in the X coordinate, and n in the Y coordinate. Thus $0 < |m| < N_x$, $0 < |n| < N_y$. The two dimensional array factor is then

$$(D.13)$$

$$A(\theta,\phi) = \sum_{m=-N_x}^{N_x} \sum_{n=-N_y}^{N_y} I_{mn} \exp\left\{j\, \frac{2\pi}{\lambda}\, \sin\,\theta\left[md_x \cos\,\theta + nd_y \sin\phi\right]\right\}.$$

If I_{mn} is constant amplitude, uniform phase, i.e.:

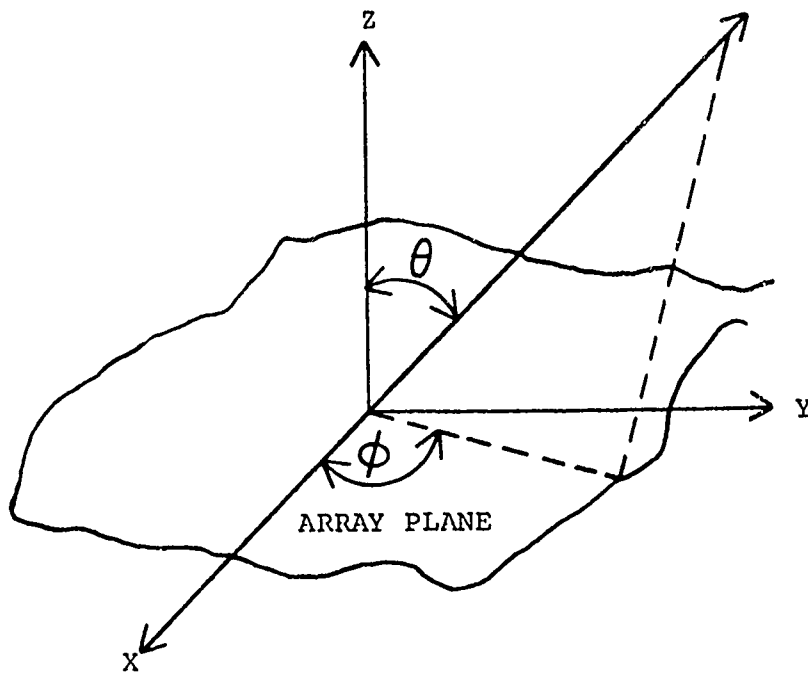$$I_{mn} = \exp\left\{-j\left(m\alpha_x + n\alpha_y\right)\right\}, \qquad (D.14)$$
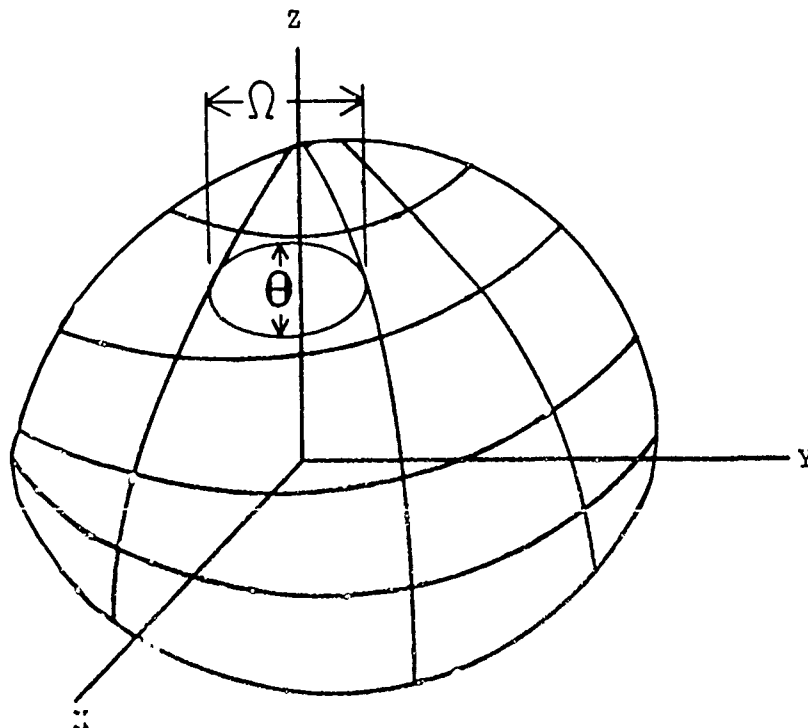
Figure D-3   Planar Array Coordinates

Figure D-4   Projection Hemisphere

D-8

then

$$A(\theta,\phi) = \sum_{n} \sum_{m} \exp\left\{j\left[m\left(\frac{2\pi}{\lambda} d_x \sin\theta \cos\phi - \alpha_x\right)\right.\right.$$

$$\left.\left. + n\left(\frac{2\pi}{\lambda} d_y \sin\theta \sin\phi - \alpha_y\right)\right]\right\} \qquad (D.15)$$

The array factor in power, $S(\theta,\phi)$ is:

$$S(\theta,\phi) = \left|A(\theta,\phi)\right|^2. \qquad (D.16)$$

Substituting Eq. (D.15) into Eq. (D.16),

$$S(\theta,\phi) = \frac{\sin^2\left[\frac{1}{2}(2N_x+1)\left(\frac{2\pi}{\lambda} d_x \sin\theta \cos\phi - \alpha_x\right)\right]}{\sin^2\left[\frac{1}{2}\left(\frac{2\pi d_x}{\lambda} \sin\theta \cos\phi - \alpha_x\right)\right]}$$

$$(D.17)$$

$$\frac{\sin^2\left[\frac{1}{2}(2N_y+1)\left(\frac{2\pi}{\lambda} d_y \sin\theta \cos\phi - \alpha_x\right)\right]}{\sin^2\left[\frac{1}{2}\left(\frac{2\pi}{\lambda} d_y \sin\theta \sin\phi - \alpha_y\right)\right]}$$

Equation (D.17) shows that in the absence of tapering, the array pattern of the planar array is the product of the patterns of two equivalent linear arrays, one in the X direction and one in the Y direction. As in the linear array, the elements must be spaced at half-wavelength intervals to avoid grating lobes. The concept of beamwidth is somewhat complex for a planar array, and is best described in terms of a hemisphere, as in Figure D-4. The intersection of the antenna beam and the hemisphere is an elliptical surface. The geometry of the projection of the pencil

beam onto the surface of the hemisphere is conventionally defined in terms of the following parameters. Let Θ be the beamwidth in the North-South direction, and Ω be the beamwidth in the East-West direction. Furthermore, let the beam be scanned to the coordinates θ_0, ϕ_0, and define

$$\Theta_{x0} = 3 \text{ db beamwidth for } \theta_0 = 0, \phi_0 = \phi_0, \text{ i.e., if}$$

scanning is in the X-Y plane

$$\Theta_{y0} = 3 \text{ dB beamwidth for } \theta_0 = 90^0, \phi_0 = \phi_0, \text{ i.e., if}$$

scanning is in the Y-Z plane. In this case, Θ_{x0} and Θ_{y0} are given by Eq. (D.12). It can then be shown that

$$\Theta^{-2} = \cos^2 \theta_0 [\Theta_{xo}^{-2} \cos^2 \phi_0 + \Theta_{y0}^{-2} \sin^2 \phi_0] \qquad (D.18)$$

and

$$\Omega^{-2} = \Theta_{x0}^{-2} \sin^2 \phi_0 + \Theta_{y0}^{-2} \cos^2 \phi_0 . \qquad (D.19)$$

For a square array, $\Theta_{x0} = \Theta_{y0}$, and

$$\left.\begin{array}{l} \Theta = \Theta_{x0}\sec\theta_0 \\[2em] \Omega = \Theta_{x0} \end{array}\right\} \qquad \text{square array .} \qquad\qquad (D.20)$$

Thus an array will, from Eqs. (D.18) and (D.19) have broadening in both the Θ and Ω beams. For the square array the beamwidth is dependent only on the polar angle, θ_0, while the Ω beamwidth is angle independent. The directivity, D, is given by

$$D = \frac{9.87}{\Theta\Omega} \left.\begin{array}{l} \\ \phi_0 = 0^0 \\[1em] \theta = \theta_0 \end{array}\right. \qquad\qquad (D.21)$$

where, in Eq. (D.21), Θ and Ω are in radians. If θ and Ω are in degrees, the factor of 9.87 is replaced by 32,400.

D.2   ANTENNA BEAM FORMATION

Section D.1 has discussed the theory of beam formation given a set of antenna elements. In this section, we address the engineering aspects of this problem, namely, how does a practical beam get formed.

To begin with, let us find the dimension of the problem. In the troposcatter context, a typical antenna might be 8 feet square, and have an operating frequency range of 4.4 to 5.0 GHz. At 5.0 GHz, the wavelength is

$$\lambda = \frac{3 \times 10^8}{5 \times 10^9} = 0.06 \text{ meters} = 0.2 \text{ feet.} \qquad\qquad (D.22)$$

Assuming half-wavelength separation (0.1 ft), the antenna will
have

$$N_x/2 = N_y/2 = 80,$$

for a total of 6400 elements. If a pencil beam is to be formed,
each of these elements will have to be individually phased and
their outputs summed in order to form a pencil beam pointed in
the desired direction.

It is apparent that an approach which requires some 6400
variable phasings is an expensive undertaking. An alternate ap-
proach is to use an RF beam forming matrix or <u>Butler matrix</u>. A
Butler matrix is a hardware implementation of a Fast Fourier
Transform (FFT), although it was developed in 1960, six years
before Cooley announced the FFT. The Butler matrix has N input
and N output ports. The outputs are the Fourier transforms of
the inputs, and if the waveform incident on the antenna is a
plane wave, the output of the Butler matrix is N beams, which
simultaneously point at all visible space. To make this point
more concretely, consider the eight element Butler array shown in
Figure D-5. The notation used in the figure is as follows:

x   =   4 port quadrature hybrid
        straight-through phase shift = $90^0 = \frac{\pi}{2}$
        coupled arm phase shift = 0° .

<n   =   phase shift of $\frac{n\pi}{8}$ radians .

Digital, Matrix, and Intermediate-Frequency Scanning
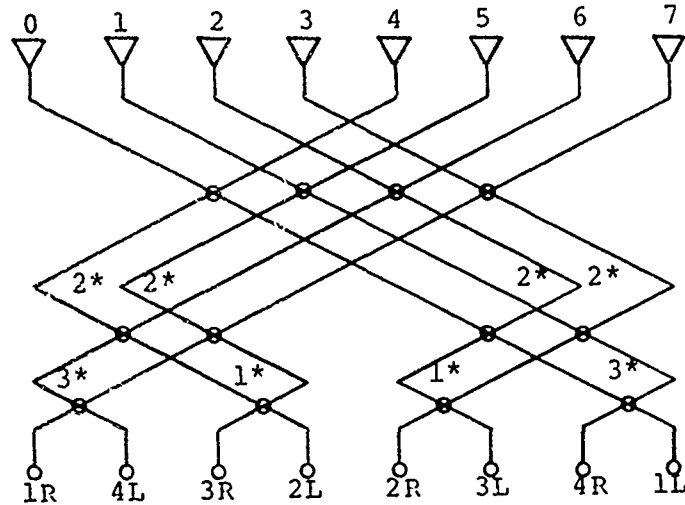
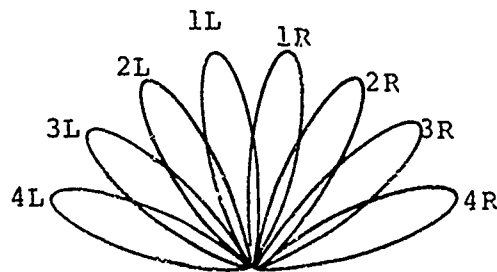* Units of Phase Shift are $\pi/8$ radians

Figure D-5   8-Element Butler Array (from Hansen, 1966)

We number the antenna elements 0 through 7 from left to right, and denote their output voltages by E_m. Tracing the signals which go to the output ports we find the output voltages:

$$
\begin{aligned}
E_{1R} = &E_0 e^{j5\pi/8} + E_1 e^{j6\pi/8} + E_2 e^{j7\pi/8} + E_3 e^{j\pi} + E_4 e^{j9\pi/8} + E_5 e^{j10\pi/8} \\
&+ E_6 e^{j11\pi/8} + E_7 e^{j12\pi/8}
\end{aligned}
\tag{D.23}
$$

Since there is a progression of $\pi/8$ radians on each term, E_{1R} will have a maximum when $E_n = e^{-jn\pi/8}$, that is, for a beam arriving at the right of broadside with a progressive phase shift of $\pi/8$ radians at each element. Similarly:

$$
\begin{aligned}
E_{2R} = &E_0 e^{j5\pi/8} + E_1 e^{j8\pi/8} + E_2 e^{j11\pi/8} + E_3 e^{j14\pi/8} \\
&+ E_4 e^{j\pi/8} + E_5 e^{j4\pi/8} + E_6 e^{j7\pi/8} + E_7 e^{j10\pi/8}
\end{aligned}
\tag{D.24}
$$

Thus, there is a progression of $3\pi/8$ radians on each term of E_{2R}, and E_{2R} will have a maximum when $E_n = e^{-jn3\pi/8}$, that is, for a beam arriving on the right of broadside with a progressive phase shift of $3\pi/8$ radians. Table D-1 summarizes the pointing angles of the eight beams.

Table D-1

Eight Beam Butler Matrix Pointing Angles

BEAM	PHASE SHIFT	POINTING ANGLE
4L	$-7\pi/8 = -157.5°$	$-61.0°$
3L	$-5\pi/8 = -112.5°$	$-38.7°$
2L	$-3\pi/8 = -\ 22.5°$	$-22.0°$
1L	$-\ \pi/8 = -\ 67.5°$	$-7.2°$
1R	$\pi/8 = +\ 22.5°$	$7.2°$
2R	$3\pi/8 = +\ 67.5°$	$22.0°$
3R	$5\pi/8 = +112.5°$	$38.7°$
4R	$7\pi/8 = +157.5°$	$61.0°$

The eight beams span ±61° of visible space.

In the general case of an N- element array, the output of the m-th port of the Butler matrix will have the amplitude

$$\frac{\sin N \left\{ \frac{\pi d}{\lambda} \sin\theta - \left(\frac{2m-1}{N} \right) \frac{\pi}{2} \right\}}{\sin \left\{ \frac{\pi d}{\lambda} \sin\theta - \left(\frac{2m-1}{N} \right) \frac{\pi}{2} \right\}} \qquad (D.25)$$

which, upon comparison with Eq. (D.4), is seen to be the amplitude array factor of an untapered array pointing at an angle

$$\theta = \sin^{-1} \frac{\lambda}{2d} \left(\frac{2Nq + 2m-1}{N} \right) \qquad (D.26)$$

from broadside. The factor q in Eq. (D.26) is an integer which can take on any value. Visible space is limited by the largest value of q for which the argument of Eq. (D.26) is less than unity. It is important to note that in $\sin\theta$ space the array

pattern is of the form sin X/X, with the beam maxima shifted π/N. Thus, the pointing angles form a linear progression in sin θ space, but are nonuniformly positioned in physical space. The angular coverage of an array is given by:

$$\text{Angular Coverage} = 2\,\sin^{-1}\frac{\lambda}{2d}\left(\frac{N-1}{N}\right). \qquad (D.27)$$

Adjacent beams cross over at the $2/\pi$ level, which is 3.92 dB down from the peak, and the maximum of each beam falls at a null of all other beams. Thus, the Butler matrix forms orthogonal beams.

The usefulness of the Butler matrix arises from the fact that it is a passive, lossless means of forming simultaneous beams which essentially cover all visible space. It is made up entirely of four-port quadrature couplers and fixed phase shifters. As it is an FFT, it can be most easily implemented when the number of elements in it are a power of 2. For an N element array, the basic unit of phase shift is 180/N degrees, which is 22.5° for an 8 element array, 11.25° for a 16 element array, etc. A two dimensional Butler array is made by forming one-dimensional arrays for each row (or column), and then combining their outputs into a second array, using the corresponding outputs of each linear array. Thus an NXN planar array would use 2N linear arrays to form the planar array pattern, giving N^2 output beams.

D.3 ARRAYS OF SUBARRAYS

The Butler matrix has provided us with a tradeoff of building a fixed multibeam system in place of a steerable single beam array. It has not, however, cut down on the number of elements. We previously have shown, for example, that an 8 foot antenna

will require 6400 elements. We now consider a reduced implementation, still using a Butler matrix, but feeding it with a reduced number of elements, each of which is a fixed subarray. A typical geometry is shown in Figure D-6; this implementation is simply shown as an example and is not necessarily a desirable approach for an adaptive troposcatter system. The array is divided into 64 subarrays, each 1' by 1'. The subarrays are identical, each having a corporate feed and phased to produce a boresight beam. No tapering is used, and the elements are spaced at half-wavelength intervals, so that the subarray pattern is

$$S(\theta, \phi)\Big|_{\text{subarray}} = \frac{\sin^2\left[\frac{10}{2}\,\pi\,\sin\,\theta\,\cos\,\phi\right]}{\sin^2\left[\frac{\pi}{2}\,\sin\,\theta\,\cos\,\phi\right]}\,\frac{\sin^2\left[\frac{10}{2}\,\pi\,\sin\,\theta\,\sin\,\phi\right]}{\sin^2\left[\frac{\pi}{2}\,\sin\,\theta\,\sin\,\phi\right]} \qquad (D.28)$$

A cut through the θ plane gives:

$$S(\theta,0)\Big|_{\text{subarray}} = 100\,\frac{\sin^2\left[5\pi\,\sin\,\theta\right]}{\sin^2\left[\frac{\pi}{2}\,\sin\,\theta\right]}\ , \qquad (D.29)$$

and the boresight half-power beamwidth (Eq. (D.12)), is:

$$\Theta_0 = \Omega_0 = 0.886 \cdot \frac{1}{10} \cdot 2$$
$$= 0.18 \text{ radians} \qquad . \qquad (D.30)$$
$$= 10.2^0$$

8'

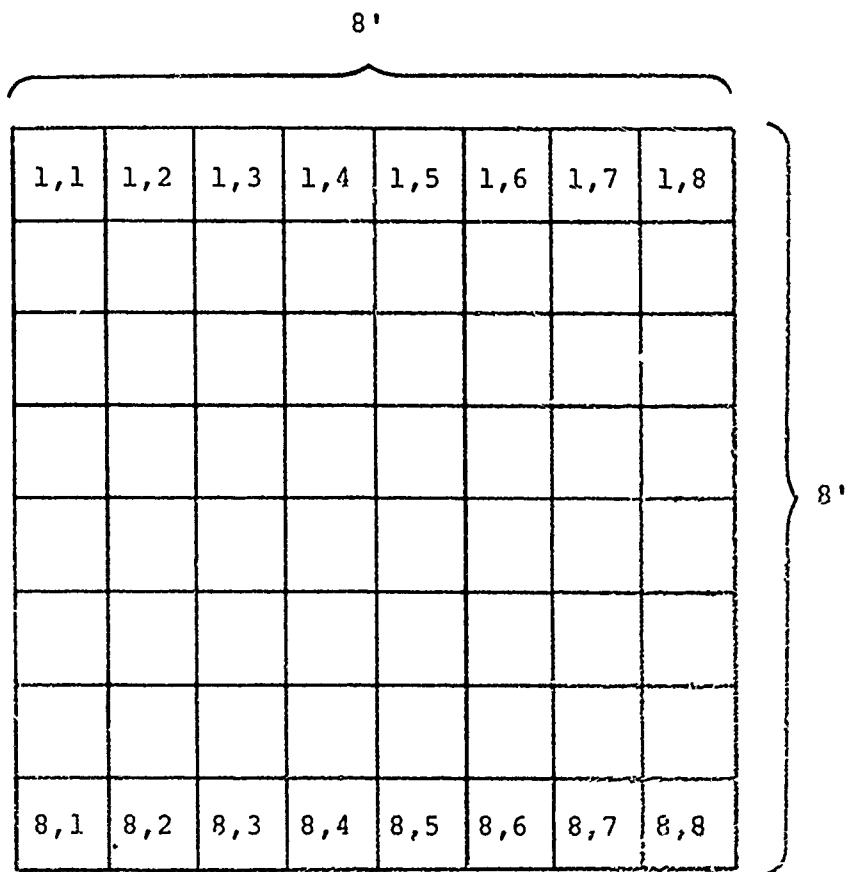| 1,1	1,2	1,3	1,4	1,5	1,6	1,7	1,8
8,1	8,2	8,3	8,4	8,5	8,6	8,7	8,8

8'

Figure D-6   An Array of Subarrays

The subarrays are spaced on 1' centers, which, at 5 GHz, are 5λ. The array factor then becomes (Eq. (D.25)) in the θ plane:

$$S(\theta)\Big|_{array} = \frac{\sin^2 8\{5\pi \sin \theta - (\frac{2m-1}{8}) \frac{\pi}{2}\}}{\sin^2\{5\pi \sin \theta - (\frac{2m-1}{8}) \frac{\pi}{2}\}} . \qquad (D.31)$$

Equation (D.30) has maxima spaced at θ given by Eq. (D.26):

$$\theta = \sin^{-1} \frac{1}{10} (\frac{16q + 2m-1}{8})$$

$$\qquad (D.32)$$

$$= \pm 0.72^0, \pm 2.15^0, \pm 3.58^0, \pm 5.02^0, \pm 6.46^0, \cdots$$

The first four sets of beams of Eq. (D.32), $\pm 0.72°$ through $\pm 5.02°$, are the eight desired antenna beams, covering a peak angular range of $10.04°$, and a 3 dB angular range of $11.3°$. The beams at $\pm 6.46°$ are grating lobes, which are due to the 5λ subarray spacing. The subarray, however, has only a $10.2°$ beamwidth, as shown by Eq. (D.36). Therefore the grating lobes will be in the sidelobe region on the subarray, and will be suppressed by the (sin X/X) subarray pattern. As long as a half-wavelength spacing is maintained on the subarray, and neither the subarray nor the array have amplitude tapering, the subdivision of an array into an array of subarrays will always result in the grating lobes being reduced by the subarray sidelobes. Therefore, the array antenna will have a region which can be defined as the "main beam", with the remainder of visible space being in the sidelobe region. The penalty which is paid for this is the narrower scan angle range which the main beam covers. In our example, the eight subarrays from beams covering a 10° range, whereas the full eighty element array, with steering capability on each element, would, from Eq. (D.27), have an angular coverage

of 162°. It is evident that a tradeoff is possible between the number of subarrays and the angular coverage of the beams, in general, if there are N elements in the subarray, each spaced at $\lambda/2$, and M subarrays, the antenna pattern in the θ plane formed by a Butler matrix will be:

$$D(\theta) = \frac{\sin^2(N \frac{\pi}{2} \sin \theta)}{\sin^2(\frac{\pi}{2} \sin \theta)} \cdot \frac{\sin^2(M \frac{\pi}{2} \{N \sin \theta - (\frac{2m-1}{M})\})}{\sin^2(\frac{\pi}{2} \{N \sin \theta - (\frac{2m-1}{M})\})} \qquad (D.33)$$

MISSION

of

Rome Air Development Center

RADC plans and executes research, development, test and selected acquisition programs in support of Command, Control Communications and Intelligence (C^3I) activities. Technical and engineering support within areas of technical competence is provided to ESD Program Offices (POs) and other ESD elements. The principal technical mission areas are communications, electromagnetic guidance and control, surveillance of ground and aerospace objects, intelligence data collection and handling, information system technology, ionospheric propagation, solid state sciences, microwave physics and electronic reliability, maintainability and compatibility.